

# Annual progress report of the Department of Solid State Physics 1 January - 31 December 1992

**Pedersen, J.S.; Lebech, B.; Lindgård, P.-A.**

*Publication date:*
1993

*Document Version*
Publisher's PDF, also known as Version of record

RISØ

Risø-R-660(EN)

# Annual Progress Report of the Department of Solid State Physics

## 1 January – 31 December 1992

Edited by J. Skov Pedersen, B. Lebech and P.-A. Lindgård

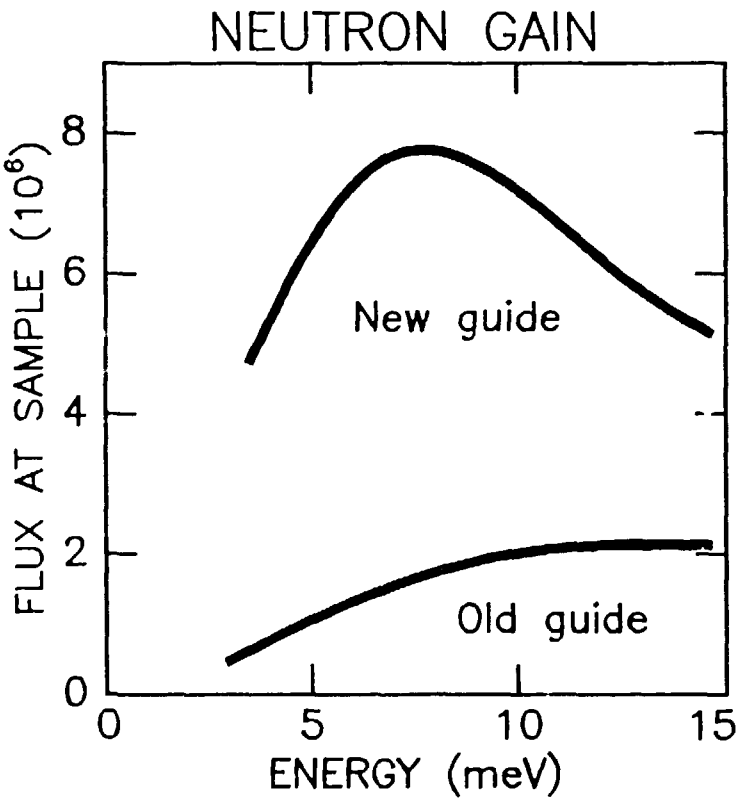


Risø National Laboratory, Roskilde, Denmark
January 1993

# Annual Progress Report of the Department of Solid State Physics 1 January – 31 December 1992

Risø-R-660(EN)

Edited by J. Skov Pedersen, B. Lebech and P.-A. Lindgård

Risø National Laboratory, Roskilde, Denmark
January 1993

**Abstract**

Research in the department is in the field of condensed matter physics. The principal activities of the department in the period from 1 January, to 31 December, 1992, are presented in this Progress Report.

The department's research is predominantly experimental – utilising diffraction of neutrons and X-rays – and includes studies of two- and three-dimensional structures, magnetic ordering, heavy fermions, high $T_c$ superconductivity, phase transitions in model systems, precipitation phenomena, and nano-scale structures in various materials. The major interest of the department is in basic research but projects of a more applied nature are often taken up, prompted by the applicability of the developed techniques and expertise.

For clarity, the contributions to this report are organized into 12 categories with the following headings:

- Theory, Monte Carlo simulations, and methods for data analysis
- Magnetic structures, magnetic phase transitions, and spin dynamics
- High $T_c$ superconductivity
- Structures and structural phase transitions
- Inclusions and precipitates in alloys and metals
- Interaction of particles and photons with surfaces
- Surfaces, interfaces, and amorphous structures
- Langmuir films
- Polymers
- Microemulsions and biological systems
- Instrumental developments
- Other activities



ISBN 87-550-1868-8
ISSN 0106-2840
ISSN 0907-0249

Grafisk Service Risø, 1993

## Contents

# 1 INTRODUCTION

The department's research is concentrated on structural measurements using the techniques of neutron and X-ray scattering. Both of these types of measurements are performed at *large facilities*, namely, the DR3 research reactor at Riso and synchrotron X-ray sources in other countries (primarily HASYLAB in Hamburg, Germany). The experimental measurements are complimented by theoretical studies and computer simulations. Most of the research is fundamental. The approach is to understand the physical properties of matter via its atomic and molecular structures. The department also has close contacts to industry; several research projects are of an applied nature.

In 1992, three major events dramatically improved the experimental capabilities of the department:

- Research at the DR3 research reactor was greatly influenced by the CEC "Large Installation" Program (LIP). LIP made it possible to improve the instrumentation at DR3 for neutron scattering and to financially support users coming to Riso. In particular, during the autumn the old neutron wave guide was replaced with a new one having individually optimised components. A neutron spectrum of higher intensity and lower peak energy was obtained. For all the instruments in the neutron house, this translates to an incident neutron flux 3-5 times greater than before. A very active user research programme is now ongoing.
- At HASYLAB, two new diffractometers built by the department became fully operational. In addition, several experiments were performed. Most noteworthy was that in the autumn the X-ray diffractometer at the undulator beamline BW1 was fully optimised for the first time. A large increase ($\times 100$) in X-ray intensity for surface reflection and refraction experiments was obtained and completely new scientific results immediately followed.
- With the participation of the department, the first preliminary X-ray scattering measurements were performed at the first beamline at the ESRF. A newly developed monochromator system using a diamond crystal was implemented and a monochromatic X-ray beam of unprecedented intensity and coherence was observed. Completely new types of X-ray scattering experiments will soon be feasible there.

## 1.1 Spin Wave Theory for Small Ferromagnetic Clusters

P.V. Hendriksen, S. Linderoth, *Laboratory of Applied Physics, Technical University of Denmark, Lyngby,* and P.-A. Lindgård, *Department of Solid State Physics, Risø National Laboratory, Denmark.*

In recent years there has been a rising interest in the properties of nano-size particles. We have studied the thermodynamic and spin dynamic properties of small ferromagnetic clusters using spin wave theory, and the spherical model for a calculation of the transition temperatures $T_c$ as a function of the size, the structure and possible disorder. In deriving the magnetic properties of a bulk system one uses the translational symmetry. This does not hold in the limit of very small systems, and therefore the predictions of the bulk model, *e.g.* the Bloch $M \sim T^{3/2}$-law for the magnetization cannot be expected to hold. The limited degrees of freedom, on the other hand, allows a numerical approach. Using an exact numerical diagonalization of the equation of motion for spins governed by the Heisenberg Hamiltonian $\mathcal{H} = -\frac{1}{2}\sum_{ij}\mathcal{J}\mathbf{S}_i \cdot \mathbf{S}_j$, we have calculated the spin wave spectrum and the neutron scattering cross section $\mathcal{S}(q,\omega)$. This is shown in Fig. 1. for a cluster with different number of spins and also for clusters in which there are introduced non-magnetic particles. In Fe clusters there is often a small concentration of carbon. The smallness of the clusters produces energy gaps in the spectrum, in particular to the first excited state $\Delta E$. This is very important for the thermodynamic properties. A simple theory relating $\Delta E$ to the maximum possible spin wave length in a cluster allow us to predict accurately the size-dependence of $\Delta E$ s a function of $1/r$, where $r$ is the cluster radius. Thus we are able to predict the magnetic properties for larger cluster sizes than treatable by the numerical method and to interpolate the values for the small clusters to the bulk values. We find that an effective power law holds in a large temperature interval $M = BT^{\alpha}$, where $\alpha$ varies between 3 and 3/2 from the smallest to the largest clusters, Fig. 2. We have also calculated the effective transition temperature $T_c$ as a function of $1/r$, reproducing the best available high temperature expansion value for $r \to \infty$. For the smallest clusters it is reduced to about half that value. This is shown in Fig. 3.

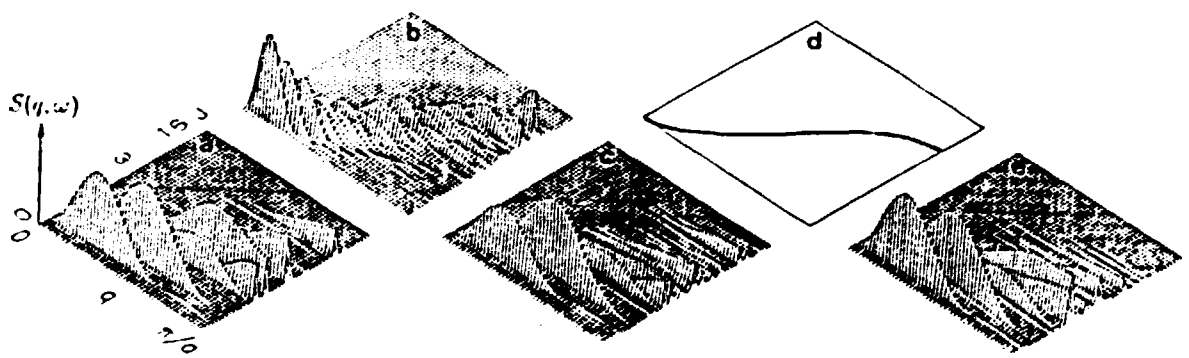


*Fig. 1. The neutron scattering cross section $\mathcal{S}(q,\omega)$ for various clusters. (a) for $N = 55$, (b) for $N = 225$, (c) including disorder by non-magnetic atoms, (d) the bulk spectrum and (e) introducing disorder by variations in the interaction strengths.*

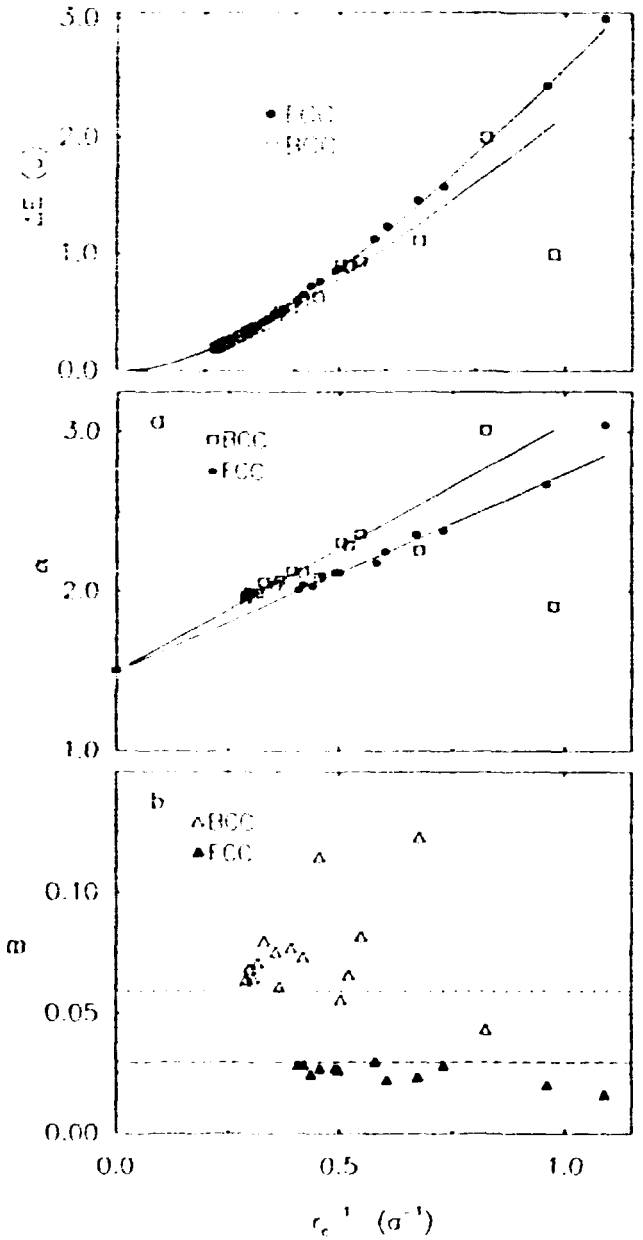


*Fig. 2. The size-dependence of the energy gap $\Delta E$, the effective exponent $\alpha$, and the prefactor $B$ for ferromagnetic clusters.*

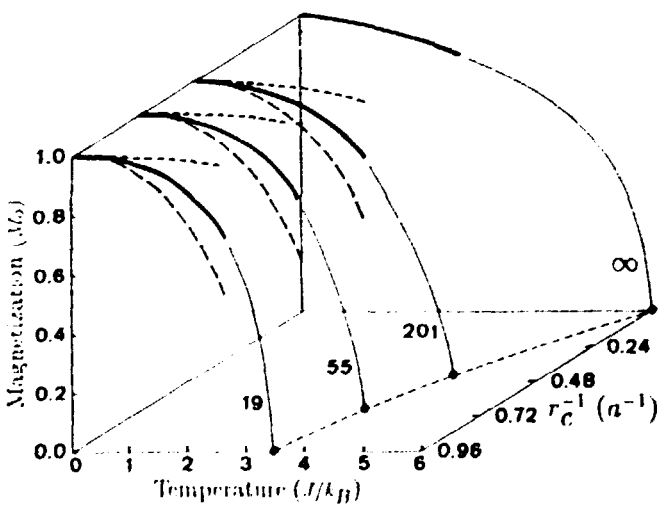


*Fig. 3. Plot showing the size dependence of the mean magnetization vs. temperature (thick line), the surface magnetization (long dashed line), and the center spin (short dashed line). In the bottom plane is shown the size dependence of the transition temperature $T_c$.*

## 1.2 Theory of the Frustrated 2D Quantum Antiferromagnet on a Triangular Lattice

K. Lefmann, *Department of Solid State Physics, Risø National Laboratory, Denmark*, and P. Hedegård, *Physics Laboratory, University of Copenhagen, Denmark*

For nearly two decades the magnetic properties of the antiferromagnetic 2D triangular lattice has been a matter of debate. The classical solution of the problem is the *Néel structure* having three sublattices. The ordering vector for this state is (1/3 1/3). Physical realizations of a triangular lattice $S = 1/2$ system are the compounds $LiNiO_2$ and $NaTiO_2$. Neutron scattering experiments on these materials have not revealed any magnetic ordering along the (1/3 1/3 $n$) directions[1].

We have been studying quantum mechanical methods of solving this problem. As a model we have chosen the Heisenberg Hamiltonian for localised spin including only nearest neighbour interactions:

$$\hat{H} = J \sum_{<i,j>} \mathbf{S}_i \cdot \mathbf{S}_j$$

For studying this system we have used the Schwinger boson formalism. Here the spins are replaced by two essentially different types of $S = 1/2$ Bose particles, one type having spin up - the other spin down. The number of these particles are then allowed to fluctuate requiring that the mean number of spins per site should be unity: $< \hat{n}_{i,\uparrow} + \hat{n}_{i,\downarrow} >= 1$.

A mean field solution of this model corresponds to Andersons resonating-valence-bond state[2] and describes a condensate of singlet pairs. It introduces an order parameter, $\Delta$, which is a measure of the density of singlets. The elementary exitations are seen to be bosonic $S = 1/2$ spin waves (*spinons*). We have obtained two different self consistent solutions (Fig. 1).

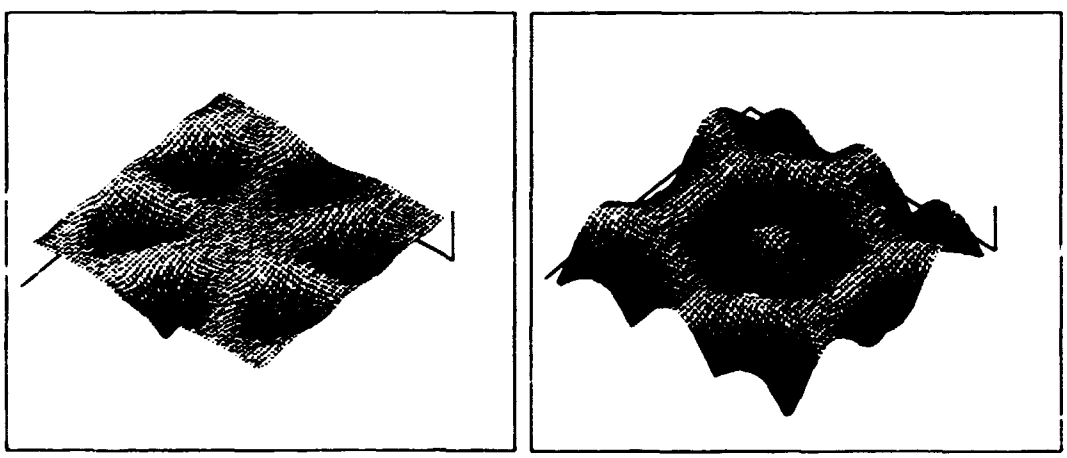

*Fig. 1. Spinon energy vs. wave vector, $\vec{k}$. Left: Solution A. The six minima are at the (1/3 1/3) position and at the other five corners of the Brillioun zone. Right: Solution B. The minima resides in a "ring" inside the Brillioun zone.*

Solution A has spinon energy minima at six points at the edge of the Brillioun zone. This corresponds to the Neél structure. Solution B is seen to have a ring of low energy spinons around the centre of the Brillioun zone. A contour plot (Fig. 2) reveals six minimum points along the same direction as the Neél structure but at an incommensurate $k$-value. At low temperatures a possibility of condensation of the spinons exists. Such a Bose condensate corresponds to magnetic ordering in contrast to the spin liquid structure that would otherwise occur.

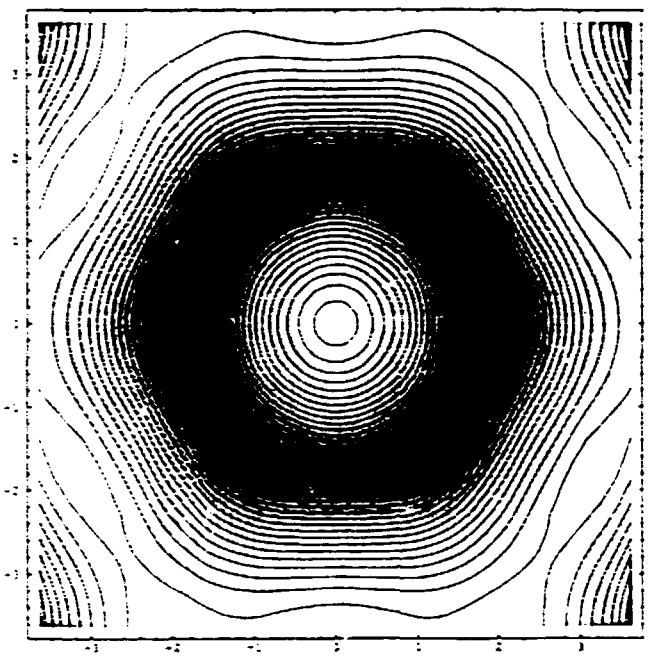

*Fig. 2. Spinon energy vs. wave vector, $\vec{k}$. A contour plot of solution B. The minima reside along the $\langle \eta\, \eta \rangle$ direction - and the five equivalent directions. The wave number for the minima is $|\vec{k}_{\min}| \approx 1.872/a$ where $a$ is the lattice spacing.*

In this model neutron scattering involves two spinons to secure $\Delta S = 0, \pm 1$, as each spinon has spin $S = 1/2$. In the ordered state magnetic Bragg peaks occur at the scattering vector, $\boldsymbol{\kappa}$ equal to the sum of two minimum points. In $NaTiO_2$ the lattice spacing is $a = 3.02$ Å. Thus, solution A predicts magnetic peaks at $\kappa_A = 1.39$ Å$^{-1}$, (1/3 1/3 0), while solution B has its innermost peaks at $\kappa_B = 0.62$ Å$^{-1}$. The inelastic scattering is similar in the ordered and the non-ordered states. For solution B we expect at low temperatures a broad maximum at $\kappa = 0$ and a small peak at $\kappa = 2\kappa_B$.

During this year a few powder samples of $NaTiO_2$ have been investigated at Riso. These experiment were done in collaboration with Andrew Harrison and Simon J. Clarke, Dep. Inorg. Chem., Oxford Univ. Because of problems with the samples quality no reliable experimental results were obtained, but these experiments will continue when better samples are available.

[1] K. Hirakawa, H. Kadowaki, and K. Ubukoshi, (1985). J. Phys. Soc. Jpn. **54**, 3526.
[2] P.W. Anderson, (1973). Mat. Res. Bull. **8**, 153.

## 1.3 Theory and Simulation of Epitaxial Rotation: Light Particles adsorbed on Graphite

E. Vives* and P.-A. Lindgård, *Department of Solid State Physics, Risø National Laboratory, Denmark*

We have developed a theory for epitaxial rotation and have performed Monte Carlo computer simulations of adsorbed particles on a corrugated surface. We have focussed on the case of rare gases and light molecules $H_2$ and $D_2$, adsorbed on graphite. The competition between the particle-particle and particle-substrate interactions gives rise to frustration phenomena. From our model predictions for the epitaxial rotation angle of the adsorbed phases are determined. Our results extend and unify previously known descriptions. In particular we find the same relations as found by Grey and Bohr[1] based on a consideration of Moiré patterns and a symmetry principle. We have given a theory which relates this to energy minimization and have identified a new class of stabilization: stabilization by disorder. Further, we have studied phase diagrams as a function of temperature and coverage. Emphasis has been on the intermediate phases appearing between the commensurate and incommensurate phase for the adsorbed systems. A comparison between the experimental[2] and the simulated the phase diagram for $D_2$ is shown in Fig. 1.

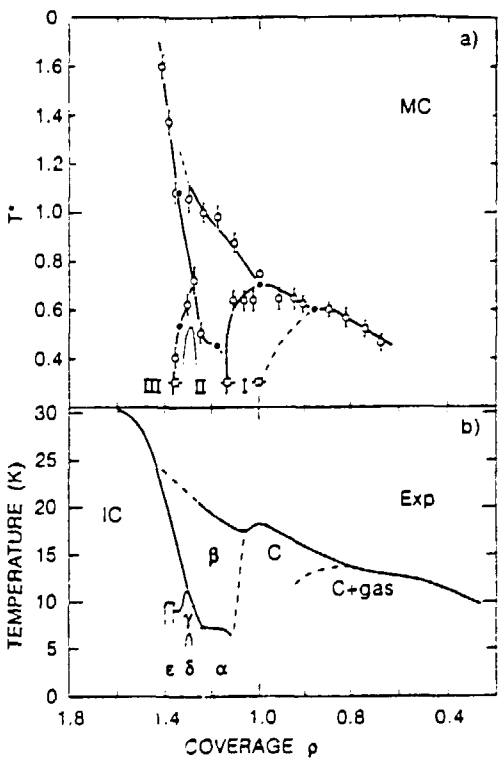


*Fig. 1. Simulated (top panel) and experimental[1] (bottom panel) phase diagrams for $D_2$ on graphite. The simulation data has been obtained from energy versus temperature scans for different coverages (indicated by ○, and ●) as well as from the analysis of the intensities of the different peaks in the structure factor (indicated by □).*

*On leave from: Department E.C.M., Universitat de Barcelona, Catalonia, Spain. Supported by the Ministerio de Educación y Ciencia (Spain).

From our simulations and our theory, we are able to understand the $\gamma$-phase of $D_2$ as an ordered phase stabilized by disorder. Such a situation is similar to the stabilization of intriguing magnetic structures in frustrated magnets. One example of which is the nuclear magnetic order in Cu. In the magnetic case quantum fluctuations select an ordered phase out of a infinite number of degenerate mean-field states. The adsorbed structure has also similarities to the complicated multi-$q$ magnetic structure observed in Nd. In the adsorbed case the $\gamma$-phase can be described as a $2q$-modulated structure. The transition between the incommensurate phase and the $\gamma$-phase is a transition between a $1-q$- and a $2-q$ structure (see Fig. 2). In agreement with the experiments, we have also found a modulated $4 \times 4$ structure. Energy, structure-factor intensities, peak positions, and epitaxial rotation angles as a function of temperature and coverage have been determined from the simulations. Good agreement with theory and experimental data is found.

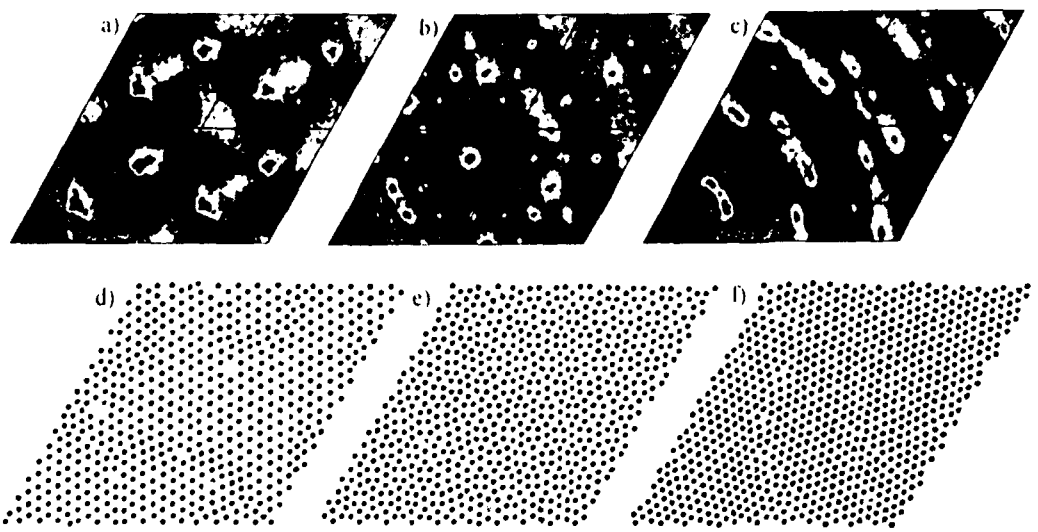


*Fig. 2. Top, intensity plots of the two-dimensional structure factor $S(\mathbf{q})$. The scale is logaritmic and the black regions inside white rings have the highest intensity. Below, small fractions (11%) of the corresponding real space snapshots (• particles, · substrate wells) obtained by Monte Carlo simulation for coverages $\rho = 1.10$ (a,d), $\rho = 1.27$ (b,e) and $\rho = 1.47$ (c,f) and temperature $0.3\epsilon/k_B$, where $\epsilon$ is the Lennard-Jones energy parameter. In experiments only the smallest $\mathbf{q}$ corner is accesible and therefore it is very difficult to see the $1-q$ to the $2-q$ transition, having only the first pair of Bragg-peaks.*


[1] F. Grey and J. Bohr, (1992). Europhys. Lett. **18**, 717.
[2] H. Freimuth and H. Weichert, (1986). Surf. Sci. **189**, 548.

## 1.4 Elastically Driven Phase Transitions Studied by a Continuous Monte Carlo Method

P.-A. Lindgård and E. Vives*, *Department of Solid State Physics, Risø National Laboratory, Denmark*

An important element in phase transitions occurring between different solid phases is the accommodation problem. The formed structure may not fit with its parent phase in respect to either the lattice constants or to the symmetry. This gives rise to elastic deformations and large scale epitaxial rotations and twin formation. The phenomena are difficult to treat accurately by means of standard lattice gas models and Monte Carlo simulations. The continuous Monte Carlo method developed to describe adsorbed particles on graphite is however well suited. That problem is in fact closely related to an alloy problem, namely, that in which one of the elements ($B$) is represented by vacancies, which only interact via "elastic" forces originating from the interaction between the other elements ($A$). As a test case the 2D-system is ideal since the "elastic" forces are emphasized, and because it allows a study of large systems by means of Monte Carlo simulations. This is in particular important when dealing with the effectively long ranged "elastic" forces and with the resulting formations of twin domains of meso-scale dimensions. The equivalence can be seen by reformulating the usual Hamiltonian for the alloy case

$$\mathcal{H}_{alloy} = \sum_{\alpha,\beta}^{A,B} \sum_{ij} V^{\alpha\beta}(r_{ij}) + \sum_{i} U^{\alpha}(\alpha, r_i)\,,$$

where $V^{\alpha,\beta}(r_{ij})$ is the interaction between atoms of type $A$ and/or $B$, and $U^{\alpha}(r_i)$ is a corrugation potential set up by the parent structure. The simple case studied considers only one set of pair interactions

$$V^{AA}(r_{ij}) = V_{Lennard-Jones}(r_{ij})\,, \quad V^{AB}(r_{ij}) = V^{BB}(r_{ij}) = 0\,,$$

$$U^{A}(r_i) = \sum_{HK} U_{HK} e^{iQ_{HK}\cdot r_i}\,, \qquad U^{B}(r_i) = 0\,,$$

where $U_{HK}$ are the first six equivalent Fourier components of the corrugation potential for a hexagonal phase. However, the model calculation can be extended considerably and made more realistic. We have generalized it to be able to treat corrugation potentials of any tetragonal of cubic symmetry. This enable us to study surfaces cut in other than the (111) symmetry directions. It also yields a more realistic model for treating strain effects for the oxygen ordering in YBaCuO, than possible by the ASYNNNI lattice gas model. Further it might be relevant for studying the properties of small inclusions of one phase into another.

*On leave from: Department E.C.M., Universitat de Barcelona, Diagonal 647, 08028 Barcelona, Catalonia, Spain.
Supported by the Ministerio de Educación y Ciencia (Spain).

## 1.5 3D-Monte Carlo Simulation of Oxygen Ordering in YBaCuO

T. Fiig, H.F. Poulsen, N.H. Andersen, P.-A. Lindgård, *Department of Solid State Physics, Risø National Laboratory, Denmark*, and O.G. Mouritsen, *Department of Physical Chemistry, The Technical University of Denmark, Denmark*

There is clear evidence that the superconducting transition temperature depends on the oxygen order in $YBa_2Cu_3O_{6+x}$. It is therefore essential to establish the local oxygen order in the material. Recent neutron diffraction experiments[1] on $YBa_2Cu_3O_{6.4}$, show diffuse superstructure reflections due to the ortho-II phase, which corresponds to a doubling of the unit cell along the $a$-axis. The correlation lengths, along the crystallographic axis are $10a$, $24b$ and $2c$. The existence of only short range order is in contrast to the orthorhombic symmetry of the sample, which is expected to originate from long range oxygen ordering.

To explain the experimental findings, we have modeled the oxygen order, by an extension of well established 2-D ASYNNNI model, by adding an attractive interaction between the basal planes of $YBa_2Cu_3O_{6+x}$, which gives the following Hamiltonian[2],

$$H = V_1 \sum_{\langle ij \rangle}^{NN} \sigma_i^k \sigma_j^k + V_2 \sum_{\langle ij \rangle}^{NNNCu} \sigma_i^k \sigma_j^k + V_3 \sum_{\langle ij \rangle}^{NNNV} \sigma_i^k \sigma_j^k + V_4 \sum_{\langle kl \rangle}^{NN} \sigma_i^k \sigma_i^l,$$

where $\sigma_i^k$ is the site occupation variable for the oxygen atoms at site $i$ in plane $k$. The first three terms constitute the 2-D ASYNNNI model, while the last term represents an attractive interaction between plane $k$ and $l$. We have calculated the 3D-structure factor by means of Monte Carlo simulation (see Fig. 1). The correlation lengths obtained by fitting to a Lorentzian, agrees reasonably with the experimental value. However, the important point here is that the experiment was performed at room temperature (which is deep into the ortho-II phase) while the calculation was done at a temperature above the transition from tetragonal to ortho-II. The calculation of the phase diagram indicates that the transition from tetragonal to ortho-II at $x = 0.4$ is separated by a finite region of ortho-I. Therefore, the transition from tetragonal to orthorhombic phase is associated with the onset of long range ortho-I oxygen ordering in the presence of short range ortho-II fluctuations.

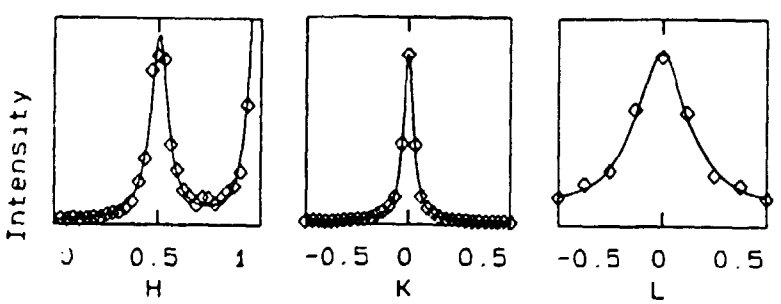


*Fig. 1. Profiles of the [1/2 0 0] superstructure reflection along the crystallographic axis. The calculated correlation lengths are 10a, 20b and 3c.*

[1] T. Zeiske, R. Sonntag, D. Hohlwein, N.H. Andersen, and T. Wolf, (1991). Nature **353**, 542.

[2] Contribution 1.22 in this report.

## 1.6 Diffusive Description of Lattice Gas Models

T. Fiig, *Department of Solid State Physics, Riso National Laboratory, Denmark*, H. J. Jensen, *Department of Mathematics, Imperial College, London, U.K.*

We have investigated a lattice gas model consisting of repulsive particles following deterministic dynamics[1]. Two versions of the model are studied. In one case we consider a finite open system in which particles can leave and enter the lattice over the edge. In the other case we use periodic boundary conditions. In both cases the power spectrum $S(f)$ of the total number of particles on the lattice exhibits a $1/f$ power spectrum, see Fig. 1 (a). The individual particles behave asymptotically as ordinary random walkers, which for instance can be seen by the lifetime distribution $D(T)$ of the time $T$ the particles spend on the lattice from they enter at an edge until they leave. The distribution scales as a power law with exponent $\alpha = 3/2$, see Fig. 1 (b).

The appropriate Langevin-like diffusion equation in terms of a coarse grained particle density $n(\mathbf{r}, t)$ can be written

$$\partial_t n = \gamma \nabla^2 n + F[n, \nabla n] + \rho,$$

where $F[n, \nabla n]$ denotes some general function which takes care of all the higher order terms in the expansion in $n$ and $\nabla n$ and $\rho$ is a noise term acting in the bulk. The analytical solution of the equation reproduces our numerical findings. The conclusion is that the deterministic lattice gases are described by a diffusion equation without any bulk noise ($\rho = 0$). The open lattice gas exhibits a cross-over behavior as the probability for introducing particles at the edge of the system becomes small. The power spectrum changes from a $1/f$ to a $1/f^2$ spectrum. The diffusive description, proven to be valid for a moderate boundary drive, fails altogether when the drive goes to zero.

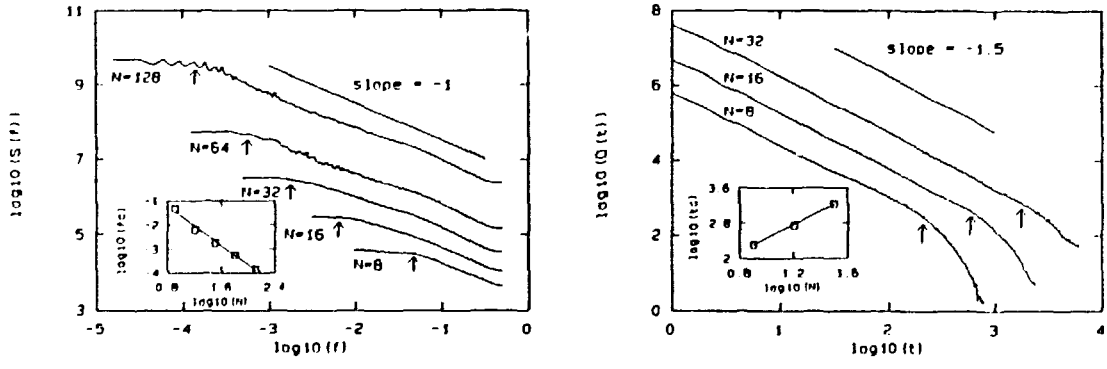


*Fig. 1. Power spectra $S(f)$ (a) and lifetime distribution $D(T)$ (b) for the deterministic lattice gas model for different lattice sizes. Inset shows cross-over frequencies $f_c$ and cross-over times $t_c$ indicated by arrows as function of system size.*

[1] T. Fiig and H. J. Jensen, (1993). *Accepted for publication in Journal of Statistical Physics.*

## 1.7 Analysis of Neutron and X-ray Reflectivity Data by Constrained Least-squares Methods

J. Skov Pedersen *Department of Physics, Riso National Laboratory, Denmark*, and I. W. Hamley, *University of Minnesota, Minneapolis, USA*

Recently, the analysis of specular reflectivity data by model-independent methods has been introduced[1-3]. The method of Skov Pedersen[2] is based on methods for analysing small-angle scattering data[4,5], and it has the limitation that the reflectivity is calculated using kinematical theory. In the method the correlation function is parameterized as a linear combination of cubic spline functions. The coefficients are determined by constrainted least-squares methods, in which the smoothest solution that agree with the data is chosen. The correlation function is then deconvoluted to give the actual scattering length density profile. In the recent method introduced by Singh *et al.* the profile is expressed as a series of sine and cosine terms and the reflectivity of this profile is fitted directly to the reflectivity data. Both kinematical and dynamical theory can be applied. This method is well-suited for periodic structures, for which the symmetry of the problem can be used for reducing the number of fitting parameters.

We have modified the method by Skov Pedersen, so that the reflectivity is calculated directly from the profile by kinematical or dynamical theory. The scattering density is again parameterized using cubic splines and a constraint is used which reduces the differences between successive cubic spline coefficients and which bias towards the mean scattering density of the material.

We have also introduce several new features in the method of Singh *et al.* of which the inclusion of a smoothness constraint is the most important. We use a contstraint which reduced the coefficients of the higher harmonics in the Fourier series. This makes it possbile to apply the method also on non-periodic profiles.

The two methods have been applied to several sets of simulated reflectivity data based on examples from the literature including an amphiphilic monolayer and block copolymer thin films. The calculations show that the two methods in most situations work equally well, and that they are able to recover the original profiles. In general, the method using spline functions as the basis is better suited for non-periodic than for periodic structures. The sine/cosine basis is well-suited for periodic and nearly periodic structures.

[1] D.S. Sivia, W.A. Hamilton, and G.S. Smith (1991). Physica **B173**, 121.
[2] J. Skov Pedersen, (1992). J. Appl. Cryst. **25**, 129.
[3] N. Singh, M. Tirrell, and F.S. Bates (1993). Applications of Fourier synthesis methods to specular reflection. *preprint.*
[4] O. Glatter, (1977). J. Appl. Cryst. **10**, 415.
[5] O. Glatter, (1981). J. Appl. Cryst. **14**, 101.

## 1.8 On Estimation of Error Propagation in Small-angle Scattering Data Treatment

D.I. Svergun, *EMBL, Hamburg Outstation, Germany*, and J. Skov Pedersen, *Department of Solid State Physics, Ris National Laboratory, Denmark*

Small-angle scattering data treatment aims at restoration of a real space distribution function $p(r)$ from the experimentally measured scattering intensity in reciprocal space. In modern research, the so-called indirect transform methods are normally used to this end. When using these methods, the parameters to be obtained cannot be directly deduced from the experimental data (an integral equation needs to be solved), therefore the problem of proper estimation of error propagation is non-trivial. In particular, error estimates may differ depending on the way of parameterizing $p(r)$.

We considered three indirect methods, where a different parameterization of $p(r)$ is used. The method of Moore[1] is based on the Shannon sampling theorem, and $p(r)$ is represented as a sum of a few (normally, less than 10) sine functions. In the original indirect method of Glatter[2], cubic *b*-splines are used (the number of splines in practical applications is 25–30). In the method of Svergun *et al.*[3], $p(r)$ is represented as a histogram, and a larger number of knots (around 40–50) is normally required. In the last two cases, the problem is ill-posed and the regularization method is used to stabilize the solution.

For the methods of Moore and of Glatter, the error propagation is evaluated via the error matrix (which is the inverse of the matrix of normal equations). In the method of Svergun *et al.*, a Monte-Carlo simulation approach is implemented. It consits of simulating typically 50–100 scattering curves from the the original measured data. These curves are then analyzed, and the standard errors are calculated from the variance of $p(r)$.

In our model calculations, the methods of Moore and Svergun *et al.* gave approximately the same error estimates for $p(r)$, whereas for the original method of Glatter, overestimated errors are typically obtained. This can be explained by poor stability of the error matrix, though the solution itself appears to be properly stabilized. In the method by Svergun *et al.*, when using Monte Carlo simulations, the problem is solved without matrix inversion, thus leading to reliable error estimates. We implemented similar techniques in a program based on the method of Glatter and have obtained propagated errors similar to those given by the method of Svergun *et al.*. In the method of Moore, error estimates via the error matrix are reliable due to a low number of unknowns, but this parametrization may lead to systematic deviations exceeding the estimated error bars.

Our main conclusion is that, when solving ill-posed problems using the regularization technique, error propagation should not be evaluated using the error matrix; instead, the Monte-Carlo method has to be used.

[1] P.B. Moore, (1980). J. Appl. Cryst., **13**, 168.
[2] O. Glatter, (1977). J. Appl. Cryst., **10**, 415.
[3] D.I. Svergun, A.V. Semenyuk, and L.A. Feigin, (1988). Acta Cryst. **A44**, 244.

## 1.9 Magnetic Structure of Erbium under High Pressure

B. Lebech, *Department of Solid State Physics, Risø National Laboratory, Denmark*, S. Kawano, *Research Reactor Institute, Kyoto University, Osaka, Japan*, and N. Achiwa, *Department of Physics, Kyushu University, Japan*

The various oscillatory, cycloidal or helical orderings of the magnetic moment observed in rare earth metals and their alloys are the result of a compromise between competing magnetic interactions such as the Ruderman-Kittel-Kasuya-Yoshida (RKKY) interaction, one-ion and two-ion anisotropy effects, and magnetoelastic effects[1]. Pressure induced changes of the interatomic distances may lead to changes in the magnetic structures and hence provide information about these interactions. Until quite recently, low temperature studies of the effects of high-pressures on the properties of rare earth metals and alloys have been rather sparse and limited to bulk methods such as measurements of electrical resistivity or intial permeability.

During the last years, the effects of high-pressure on the magnetic structures of Tb and Ho have been studied by means of neutron diffraction[2-4]. We have used a McWhan-type pressure cell developed by Onodera *et al.*[5] for similar studies of the magnetic structures of a single crystal of Er ($3 \times 3 \times 4$ mm$^3$). The data show that at 4.5 K, 11.5 kbar hydrostatic pressure suppresses the transition to a conical structure observed below 20 K at ambient pressure. Furthermore, we find that the ambient-pressure high-temperature cycloidal structure, with modulation vector $\mathbf{Q} \simeq (\frac{2}{7} \cdot \frac{2\pi}{c})\hat{\mathbf{c}}$ persists down to 4.5 K. The existence of higher-harmonic magnetic satellites indicates that the cycloid is squared up. Preliminary data at higher temperatures further show that the modulation vector is unchanged between 4.5 K and $\sim$ 50 K. Above $\sim$ 50 K the structure changes to a longitudinally-modulated structure and $Q$ tends to increase. The intensities of the magnetic satellites originating from higher-order harmonics of the **c**-axis-moment component which are observed at 4.5 K decrease slowly with increasing temperature, but they persist up to $\sim$ 60 K.

The intensities of the magnetic Bragg peaks observed at 4.5 K and 11.5 kbar hydrostatic pressure have been analyzed in terms of a cycloidal structure given by:

$$\begin{aligned} \mu_x(\mathbf{r}_n) &= \mu_{x0}\cos(\mathbf{r}_n \cdot \mathbf{Q} + \alpha_x) \\ \mu_y(\mathbf{r}_n) &= \mu_{y0}\cos(\mathbf{r}_n \cdot \mathbf{Q} + \alpha_y) \sim 0 \\ \mu_z(\mathbf{r}_n) &= A_1\cos(\mathbf{r}_n \cdot \mathbf{Q} + \gamma_1) + A_3\cos(3\,\mathbf{r}_n \cdot \mathbf{Q} + \gamma_3) + A_5\cos(5\,\mathbf{r}_n \cdot \mathbf{Q} + \gamma_5) \\ &\quad + A_7\cos(7\,\mathbf{r}_n \cdot \mathbf{Q} + \gamma_7) \end{aligned} \qquad (1)$$

where $x$, $y$, and $z$ refer to moment components along the **a** , **b** , and **c** directions of the real space lattice. The modulation vector $\mathbf{Q} = (\frac{2}{7} \cdot \frac{2\pi}{c})\hat{\mathbf{c}}$, and the moment components $\mu_{x0}$ and $\mu_{y0}$ are perpendicular to **c**, while $A_i$ ($i$ = 1, 3, 5, and 7) are parallel to **c**. The phases, $\alpha_x$, $\alpha_y$, and $\gamma_i$, where $i$ = 1, 3, 5, and 7, between the individual moment components in were estimated by a trial and error method with the following conditions: (1) The total moment on any atom $i$ should not exceed the free ion value of 9 $\mu_B$ per Er atom. (2) the moments of all atoms should be as large and of as equal length as possible, and (3) $\mu_{y0}$ should be negligible.

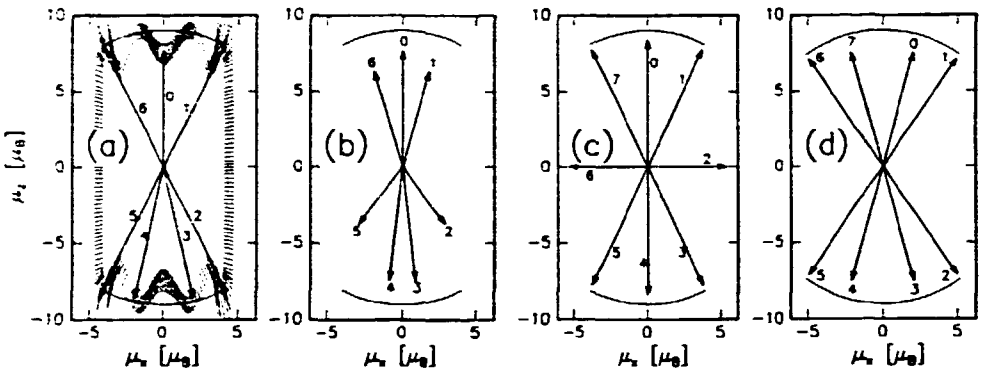


*Fig. 1. Spin configuration for a cycloidal structures of Er. (a) at 4.5 K and at 11.5 kbar hydrostatic pressure. (b) at 49 K and ambient pressure*[6] *and (c) and (d) at 22 K and ambient pressure*[7]*. The moments have been projected onto the xz-plane and displaced to a common origin. The numbers i = 0, 1, 2, ...., 6 (,7) refer to spins in the ith layer of atoms.*

The results are summarized in Fig. 1. Figure 1a shows the spin configuration of a cycloidal structure given by eq. (1) for Er at 4.5 K and 11.5 kbar hydrostatic pressure. For comparison, Fig. 1b shows the moment-configuration derived by Cowley and Jensen[6] for Er at ambient pressure and 49 K. Figures 1c and 1d show the results of an analysis similar to the one at 4.5 K and 11.5 kbar hydrostatic pressure for the data of Habenschuss *et al.*[7] for Er at 22 K. From the neutron-diffraction data alone, it is impossible to decide which of these two structures is the correct structure of Er at 22 K and ambient pressure. For the highly anisotropic structure shown in Fig. 1c, the spins in the second and sixth layers lie entirely in the basal plane while the remaining spins lie predominantly along the **c** axis. Because of the strong magnetoelastic couplings in Er[1] this configuration will lead to lattice distortions with a periodicity of $q = 4/8$. In contrast, the structure shown in Fig. 1d is relatively isotropic with all spins predominantly along the **c**-axis and will presumably only accomadate relatively small lattice distortions. Therefore, precise X ray diffraction measurements may allow us to distinguish between these two structures.

[1] J. Jensen and A.R. Mackintosh, (1991). *Rare Earth Magnetism: Structures and Excitations* (Clarendon Press, Oxford).

[2] H. Umebayashi, G. Shirane, B.C. Frazer, and W.B. Daniels, (1968). Phys. Rev. **165**, 688.

[3] S. Kawano, N. Achiwa, A. Onodera, and Y. Nakai, (1992). Physica B **180** & **181**, 46.

[4] N. Achiwa, S. Kawano, A. Onodera, and Y. Nakai, (1988). J. de Phys. **49**, C8-349.

[5] A. Onodera, Y. Nakai, N. Kunitomi, O.A. Pringle, H.G. Smith, R.M. Nicklow, R.M. Moon, F. Amita, N. Yamamoto, S. Kawano, N. Achiwa, and Y. Endoh, (1987). Jpn. J. Appl. Phys. **26**, 152.

[6] R.A. Cowley and J. Jensen, (1992). *Magnetic structures and interactions in Erbium, accepted for publication in J. Phys. Condens. Matt.*

[7] H. Habenschuss, C. Stassis, S.K. Sinha, H.D. Deckman, and F.H. Spedding, (1974). Phys. Rev. **B10**, 1020.

## 1.10 Crystal and Magnetic Structure of $ErRh_3B_2$

P. Harris, B. Lebech, *Department of Solid State Physics, Risø National Laboratory, Denmark*, J. Bernhard, *Department of Electrical Engineering, University College of Falun/Borlänge, Sweden*, and I. Higashi, *Inorganic Chemical Physics Laboratory, The Institute of Physical and Chemical Research, Wako-Shi, Saitama, Japan*

The ternary system $ErRh_3B_2$ is known to be ferromagnetic and to crystallize in a base-centered monoclinic structure (space group $C2/m$), which is slightly distorted from hexagonal symmetry. A recent X-ray study and magnetic susceptibility measurements[1] show that the system is more complex.

From single crystal X-ray diffraction the lattice constants are determined to be $a = 5.32$ Å, $b = 9.21$ Å, $c = 3.077$ Å, and $\beta = 90.6°$. The compound shows twinning. Positive a- and b-axes from one twin individual are directed along negative a'- and b'-axes of the other twin individual. As the c- and c'-axes are not parallel, but inclined 1.2° to each other, the reflections will split along the c*-axis. In addition a six doubling of the c-axis is seen by the X-ray oscillation film technique. The diffraction peaks were weak and complicated by the twinning, why the superstructure has not been determined.

Magnetization measurements show considerable anisotropy. At $T_N = 27$ K, the data indicates ferromagnetic order with the spins directed parallel to the c-axis. However, the magnetization curve shows a maximum at 27 K. The magnetization decreases on further cooling and ends up at a value of 75 % of it's maximum value.

In order to investigate both the crystal and the magnetic structure, initial investigations of $ErRh_3B_2$ has been performed on a 4-circle neutron diffractometer using neutrons of wavelength 1.013 Å. Scans parallel to the c*-axis indicated clearly a doubling of the c-axis, but no six doubling was seen. However, the resolution was too low to eliminate the presence of additional satellite reflections.

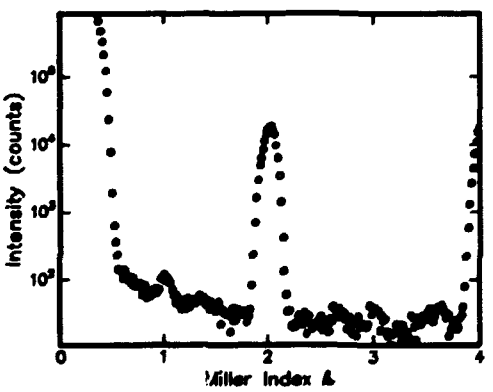


*Fig. 1. Scan at 15 K along the* $(0\,k\,0)$ *direction. Weak diffraction are seen at the positions* $(0\,1\,0)$, $(0\,\frac{4}{3}\,0)$, $(0\,\frac{8}{3}\,0)$ *and* $(0\,3\,0)$.

At 15 K we observed strong ferromagnetic scattering. In addition we observed some scattering at $(0\,1\,0)$, $(0\,3\,0)$ and $(1\,0\,0)$, all three of them systematically extinct above $T_N$. There also seemed to be weak scattering at $(0\,\frac{4}{3}\,0)$ and $(0\,\frac{8}{3}\,0)$ (see Fig. 1). This indicates that the magnetic ordering is not as for a simple ferromagnet.

In the near future we plan to do an experiment on a triple-axis spectrometer, using cold neutrons ($\lambda \approx 4$ Å). In this experiment we expect to be able to resolve the crystalline superstructure and follow the magnetic scattering as a function of temperature.

[1] J. Bernhard, H. Kitazawa, I. Higashi, T. Shishido, T. Fukuda, and H. Takei, (1992). J. Metals Alloys, *In the press.*

## 1.11 Unusual Polarization and Energy Dependence in Magnetic Diffraction from a HoEr Alloy

D.B. Pengra, N.B. Thoft, R. Feidenhans'l, and J. Bohr, *Department of Solid State Physics, Riso National Laboratory, Denmark*, and M. Wulff, *European Synchrotron Radiation Facility, Grenoble, France*

We have studied the energy and polarization dependence of X-ray diffraction peaks arising from the magnetic structure of a single-crystal random alloy, $Ho_{0.5}Er_{0.5}$ at different temperatures. Diffraction peaks, which are satellites to the principle Bragg reflections of the crystal lattice, show a surprising energy and azimuthal-angle dependence that has so far resisted explanation.

The HoEr crystal, which has previously been studied with neutron diffraction[1], has a low-temperature phase consisting of of a single, conical-spiral magnetic structure. Our X-ray diffraction data show that this phase is accompanied by a basal-plane lattice modulation, as we see only magnetic-scattering satellites along the [00$\ell$] direction, but much stronger charge-scattering satellites along the [10$\ell$] direction. The magnetic phase transforms to a basal-plane spiral, and the lattice modulation vanishes, at 35 K. To perform the energy analysis of the magnetic peaks, we maintain the Bragg condition at the $(0,0,4-q)$ satellite while varying the incident energy through the Ho $L_{III}$ absorption edge (8069 eV), and collect the signal for both in-plane ($\sigma$-$\sigma$) and out-of-plane ($\sigma$-$\pi$) polarizations. In Fig. 1, one can see that well below the resonance energy at 8067 eV there is additional intensity at 8051 eV and about 8015 eV. These peaks vanish upon warming the sample to 40 K.

The strengths and energies of the extra resonances vary as a function of the azimuthal angle about the principle diffraction vector. Such behavior is expected from peaks arising from multiple, or "Renninger" reflections[2], but a careful analysis of the data suggests these peaks are not due to this mechanism. We are currently considering other possible explanations for this phenomenon.

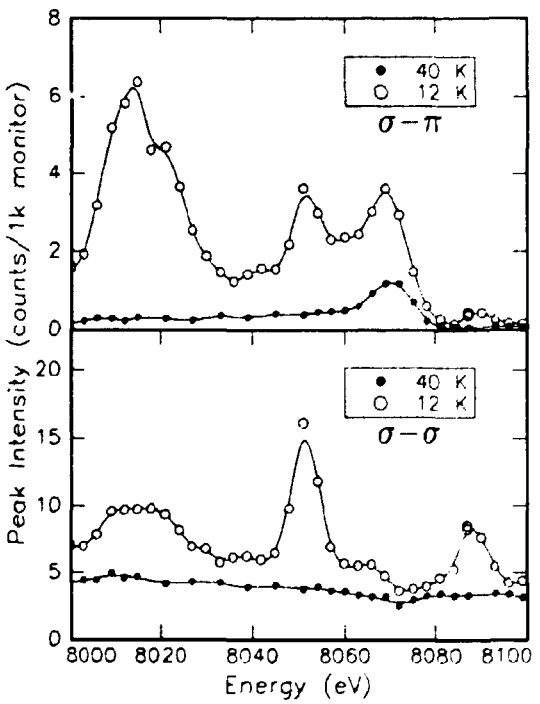


*Fig. 1. Energy and temperature dependence of the peak intensity of the $(0,0,4-q)$ satellite, measured in in-plane ($\sigma$-$\sigma$) and out-of-plane ($\sigma$-$\pi$) polarizations. Solid lines are guides to the eye.*

[1] B.K. Howard and J. Bohr, (1991). Physica Scripta **T39**, 96.
[2] H. Cole, F.W. Chambers, and H.M. Dunn, (1962). Acta Cryst. **15**, 138.

## 1.12 Anomalous X-Ray Diffraction Study of Ho-Y Multilayers

N.B. Thoft, D.B. Pengra, J. Bohr, *Department of Solid State Physics, Riso National Laboratory, Denmark*, G. Helgesen, and D. Gibbs, *Brookhaven National Laboratory, USA*

Ho-Y superlattices have been studied by synchrotron X-ray scattering, making use of the enhanced scattering obtained by tuning the incoming X-ray energy near the Ho absorption edge. Magnetic rare earth superlattices have previously been studied[1]. In this study we attempt to understand the effect of the artificial periodicity or compositional modulation, finite layer thickness, and epitaxial strain on the magnetic structure in more detail.

An example of the data for the $Ho_{15}Y_5$ sample is shown below. As the incoming X-ray energy is changed from 8055 eV through 8068 eV (the Ho absorption edge) to 8085 eV, it is clearly seen that the intensity of the peak at 2.262 $c^*$, which stems from the magnetic structure, comes up and falls away. This illustrates the resonance in the magnetic scattering cross-section at the Ho absorption edge. (The curves are offset for clarity.) These scans were taken using a polarization analyser in the $\sigma$-$\pi$ orientation, which favours magnetic scattering. As the incoming beam is not completely polarized several charge scattering peaks arising from the multilayer structure are also observed.

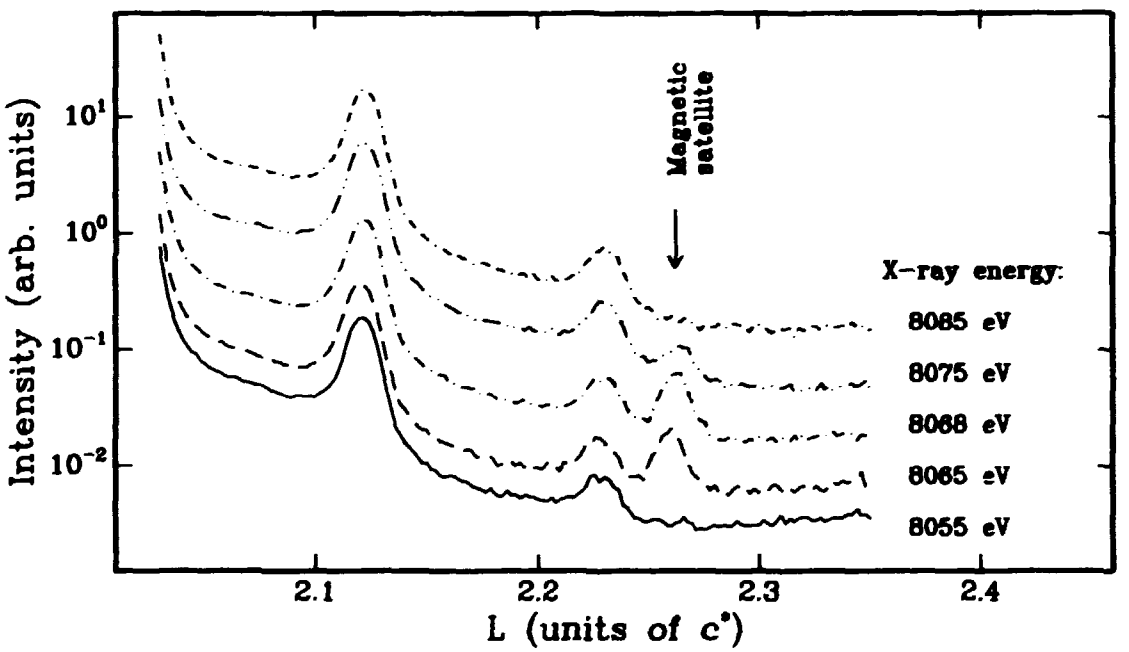


[1] For a review, see *e.g.* C.F. Majkrzak, J. Kwo, M. Hong, Y. Yafet, D. Gibbs, C.L. Chen, and J. Bohr, (1991). Advances in Physics **40**, 99.

## 1.13 The Magnetic Structure of Holmium-Yttrium Superlattices

D. A. Jehan, D. F. McMorrow, R. A. Cowley, R. C. C. Ward, M. R. Wells, N. Hagmann, *Oxford Physics, Clarendon Laboratory, UK*, M. C. Gerstenberg, and K. N. Clausen, *Department of Solid State Physics, Riso National Laboratory, Denmark*

The chemical and magnetic structures of a series of holmium-yttrium superlattices and a single 5000 Å film of holmium have been investigated by high-resolution X-ray and neutron diffraction measurements. The samples have all been grown by molecular beam epitaxy, which allow a pre-selected number of atomic planes to be grown. This provides a unique method of producing single crystals which are "model" magnetic systems and allows fundamental theories of magnetism to be tested. The epitaxial relationships are [120] $Al_2O_3$ || [110] Nb || [001] Y, Ho, where both the bcc niobium and hcp rare-earth metals grow with their respective densest-packed atomic planes parallel to the substrate plane.

Other multilayer systems, which consist of alternating layers of a magnetic rare-earth and the non-magnetic yttrium, have already been studied[1]. The most important feature of the magnetism in these superlattices is that there is coherence in the ordering between adjacent blocks of magnetic material. The aim of the present study is to investigate more thoroughly the effect of strain and different thicknesses of the Ho and Y blocks on the magnetic structures, and compare the results with bulk Ho.

X-ray diffraction with detailed modelling showed that the structural coherence length is typically in excess of 2000 Å. The superlattice interfaces, made up of surface roughness and interdiffusion, extend over 4-5 lattice planes. Furthermore, the study showed that the c-axis-spacing in the Ho-layers is strained to be smaller than the bulk value of 2.808 Å, while in the Y-layers the spacing is increasing with respect to the bulk value of 2.865 Å. In general the strain is increased with thinner layers of either material.

The magnetic structure was determined by neutron scattering techniques using TAS1 and TAS7. Figure 1 shows a series of scans of the wave vector transfer **Q** taken along the [00*l*]-direction between 10 and 130 K at 10 K intervals from the $[Ho_{40}|Y_{15}]_{50}$ superlattice. The data were analyzed using a model in which it is assumed that the magnetic moment associated with the Ho atoms and the turn angle of the helical structure is dependent on the concentration of the Ho and Y ions. The layer thicknesses and interface widths found from the neutron data showed good agreement with the X-ray measurements. Subsequently, the magnetic moments were shown to be confined to the basal plane at all temperatures to form a simple helical structure with no clear evidence of any "spin-slip" phases[2] in any of the superlattices. The model provided good agreement with the measurements over several decades of intensity.

The Neel Temperature was found to decrease with decreasing Ho layer thicknesses and is independent of the Y blocks (for Y blocks between 6 and 30 layers). The magnetic coherence length is at least 750 Å or 5 bilayers for $[Ho_{40}|Y_{15}]_{50}$.

The contributions to the total helical turn angle made by the holmium and yttrium was determined by the modelling. It was found that the effective turn angle in the yttrium is approximately 51° and independent of both temperature and the number of yttrium and

holmium planes. In contrast the turn angle in the holmium layers changes with temperature, but with an overall variation that is less than in bulk holmium, and in a manner which depends on the thickness of the holmium blocks alone.

The strain induced in the sample by the mismatch in the lattice parameters of Ho and Y is sufficient to change radically the magnetic structure: The variation of the wave vector of the helix with temperature is reduced, and as far as we could ascertain no conical phase occurs as in bulk Ho. This reduction might arise from a coupling of the strain to the exchange which will occur as a magneto-elastic energy term in the Hamiltonian. The effect of the strain will be further investigated by experiments on holmium/lutetium superlattices. Lu has a basal plane parameter that is smaller than Ho, whereas that of Y is larger. Thus any strains induced in Ho will be in the opposite sense to those induced in Y.

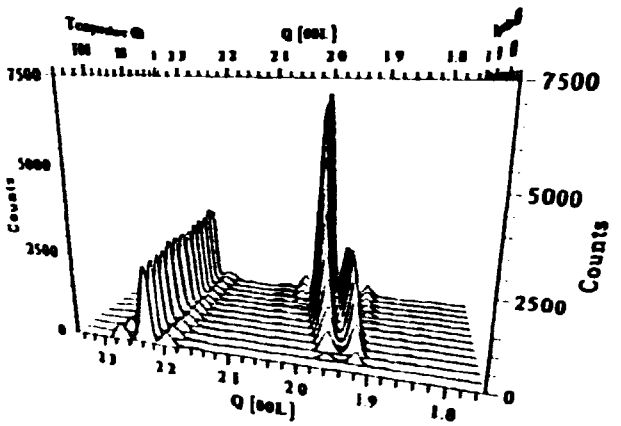


*Fig. 1. A series of scans taken along the* [00*l*]*-direction between 10 and 130 K at 10 K intervals from the* $[Ho_{40}|Y_{15}]_{50}$ *superlattice. The scan in the foreground was taken above the Neel temperature,* $T_N$*, and only the nuclear scattering is evident at* $Q = 2.23$ Å$^{-1}$*. At* $T_N$ *the turn angle per Ho layer is approximately 50° which is lower than the bulk value of Ho. As the temperature is decreased the magnetic peaks move towards the nuclear peaks indicating a decrease in the turn angle of the Ho. Furthermore, the magnetic peaks increase in intensity as the temperature decreases due to increased ordering of the magnetic moments.*

[1]C. F. Majkrzak, J. Kwo, M. Hong, Y. Yafet, D. Gibbs, C. L. Chien, and J. Bohr, (1991). Advances in Physics **40**, 99.
[2]D. Gibbs, D. E. Moncton, K. L. D'Amico, J. Bohr, and H. Grier, (1985). Phys. Rev. Lett. **55**, 234.

## 1.14 Magnetism in the Nearly Ferromagnetic Helix, FeGe

B. Lebech and P. Harris, *Department of Solid State Physics, Riso National Laboratory, Denmark*

The cubic polymorph of FeGe and MnSi belongs to a class of magnetic intermetallic compounds with the B20 crystal structure ($P2_13$). Materials with this crystal structure lack inversion symmetry; they have chirality and are capable of supporting a static spin density wave at low temperatures. Within current theories the static spin density wave corresponds to a long range antiferromagnetic helical structure, a so-called Dzyaloshinskii-Moriya helix. The helix propagates along high symmetry directions in the crystal, and it is extremely long range with repeat distances ranging from 45 to 175 lattice units. This means that locally, along the direction of propagation, the spin arrangement can be considered ferromagnetic. The randomly substituted $Mn_xCo_{1-x}Si$ and $Fe_xCo_{1-x}Si$ alloys have the same crystal structure as the parent compounds and similar magnetic properties with antiferromagnetic order of even longer range than that observed in MnSi or FeGe. Figure 1 illustrates this. It shows the relation between the number of 3*d*-electrons and the modulation vector (*i.e.* inverse repeat distance) of the antiferromagnetic order[*,1]. At least for $Fe_xCo_{1-x}Si$, the modulation vector versus the 3*d*-electron concentration lies on a smooth curve.

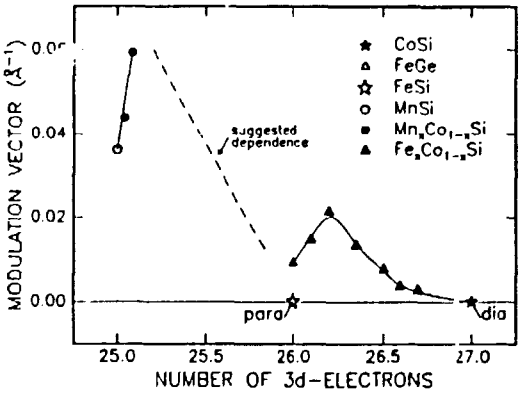


*Fig. 1. Summary of the relation between the number of 3d-electrons and the reported modulation vectors in the isomorphous, magnetically ordered cubic structures of MnSi, FeGe, $Mn_xCo_{1-x}Si$ and $Fe_xCo_{1-x}Si$. For completeness the paramagnetic FeSi and the diamagnetic CoSi are included.*

FeGe has a critical temperature of $T_N \sim 278.7$ K. The magnetic structure is a helix propagating along equivalent (100) directions above 211 K and along equivalent (111) directions below 211 K (for decreasing temperatures). The periodicity is $\sim 700$ Å and the spins are confined to lie in planes perpendicular to the direction of the propagation of the helix. Within each plane, the spins are ferromagnetically aligned, but the spins in neighbouring planes are turned an angle, determined by the repeat distance, with respect to each other.

Recent detailed magnetization studies of both MnSi and FeGe[*,2,3] and a theoretical treatment by Plumer[*,4] of the effects of applied magnetic fields have led to a re-analysis of the small-angle neutron scattering data of FeGe in an applied magnetic field. Some results are summarized in Fig. 2, which show the field dependencies at 250 K, of the angle between the modulation vector **q** and the field **H**. The field is applied in the [011] direction, *i.e.* vertically and perpendicular to the incident neutron beam. At 250 K, the initial propagation vector **q**(0) is along equivalent (100) directions and the spins are confined to

planes perpendicular to the direction of propagation. The insets illustrates the scattering geometries. In Figs. 2a and 2b the incident neutron beam is along the $[0\bar{1}1]$ and $[\bar{1}00]$ directions, respectively. It is important to note that the crystal orientation in Fig. 2b corresponds to a 90° rotation of the crystal around the direction of the field when compared to the crystal orientation in Fig. 2a, *i.e.* at each field the data shows "snapshots" of the orientation of the two types of wave vectors that coexist in the crystal.

The obvious differences are the following:
In Fig. 2a, when the initial modulation vector **q**(0) is perpendicular to the applied field the transition is a regular first order spin flop transition, where the modulation vector flop to the field direction at $\mathbf{H}_f$ = 6.3 mT, while keeping the spins perpendicular to the modulation vector. This result is in complete agreement with the prediction of Plumer*,[4].

In Fig. 2b, when **q**(0) is at 45° to the applied field the transition is a second order transition, where the modulation vector turns parallel and the spins perpendicular to the field direction at $\mathbf{H}_f$ = 13.2 mT. This behaviour is similar to the behaviour calculated by Plumer[4] at 250 K for a field applied along the [111] direction with the initial wave vector along the [001] direction.

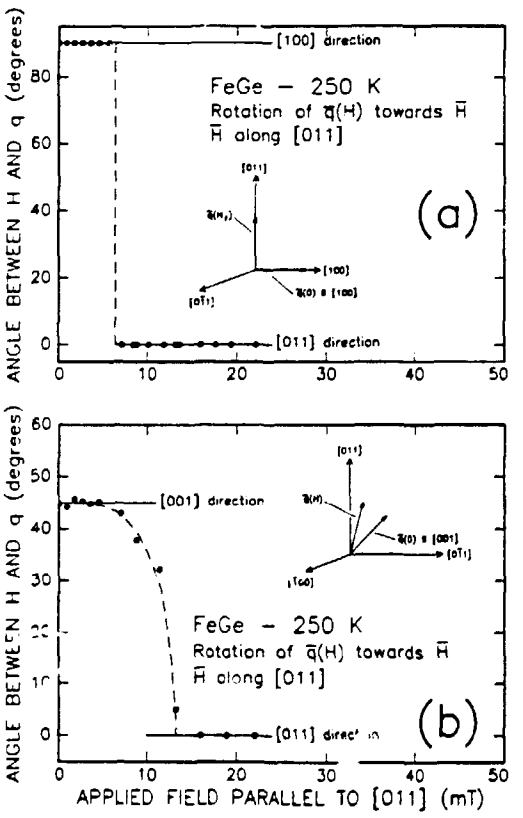


*Fig. 2. Field dependencies of the angle, between the modulation vector q and the direction of the applied field* **H** *at 250 K in cubic FeGe. The insets show the relevant parts of reciprocal space and define the orientations of the initial modulation vector* **q**(0) *and the modulation vector* **q**(*H*) *for a field* **H** *along [011]. Both these vectors lie in a vertical plane parallel to the area sensitive detector.*

The field dependence in the low temperature phase*,[5] (at 140 K) is analogous to the field dependence observed at 250 K. When the angle between the applied field and the initial modulation vector **q**(0) is 90°, the field induced transition is a first order spin flop transition ($\mathbf{H}_f$ = 16.9 mT), whereas the rotation of the modulation vector is a second order transition ($\mathbf{H}_f$ = 39.5 mT), when the angle between the applied field and the initial

modulation vector $\mathbf{q}(0)$ is less than 90°. Therefore, the experimental results seem to imply that at both temperatures, the important parameter governing the nature of the field induced transition is the initial angle $\theta(0)$, between the applied field and the modulation vector - not the particular crystallographic direction of the modulation vector.

*) For references see the following contribution.

## 1.15 Critical Scattering in the Nearly Ferromagnetic Helix, MnSi

C.I. Gregory, N.R. Bernhoeft, *Department of Physics, University of Durham, U.K.*, B. Lebech, and P. Harris, *Department of Solid State Physics, Risø National Laboratory, Denmark*

MnSi is an example of a system intermediate between a weakly ferromagnetic material and a heavy electron system[6] with a relatively low ordering temperature as compared to FeGe[1] (see 1.14). The critical temperature is ~29 K, below which MnSi orders magnetically into a helical spin structure similar to the one found in FeGe. However, MnSi has only one magnetically ordered phase, in which the spiral propagates along equivalent ⟨111⟩ directions with a period of ~180 Å[7]. Several neutron diffraction studies have indicated that the magnetic ordering is a two stage process where a ring of critical scattering with periodicity ~180 Å appears as precursor scattering several degrees above the onset of true long range order[8,9,3]. Recent measurements of heat capacity[10] confirm the two stage transition to magnetic order. In agreement with the neutron diffraction data, the heat capacity mesurements show a very sharp peak at ~29 K followed by a much broader

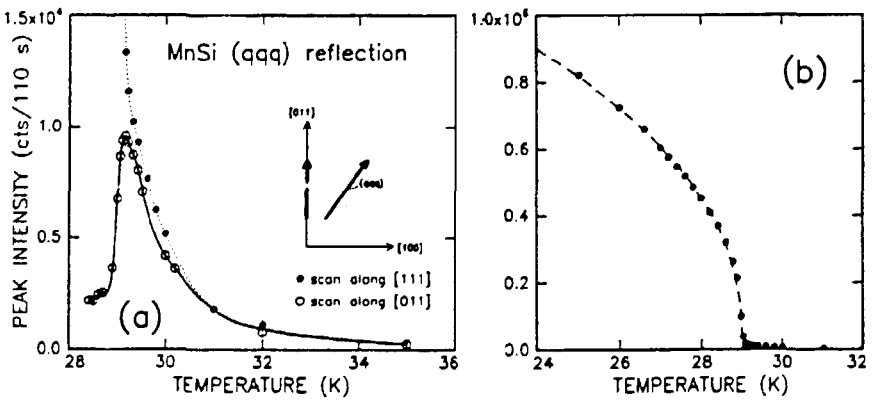


*Fig. 1. (a) Temperature dependence of the peak intensity of the magnetic scattering in MnSi near $T_N$. The data were collected by scanning through (q q q) and (0 q q) in the [111] and [011] directions as illustated by the reciprocal lattice plane sketched in the right hand side of the figure. The solid and dotted curves are guides to the eye. (b) The magnetic Bragg scattering in the (q q q) magnetic Bragg peak below the critical regime. The dashed curve is the result of a fit to a power law (see text) of the intensity versus temperature.*

hump which extends above 31 K. By means of cold neutron diffractometry, we have made a detailed study of the critical scattering in MnSi both well above and below $T_N$. Extended scans through a ring with radius $\sqrt{3}Q \sim \frac{2\pi}{180}$ Å$^{-1}$ around origo in several directions of reciprocal space (including the high symmetry directions) indicated that in the [100], [011] plane critical scattering collapsed to Bragg scattering in $(q\,q\,q)$ (where q is in relative lattice units) at $T_N$. The measurements were done at a triple-axis spectrometer in the elastic mode using neutrons of incident energy 5 meV selected by scattering from the (0 0 2) planes of a pyrolytic graphite monochromator and analyser. A cooled Be filter was inserted in front of the monochromator in order to remove the higher order contamination of the incident beam. The horizontal and vertical collimations were 60'/30'/30'/60' and 120'/120'/120'/120', respectively.

As an example Fig. 1*a* shows the peak height observed when scanning along two high symmetry directions close to $T_N$. The observed scattering were background corrected by subtracting the scattering observed for the same scans made at 45 K, and the residual scattering (in both directions) were fitted to Gaussian line shapes (below $T_N$) or a shape correspoding to a Lorentzian function folded with Gaussian (above $T_N$). In the [111] direction, the modulation vector shows an abrupt increase of $\sim 0.006$ Å$^{-1}$ at $T_N$. Below $T_N$, $\sqrt{3}Q$ increases slowly to reach a maximum value of 0.036 Å$^{-1}$ ~1 K below $T_N$ whereafter it decrease slowly. Not unexpectedly, the width decreases smoothly with temperature above $T_N$ with an abrupt decrease at $T_N$ to the resolution limited width below $T_N$. In the [011] direction the width (28 K < T < 35 K) is considerably wider than that given by the resolution, with a broad minimun around $T_N$. Figure 1*b* shows the magnetic Bragg scattering observed at $(q\ q\ q)$ in a wider temperature region. Below $T_N$, this data has been fitted to a power law of the form

$$I(T) = I_0(T_N - T)^{2\beta}, \quad \text{for } T < T_N \tag{1}$$

The resulting parameters are $T_N = (29.03 \pm 0.05)$ K and $\beta = (0.208 \pm 0.010)$. This value of $\beta$ is rather low, and reflects perhaps a first order transition although the implication of the two stage transition is not yet fully accounted for.


[1] B. Lebech, J. Bernhard, and T. Freltoft, (1989). J. Phys.: Condens. Matter **1**, 6105 *and references therein.*

[2] C.I. Gregory, D.B. Lambrick, and N.R. Bernhoeft, (1992). J. Magn. Magn. Mat. **104-107**, 689.

[3] C.I. Gregory, B. Lebech, N.R. Bernhoeft, P. Harris, K. Mortensen, and J. Skov Pedersen, (1993). *To be published*, (see also the Annual Progress Report, 1991).

[4] M.L. Plumer, (1990). J. Phys.: Condens. Matter **2**, 7503.

[5] B. Lebech, (1993). In: *Recent advances in Magnetism of Transition Metal Compounds* (1993) (World Scientific Publishing Co.). *To be published.*

[6] G.G. Lonszaricch, (1986). J. Magn. Magn. Mater. **54-57**, 612.

[7] Y. Ishikawa, K. Tajima, D. Bloch, and M. Roth, (1976). Solid State Commun. **19**, 525.

[8] Y. Ishikawa and M. Arai, (1984). J. Phys. Soc. Jpn. **53**, 2726.

[9] S. Hayden and S. Brown, (1991). *Private communication.*

[10] N.R. Bernhoeft, C. Marcenat, and R. Calemiznk, (1992). *Private communication.*

## 1.16 Crystalline and Magnetic Ordering in the Monoclinic Phase of the Layered Perovskite PAMC

P. Harris, B. Lebech, *Department of Solid State Physics, Riso National Laboratory, Denmark*, N. Achiwa, *Department of Physics, Kyusho University, Japan*, and F.K. Larsen, *Department of Chemistry, University of Århus, Denmark*

The layered perovskite $(CH_3CH_2CH_2NH_3)_2MnCl_6$ (PAMC) is an example of an antiferromagnet that shows weak ferromagnetism. The small ferromagnetic moment is believed to originate in anisotropic exchange interactions of the form $\mathbf{D} \cdot (\mathbf{S_1} \times \mathbf{S_2})$[1], an interaction which is possible because the low crystal symmetry allows the magnetic moments in the pure antiferromagnet to tilt without change of symmetry. In addition PAMC exhibits a large sequence of structural phases. It consists of ($MnCl_6$) octahedra sandwiched between propylammonium chains. The ammonium group hydrogens may bond to the $Cl^-$ ions in the octahedra in four different positions[2]. At high temperatures all four positions are equally possible (tetragonal symmetry), but upon cooling there is a gradual freezing of the bonds and the structure becomes orthorhombic and finally monoclinic. The structural phase sequence is as follows: $\alpha$ phase $I4/mmm$; 441 K; $\beta$ phase $Abma$; 388 K; $\gamma$ phase $N_{111}^{Abma}$; 339 K; $\delta$ phase $Abma$; 168 K; $\epsilon$ phase $P_{s11}^{Abma}$; 112 K; $\eta$ phase $P_{1s}^{P2_1/c}$; 39 K; magnetic ordered phase.

In order to understand the interactions between the crystal structure and the magnetic structure we have performed an elastic neutron scattering experiment and a 4-circle X-ray experiment on the low temperature monoclinic $\eta$ phase of PAMC. The neutron experiment was done on the double axis spectrometer TAS3, using neutrons of wavelength 1.29 Å. The X-ray experiment at 8 K was done at Department of Chemistry, University of Århus, Denmark, using $MoK_\alpha$ radiation.

The orthorhombic $\epsilon$ phase is modulated with an incommensurate modulation vector of $(\frac{1}{3} + \delta)\mathbf{c}^*_{ortho}$ which at the phase transition at 112 K locks-in *and* turns to a value of $\frac{1}{3}\mathbf{c}^*_{mono} \sim \frac{1}{3}(\mathbf{c}^*_{ortho} + \mathbf{a}^*_{ortho})$. The direct axes $\mathbf{c}_{ortho}$ and $\mathbf{c}_{mono}$ are parallel and therefore the direction of the modulational wave does not turn in direct space, the turning rather indicates a phase shift of the modulational wave across the layers (perpendicular to the **bc**-plane). Unlike the preliminary phases of PAMC the $\eta$ phase shows multiple twinning in the **bc**-plane and therefore the reflection split along the $\mathbf{a}^*$-axis. Because the twinning could not be resolved in the X-ray experiment we had to incorporate it in the model for data refinement[3] of the 4-circle data.

From the reflection conditions: $(h0lm)$, $l + m = 2n$; $(0k00)$, $k = 2n$, the superspace group $I_{1s}^{P2_1/c}$ was derived[4]. As only first order satellites were observed, we used simple harmonic functions to describe the deviation from the basic structure. In principle it should be possible to refine the data in the supercell of $\mathbf{a}_{mono}$, $\mathbf{b}_{mono}$ and $3\mathbf{c}_{mono}$, but as the satellite reflections are very weak it is not possible in practice. The average unit cell and crystal structure of the $\eta$ phase of PAMC is shown in Fig. 1. When the crystal transforms from the orthorhombic $\epsilon$ phase to the monoclinic $\eta$ phase the reflections split into two components parallel to the $\mathbf{a}^*$-axis.

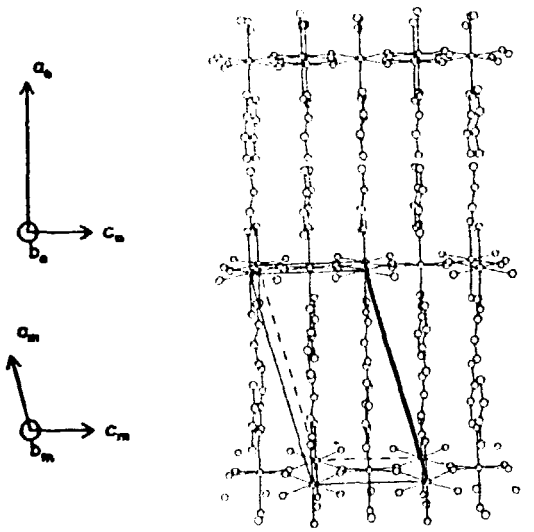

*Fig. 1. The average crystal structure of $\eta$ PAMC at 8 K.*

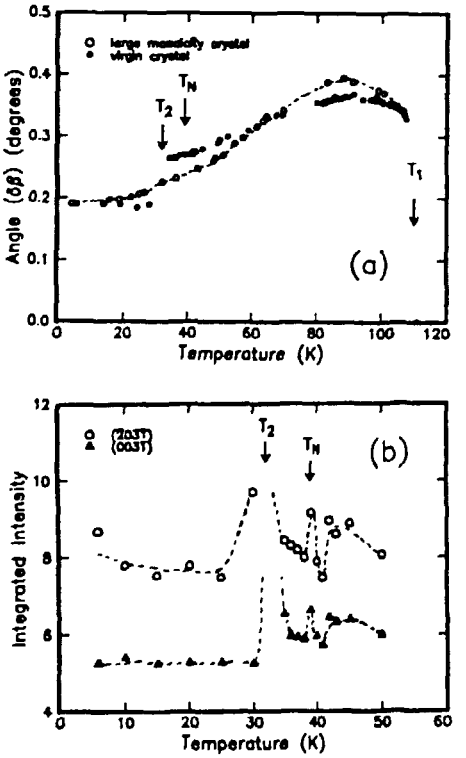


*Fig. 2. (a) The angular splitting of the orthorhombic (0040) reflection into the two (2040) and (2040)′ reflections of the monoclinic system. • virgin crystal, o non-virgin crystal with large mosaicity[5]. (b) Integrated intensities of two satellite reflections (virgin crystal, cooling). Dashed curves are guides to the eye.*

When the crystal transforms from the orthorhombic $\epsilon$ phase to the monoclinic $\eta$ phase the reflections split into two components parallel to the $\mathbf{a}^*$-axis. This allows determination of the angular deviation from orthorhombic symmetry which is related to the order parameter of the crystal structure in the $\eta$ phase. Figure 2*a* shows the temperature dependence of the deviation from orthorhombic symmetry for a virgin crystal determined by neutron scattering (•). After a small increase, the angle does not remain constant as expected, but instead decreases upon cooling. The rate of decrease flattens somewhat around 50 K, and at $T_2 = 32$ K the angle decreases abruptly to a constant value. After several thermal cycles through the orthorhombic-monoclinic transition at 112 K the mosaicity of the crystal increases. Measurements on such a crystal are also shown in Fig. 2*a* (o)[5], and it is evident that the abrupt decrease at 32 K smears out, and altogether, the whole curve seems smoother (dashed).

The satellite reflections may gain intensity from the magnetic ordering due to two different mechanisms. One possibility is a contribution from a positional modulation of the Mn atoms and another is a contribution from a rotational modulation of the tilted magnetic moments, originating from an interaction between the magnetic moments and the tetrahedra. Therefore, we investigated the integrated intensities of some nuclear satellites as a function of temperature. This was done by scanning in nets in reciprocal space around the satellites at each temperature. The somewhat surprising results are shown in Fig. 2*b* for the satellites $(2\,0\,3\,\bar{1})$ and $(0\,0\,3\,\bar{1})$. The two reflections show similar behaviors, and definitely no systematic increase in intensity below 39 K is seen. The intensity is constant below 30 K, but there is a sharp peak around 32 K ($T_2$), and a smaller peak at 39 K ($T_N$). On an absolute scale these increments are small, but statistically significant.

After accurately measuring the intensities of the satellite reflections, we may say that the magnetic order do not give any notable contribution to the satellite intensities. The positional modulation of the Mn atoms is too small to contribute significantly and the tilt of the magnetic moments must be confined to the **b**-direction. Also the monoclinic angle $\delta\beta$ has an unexpected temperature dependence, *i.e.* because no structural phase transition occurs below 112 K, the decrease between 80 K and 35 K as well as the abrupt change at 32 K is unexpected. Assuming that the intensities of the satellites are very sensitive to small changes in the crystal structure, there is a good agreement between the different types of information: At 39 K, the crystal undergoes a second order magnetic phase transition, and there is an associated small peak in the intensities of the satellites; at 32 K the monoclinic angle jumps to a constant value, and there is a corresponding peak in the satellite intensity. One could therefore expect the peak at 32 K to disappear as the mosaicity increases. This is in agreement with the fact that we have not observed a peak at 32 K in crystals with larger mosaicity.

The anisotropic exchange vector **D** is determined by the crystal symmetry that confines it to the **ac** plane. For the very small changes in this crystal system ($\delta\beta_{max} \approx 0.4°$) we may assume that the orientation of **D** with respect to the *unit cell* will be constant – in other words, there is a coupling between the anisotropic exchange and the monoclinic angle between the **a**- and **c**-axes. One also has to consider the strong in-plane antiferromagnetic interactions and the weak out-of-plane ferromagnetic interactions. The in-plane antiferromagnetic interactions are perpendicular to the **ac**-plane, and therefore not influenced by changes in the monoclinic angle. In contrast the out-of-plane ferromagnetic interactions must be influenced by changes in the monoclinic angle, because the relative positions of two interacting atoms change.

The temperature dependence of the monoclinic angle, indicates that the coupling between the magnetic structure and the monoclinic distortion is significant. The fact that the monoclinic distortion appears simultaneous with the lock-in and rotation of the modulation vector indicates a strong coupling between the monoclinic distortion (the monoclinic angle) and the modulation. The actual temperature dependence of the angle may then be a weighted average of the preferred angle for the structural interactions, and the preferred angle for the magnetic interactions. In other words, the change in the monoclinic angle will be a weigted average of the constant monoclinic angle expected below the structural phase transition and the decreasing monoclinic angle imposed by the magnetic order, in qualitative agreement with the experimental data shown in Fig. 2*a*.


[1] N. Achiwa, T. Matsuyama, and T. Yoshinari, (1990). Phase Transitions **28**, 79.
[2] P. Muralt, R. Kind, and W. Bührer, (1988). Phys. Rev. **B38**, 666.
[3] V. Petříček, P. Coppens, and P. Becker, (1985). Acta Cryst. **A41**, 478.
[4] P.M. de Wolff, T. Janssen, and A. Janner, (1981). Acta Cryst. **A37**, 625.
[5] N. Achiwa, S. Kawano, and B. Lebech, (1990). *Physics Department. Annual Progress Report*, (Riso National Laboratory, Denmark)

## 1.17 Magnetic Fluctuations in Superconducting $La_{1.86}Sr_{0.14}CuO_4$

T.E. Mason, *Department of Solid State Physics, Riso National Laboratory, Denmark*, G. Aeppli, A.P. Ramirez, *AT&T Bell Laboratories, U.S.A.*, S.M. Hayden, *H.H. Wills Physics Laboratory, Bristol University, U.K.*, and H.A. Mook, *Solid State Division, Oak Ridge National Laboratory, USA*

Recently we have shown that the low frequency inelastic magnetic response of metallic $La_{2-x}Sr_xCuO_4$, associated with the proximity to Fermi surface nesting, is largest at $(\pi,\pi) \pm \delta(\pi,0)$ and $(\pi,\pi) \pm \delta(0,\pi)$ where $\delta \approx 2x$[1,2]. Because inelastic neutron scattering probes transitions across the Fermi surface it should be suppressed in the superconducting state for energies less than $2\Delta$. This has been observed[2], however, a residual response at low temperatures and frequencies was found. (See Fig. 1.)

It has been suggested that the presence of low frequency excitations in the superconducting state may be due to *d*-wave superconductivity[3,4], a state also invoked to explain other anomalous behaviour of the high $T_c$ materials. If this is the case then there are specific implications for the $q$-dependence of the magnetic response in the superconducting state. In particular the peaks should be rotated by 45° so that they lie along the $(\pi,\pi)$ and $(\pi,-\pi)$ directions.[4]

In order to be more sensitive to the very low intensities found below $T_c$ we have improved the efficiency of TAS6 by a factor of 2 and increased the sample volume by the same amount (compared with our previous measurements). We find that $\chi''$ is reduced to about 60 % of the value at 35 K below $T_c$ (=33 K) for $\hbar\omega < 6$ meV. There is no change in the position of the incommensurate response, the peak shape, or its width. This rules out any simple *d*-wave gap function which would introduce a new $q$-dependence in $\chi''$. It is, however, consistent with a conventional gapless superconductor where the states below the gap are introduced by the presence of pair-breaking magnetic impurities. This scenario is supported by specific heat measurements which show a residual linear contribution to the specific heat of about 20% of the normal state value and a magnetic impurity concentration of 0.4% .

[1] S.W. Cheong, G. Aeppli, T.E. Mason, H.A. Mook, S.M. Hayden, P.C. Canfield, Z. Fisk, K.N. Clausen, and J.L. Martinez, (1991). Phys. Rev. Lett. **67**, 1791.
[2] T.E. Mason, G. Aeppli, and H.A. Mook, (1992). Phys. Rev. Lett. **68**, 1414.
[3] T.R. Thurston, P.M. Gehring, G. Shirane, R.J. Birgeneau, M.A. Kastner, Y. Endoh, M. Matsuda, K. Yamada, H. Kojima, and I. Tanaka, (1992). Phys. Rev. B**46**, 9128
[4] Y. Zha, K. Levin, and Q. Si, (1993). Phys. Rev. B. *In press.*

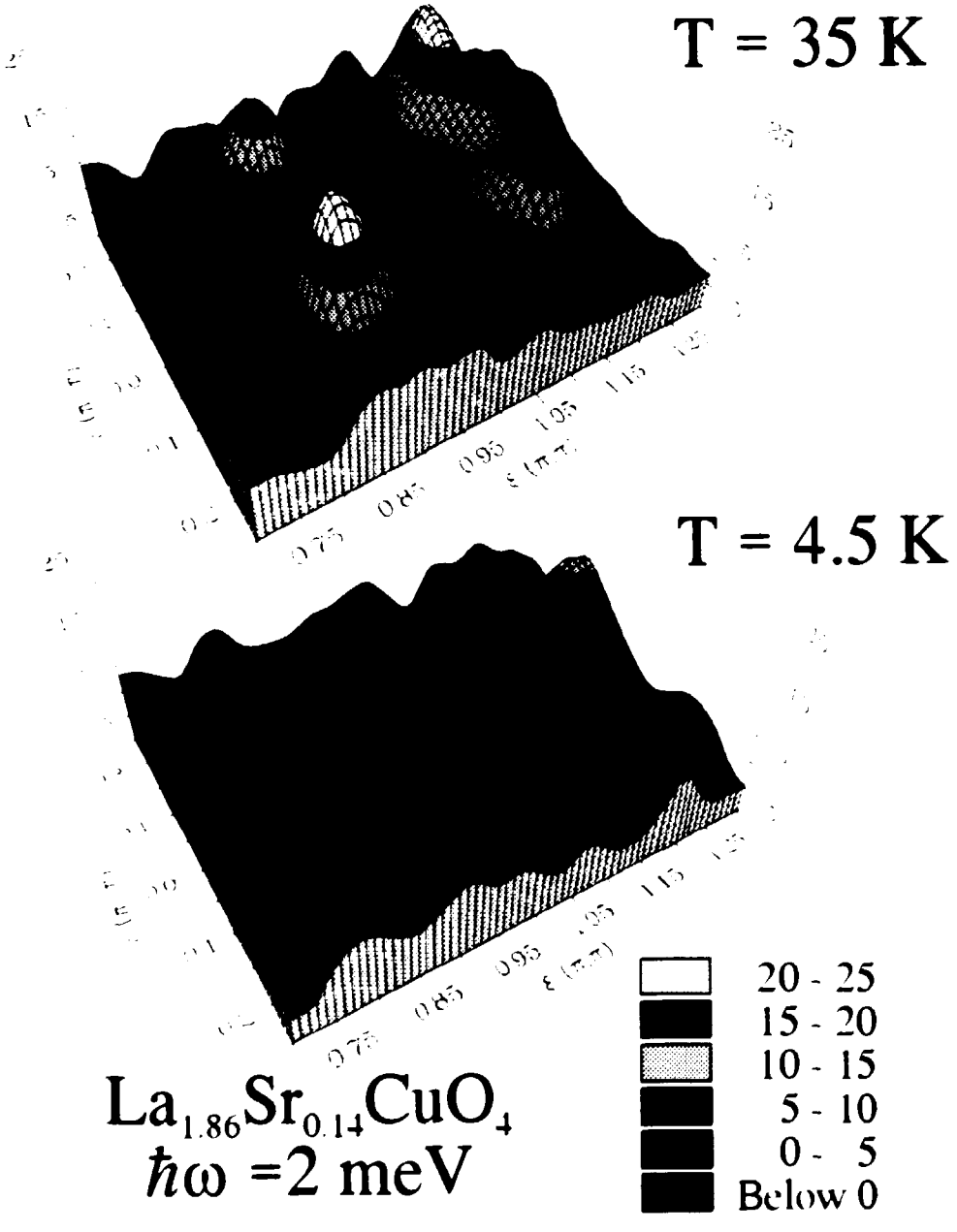


*Fig. 1: Contour map of the intensity at scattering in the 2D zone, $(\xi, 0, \xi)$, near the commensurate position for $\hbar\omega = 2$ meV at $T = 35$ K$(> T_c)$ and $T = 4.5$ K$(< T_c)$*

## 1.18 Measurement of Spin Waves in Copper (II) Deuteroformate Tetradeuterate: An S=$\frac{1}{2}$ Square Heisenberg Antiferromagnet

S.J. Clarke, A. Harrison, *Inorganic Chemistry Laboratory, University of Oxford, UK*, and T.E. Mason, *Department of Solid State Physics, Risø National Laboratory, Denmark*

The layered cuprates such as $La_2CuO_4$, which provide parent compounds of high $T_c$ superconducting ceramics, are rare examples of $S=\frac{1}{2}$ square Heisenberg antiferromagnets. Unfortunately, they are not good model magnets because they are difficult to prepare as high-quality single crystals and the magnitude of the intraplane exchange constant of around 100 meV makes them difficult to characterize using techniques such as inelastic neutron scattering.

We have recently shown[1-3] that copper formate tetrahydrate, $Cu(HCO_2)_2{\cdot}4H_2O$, (CFTH) is a good example of this class of magnet and can be prepared as large, high-quality single crystals. The ratio of the inter- and intralayer coupling is less than $10^{-4}$. Antiferromagnetic ordering driven by the interlayer coupling in CFTH occurs at $T_N$=16.5 K. We have already studied the spin waves at low energies close to the zone centre in the fully deuterated form of the compound CFTD using TAS1[2]. On TAS6 we mapped out the whole dispersion surface from the zone centre to the zone boundary[4]. We used five oriented single crystals with a total volume of 2.5 $cm^3$ cooled to 4.3 K in a Cryogenic Associates Inc. CT14 $^4$He flow cryostat. We used mainly constant-energy scans with energy transfers ranging from 3.0 to 14 meV to map out the dispersion. These were carried out in both the 010 and 210 zones. We fitted the spin-wave cross-section to a classical expression and convolved this with the experimental resolution function using a Monte-Carlo integration technique. The data and fit for a scan with energy transfer of 3.0 meV along the **b*** direction are shown in Fig. 1.

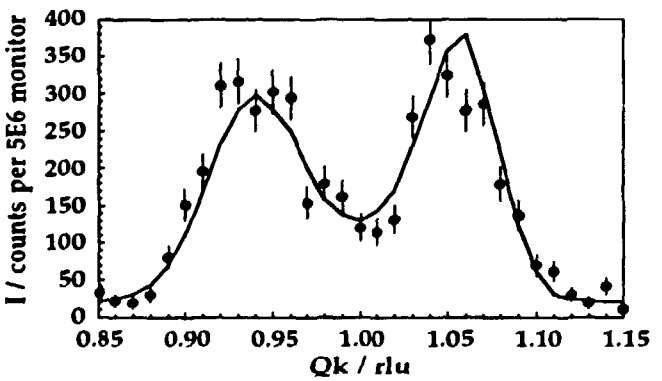


*Fig. 1. Spin-wave peaks obtained using a scan along* **b*** *from the centre of the 010 zone with energy transfer of 3.0 meV. The solid line is a fit to eq. 1.*

We fitted the spin waves to the classical expression:

$$E(\mathbf{q}) = [(c+\Delta)^2 - (c\gamma_{\mathbf{q}} - \Delta)^2]^{1/2} \qquad (1)$$

where $\gamma_{\mathbf{q}} = \cos(\mathbf{q}\cdot\mathbf{a}/2)\cos(\mathbf{q}\cdot\mathbf{b}/2)$, $c$ is the spin wave velocity and $\Delta$ is a parameter

which produces a gap at the zone centre.

This is equivalent to:

$$E(\mathbf{q}) = 4S[(D + J(1 - \gamma_{\mathbf{q}}))J(1 + \gamma_{\mathbf{q}})]^{1/2} \quad (2)$$

where $S = \frac{1}{2}$ is the value of the spin, $J$ is the intraplane exchange constant and $D$ is equivalent to $\Delta$. The solid line in the dispersion curve in Fig. 2 is a fit to eq. 2 with a $J$ of 7.4 meV and a $D$ of 0.0042 meV. This combination of $J$ and $D$ produces a gap at the zone centre of 0.5 meV.

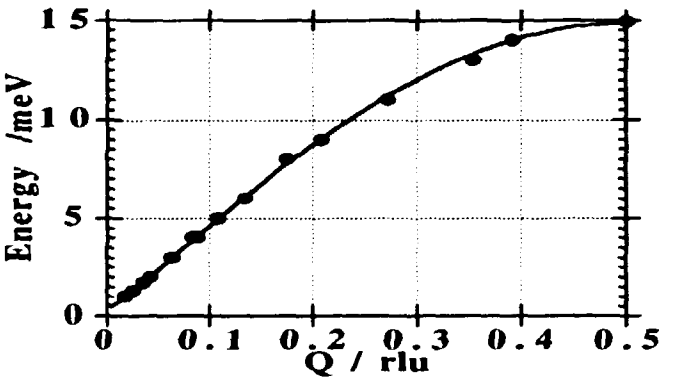


*Fig. 2. Spin-wave dispersion curve for CFTD.*


[1] S.J. Clarke, A. Harrison, T.E. Mason, G.J. McIntyre, and D. Visser, (1992). J. Phys. Condens. Mat. **4**, L71.

[2] A. Harrison, S.J. Clarke, T.E. Mason, and D. Visser, (1992). J. Magn. Magn. Mat. **104–107**, 557.

[3] S.J. Clarke and A. Harrison, (1992). J. Phys. Condens. Mat. **4**, 6217.

[4] S.J. Clarke, A. Harrison, and T.E. Mason, (1992). *Presented at the 37th Annual Conference on Magnetism and Magnetic Materials.*

## 1.19 Magnetic Fluctuations in the Superconducting Heavy Fermion System $UPd_2Al_3$

T.E. Mason, T. Petersen *Department of Solid State Physics, Riso National Laboratory, Denmark*, G. Aeppli, A.P. Ramirez *AT&T Bell Laboratories, Murray Hill, USA*, E. Bücher, and J. Hufnagl *Universität Konstanz, Germany*

The heavy fermion compound $UPd_2Al_3$ exhibits simultaneous antiferromagnetic and superconducting order. To determine if the superconductivity is induced by spin fluctuations, or if there exists some other coupling between the superconductivity and antiferromagnetism in this material, we have measured the spin dynamics at temperatures above and below the superconducting transition temperature $T_c \sim 2\,K$ in two single crystals using the TAS6 spectometer.

We have measured the temperature dependence of the antiferromagnetically ordered moment and obtained results for the energy and damping of the spin-waves with momentum transfers along the $(00\ell)$, $(hh\ell)$ and $(h0\ell)$ directions in the first Brillouin zone. Our results do not show any significant changes at $T_c$; neither in the antiferromagnetically ordered moment (Fig. 1) as is the case in the similar compound $UPt_3$[1], nor in the energy or damping of the spin excitations near the antiferromagnetic wavevector $(00\frac{1}{2})$ as one would expect if the superconductivity was induced by spin waves.

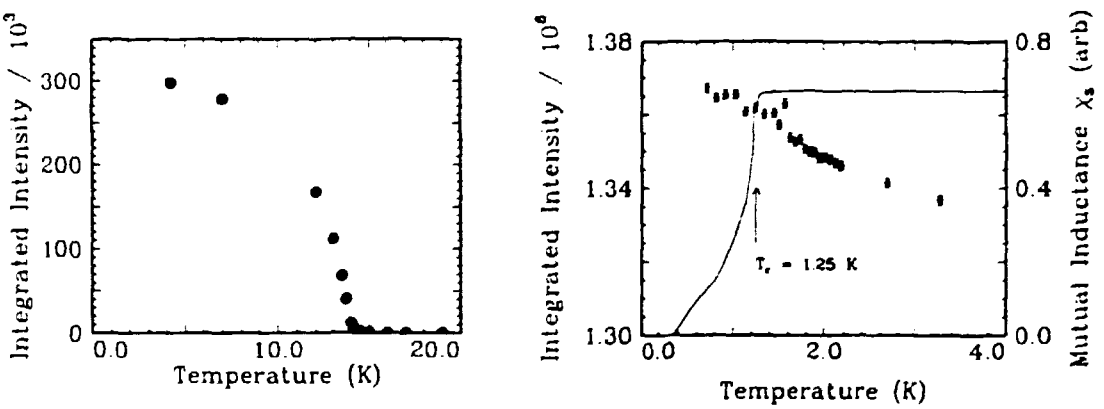


*Fig. 1. Integrated intensity of magnetic Bragg peak. Detail at right shows Bragg intensity and AC susceptibility (solid line) at low temperatures. The superconduting transition is visible as the sudden increase in diamagnetic susceptibility.*

Figure 2 shows the dispersion relationship for the spin waves in $UPd_2Al_3$. The data were obtained with constant-$q$ scans and analyzed with a resolution convolution program. We find that our measurements may be described by a model of the spin waves as having no or only a small gap (of magnitude smaller than 0.3meV) at $(00\frac{1}{2})$. Moreover we find that a realistic model of the spin dynamics must include interactions between next-nearest neighbours.

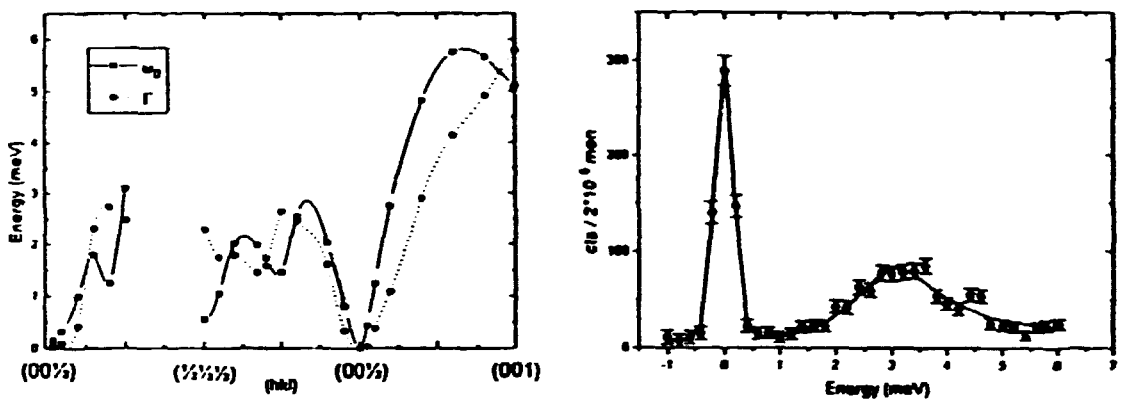


*Fig. 2. Spin wave dispersion relation for $UPd_2Al_3$. The circles are energies and the triangles are dampings. The lines are only guides to the eye. At the right is shown a constant-q scan. The left peak is diffuse scattering and the right one is the spin wave.*

[1] G. Aeppli, D. Bishop, C. Broholm, E. Bücher, K. Siemensmeyer, M. Steiner, and N. Stüsser, (1989). Phys. Rev. Lett. **63**, 676.

## 1.20 Magnetic Microstructure of Nearly Ferromagnetic, Frustrated Pyrochlore Oxides $Y_2Mn_2O_7$ and $Lu_2Mn_2O_7$

J.E. Greedan, *Institute for Materials Research, McMaster University, Hamilton, Canada,* J. Skov Pedersen, *Department of Solid State Physics, Riso National Laboratory, Denmark,* and M.A. Subramanian, *CR and D, E.I. DuPont, Wilmington, Delaware, USA*

The pyrochlore structure oxides $Ln_2Mn_2O_7$ (Ln=lanthanide or Y) show complex magnetic properties. Susceptibility and magnetization measurements suggest ferromagnetic order at temperatures between 40 K and 17 K (depending on Ln) but also spin glass-like behaviour at lower temperatures[1,2]. As these compounds show negligible crystallographic disorder, the spin glass behaviour may be due to the high degree of topological frustration inherent in the Ln and Mn sublattices which each consist of three dimensional arrays of corner-shared tetrahedra[2].

SANS measurements were carried out over extensive $Q$ and temperature ranges in order to better characterize the apparently complex magnetic microstructure in two of these compounds, $Y_2Mn_2O_7$ and $Lu_2Mn_2O_7$. The magnetic component, obtained by subtracting a 50 K data set from those obtained at low temperatures, was found to be significant below about 20 K for both compounds. The magnetic scattering could be fit to a model cross-section consisting of a Lorentzian plus a Lorentzian-squared term.

$$\frac{d\sigma(Q)}{d\Omega} = \frac{A_1}{1/\xi_1^2 + Q^2} + \frac{A_2}{(1/\xi_2^2 + Q^2)^2}$$

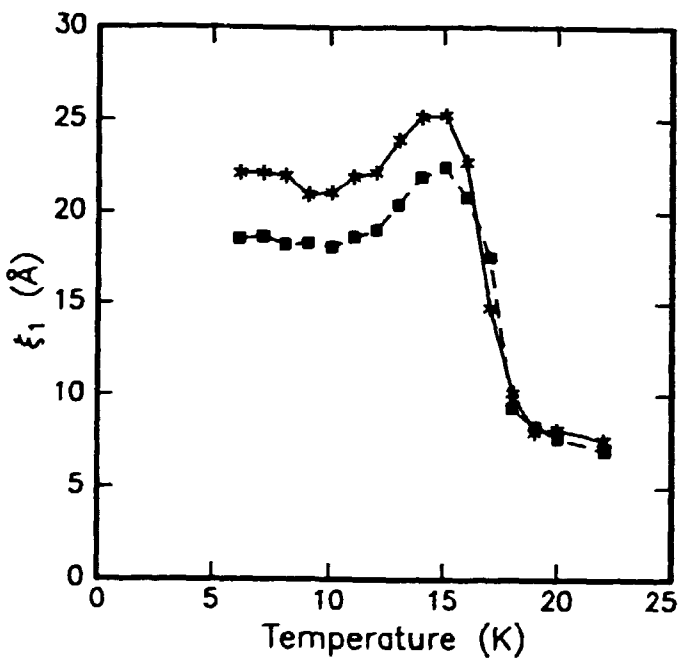


*Fig. 1. The correlation length $\xi_1$ of the Lorenzian term as a function of temperature: (*) $Y_2Mn_2O_7$ and (■) $Lu_2Mn_2O_7$*

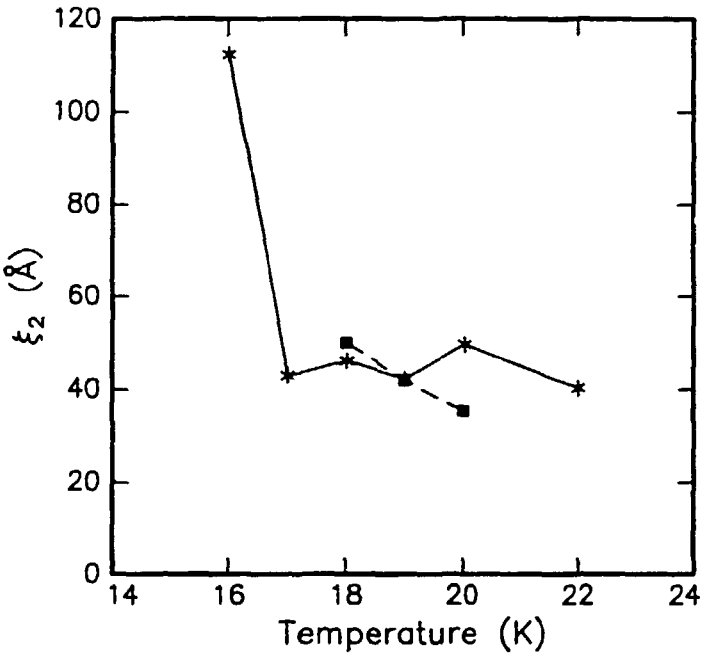


*Fig. 2. The correlation length $\xi_2$ of the Lorenzian squared term as a function of temperature: (*) $Y_2Mn_2O_7$ and (■) $Lu_2Mn_2O_7$. Below the lowest temperature indicated, 16 K (Y) and 18 K (Lu) $\xi_2$ becomes resolution limited.*

Such a cross section has been found previously for magnetic metallic glasses[2,3]. The fits to the data using this cross section are excellent over the entire $Q$-range investigated. The Lorenzian correlation length, $\xi_1$, which measures the ferromagnetic cluster size shows growth from ~6 Å at 20 K to ~25 Å at 17 K which corresponds to the susceptibility anomaly in $Y_2Mn_2O_7$. Similar results have been reported from data obtained over a much more truncated $Q$-range[5]. In the present previous work the Lorentzian-squared term was not seen and the $\xi_1$ values were somewhat overestimated. In the present study $\xi_1$ remains constant from 17 K to 6 K. Very similar results were found for $\xi_1$ in $Lu_2Mn_2O_7$.

The Lorentzian-squared length, $\xi_2$, is thought to arise from random-field effects[3]. For both Ln=Y and Lu, $\xi_2 > \xi_1$ and $\xi_2$ has a different temperature dependence remaining constant above 17 K with a finite value of about 30-40 Å but rising sharply at 17 K and attaining resolution limited values below that temperature as seen in Fig. 2.

[1] M.A. Subramanian, C.C. Torardi, D.C. Johnson, J. Pannetier, and A.W. Sleight, (1988). J. Solid State Chem **72**, 24.
[2] J.N. Reimers, J.E. Greedan, R.K. Kremer, E. Gmelin, and M.A. Subramanian, (1991). Phys. Rev. **B43**, 3387.
[3] G. Aeppli, S.M. Shapiro, R.J. Birgeneau, and H.S. Chen, (1983). Phys. Rev. **B28**, 5160.
[4] M.L. Spano, J.J. Rhyne, S.J. Pickart, S.K. Hasanain, R.J. Gambino, and T.R. McGuire, (1987). J. Appl. Phys. **61**, 3639.
[5] J.E. Greedan, J. Avelar, and M.A. Subramanian, (1982). Solid State Comm. **82**, 797.

## 1.21 Small-Angle Neutron Scattering from the Flux Lattice in the High-$T_c$ Superconductor YBCO

E.M. Forgan, S.L. Lee, *School of Physics and Space Research, University of Birmingham, UK*, D. McK. Paul, *Department of Physics, University of Warwick, Coventry, UK*, H.A. Mook, M. Yethiraj, *Oak Ridge National Laboratory, Tennessee, USA*, D.J. Bishop, P.L. Gammel, R. Kleiman, *AT&T Bell Laboratories, Murray Hill, New Jersey, USA*, and K. Mortensen, *Department of Solid State Physics, Risø National Laboratory, Denmark*

Neutron scattering is the only technique which give *direct* information about the spatial distribution of magnetic flux lines within the bulk of a superconductor. However, the diffraction angles are small because the flux line spacing ($\propto B^{-\frac{1}{2}}$, $B$ being the magnetic field) is much larger than neutron wavelengths at accessible fields. On the Risø SANS facility we have used a scattering geometry with the incident neutron beam approximately parallel to the magnetic field. This means that the pattern of scattered neutrons on the planar multi-detector is an image of the (two-dimensional) reciprocal lattice of the flux lines. When the sample was rotated, the intensity of the diffracted spots varied, as shown in Fig. 1. The width of this rocking curve is a measure of the perfection of the flux line structure. The measurements indicate that the flux lines are parallel to the crystal $c$-axis within 2°, and extend over a distance of at least 1.5 $\mu$m along the field direction. The *shape* of each diffracted spot can also give information: the radial width may be related to the spread of diffracting plane *spacings*; the tangential width is connected to the spread of plane *orientations*. After deconvolution of the wavelength spread and collimation of the incoming beam, (see *e.g.* ref. 1), we find that the spread of plane spacings is quite large, with a fractional width ~0.2 FWHM. This disorder is doubtless related to the fact that second order diffraction spots from these planes are very much weaker than expected from the London model applied to a perfect lattice. However, the tangential width is resolution limited; we ascribe this to the pinning of flux-line planes to twin planes. This pinning is also the cause of the square symmetry of the patterns seen in Fig. 1. We followed the flux lattice signal down to a field of 0.06 T, increasing the neutron wavelength to give large enough Bragg diffraction angles. We saw no sign of an expected square-to-hexagonal transition at low fields; instead, the signal became much weaker, presumably because at small flux line densities the intervortex interactions become weak relative to the effects of random pinning.

The total intensity of the spots, integrated over the rocking curve, has been followed as a function of temperature at an applied field of 2 T. As can be seen in Fig. 2, the intensity goes to zero well below $T_c(B)$, which is 91.5 K. It seems likely that zero intensity occurs instead at the *irreversibility line*, which has been measured at Oak Ridge by macroscopic measurements. This is the first real hint, by our technique, of flux lattice melting.

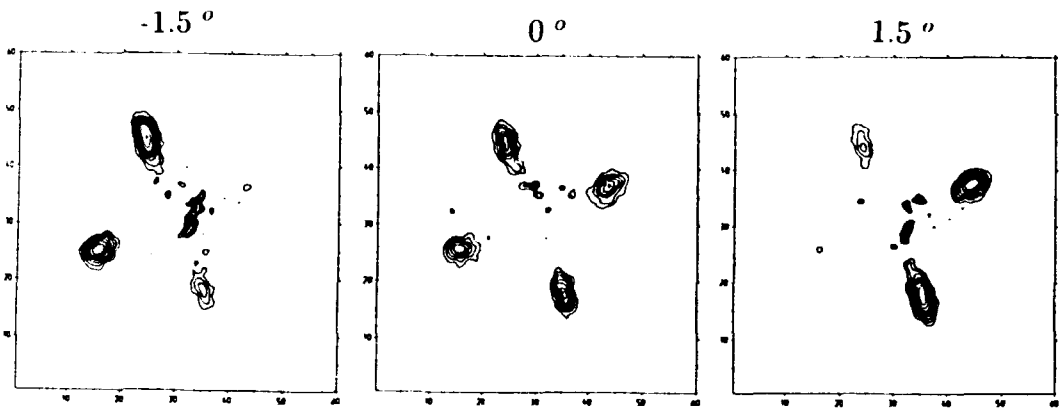


*Fig. 1. Diffracted intensity due to flux lines in YBCO cooled in a field of 2 T to base temperature. Background scattering due to the cryostat and sample has been subtracted. Between each picture, the sample and cryostat have been rotated by 1.5° about a vertical axis.*

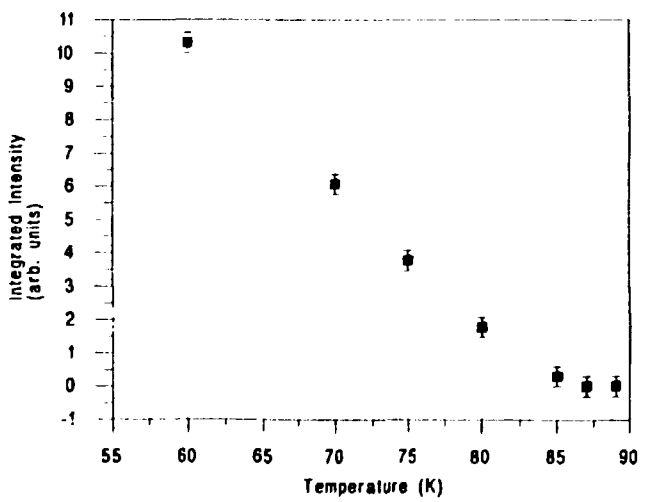


*Fig. 2. Integrated intensity of flux line scattering versus temperature near $T_c$. The field strength is 2 T, applied at an angle of 3° to the crystal c-axis.*

[1] R. Cubitt *et al.*, (1992). Physica B **180-181**, 377.

## 1.22 Structure and Superconductivity in Co-doped $YBa_2Cu_3O_{6+x}$

N.H. Andersen, H.F. Poulsen, *Department of Solid State Physics, Riso National Laboratory, Denmark*, J.V. Andersen, O.G. Mouritsen, *Department of Physical Chemistry, The Technical University of Denmark, Lyngby, Denmark*, L. Börjesson, M. Kakihana, *Physics Department, Chalmers Institute of Technology, Gothenburg, Sweden*, R. Hadfield, and R. McGreevy, *Clarendon Laboratory, Oxford, England*

Oxygen depletion and chemical substitutions in the basal $CuO_x$-plane of the high temperature superconductor $YBa_2Cu_3O_{6+x}$ ($0 < x < 1$) (YBCO) have a detrimental influence on the superconducting properties. For oxygen deficient YBCO, dynamic[1] and static[2] variations of $T_c$ have been correlated with similar variations in the coherence of the oxygen ordering. However, the role of doping with Co, Fe, or Al in the suppression of $T_c$ is not yet well understood. Since Co, Fe, and Al have a preference for higher oxidation levels than Cu, they tend to increase their oxygen coordination number and cause oxygen disordering.

The effect of Co doping on the oxygen disordering and superconducting transition temperature in $YBa_2Cu_{3-y}Co_yO_{6+x}$ has been studied experimentally and by Monte Carlo simulations. Samples with Co doping levels, $0 \leq y \leq 0.5$, have been prepared and characterized by standard DC resistivity and AC susceptibility measurements. The resulting superconducting transition temperatures are shown in Fig. 1. The structural ordering phenomena have been studied by neutron powder diffraction and EXAFS measurements.

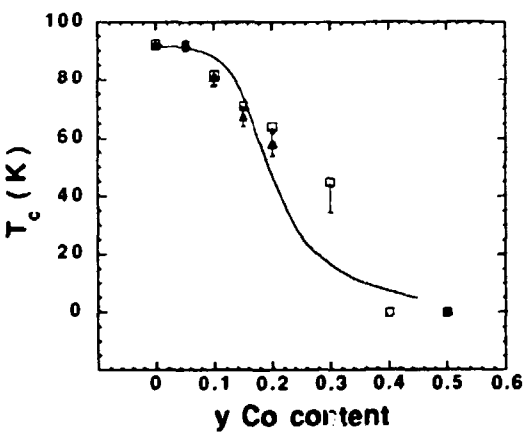


*Fig. 1. The superconducting transition temperature $T_c(y)$ of $YBa_2Cu_{3-y}Co_yO_{6+x}$. □ are ac susceptibility data and ▲ are resistivity data. The full line is the prediction of the minimal model calculation described in the text.*

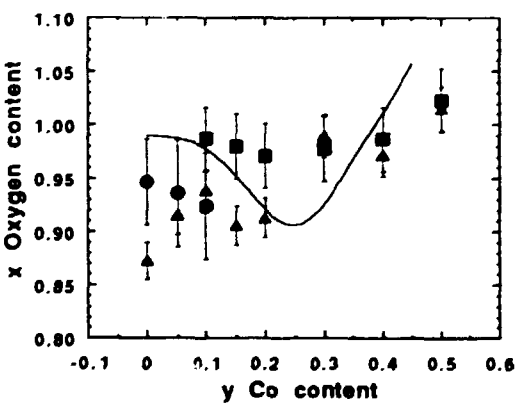


*Fig. 2. The oxygen content (x) of $YBa_2Cu_{3-y}Co_yO_{6+x}$ determined from neutron powder diffraction data in the tetragonal (□) and orthorhombic (●) phases. ▲ is the oxygen content derived from iodometric titration analysis. The full line is the result of model calculations described in the text.*

Full profile structural refinements of the neutron powder diffraction data show that $YBa_2Cu_{3-y}Co_yO_{6+x}$ is orthorhomic for $y < 0.1$ and tetragonal for $y \geq 0.1$. Using a model with isotropic Debye Waller factors and without split sites, we find full occupation

on almost all sites. Minor deficiencies are found on the apical oxygen site (the oxygen bridging the basal $CuO_x$ and the superconducting $CuO_2$ planes) and on the Cu/Co site. More pronounced variations are found on the oxygen sites in the basal $Cu_{1-y}Co_yO_x$ plane as shown in Fig. 2. Preliminary analysis of the EXAFS data show that Co has an almost concentration independent oxygen coordination number of five.

The oxygen ordering phenomena in the basal $Cu_{1-y}Co_yO_x$ plane of the structure have been studied by model calculations based on a modified version of the so-called ASYNNNI model using Monte Carlo techniques. The three interaction parameters in the model, $V_1$ (repulsive), $V_2$ (attractive), and $V_3$ (repulsive), shown in Fig. 3, and the chemical potential corresponding to one atmosphere of oxygen have been fixed at the values determined from comparison with experimental data on undoped YBCO. The increased probability of excess oxygen around the Co atoms has been incorporated into the model in a simple way by making the nearest-neighbor interaction parameter, $V_1^{Co}$, around randomly distributed Co atoms less repulsive. Comparison with the diffraction (Fig. 2) and the EXAFS data shows that $V_1^{Co} = 0.0$ is a likely value for the interaction parameter around the Co atoms, and that the modified ASYNNNI model is an appropriate starting model for oxygen ordering in Co-doped YBCO.

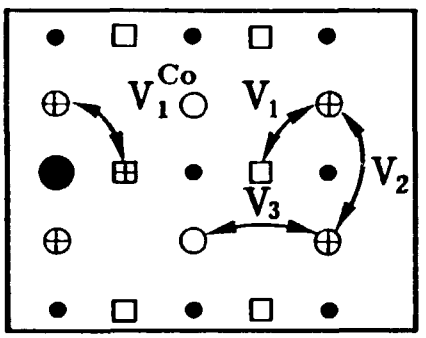


*Fig. 3. The oxygen interactions $V_1$, $V_1^{Co}$, $V_2$, and $V_3$ in the modified ASYNNNI model for Co doped YBCO. • are Cu atoms, and ● a Co atom. ⊕ are occupied oxygen sites in both ortho-I and ortho-II, but ○ are only occupied in ortho-I. □ oxygen sites are not occupied in the ground state, but Co doping increases the occupation of the ⊞ oxygen sites.*

The experimental data of the superconducting transition temperature, $T_c(y)$, have been analyzed within the context of a previously established so-called *minimal model* for undoped YBCO[2]. In this model the superconducting transition temperature, $T_c(x)$, is related to a weighted average of ordered oxygen domains of the thermodynamically stable ortho-I and ortho-II phases (see Fig. 3). The statistics of the oxygen ordering is established from ASYNNNI model calculations. We have adopted the minimal model without modifications and adjustable parameters for Co doped YBCO and calculated the $T_c(y)$ variation based on the ordering properties derived from the modified ASYNNNI model. As shown in Fig. 1, the results are in surprisingly good agreement with the experimental data, especially, when it is considered that only one adjustable parameter $V_1^{Co}$ (which, in principle, may be obtained from the structural data) has been introduced. The results indicate that the oxygen disordering in YBCO resulting from oxygen deficiency and Co doping, influence the superconducting transition temperature in a unified way.

[1]H.F. Poulsen, N.H. Andersen, J.V. Andersen, H. Bohr, and O.G. Mouritsen, (1991). Phys. Rev. Lett. **66**, 465.
[2]H.F. Poulsen, N.H. Andersen, J.V. Andersen, H. Bohr, and O.G. Mouritsen, (1991). Nature **349**, 594.

## 1.23 Effects of Deposition Temperature on Microstructure and Critical Current Density of Epitaxial $YBa_2Cu_3O_{6+x}$ Thin Films Grown on $SrTiO_3(001)$

R. de Reus*, N.H. Andersen, *Department of Solid State Physics, Riso National Laboratory*, P. Kringhøj, *Institute for Physics and Astronomy, University of Århus, Denmark*, P. Vase, and K. Linkenkær-Hansen, *NKT Research Center, Brøndby, Denmark*

Thin $YBa_2Cu_3O_{6+x}$ films were deposited by laser ablation on MgO(001) and $SrTiO_3(001)$ substrates at elevated temperatures. Using laser ablation the target stoichiometry is easily retained. Stoichiometric $YBa_2Cu_3O_{6+x}$ films of high quality were prepared. Critical temperatures above 90 K were achieved with transition widths less than 1.5 K. However, strong variations in the critical current densities were measured, ranging from $3.7 \times 10^5$ A/cm$^2$ ("bad sample") to $1.0 \times 10^7$ A/cm$^2$ ("good sample"). Conventional X-ray powder diffraction analysis showed that all films were *c*-axis oriented and single phase. We were able to show that the reduction in critical current density from $1.5 \times 10^6$ A/cm$^2$ to $3.5 \times 10^5$ A/cm$^2$ of films deposited on MgO(001) is due to the occurrence of 5 % of the material with a misorientation of 45° in the *ab*- plane (parall el to the substrate surface). For films deposited on $SrTiO_3(001)$ it was found that an increase of *a*-axis oriented material from 0.6 % to 8.3 % reduced the critical current density from $1.0 \times 10^7$ A/cm$^2$ to $2.9 \times 10^6$ A/cm$^2$. The higher critical current densities of films deposited on $SrTiO_3$ as compared to films deposited on MgO, are attributed to the better lattice match of $YBa_2Cu_3O_{6+x}$ with $SrTiO_3$ resulting in a smaller mosaic spread and la ger domain size[1].

Interesting results were obtained from experiments where the deposition temperature was changed under otherwise ideal conditions. Similar to the previous experiment all $YBa_2Cu_3O_{6+x}$ films deposited on $SrTiO_3(001)$ were *c*-axis oriented and exhibited comparable critical temperatures. For all deposition temperatures, which ranged from 690 to 900°C, no 45°-rotated domains or *a*-axis oriented material could be detected by X-ray diffraction (XRD). However, as shown in Fig. 1, the critical current density showed a maximum for deposition temperatures between 780 and 810°C. Channeling experiments using Rutherford backscattering spectrometry (RBS) showed that these films were of high crystalline quality as indicated by the low backscattering yield. For films deposited at lower temperatures, significantly higher backscattering yields, due to the presence of local defects in the films, were observed. Also, the XRD studies reveal a deterioration of crystalline quality for the films deposited below 780°C, which may explain the decrease in critical current density. In these films a decrease in domain size as well as an increased in plane mosaicity were observed. This is exemplified in Fig. 2 where the rocking curve through the (112) Bragg reflection is shown for two films. Due to twinning, this Bragg reflection should split into three distinct peaks as observed for the high quality film deposited at 810°C. For the film deposited at 690°C, these three peaks merge. For samples deposited above 810°C significant amounts of impurity phase were observed.

*Present and permanent address: Mikroelektronik Centret, The Technical University of Denmark, Lyngby, Denmark.

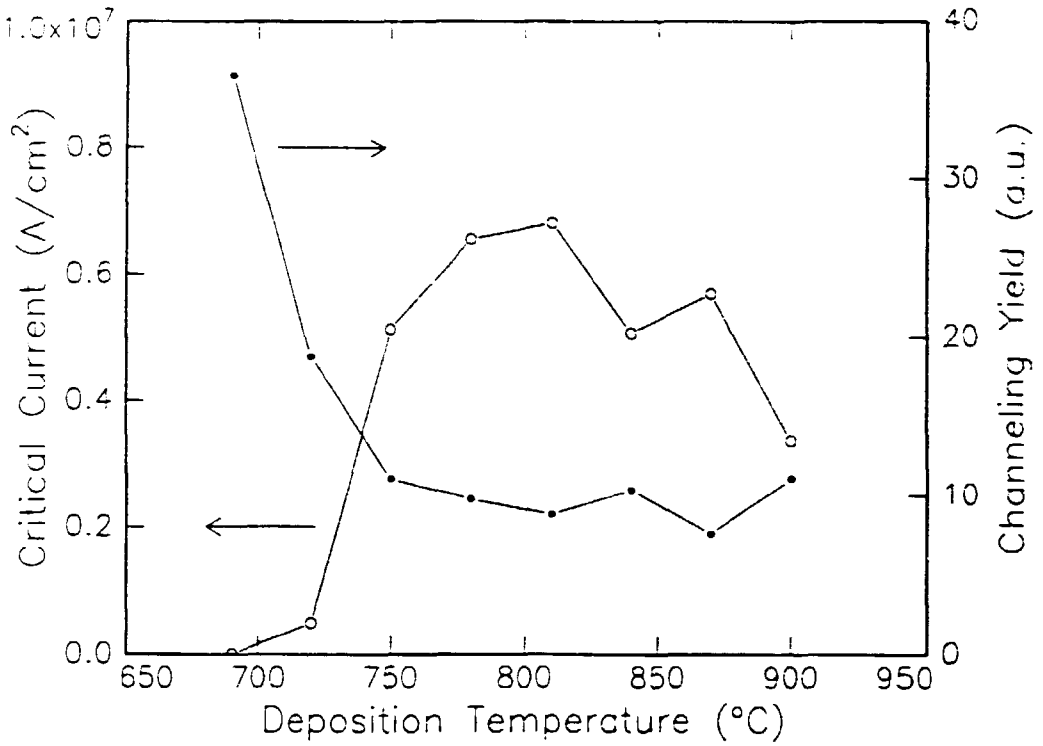


*Fig. 1. Rutherford backscattering (RBS) channeling yield, and critical current densities of $YBa_2Cu_3O_{6+x}$ on $SrTiO_3(001)$ at 77 K measured as a function of deposition temperature. The optimum deposition temperature is between 780°C and 810°C. In this temperature interval the maximum critical current density and, according to RBS and XRD (cf. Fig. 2), a high crysstalline quality, are obtained.*

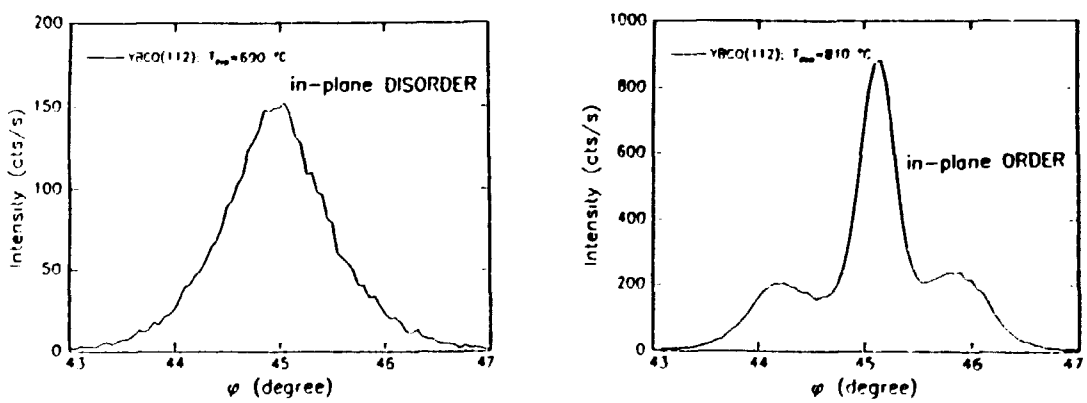


*Fig. 2. X-ray diffraction rocking curves through the (112) Bragg reflection of $YBa_2Cu_3O_{6+x}$ films deposited at 690°C (left) and 810°C (right).*

[1]R.F. Kromann, J.B. Sørensen, R. de Reus, N.H. Andersen, P. Vase, and T. Freltoft, (1992). J. Appl. Phys. **71**, 3119.

## 1.24 Crystal Structure, Magnetic Susceptibility and Thermopower of Superconducting and Non-Superconducting $Nd_{1.85}Ce_{0.15}CuO_{4+y}$

N.H. Andersen, B. Lebech, *Department of Solid State Physics, Riso National Laboratory, Denmark*, I. Mangelschots, *IBM Research Laboratory, Rüschlikon, Switzerland*, A. Wisniewski, *Polish Academy of Sciences, Warszawa, Poland*, and C.S. Jacobsen, *Physics Laboratory 3, The Technical University of Denmark, Lyngby, Denmark*

The superconducting properties of $Nd_{2-x}Ce_xCuO_{4+y}$, NCCO, have attracted considerable interest. NCCO has the highest critical temperature ($T_c$ = 25 K) for $x \approx 0.15$, and superconductivity is only observed in reduced samples. Based on these observations, and because cerium is most likely $Ce^{4+}$, NCCO is expected to be an electronic conductor and not as the other high temperature superconductors, a hole conductor.

For superconducting (reduced) and non-superconducting (oxidized) $Nd_{1.85}Ce_{0.15}CuO_{4+y}$, an experimental study, including structure determination by neutron powder diffraction, recording of oxygen changes by gas volumetry, and susceptibility and thermoelectric measurements, has been carried out[1]. Difference neutron diffraction patterns from samples prepared on line at the spectrometer show that the structures of superconducting and non superconducting samples are identical within the limits set by the statistical errors of our data. Simultaneous gas volumetric measurements reveal that $\Delta y < 0.03(1)$ when the sample is oxidized from the superconducting to the non-superconducting state. Structural refinements confirm that $Nd_{1.85}Ce_{0.15}CuO_{4+y}$ has the T'-type tetragonal structure reported in the literature, but additional oxygen may be located on the apical O3 oxygen site of the T type structure, with a total oxygen content of $4 + y = 4.03(5)$ (*cf.* Fig. 1). Consistent with this result, we find very small values of the thermoelectric power indicating that $Nd_{1.85}Ce_{0.15}CuO_{4+y}$ is close to the formal threshold, $y_c = 0.075$, between electron and hole conduction but, surprisingly, the thermoelectric power of the superconducting sample is positive, while it is negative below 210 K in the non-superconducting sample.

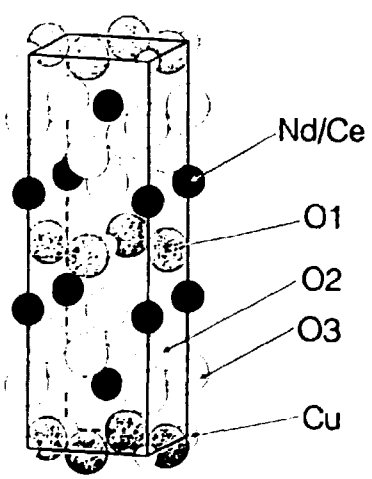


*Fig. 1. The T'-type crystal structure of $Nd_{2-x}Ce_xCuO_{4+y}$. The oxygen sites O1 and O2 are essentially fully occupied in the T'-structure. In the T type structure of archetype $La_{2-x}Ba_{-x}CuO_{4+y}$, the occupied oxygen sites are O1 and O3. Additional oxygen may be located on the O3 site in $Nd_{2-x}Ce_xCuO_{4+y}$. The atoms displayed are half the size of their actual ionic radii, and excess oxygen on the O3 site requires relaxation of the neighboring sites.*

[1] I. Mangelschots, N.H. Andersen, B. Lebech, A. Wisniewski, and C.S. Jacobsen, (1992). Physica C **203**, 369.

## 1.25 Crystal Structure and Charge Localization in $Pb_2Sr_2Y_{1-x}Ca_xCu_3O_8$ for x = 0.0 – 0.5.

J.E. Jorgensen, *Department of Chemistry, Aarhus University, Denmark*, and N.H. Andersen, *Department of Solid State Physics, Risø National Laboratory, Denmark*

Compounds with formula $Pb_2Sr_2Ln_{1-x}Ca_xCu_3O_8$, where Ln represents a lanthanide were synthesized and shown to be superconductors with critical temperatures close to 70 K by Cava *et al.*[1] in 1988. Superconductivity is only observed for samples prepared in a mildly reducing atmosphere. The maximum $T_c$ value is obtained for calcium doping levels close to $x = 0.5$. These compounds are pseudo-tetragonal, but actually orthorhombic, and they have a stacking sequence -Ln-$CuO_2$-SrO-PbO-SrO-$CuO_2$-. The $CuO_2$ layers contain the basic electronic structure for all high $T_c$ superconducting compounds, but superconductivity is only observed if holes are introduced into the $CuO_2$ planes by suitable electron acceptor units in the structure. The aim of the present neutron powder diffraction study was to determine the structural changes induced by Ca-doping of $Pb_2Sr_2YCu_3O_8$. Special attention was paid to changes in the axial Cu–O bond length which is usually considered to be essential for effective charge transfer to the $CuO_2$ planes.

Powder samples of $Pb_2Sr_2Y_{1-x}Ca_xCu_3O_8$ with $x = 0.0–0.5$ were prepared and their superconducting properties were characterized by resistivity measurements. Superconductivity was only observed in the $x = 0.5$ sample. Analyses of the neutron powder-diffraction data were carried out by Rietveld analysis. Bond valencies for all cations were calculated from the interatomic distances. The axial Cu–O bond length and the bond valency of the copper ions in the $CuO_2$ planes are shown in Fig. 1. Ca doping has little influence on the axial Cu–O bond length for doping levels up to $x = 0.4$, while the total copper–bond valency, determined from the bond length sums of all the neighboring ions, increases. The bond valency of the Pb ions increases up to $x = 0.4$ and then saturates. Based on these observations we conclude that upon calcium doping both the $CuO_2$ planes and the Pb are oxidized. Our results explain why the calcium doping, which should introduce the necessary holes into the superconducting $CuO_2$ planes, only becomes effective for doping levels $x > 0.4$.

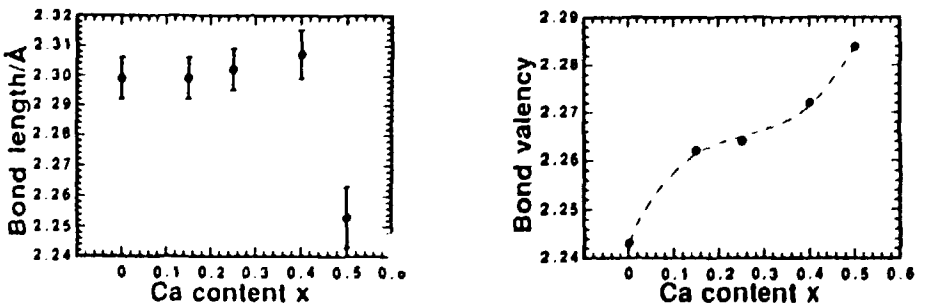


*Fig. 1. Left: Axial Cu–O bond length as a function of the Ca doping level. Right: Bond valency of the copper ions in the $CuO_2$ layers.*

[1] R.J. Cava *et al.*, (1988). Nature, **336**, 211.

## 1.26 Preparation and Structural Analysis of Epitaxial $Bi_2Sr_2CaCu_2O_{8+x}$ Thin Films on MgO(001), $LaAlO_3$(001), and $NdGaO_3$(001)

R. de Reus*, M. Nielsen, *Department of Solid State Physics, Risø National Laboratory, Denmark.* R. Seemann, A. Sewing, and R.L. Johnson, *II. Institut für Experimentalphysik, Universität Hamburg, Germany*

From the point of view of applications, $Bi_2Sr_2CaCu_2O_{8+x}$ is a promising high-$T_c$ superconductor because of its high stability and critical magnetic field at low temperatures in comparison to $YBa_2Cu_3O_{6+x}$. Laser ablation was used to deposit thin films of $Bi_2Sr_2CaCu_2O_{8+x}$ on different substraters. The deposition process was optimized and the influence of the deposition parameters on the electrical and structural properties of the films was investigated. The highest quality films are expected for deposition temperatures higher than the recrystallization temperature of Bi–Sr–Ca–Cu–O, so that crystalline films are grown during deposition. Unfortunately, for temperatures higher than 500°C a severe loss of Bi is observed, resulting in formation of phases other than the desired $Bi_2Sr_2CaCu_2O_{8+x}$. Therefore, amorphous Bi–Sr–Ca–Cu–O films were deposited around 500°C and subsequently annealed in air. The post-annealing temperature of the critical parameter and the optimal temperature is 850°C. On MgO(001), $NdGaO_3$(001), and $LaAlO_3$(001) substrates, *c*-axis-oriented films were obtained with critical temperatures higher than 80 K. Since growth of the crystalline $Bi_2Sr_2CaCu_2O_{8+x}$ takes place during annealing, the formation of the epitaxial phase is hindered. Primary nucleation of the crystalline phase is expected at the substrate interface and at the surface. At the interface, epitaxial growth of $Bi_2Sr_2CaCu_2O_{8+x}$ is promoted by a good lattice match with the substrate. This is the case for the $LaAlO_3$ and $NdGaO_3$ substrates (lattice mismatch less than 1 %), where approximately 50 % of the film is fully epitaxial, whereas the remainder is randomly oriented in the *ab*-plane. For MgO substrates (lattice mismatch 10 %) some preferential in-plane orientations of the $Bi_2Sr_2CaCu_2O_{8+x}$ are observed, but the majority of the film is randomly oriented in the *ab*-plane[1,2].

[1] R. Seemann, F. Hänisch, M. Peyerl, A. Sewing, R.L. Johnson, R. de Reus, and M. Nielsen, (1992). Physica **C199**, 112.
[2] R. de Reus, M. Nielsen, R. Seemann, A. Sewing, and R.L. Johnson, (1992). In: *Electronic Properties of High-$T_c$ Superconductors*, H. Kuzmany, M. Mehring, and J. Fink (Eds.), (Springer Verlag, Heidelberg).

*Present and permanent address: Mikroelektronik Centret, The Technical University of Denmark, Lyngby, Denmark.

## 1.27 Neutron Diffraction on Ternary Alkali Metal Palladium Deuterides

G. Auffermann, W. Bronger, P. Müller, *Institut für Anorganische Chemie der RWTH Aachen, Germany*, and K. N. Clausen, *Physics Department, Risø National Laboratory, Denmark*

Ternary alkali metal palladium hydrides $A_xPdH_z$ (A = alkali metal) were synthesized by the reaction of alkali metal hydride with palladium sponge in a hydrogen atmosphere at temperatures between 570 K and 700 K. The experimental conditions show that higher oxidation states of palladium are stabilized with increasing hydrogen pressure. Recently hydrogen reaction pressures between 20 and 100 bar led to five new colourless hydrides with the compositions $A_2PdH_4$ (A = Rb or Cs) [1] and $A_3PdH_5$ (A = K [2], Rb [3] or Cs [2]).

X-ray investigations on powdered samples revealed the atomic positions of the metal atoms. To determine the hydrogen positions neutron diffraction experiments on the deuterated compounds were carried out on TAS1. These experiments led to the complete structure determination. The characteristic features of the structures are square planar $[PdD_4]^{2-}$-groups. Structural studies on the $A_2PdD_4$ phases (see Fig. 1 and Table 1) down to 15 K showed that phase transitions occur which are caused by motional processes in the sphere of the hydrogen ligands, whereas the $A_3PdD_5$ phases (see Fig. 2 and Table 2) decompose to the low pressure phase $A_3PdD_3$ [3,4] and $D_2$ before a structural change occurs.

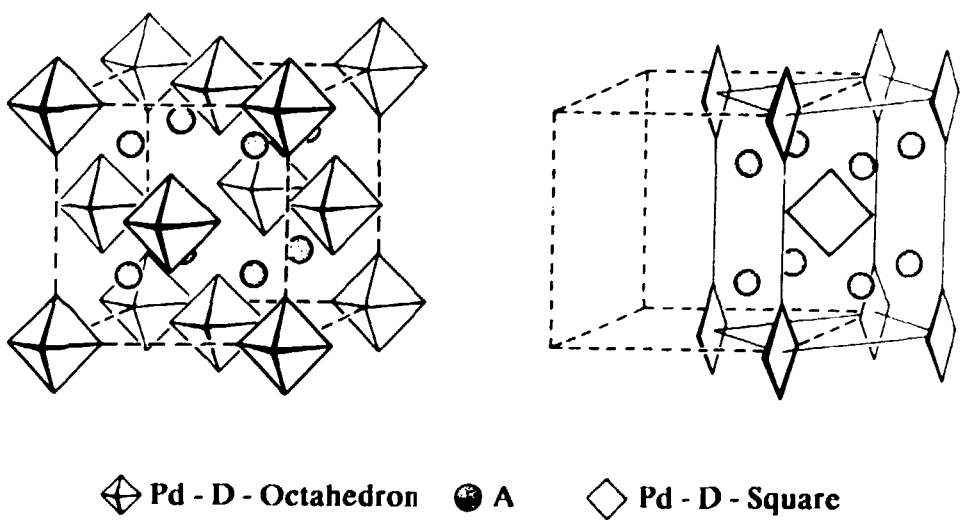


*Fig. 1: $A_2PdD_4$ (A = Rb, Cs); structures of the high temperature (left side) and low temperature modifications (right side). The corners of the Pd-D-octahedra are statistically occupied by deuterium with a population factor of two thirds.*

*Table 1: $A_2PdD_4$ (A = Rb, Cs); structural parameters of the high temperature modifications (295 K; space group Fm3m, Z = 4; A in 8c ($\frac{1}{4}\frac{1}{4}\frac{1}{4}$), Pd in 4a (0 0 0), D in 24e (x 0 0 with pp = 2/3) and the low temperature modifications (15 K; space group $P4_2/mnm$, Z = 2; A in 4d ($0\frac{1}{2}\frac{1}{4}$), Pd in 2a (0 0 0), D1 in 4e (0 0 z), D2 in 4f (x x 0)) from neutron diffraction experiments.*

| | High temperature phase | | Low temperature phase | | | |
|---|---|---|---|---|---|---|
| Compound | a[Å] | $x_D$ | a[Å] | c[Å] | $z_{D1}$ | $x_{D2}$ |
| $Rb_2PdD_4$ | 8.431(1) | 0.1938(7) | 5.827(1) | 8.495(2) | 0.1971(8) | 0.2023(9) |
| $Cs_2PdD_4$ | 8.872(9) | 0.180(2) | 6.17(1) | 8.85(1) | 0.185(3) | 0.182(3) |

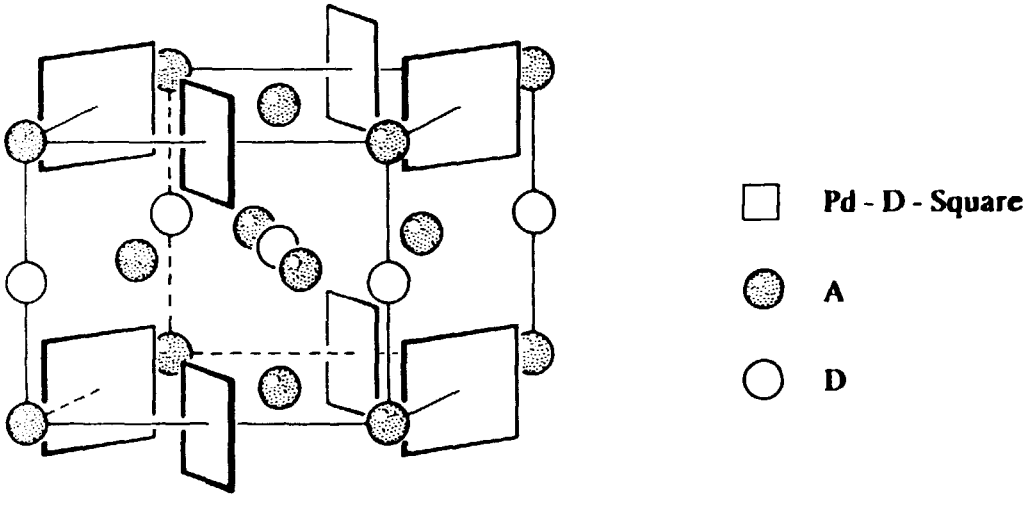


*Fig. 2: $A_3PdD_5$ (A = K, Rb, Cs); structure of the room temperature modifications.*

*Table 2: $A_3PdD_5$ (A = K, Rb, Cs); structural parameters from neutron diffraction experiments at room temperature (space group P4/mbm, Z = 2; A1 in 2a (0 0 0), A2 in 4h (x x+$\frac{1}{2}\frac{1}{2}$), Pd in 2d (0 $\frac{1}{2}$ 0), D1 in 2b (0 0 $\frac{1}{2}$), D2 in 8k (x x+$\frac{1}{2}$ z))*

| Compound | a[Å] | c[Å] | $z_{A2}$ | $x_{D2}$ | $z_{D2}$ |
|---|---|---|---|---|---|
| $K_3PdD_5$ | 7.432(3) | 5.811(2) | 0.678(3) | 0.114(1) | 0.189(2) |
| $Rb_3PdD_5$ | 7.800(3) | 5.987(2) | 0.684(1) | 0.1079(8) | 0.181(1) |
| $Cs_3PdD_5$ | 8.301(7) | 6.024(5) | 0.679(3) | 0.100(3) | 0.191(4) |


[1] W. Bronger and G. Auffermann, (1992). J. Alloys Comp. **187**, 87.
[2] W. Bronger and G. Auffermann, (1992). J. Alloys Comp. **187**, 81.
[3] W. Bronger and G. Auffermann, (1992). J. Alloys Comp. **179**, 235.
[4] W. Bronger and G. Auffermann, (1990). J. Less-Common Met. **158**, 163.

## 1.28 Structural Phase Transition in a Buried Layer of $CoSi_2$: X-Ray-Scattering Measurements

A.R. Sandy, E. Findeisen, M. Nielsen, J. Bohr, *Department of Solid State Physics, Riso National Laboratory, Denmark*, W.G. Spanninga, and L. Niesen, *Nuclear Solid State Physics and Materials Science Centre, Rijksuniversiteit Groningen, The Netherlands*

Motivated by recent Mössbauer-spectroscopy measurements which indicate that a $CoSi_2$ layer buried in Si(111) undergoes a structural phase transformation at low temperatures[1], we have initiated an X-ray-scattering study of this system. Our preliminary results, highlighted below, confirm this observation and warrant further investigation.

The samples we have studied were formed by high-dose $Co^+$ implantation into Si(111) single crystals and subsequent annealing[2]. At room temperature, transmission electron microscopy, high-resolution electron microscopy, and X-ray diffraction measurements[2] reveal macroscopically smooth interfaces between a 700 Å epitaxial, aligned, crystalline $CoSi_2$ layer buried 450 Å below the surface of a Si(111) crystal. The buried layer of $CoSi_2$ has the same structure as bulk samples of $CoSi_2$—the $CaF_2$ structure—though its lattice constants parallel and perpendicular to the buried layer are 1.2 % larger and 0.6 % smaller, respectively, than in bulk samples.

Figure 1 displays measured X-ray intensities obtained along the surface-normal direction ($L$) in the vicinity of the Si(111) bulk Bragg reflection as a function of temperature. Data were obtained at BW2, HASYLAB. [$c^* \equiv 2\pi/(\sqrt{3}d) = 0.6680$ Å$^{-1}$ at 300 K, where $d$ is the conventional unit cell size.] The peaks at $L = 3$ and $L \approx 3.054$ are the Si(111) and the $CaF_2$-like, $CoSi_2$(111) bulk Bragg reflections, respectively. In addition, oscillations separated by $\Delta L \approx 0.0135$ are visible in Figs. 1(*a*)–1(*g*). At high temperatures (300 and 260 K), close to 20 such oscillations are observed in the vicinity of the Si(111) Bragg reflection. These oscillations arise because of the finite thickness (700 Å) of the buried layer. The large number of oscillations that we have observed confirm that the Si-$CoSi_2$ interfaces are smooth over large length scales parallel to the buried interfaces.

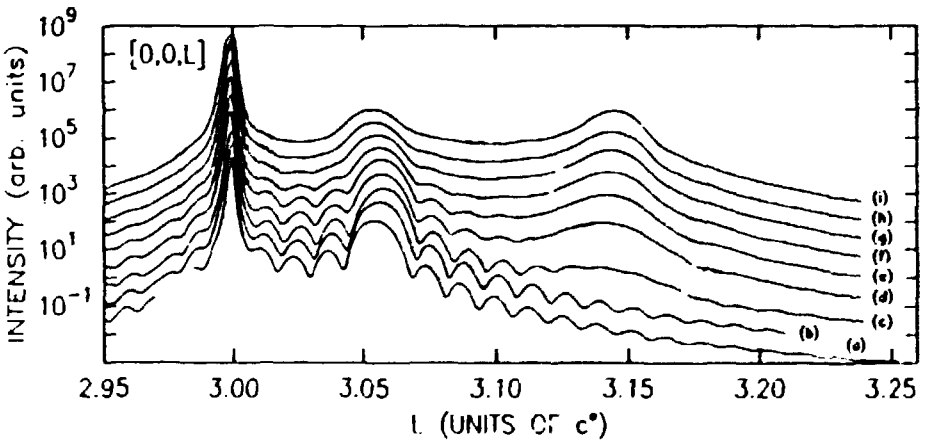


*Fig. 1. X-ray intensity vs. wave-vector transfer along [0, 0, L]. The solid lines join the measured data points. Data obtained at (a) 300, (b) 260, (c) 220, (d) 200, (e) 180, (f) 160, (g) 140, (h) 120, and (i) 80 K. Successive scans have been vertically offset for clarity.*

As the temperature is decreased below 260 K (Figs. 1(*c*)-1(*i*)), the number and amplitudes of these oscillations decrease and then vanish (Fig. 1(*i*)), the integrated intensity from the $CaF_2$-like, $CoSi_2$(111) Bragg reflection decreases significantly, and a new peak appears at $L \approx 3.145$ and intensifies. Additional scans performed below 80 K (not shown) are nearly identical to that obtained at 80 K (Fig. 1(*i*)). The transformation shown is reversible with temperature but there remain time[1]/hysteresis effects to unravel.

Scans performed in the vicinity of the Si(111) ($L = 3$) and Si(333) ($L = 9$) bulk Bragg reflections, and in the vicinity of the Si(222) ($L = 6$) bulk-forbidden reflection (Fig. 2) lead us to conclude that the peaks at $L \approx 3.145$, 6.290, and 9.435 correspond to a new structure of $CoSi_2$ coexisting with the bulk, $CaF_2$-like, $CoSi_2$ structure. We speculate that the structural phase transformation is driven by differences in the thermal expansion of Si and $CoSi_2$ at low temperatures. This results in large elastic strains at the Si-$CoSi_2$ interfaces which may be sufficient to distort the $CaF_2$ structure of $CoSi_2$. The perturbation is relaxed and the bulk $CoSi_2$ structure obtained over a characteristic elastic length which is less than half the thickness of the buried layer. Because the finite-size oscillations vanish at low temperatures (Fig. 1), we suggest that the interfaces between these two structures are "rough"; for instance, the interfaces may be buckled.

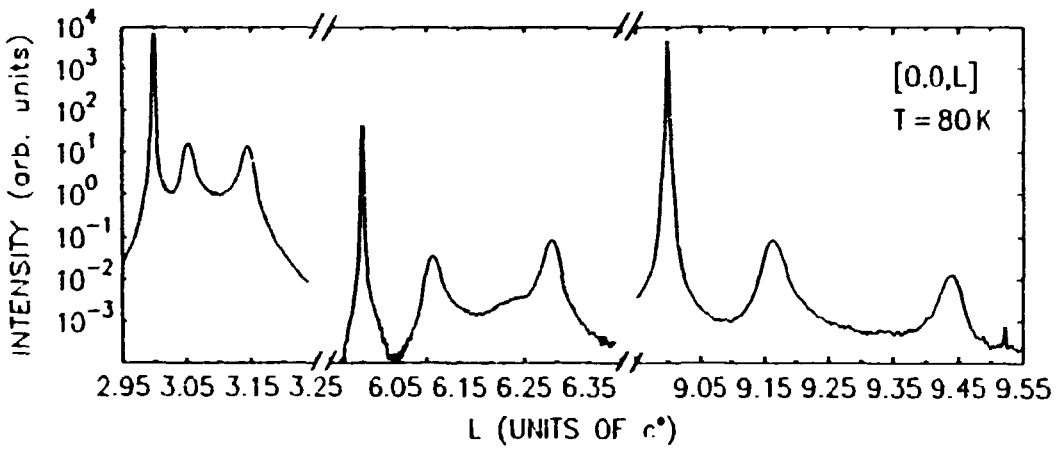


*Fig. 2. X-ray intensity vs. wave-vector transfer along* $[0, 0, L]$. *The solid lines join the measured data points.*

It remains to determine how and if the structure of the buried layer parallel to the Si-$CoSi_2$ interfaces changes at low temperatures and whether the structural phase transformation occurs at neither, one, or, as we intuitively expect, both of the Si-$CoSi_2$ interfaces. As alluded to above, future research should include an investigation of the buried-layer thickness on the above properties.

[1] W.G. Spanninga, P.J.M. Smulders, and L. Niesen, (1992). Nucl. Inst. Meth. **B63**, 138.
[2] C.W.T. Bulle-Lieuwma, A.H. van Ommen, and L.J. van IJzendoorn, (1989). Appl. Phys. Lett. **54**, 211.

## 1.29 X-Ray Studies of Charge-Density-Wave Phases in $TaS_2$

D.B. Pengra and J. Bohr, *Department of Solid State Physics, Risø National Laboratory, Denmark*

The metastable 1T polytype of $TaS_2$ has charge-density wave (CDW) phases which adopt three different structures; in order of decreasing temperature, they are incommensurate (IC), nearly-commensurate (NC) and commensurate (C)[1]. We have used X-ray diffraction to study the correlation between the orientation of the CDW lattice and its commensurability with the atomic lattice. We are investigating whether the rotation of the CDW state is governed by a symmetry principle recently applied to epitaxial rotations[2]. The principle states that in a system composed of two interacting two-dimensional lattices with different periodicities, the energy is minimized when one lattice rotates with respect to the other such that domain walls are formed that lie along high symmetry directions of one of the lattices. These *high symmetry solutions* have been found to give some of the rotation angles that have been measured for gases adsorbed on graphite substrates. The argument is general enough that the effect may be seen in other kinds of systems with competing periodicities. Such a system may be CDWs in $TaS_2$. Figure 1 shows the correspondance between one set of high symmetry solutions (denoted by the line) and the measurements of the CDW satellite location for the C and NC structures. These solutions are for a domain-wall angle oriented by 60° with respect to the CDW lattice. The C phase is by definition a high symmetry solution.

We have been investigating evidence of a continuous rotation in the CDW wavevector as the temperature approaches the C-NC phase transition, as has been seen in other studies[3], and whether such a rotation follows the line in Fig. 1. Our data do not show a continuous change in the CDW vector, but an abrupt C-NC transition, and a persistence (probably due to quenching) of one of the NC satellites down to lowest temperatures. This behavior indicates that the NC position represents a comparatively deep energy minimum in the system, and thereby indicates that the NC structure is probably a relaxed commensurate structure of a higher order[2].

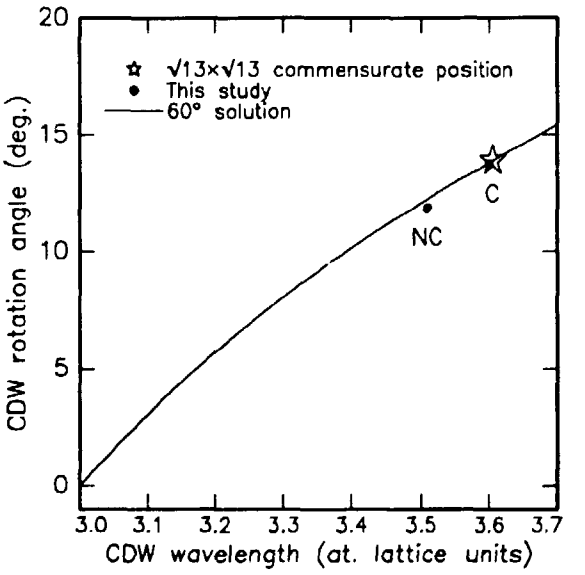


*Fig. 1. CDW satellite locations for the NC and C phases compared to high symmetry solutions from reference 2.*

[1] J.A. Wilson, F.J. Di Salvo, and S. Majahan, (1975). Adv. Phys. **24**, 117.
[2] F. Grey and J. Bohr, (1992). Europhys. Lett. **18**, 717.
[3] T. Ishiguro and H. Sato, (1991). Phys. Rev. B **44**, 2046; R.E. Thompson *et al.* (1988). Phys. Rev. B **38**, 10 734.

## 1.30 Melting and Solidification of Bismuth Inclusions in Aluminium

N.B. Thoft, J. Bohr, B. Buras, *Department of Solid State Physics, Risø National Laboratory, Denmark*, E. Johnson, H.H. Andersen, A. Johansen, and L. Sarholt-Kristensen, *Physics Laboratory, H.C. Orsted Institute, University of Copenhagen, Denmark*

The melting and solidification of bismuth inclusions in aluminium single crystals and structural phenomena at the bismuth aluminium interface are studied by X-ray diffraction. Bi and Al are immiscible, and Bi inclusions are formed by ion implantation into aluminium.

In earlier X-ray diffraction studies[1] of lead inclusions in aluminium large superheating (up to 67 K) and large supercooling (at least 18 K) were observed. In contrast to lead, bismuth has a smaller thermal expansion than aluminium and, furthermore, bismuth contracts upon melting.

Figure 1 shows the intensity of the Bi (011) diffraction peak during one temperature cycle (upper curve: room temperature → 275°C, lower curve: 275°C → room temperature). The melting of Bi inclusions starts around 80 K below the bulk melting point ($T_B$=271°C), and at $T_B$ all inclusions have melted. Additionally a large supercooling is observed. This confirms the importance of the previously mentioned differences between the lead and the bismuth systems, when considering the melting and the solidification of inclusions.

Future experiments will aim at studying the observed features in greater detail, both by X-ray diffraction and electron microscopy. For instance we intend to study the growth of the bismuth inclusions as a result of annealing, and hope to learn about the dependence of the onset of melting and solidification on the inclusion size distribution

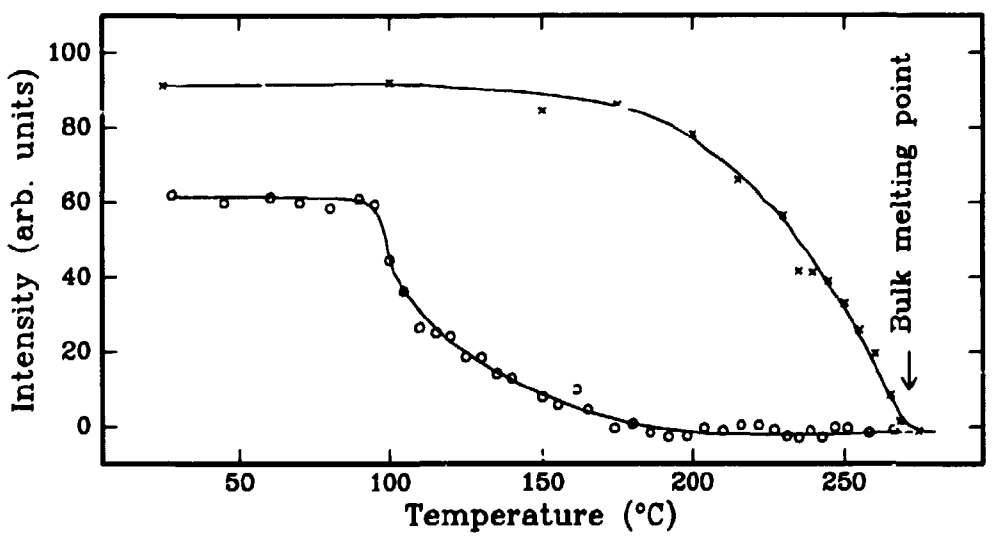


*Fig. 1. Background-subtracted intensity of Bi (011) diffraction peak. × heating data, o cooling data. The curves should only be taken as guides for the eye.*

[1] L. Gråbæk, J. Bohr, E. Johnson, A. Johanson, L. Sarholt-Kristensen, and H.H. Andersen, (1990). Phys. Rev. Lett. **64**, 934.

## 1.31 Small-angle Scattering from Precipitates: Analysis by Use of a Polydisperse Hard-sphere Model

J. Skov Pedersen, *Department of Solid State Physics, Riso National Laboratory, Denmark*

A general polydisperse hard-sphere model for analysing small-angle scattering data from spherical precipitates in alloys has been introduced. The scattering intensity is calculated using the analytical expressions given by Vrij[1] for a polydisperse hard-sphere interacting system. In the model the size distribution is chosen as a Weibull density distribution and the hard-sphere interaction radius is taken as being proportional to the radius of the precipitates. The Weibull distribution is monomodal, and depending on the parameters describing the distribution, it can be skew to either side. This distribution has been found to describe the size distribution of $\delta'$-precipitates in Al-Li alloys determined by transmission electron microscopy[2].

Small-angle X-ray[3,4] and neutron scattering data[5], taken from the literature, for spherical $\delta'$-precipitates in Al-Li alloys have been analysed by the model. It gives very good fits to the experimental data and the results are in agreement with a Li content of 25% in the precipitates. The concentration of Li in the matrix is also in good agreement with the phase diagram of Al-Li found in the literature. The results we have obtained contradict the previously claimed inability of the such a model to fit the small-angle scattering data from Al-Li[3,4].

We have also applied a monodisperse hard-sphere model to the scattering data and have pointed out previous, erroneous, interpretations of the model, found in the literature[3,4]. The fits we obtain give a too high Li content in the $\delta'$-precipitates. However, one should note that the monodisperse model does not agree with the data at large scattering vectors, and that it therefore is a low-resolution interpretation of the data from a sytem which is actually polydisperse. We have investigated the systematic errors arising from this by simulating the scattering fom a polydisperse system and anlysing them by a monodisperse model. The results show that this does lead to higher Li concentration in the precipitates.

In the present work we have only considering small-angle scattering data from the Al-Li alloys, however, most of the results and conclusions are also valid for other system with spherical precipitates.

[1] A. Vrij, (1979). J. Chem. Phys. **71**, 3267.
[2] K. Maghalingam, B.P. Gu, G.L. Liedl, and T.M. Sanders, Jr., (1987). Acta Metall. **35**, 483.
[3] R. Triolo, E. Caponetti, and S. Spooner, (1989). Phys. Rev. **39**, 4588.
[4] R. Triolo, E. Caponetti, S. Spooner, and F. Boschetti, (1989). Phil. Mag. A **60**, 401.
[5] S. Abis, R. Caciuffo, F. Carsughi, R. Coppola, M. Magnani, F. Rustichelli, and M. Stefanon, (1990). Phys. Rev. **42**, 2275.

## 1.32 In-situ Time-resolved SANS Measurement on Krypton Bubbles in Copper

J. Skov Pedersen, *Department of Solid State Physics, Riso National Laboratory, Denmark*, and M. Eldrup, *Material Department, Riso National Laboratory, Denmark*

Last year *in-situ* time-resolved SANS measurement on the behaviour of Kr Bubbles in Cu under isothermal annealing were initiated. These measurements have been continued this year. In order to have a reliable control of the sample temperature in the range 100-500°C, we have developed a new furnace which is placed directly in the integrated vacuum of the SANS instrument. Thus, no neutron transparent windows are required. It is compact and relatively small, which allows a fast heating of the sample to the desired temperature. The furnace is made out of one piece of copper in order to have good thermal contact between the heating elements and the sample. The temperature is measured and controlled by two Pt resistors and two thermocouples.

Two series of measurement were performed at, respectively, 300 and 400°C. The results were analyzed by a monodisperse hard-sphere model, which includes the following parameters: bubble radius $R$, hard-sphere interaction radius $R_{hs}$, hard-sphere volume fraction $\eta_{hs}$, and an over-all scale factor, which is the number density of particles multiplied by the scattering contrast squared. At both temperatures the bubble radius follows approximately the relation:

$$R(t)^{\alpha} - R(0)^{\alpha} = K\,t$$

where $K$ is a growth constant and $t$ is the time.

At 300°C the exponent $\alpha$ is about 20, and at 400° it is about 12. The starting value of the radius $R(0)$ at 300°C is 10.1 Å and at the end of the measurements after 44 hours, it has increased to 13.0 Å. The corresponding change in the factor $R_{hs}/R$ is from 2.0 to 1.75. The volume fraction, calculated as $\eta_{hs}R^3/R_{hs}^3$ is nearly constant and equal to 0.01. The measurements at 400°C were performed on the sample already annealed at 300°C. The first measurement after the temperature has stabilized gives a radius of 14.4 Å, which increases to 23.7 Å after 45 hours. The ratio $R_{hs}/R$ decreases from 1.89 to 1.62 at the end of the measurements, while the volume fraction increases from 0.011 to 0.03.

The exponent determined for the two annealing series are much higher than expected from theory. Classical Ostwald ripening theory predicts a exponent of 2, whereas theories including bubble migration and coalescence gives exponents of 3-6 depending on the diffusion mechanism[1]. For high pressure bubbles the exponent is expected to increase both for the ripening theory and the migration and coalescence theories[2].

We have recently initiated analysis of the data in terms of polydisperse models, which also include the bubble interference effects. The size distributions are broad with a shape in qualitative agreement with shapes obtained from model calculations[1].

[1] D. Kaletta, (1983). Radiation Effects **78**, 245.
[2] P.F.P. Fichter, H. Schroeder, and H. Trinkaus, (1991). In *Fundamental Aspects of Inert Gas Behaviour in Solids*. S.E. Donnelly and J.H. Evans (eds.) (Plenum) p. 221.

## 1.33 Small-Angle Neutron Scattering on Ni-11 at.% Ti

P. Vyskocil, B. Schönfeld, G. Kostorz, *Institute of Applied Physics, ETH Zurich, Switzerland*, and J. Skov Pedersen, *Department of Solid State Physics, Riso National Laboratory, Denmark*

The decomposition process of Ni-Ti alloys strongly depends on Ti-concentration and aging temperature. It was suggested[1] that in a distinct region of the phase diagram the decomposition starts with the formation of periodically arranged particles having a titanium concentration of 17 at.% ($\alpha_2$-phase) before the still metastable $\gamma'$-phase ($Ni_3Ti$, $L1_2$-superstructure) develops. Classical nucleation and growth with $\gamma'$-precipitates appearing from the earliest observable stages of decomposition was reported by Grüne[2]. The existence of the $\alpha_2$-phase has recently been confirmed[3,4] but not much is known about its formation. In ref. 5) the authors suggest that the $\alpha_2$-phase forms after an initial spinodal decomposition stage.

The objectives of the present study are to elucidate the nature of the decomposition and to get more information about topological changes at intermediate aging times where $L1_2$-particles are already present and aligned along the ⟨100⟩ directions.

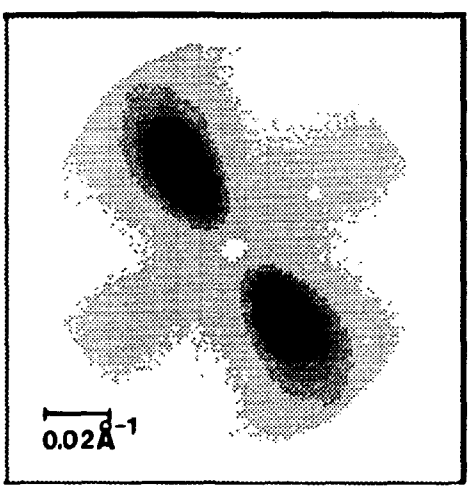


*Fig. 1. Single crystal of Ni-11.5 at.%Ti, aged for 240 hours at 580°C. The incident beam was parallel to a ⟨110⟩ direction. The peaks along [100] are a consequence of the alignment of precipitates.*

The small-angle scattering of both mono- and polycrystalline Ni-Ti samples was measured after aging at 580 °C for times ranging from 5 minutes to 900 hours. Results for polycrystals with titanium concentrations of 10.5, 10.8, 11.8 at.% were used to calculate the integrated intensity $Q = 4\pi \int I(q)q^2 dq$ and the particle size distribution for advanced stages of decomposition while the scattering of single crystals will be used for the modelling of quasi-periodic structures. A preliminary analysis of the scattering from polycrystals

shows that the metastable $\gamma'$-phase (titanium concentration inside the particles 25%, titanium concentration in the matrix 8%) is reached after 200 hours. Figures 1 and 2 show the strongly anisotropic scattering of single crystals aged for 240 hours and 500 hours, respectively.

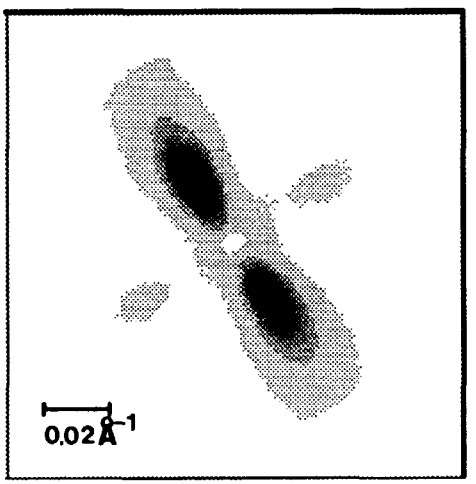


*Fig. 2. Single crystal of Ni-11.8 at.%Ti, aged for 500 hours at 580°C. Compared with Fig. 1 the peaks appear closer to the direct beam because of the coarsening of the microstructure.*


[1] K. Hashimoto and T. Tsujimoto, (1978). Trans. JIM **19**, 77.
[2] R. Grüne, (1988). Acta metall. **36**, 2797.
[3] A. Cerri, B. Schoñfeld, and G. Kostorz, (1990). Phys. Rev. **B42**, 958.
[4] T. Ungár, M. Lambrigger, and G. Kostorz, (1991). Mat. Sci. Eng. **A138**, 147.
[5] K. Hashimoto, T. Tsujimoto, and K. Saito, (1981). Trans. JIM **22**, 798.

## 1.34 Determination of $\gamma'$ Precipitate Size Distributions in Ni-Al-Mo Alloys by SANS and TEM

A.D. Sequeira, H.A. Calderon, G. Kostorz, *Institute of Applied Physics, ETH Zürich, Switzerland*, and J. Skov Pedersen, *Department of Solid State Physics, Riso National Laboratory, Denmark*

The study of alloys with unimodal particle size distribution is well documented but there have been only a few attempts to study alloys with bimodal size distributions owing to the complexity of such systems. These investigations however, have mostly ignored the determinant role of the lattice mismatch between the matrix and the precipitates $\delta = (a_{\gamma'} - a_{\gamma})/a_{\gamma}$, where $a$ is the lattice constant. This is particularly important since the effect of coherency strains, produced by the lattice mismatch $\delta$, upon phase separation is clearly recognised. In this investigation, the Mo concentration is used to tune the lattice mismatch of the $\gamma - \gamma'$ system.

Single-crystals with specific Mo concentrations were prepared to be studied in a double-step ageing. Alloys with $\delta$(1273K) negative or zero were aged at this temperature to form a first class of precipitates. Upon cooling to the second ageing temperature, $\delta$(873K) became zero or positive and a second class of smaller precipitates was formed. Each individual alloy was aged at this temperature from 1 to 1500 h.

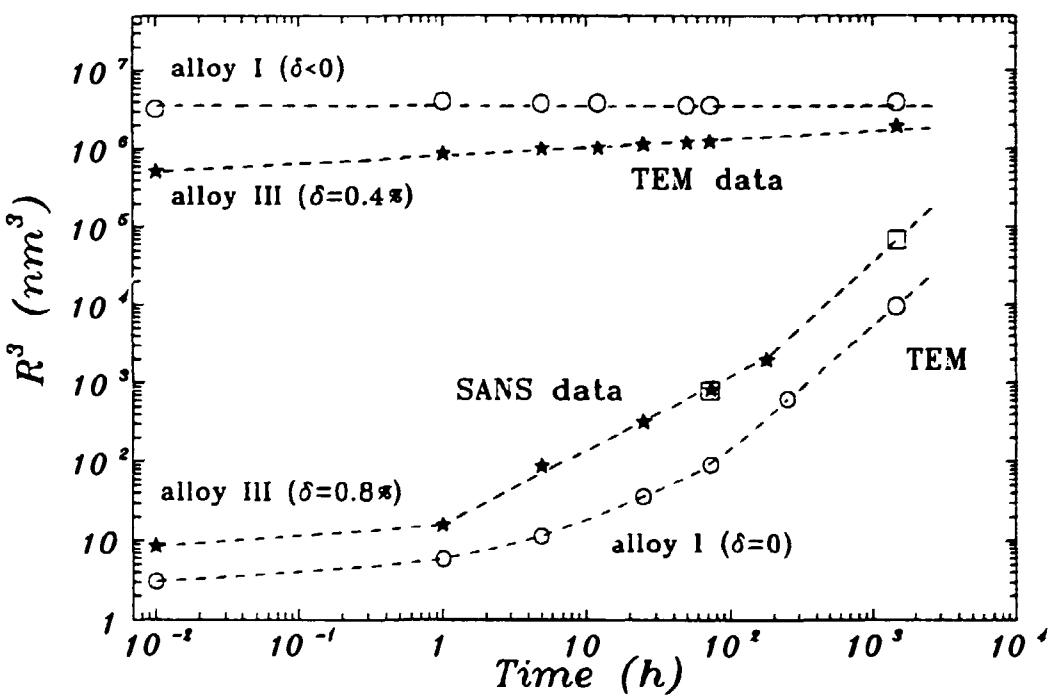


*Fig. 1. The kinetics of coarsening for both classes of precipitates in two Ni-Al-Mo alloys.*

The evolution of the microstructure during the decomposition process of the bimodal system was studied combining transmission electron microscopy (TEM) as a rather local probe with small-angle neutron scattering (SANS). With these two complementary techniques a statistically reliable determination of the particle size distributions, shape and space correlations of the precipitate ensemble was possible. To evaluate the lattice mismatch at room temperature for each class of precipitates convergent-beam electron diffraction patterns have been used.

TEM has been used for determining the particle size distributions of the class of large precipitates. In order to determine the particle size distribution for the class of smaller precipitates the SANS radial averaged curves were analysed in terms of a free-form distribution, for which a smoothness and a positivity constraint was used. The correlation effects between the precipitates were described by a local-monodisperse hard-sphere model. The instrumental resolution was taken into account for each of the three sample-to-detector distances (1, 3 and 6 m; $\lambda$ = 10 Å). A form factor of a sphere/cube was used to model the microstructure of alloy I/III, (see Fig. 1), respectively. This approach gave fits of excellent quality. For one specific stage (72 h at 873 K) it was also possible to determine the particle size distribution by TEM and the agreement is good. In the figure the kinetics of coarsening is presented for both classes of precipitates. For the later stages of ageing the small precipitates present a coarsening rate two orders of magnitude higher than the large precipitates. This indicates preferential coarsening of the smaller precipitates. This phenomenon is not predicted by the classical theories for coarsening.

## 1.35 Secondary Electron Emission from Insulators

J. Schou, *Department of Solid State Physics, Riso National Laboratory, Denmark*

The review on electron emission from surfaces during particle and photon bombardment is completed[1]. It includes primarily charged particles of energies that are representative of plasma-wall interactions, electrons and light ions from 0.1 to 10 keV.

A special subject is the secondary electron emission from condensed gases. The theoretical models for this type of emission are not yet at a level from which feasible predictions may emerge. A preliminary analysis shows that the internal diffusion prior to emission leads to features that differ substantially from electron emission from metals.

[1] J. Schou, (1992), Report Risø-I-588(EN).

## 1.36 Sputtering of Insulators

J. Schou, *Department of Solid State Physics, Riso National Laboratory, Denmark*, O. Ellegaard, *University of Odense, Denmark*, H. Sørensen, B. Stenum, *Departmen of Optics and Fluid Dynamics, Riso National Laboratory, Denmark*, R. Pedrys, *Institute of Physics, Jagellonian University, Krakow, Poland*, and R.E. Johnson, *University of Virginia, Charlottesville, USA*

The studies on sputtering of insulators have been continued with particular emphasis on the frozen gases.

The most volatile molecular gases as solid nitrogen, oxygen and the solid hydrogenic isotopes have been investigated. The sputtering yield were measured for hydrogen and helium ion bombardment. These results were compared with measurements of the energy distributions previously measured at the FOM-institute in Amsterdam by R. Pedrys. The main result is that this electronic sputtering shows similar features for nitrogen and the hydrogenic solids (Fig. 1). The yield increases with energy, but depends strongly on the sublimation energy and the internal electronic deexcitation processes. A typical yield for a 10-keV proton is 10 $N_2$ for solid nitrogen, 20 $O_2$ for solid oxygen, 200 $D_2$ for solid deuterium, and 800 $H_2$ for solid hydrogen. This difference reflects primarily the large variation in sublimation energy that ranges from 90 meV/$O_2$ to 12.6 meV/$D_2$, and 8.7 meV/$H_2$. Because the sublimation energy for solid oxygen is almost similar to that of solid nitrogen, the relatively large yield from solid oxygen is a result of the very efficient energy conversion of electronic excitations in the solid. The particle ejection from solid oxygen is partly driven by the energy release from ozone formation and reactions.

Many of the results from sputtering of condensed gases will be included in a review on insulator sputtering which is prepared in a collaboration between J. Schou and R.E. Johnson.

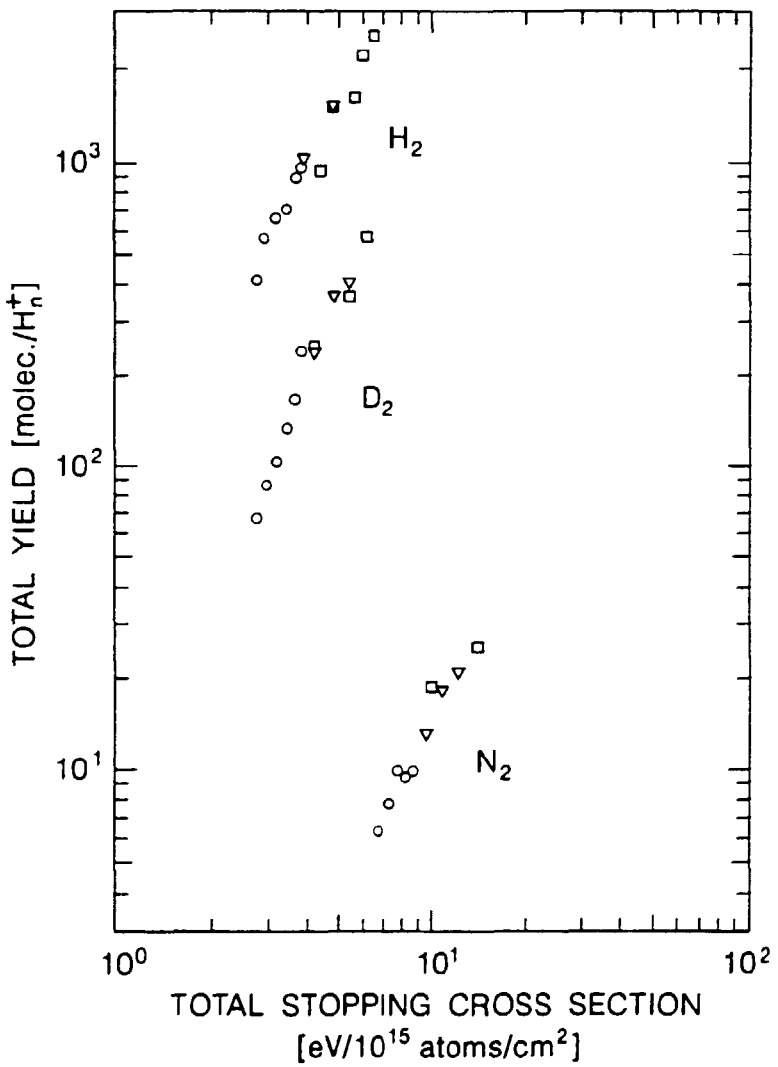


*Fig. 1. The sputtering yield for solid nitrogen, deuterium and hydrogen as a function of the sum of the stopping powers of the individual atoms for 5 to 10 keV hydrogen ion bombardment.* ○, $H^+$, ▽, $H_2^+$, □, $H_3^+$.

## 1.37 Laser Ablation from Simple Materials

J. Schou, *Department of Solid State Physics, Risø National Laboratory, Denmark*, O. Ellegaard, *University of Odense, Denmark*, and K.V. Weisberg, *Department of Optics and Fluid Dynamics, Risø National Laboratory, Denmark*

In the existing setup simple materials as silver and solid nitrogen have been irradiated by a pulsed UV-nitrogen laser. The laser has a strong line at 337.1 nm with a peak power of about 70 kW. The beam divergence is so small that intensities up to 100 GW/cm$^2$ are possible. The mass loss during irradiation can be measured by an oscillating quartz crystal monitor. In addition, the setup is equipped with a vacuum monochronomator for photon detection from 120 nm up to 900 nm. Because of the target is placed below a liquid-helium cryostat, the power can be determined directly from calorimetric measurements ( Fig. 1).

The silver electrode was irradiated by the laser with intensities around 100 GW/cm$^2$. The laser beam produced small holes in the electrode corresponding to a circular spot of diameter 0.1 mm. During the ablation a small visible plume was observed. At this intensity the ablation took place with a rate of $10^{-3}$ Ag atoms/photon. The rate turned out to be surprisingly constant until the silver spot was eroded away.

Films of solid nitrogen were deposited on the silver electrode as well. At the wavelength 337.1 nm solid nitrogen is absolutely transparent, and the energy is deposited directly into the electrode. For a 2000 Å film the yield was about $10^{-2}$ $N_2$/photon at 2 MW/cm$^2$. This erosion is caused by thermal absorption rather than ablation. The yield increases strongly with intensity up to about 1 $N_2$/photon at 10 MW/cm$^2$. The yield decreased exponentially with increasing film thickness. This behaviour means that it is possible to analyse the thermal desorption quite well. No significant multiphoton ionization process took place, since no luminescence at the characteristic atomic line around 523 nm was detected. The transition in nitrogen is forbidden in vacuum, but it is intense in a nitrogen solid. In general, UV-laser irradiation of solid nitrogen is interesting because metal nitrides are materials well suited for film production by laser ablation deposition.

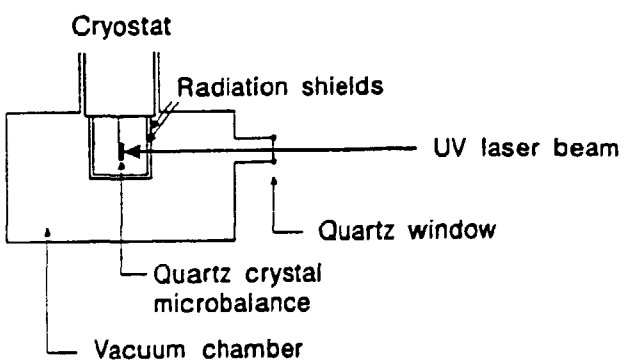


*Fig. 1. Experimental setup for laser ablation studies.*

## 1.38 STM and X-ray Diffraction Investigations of Ag on Ge(111)

L. Seehofer, R.L. Johnson, *II. Institut für Experimentalphysik, Universität Hamburg, Germany*, M. Hammar, M. Göthelid, U.O. Karlsson, *Department of Physics, Royal Institute of Technology, Stockholm, Sweden*, G. Le Lay, *CRMC-2 CNRS, Marseille, France*, R. Feidenhans'l, E. Findeisen, M. Nielsen, *Department of Solid State Physics, Riso National Laboratory, Denmark*, and M.Foss, *Institute for Physics and Astronomy, Århus University, Denmark*

There has been a long-standing controversy about the atomic structure of the Si(111)$\sqrt{3}\times\sqrt{3}$ Ag reconstruction[1,2]. It has been studied by numerous techniques and a large number of different models have been suggested. In order to provide additional information we have carried out detailed investigations of the different reconstructions induced by Ag on Ge(111). We have performed measurements with surface X-ray diffraction and scanning tunneling microscopy on the same samples. In this way we could obtain information about the surface botl, the local atomic and electronic structure as a function of Ag coverage. The X-ray diffraction measurements were performed at beamline BW2 and W1 in HASYLAB, Hamburg.

Rather surprisingly the STM images appeared very similar to those of Ag on Si(111) with a honeycomb like arrangement of protrusions, however, the atomic structure determined by X-ray diffraction is quite different. On Ge(111) Ag-trimers are formed with an Ag-Ag bond-length close to the value of bulk Ag, whereas on Si(111) a more open structure is formed. A more detailed atomic model of the $\sqrt{3}\times\sqrt{3}$ reconstruction is in progress. Eight out-of-plane fractional-order rod-scans were measured, which should allow determination of the relaxation in deeper layers.

We also obtained both STM and X-ray diffraction results for the $4\times4$ reconstruction which arises at lower Ag coverage. Below is an STM picture (Fig. 1) shown together with a Patterson map (Fig. 2) of the structure. In the STM picture the dark holes are the corners of the $4\times4$ unit cell. Clearly, there is a great difference between the two halfs in the unit cell. Unfortunately, the resolution inside the unit cell is not high enough to identify single atoms. The Patterson map shows that nearly all interatomic vectors in the unit cell are along the main symmetry axis. We do not yet have a model for the structure.

[1] Y.G. Ding, C.T. Chan, and K.M. Ho, (1991). Phys. Rev. Lett. **67**, 1454.
[2] J. Quinn, F. Jona, and P.M. Marcus, (1992). Phys. Rev. **B46**, 7288.

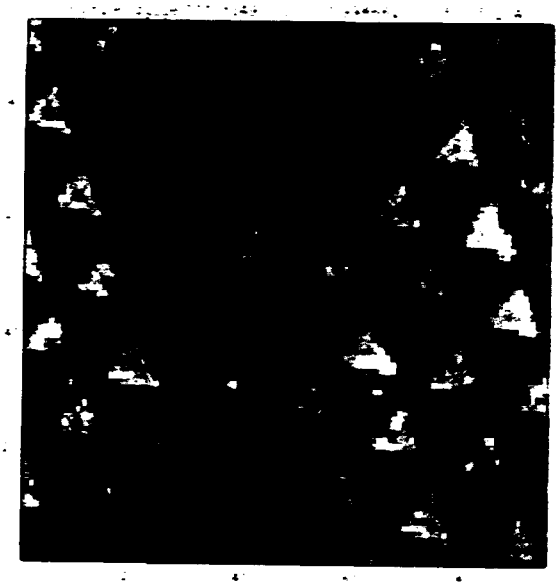

*Fig. 1. STM-image of the Ge(111)1 × 1-Ag structure. The axes are in Å*

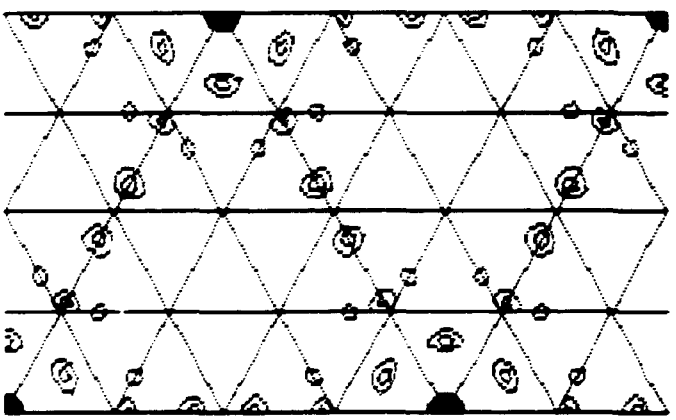

*Fig. 2. A contour map of the Patterson function for the Ge(111)1 × 1- Ag structure.*

## 1.39 The Incommensurate Structures of Ga/Ge(111): a Combined STM and X-ray Diffraction Study.

P. Molinàs-Mata, M. Böhringer, J. Zegenhagen, *Max-Planck-Institut für Festkörperforschung, Stuttgart, Germany*, L. Seehofer, T. Buslaps, R.L. Johnson, *II. Institut für Experimentalphysik, Universität Hamburg, Germany*, R. Feidenhans'l, E. Findeisen, M. Nielsen *Department of Solid State Physics, Riso National Laboratory, Denmark*, and M. Foss, *Institute for Physics and Astronomy, Århus University, Denmark*.

Metals form a large variety of structures on the surfaces of Si and Ge. Gallium and copper are specially interesting because they form incommensurate structures for coverages close to about one monolayer. We have studied the system Ga/Ge(111) by STM and X-ray diffraction. The X-ray diffraction measurements were performed partly at beamline BW2, partly at W1.

The incommensurability leads to the formation of small domains. However, Ga/Ge(111) exhibits two incommensurate phases. A $\gamma$-phase with hexagonal-shaped domains of about 28 Å in diameter and a $\beta$-phase with triangular-shaped domains. An example of the $\gamma$-phase is shown in the Fig. 1. The $\gamma$ and the $\beta$ phases have different incommensurability. This is evidenced by X-ray diffraction. In Fig. 2*a* scan along the (10) direction in the surface plane is shown. The peak at $q = 1.0$ (in reciprocal lattice units) is the crystal-truncation-rod from the substrate. The peak at $q = 0.865$ is coming from $\gamma$-phase, whereas the peak at $q = 0.925$ is from the $\beta$-phase. The $\gamma$ could therefore be labelled $\sqrt{7.4}\times\sqrt{7.4}$ and the $\beta$-phase $\sqrt{13.3}\times\sqrt{13.3}$. Special surface preparation is needed to obtained a single-phase structure exclusively. At present this is only possible for the $\gamma$-phase, but a preparation procedure for the $\beta$-phase is in progress. This would simplify the data-analysis for X-ray diffraction considerably.

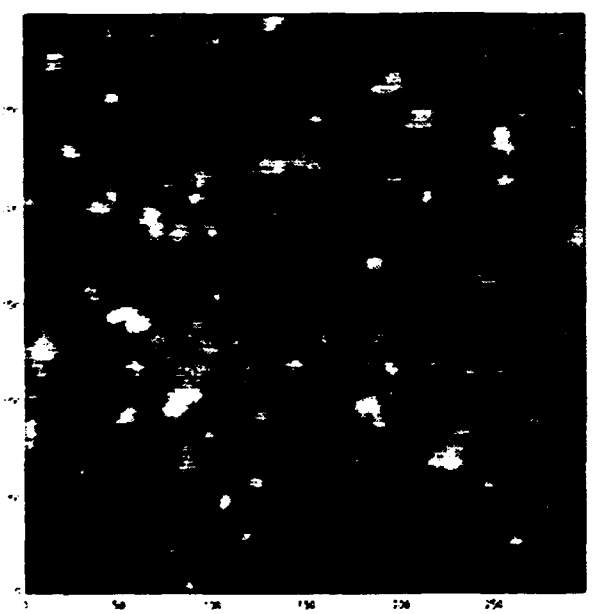

*Fig. 1. An STM image of the $\gamma$-phase of the Ga/Ge(111) structure. The domains have hexagonal shape. The axes are in Å.*

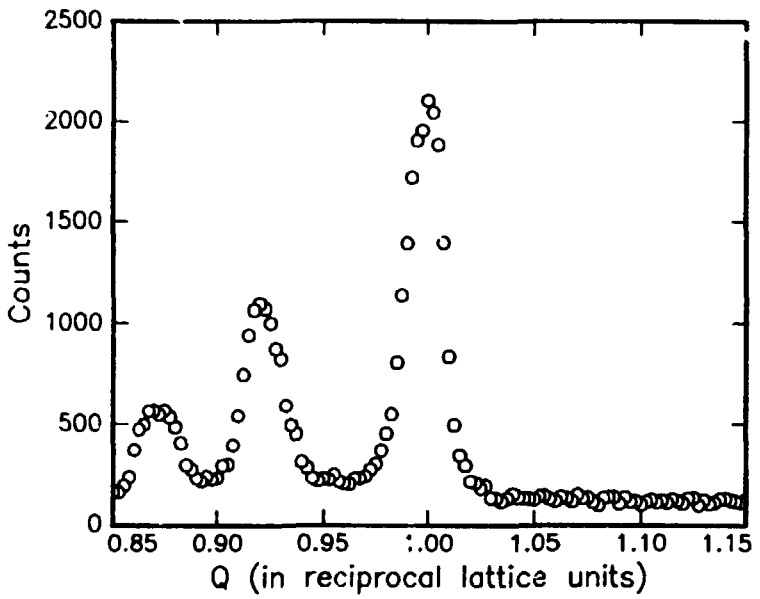


*Fig. 2. An X-ray diffraction scan along the (10) direction in reciprocal space. The peak at q=0.865 is coming from γ-phase, whereas the peak at q=0.925 is from the β-phase.*

## 1.40 X-ray Diffraction Study of Epitaxial $C_{60}$ Films Grown on GeS(001)

G. Gensterblum, J.-J. Pireaux, P.A. Thiry, *Laboratoire Interdisciplinaire de Spectroscopie Electronique, Bruxelles, Belgium*, G. Bengele, R.L. Johnson, *Institut für Experimentalphysik, Universität Hamburg, Germany*, M. Foss, *Institute for Physics and Astronomy, University of Århus, Denmark*, R. Feidenhans'l, *Department of Solid State Physics, Risø National Laboratory, Denmark*, and G. LeLay, *CRMC2-CNRS, Campus de Luminy, Marseille, France*

The epitaxial $C_{60}$/GeS films have been prepared at WINKELEMI in HASYLAB, Hamburg. The GeS(001) single crystal (7 × 7 mm$^2$) was freshly cleaved in ultra high vacuum. The chemical and crystallographic qualities of the substrate surface was checked by LEED prior to deposition. The crystallographic structure of the layered compound GeS belongs to the orthorhombic space group Pnma, so that the LEED diffraction pattern is rectangular (**a** = 4.30 Å and **b** = 3.64 Å). Cromatographically purified $C_{60}$ was then sublimed at a temperature of 400°C at constant pressure below 2 $10^{-9}$ mbar, on the GeS(001) substrate. The deposition rate was about 4 Å/minute as estimated with a quartz crystal oscillator. The final thickness of the film was about 120 Å which corresponds to about 14 monolayers. After deposition the film was annealed at about 180°C for 30 minutes. One obtains then a sharp LEED diffraction pattern, which reveals the $C_{60}$ hexagonal arrangement corresponding to the (111) plane of the room temperature fcc phase. The good epitaxial growth, which is probably favored by the weak interaction between the substrate and the molecule, stems from the peculiar corrugation of its surface which provides a preferential adsorption direction along the **b**-axis, and the close lattice match between twice the lattice parameter of GeS along its **a**-axis (2 × 4.30 Å = 8.6 Å) and the separation between rows of $C_{60}$ clusters along the ⟨ 101 ⟩ direction (8.68 Å).

X-ray diffraction measurements were performed partly at beamline W1, partly at BW2 in HASYLAB. Scans were performed along the specular direction of the GeS substrate. A scan around the expected position for the $C_{60}$ signal is shown in the figure. The parameter $Q$ is the momentum transfer in the direction normal to the surface. A clear peak at 0.774 Å$^{-1}$ is observed together with finite size oscillations. This demonstrates that the $C_{60}$ has grown in a layer by layer fashion. The peak position give an interlayer distance of 8.12 Å, slightly shorter than the (111) interlayer distance in bulk $C_{60}$. The position of the finite size oscillation shows that the numbers of layers is approximately 17.

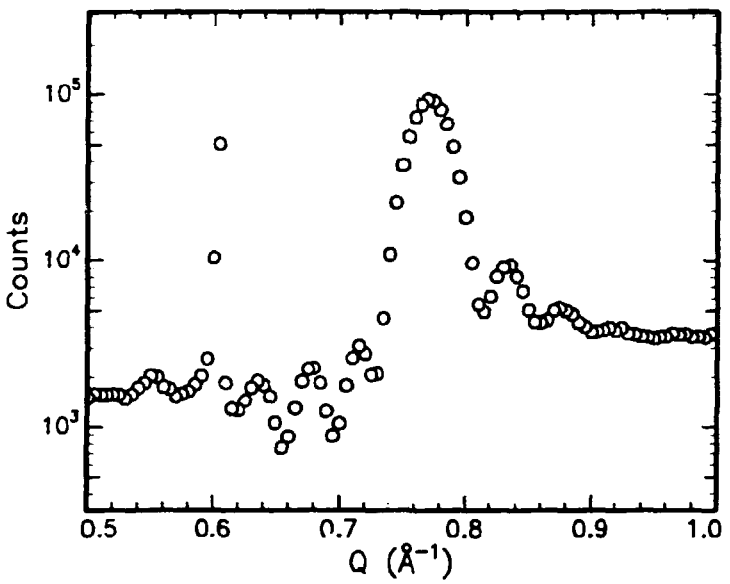


*Fig. 1. Scan along the specular direction showing diffraction from the $C_{60}$ layers. The peak at 0.6 Å$^{-1}$ is an bulk effect.*

## 1.41 Sulphur-Induced Reconstructions of the Ni(110) and Cu(111) Surface Studied by Surface X-ray Diffraction and STM

M. Foss, F. Besenbacher, L. Ruan, I. Stensgaard, *Institute of Physics and Astronomy, Aarhus University, Denmark*, E. Findeisen, R. Feidenhans'l, M. Nielsen, *Department of Solid State Physics, Riso National Laboratory, Denmark*, T. Buslaps, and R.L. Johnson, *II. Institut für Experimentalphysik, Universität Hamburg, Germany*

The determination of adsorbate-induced surface reconstructions is an important subject for understanding the fundamental interaction between surfaces and adsorabates. Especially adsorption-processes involving sulphur, which is a poison for many catalytic reactions, are of both fundamental and technological interest.

So far we have analyzed two such systems, Ni(110)(4 × 1)-S and Cu(111)($\sqrt{7} \times \sqrt{7}$)R19°-S, in detail by both Scanning Tunneling Microscopy (STM) and surface X-ray diffraction. The X-ray data were obtained at the wiggler beamline W1 in HASYLAB, Hamburg and the STM data at the Institute of Physics and Astronomy, Aarhus University. Apart from these two systems, a S reconstruction of Ni(111) is under investigation.

When a clean Ni(110) surface is exposed to $H_2S$ at room temperature a number of simple sulphur overlayer structures appear as a function of increasing S coverage, as seen by STM[1] and LEED. If, however, Ni(110) is exposed to $H_2S$ at elevated temperature, ($\sim 500K$), a p(4 × 1) structure evolves. STM images show, that the structure is mediated through a long range mass transport and that the Ni coverage is $\Theta_{Ni} = 0.5$ monolayers[2]. This information, combined with the Patterson function from the in-plane X-Ray data (see Fig. 1), gives some constraints concerning the possible models.

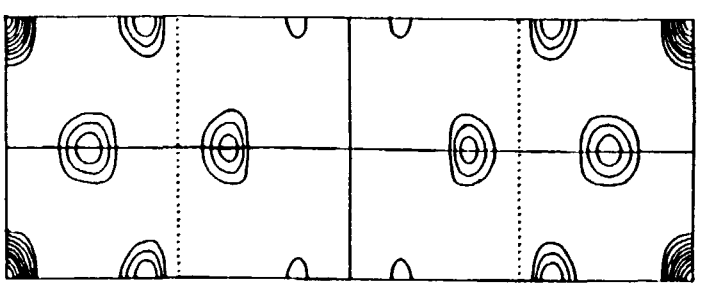

*Fig. 1. Contour plot of the experimental Patterson function for Ni(110)(4 × 1)-S.*

By including two Ni atoms and three S atoms it is possible by least-squares refinement of the atomic positions to obtain a $\chi^2 = 9$. This involves a scale factor, an overall Debye-Waller parameter and two positional coordinates. If small relaxations of the next Ni-layer is allowed, a $\chi^2 = 3.5$ is obtained. The hard-sphere model, which is shown in Fig. 2, is in

good agreement with the rod scans and the STM data. Furthermore, it seems reasonable that no subsurface S positions are present because of the large barrier of penetration for S.

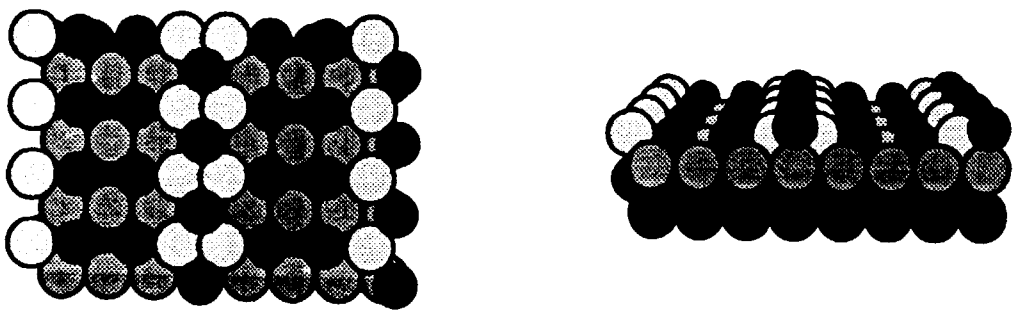

*Fig. 2. Proposed atomic structure of Ni(110)(4×1)-S as determined by X-Ray diffraction. The black atoms are S. The model is based on in-plane as well as out-of-plane data. A top-view is shown to the left and a side-view to the right.*

Several studies of Cu(111)($\sqrt{7} \times \sqrt{7}$)R19° can be found in the literature, but there is no generally accepted model for this system. In this case $H_2S$ exposure at room temperature produces the reconstruction, a slight post-anneal, however, improves the quality of the LEED-pattern. The obtained Patterson (Fig. 3), does not give as much help as would be expected due to a break in the 3-fold rotational symmetry. This symmetry break, which complicates the data analysis, is clearly seen by STM.

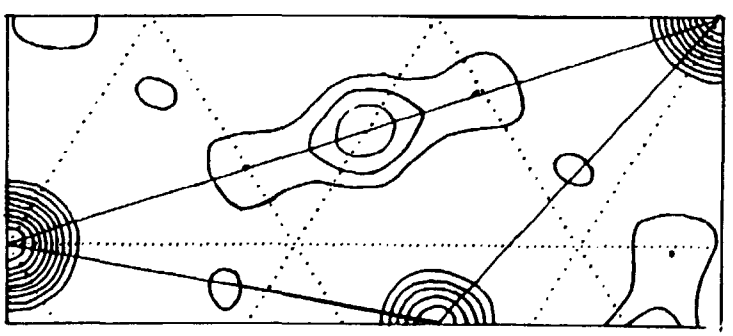

*Fig. 3. Contour plot of the experimental Patterson function for Cu(111)($\sqrt{7} \times \sqrt{7}$)R19°-S. The full line shows the irreducible unit, the dotted lines show 1x1 unit cells.*

Only the in-plane structure is so far solved. A model, which with an overall scale factor, one structural parameter and a common Debye-Waller factor gives $\chi^2 = 4$, is shown in Fig. 4.

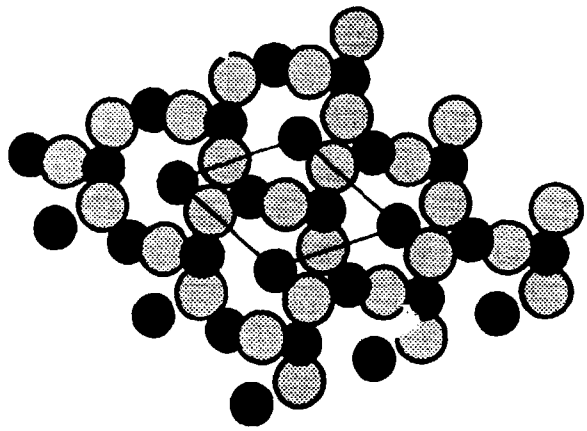

*Figure 4. The in-plane model for the Cu(111)($\sqrt{7} \times \sqrt{7}$)R19°-S. The black atoms are S and the dark grey atoms are Cu. A unit cell is also indicated.*

This model fits the experimental Cu coverage $\Theta_{Cu} = 3/7$ monolayer found by step etching in dynamic STM studies [3] and the S coverage $\Theta_S = 3/7$ monolayers found by high energy ion scattering. The out of plane structure is still under investigation by comparison with X-ray rod scans.

[1]F. Besenbacher, I. Stensgaard, L. Ruan, J.K. Nørskov, and K.W. Jacobsen, (1992). Surface Science **272**, 334.
[2]L. Ruan, F. Besenbacher, I. Stensgaard, and E. Lægsgaard, (1992). Phys. Rev. Lett. **69**, 3523.
[3]L. Ruan, I. Stensgaard, F. Besenbacher and E. Lægsgaard, (1992). Ultramicroscopy **42–44**, 498.

## 1.42 Characterization of Roughness of MgO(100) Substrates by Diffuse X-ray Scattering

C.P. Jensen and R. Feidenhans'l, *Department of Solid State Physics, Risø National Laboratory, Denmark*

A very important issue in molecular beam epitaxy (MBE) is the characterization and control of interface roughness. Very little is known about the fundamental laws governing the roughness in MBE-grown films. Recently, great progress is made in understanding diffuse X-ray scattering from rough surfaces[1,2]. The roughness of a surface gives rise to diffuse scattering around the reflection in the specular direction.

We have used this to characterize the MgO(001) substrates we use for metal MBE and are currently optimizing the preparation procedures for the substrates to minimize the roughness. Understanding the substrate roughness is a prerequisite to understand interface roughnesses. In Fig. 1, sample rocking-scans around the specular peak at $q = 0.1$ Å$^{-1}$ are shown for substrates from different suppliers. The peak in the center is the specular peak. The scattering around the specular peak is scattering from the roughness. The enhancements are refraction effects coming, when the angle of incidence or the angle of exit is close to the critical angle for MgO. As seen in Fig. 1, heating the substrates to 600°C in vacuum enhances the roughness, but is needed to remove dirt from the surface prior growth. The measurements are performed at the Risø rotating anode using Cu $K_\alpha$ radiation and a Ge(002) monochromator. This gives, however, insufficient resolution for an quantitative analysis. Experiments with better resolution are planned.

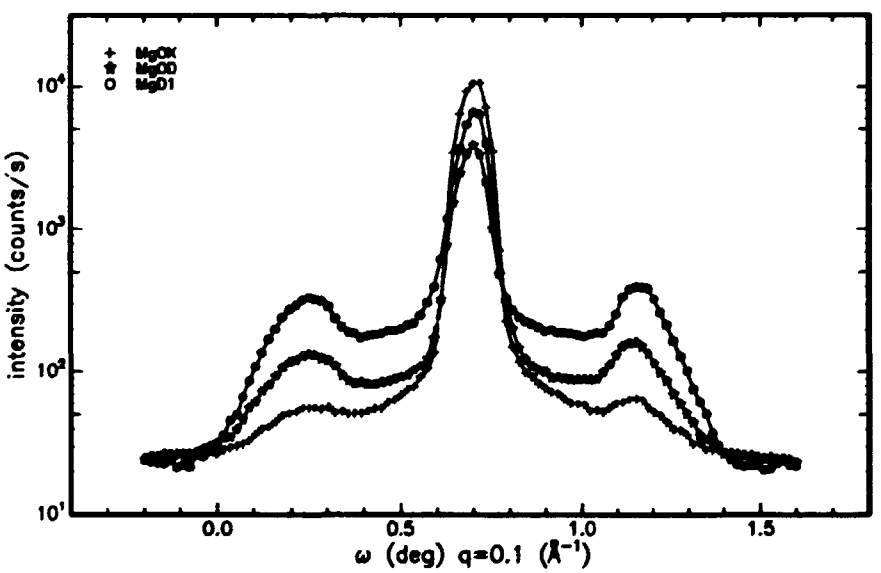


*Fig 1. Sample rocking scans (ω scans) around the specular direction at q=0.1 Å$^{-1}$ for MgO(001) substrates from two different manufactures. The sample labelled MgD1 is the same sample as MgOD, but has been heated to 600°C*

[1] S.K. Sinha, E.B. Sirota, S. Garoff, and H.B. Stanley, (1988). Phys. Rev. **B38**, 2297.
[2] W. Weber and B. Lengeler, (1992). Phys. Rev. **B46**, 7953.

## 1.43 Investigations of the Growth of Au,Ag and Cu on MgO(001)

C.P. Jensen, M.C. Gerstenberg, R. Feidenhans'l, *Department of Solid State Physics, Riso National Laboratory, Denmark*, and F. Olsen *IMFUFA, University of Roskilde, Denmark*

We have studied the growth of the noble metals Au, Ag and Cu on MgO(001) in the Metal MBE (MBE=Molecular Beam Epitaxy) apparatus in the department. Au, Ag and Cu are evaporated from Knudsen evaporation cells onto a clean MgO(001) substrate. The evaporation is performed in ulta-high vacumm at pressure in the low $10^{-10}$ torr range.

Only Ag grows epitaxially with Ag[001]||MgO[001] and Ag[100]||MgO[100]. The lattice constant of Ag is 4.09 Å, whereas the lattice constant for MgO is 4.21 Å giving a misfit of 2.9%. Although the misfit for Au is only slightly larger - 3.2% - it does not grow epitaxially but only c-axis oriented with Au(111)||MgO(001). A thin Fe or Ag buffer layer is necessary between the Au layers and the MgO(001) substrate to obtain epitaxy. The misfit for Cu 16% is too large to obtain two-dimensional growth.

$Cu_3Au$ is a classical system for studying order-disorder phase transition. The bulk phase transition is first order, but at the (100) surface it is second order. One aim of this study was to test the feasibility of making thin films of $Cu_3Au$ sandwiched between Ag layers. The depositions rates from the Knudsen evaporation cells were adjusted to obtain the right stoichiometry of Au and Cu. The films were deposited at close to room temperature. An X-ray diffraction scan along the specular (00*l*) direction is shown in Fig. 1 for a 170 Å Ag/200 Å $Cu_3Au$/230 Å Ag/MgO(001) structure. The measurements are performed at the rotating anode using a graphite monochromator. The peak at 3.35 $Å^{-1}$ is the $Cu_3Au(002)$ reflection, the peak at 1.70 $Å^{-1}$ is the $Cu_3Au(001)$ superstructure peak. The MgO(002) reflection is at 2.985 $Å^{-1}$ and the peak at 1.49 is the second-order contamination. The Ag(002) reflection is at 3.077 $Å^{-1}$.

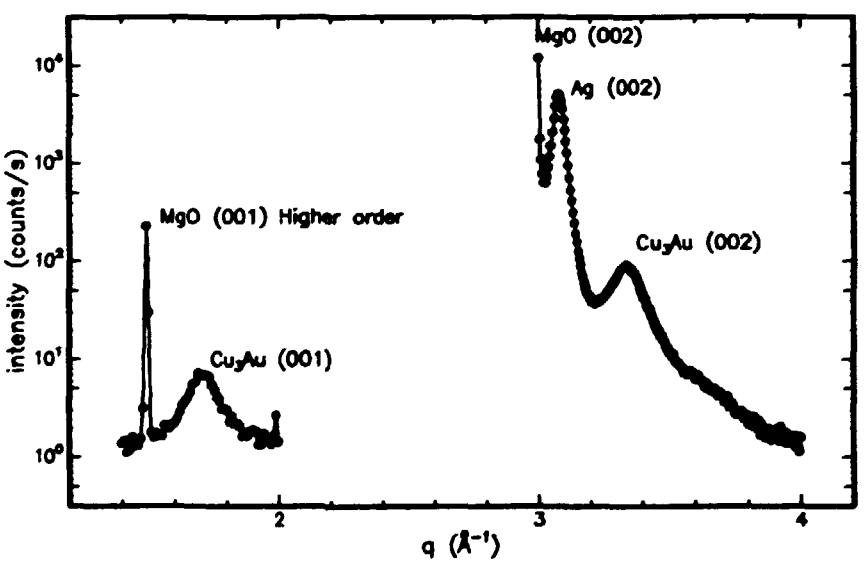


*Fig. 1. X-ray diffraction scan along the (00l) direction of a 170 Å Ag/200 Å $Cu_3Au$/230 Å Ag/MgO(001) structure.*

## 1.44 Metal-insulator-metal Structures

F. Olsen, IMFUFA, *University of Roskilde, Denmark*, and R. Feidenhans'l, *Department of Solid State Physics, Riso National Laboratory, Denmark*

Metal-Insulator-Metal (MIM) structures are used as planar electron emitters in multi-beam electron lithography. An applied field (of the order of $10^9$ V/m) between the metal electrodes allows electrons to tunnel through the insulator, and if the top metal electrode is thin enough, a fraction as high as $10^{-3}$ of the electrons will escape into vacuum. It is believed that a single crystalline MIM will produce the highest possible homogeneity in the electron emission profile. The samples are grown in the metal-MBE apparatus and they are tested at IMFUFA, University of Roskilde.

The epitaxial growth of V and Fe on MgO(001) have been perfected, but so far it has not been possible to grow an insulating insulator, neither MgO, nor $Al_2O_3$, in spite of different cleaning procedures, growth under oxygen pressure, exposure of insulator to atmosphere, or rotation of substrate under growth. The resistance of the insulator is always 10-20 Ω, independent of thickness and active area. Electron microscopy have not revealed any holes in the insulator layers. In spite of this, we have observed electron emission from two (out of ten grown) Au/Fe/MgO/Fe/MgO(001) MIMs, though highly inhomogeneous and of very low density.

Besides we have used Si(111) and Si(100) as substrates. Good epitaxial growth have been obtained after $NH_4F$ etch of the native oxide and growth of Ag and Fe/Ag on Si(111). MgO does not grow epitaxially neither on Si(111), nor on Ag(100), nor on Ag(111). Future plans include the use of GaAs substrates and *in situ* sputtering of MgO substrates.

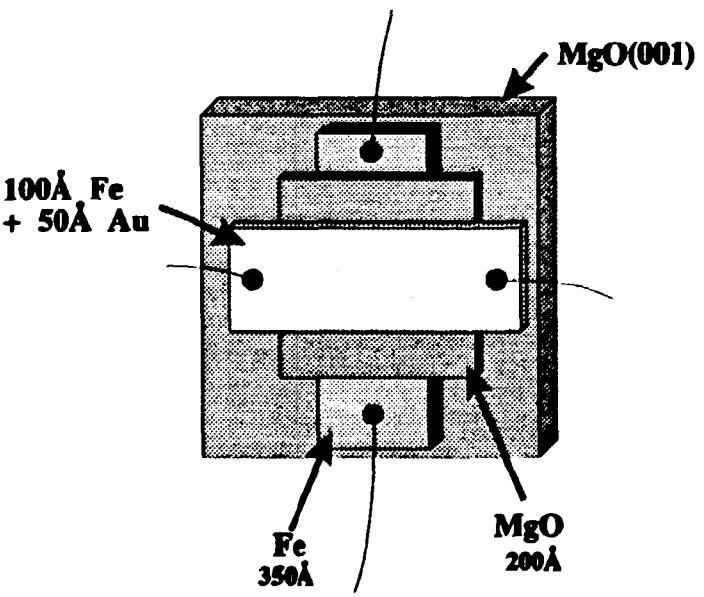


*Fig. 1. A sketch of a MIM structure, which has shown electron emission.*

## 1.45 Surface Melting of Caprolactam

S. Chandavarkar, H.A. van der Vegt, W.H. de Jeu, *FOM Institute for Atomic and Molecular Physics, Amsterdam, The Netherlands*, R.M. Geertman, *University of Nijmegen, The Netherlands*, and R. Feidenhans'l, *Department of Solid State Physics, Riso National Laboratory, Roskilde, Denmark*

In contrast to other systems[1], the surface melting of caprolactam ($C_6H_{11}ON$) has been reported[2] to proceed via a first-order "prewetting" transition 13 K below the bulk melting temperature ($T_m$= 69.2°C). In the X-ray reflectivity study carried out with a rotating anode source, there was also some indication that, at temperatures below this transition, the surface melting proceeds in a layer by layer fashion. This behaviour was interpreted in terms of a theoretical model where the competetion between short-range "layering" interactions and long-range van der Waals interactions results in the observed prewetting transition[3]. This model also predicts that, above the prewetting transition, capilliary waves at the liquid-vapour interface wash out the layering interactions and result in a continous power-law growth of the film thickness. Although a smooth increase in the film thickness was observed above the first-order transition, the nature of the divergence could not be determined as the increasing interfacial roughness made it impossible to acquire data within 3 K of $T_m$.

Additional synchrotron X-ray reflectivity experiments were therefore carried out at beamline BW2 in HASYLAB, Hamburg. In these experiments dramatic changes in the surface scattering were observed as the temperature was increased to 67°C. While below this temperature there was a well defined surface peak aligned with the bulk Bragg peak, at 67°C the surface peak was found to move *as a function of time* indicating changes in the "surface" orientation. Figure 1 shows a series of transverse scans at $2\theta = 2°$ ($Q$ = 0.134 Å$^{-1}$). In all cases the orientation of the bulk crystal, monitored by the (200) Bragg peak, did not change. In addition this behaviour was reproducible on both the crystals studied.

Subsequent cooling of the crystal to 61°C recovered the well defined surface peak. The reflectivity scans at this temperature at different times after cooling down are shown in Fig. 2. Initially the reflectivity shows no sign of the oscillations expected at this temperature possibly due to an extremely large interfacial roughness. However, over the course of the next ten hours, oscillations in the reflectivity became more pronounced indicating a surprisingly slow dynamics of the system. In addition to the data at these two temperatures the rotating anode data was also extended over a larger $Q$ range. A complete analysis of the data is currently under way.

[1] J.G. Dash, (1989). Contemp. Phys. **30**, 89.
[2] S. Chandavarkar, R.M. Geertman, and W.H. de Jeu, (1992). Phys. Rev. Lett. **69**, 2384.
[3] A.A. Chernov and L.V. Mikheev, (1988). Phys. Rev. Lett. **60**, 2488.

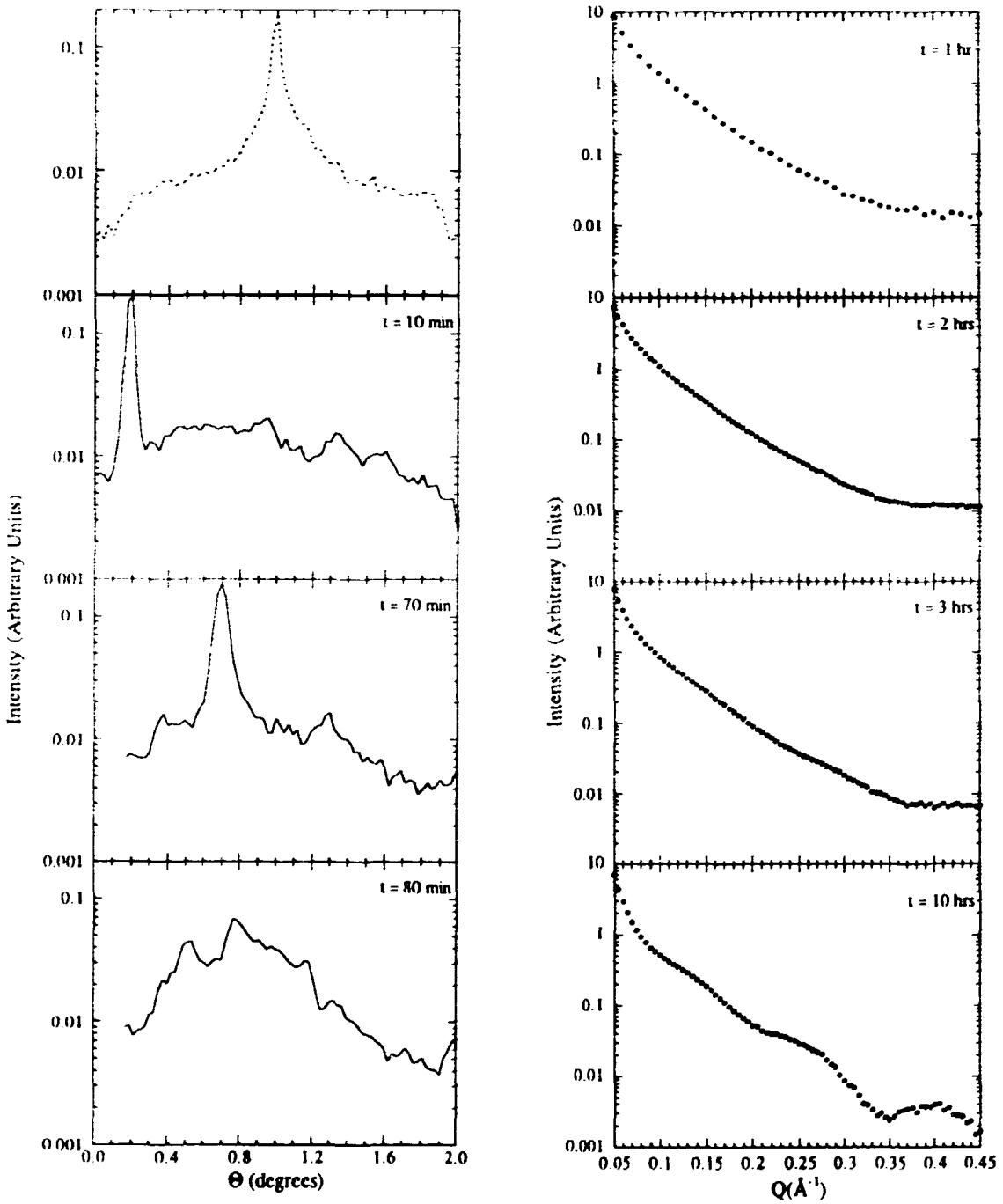


*Fig. 1. Left: Transverse scans at 2θ = 2 °. The scans at 67°C (solid line) are shown for different times after initially heating the crystal. The dashed line is a transverse scan at 65°C.*
*Right: Reflectivity scans at 61°C for different times after cooling down from 67°C.*

## 1.46 Investigations of Fe and V layers on MgO(001)

C.P. Jensen, M.C. Gerstenberg, R. Feidenhans'l, K.N. Clausen, *Department of Solid State Physics, Risø National Laboratory, Denmark*, and F. Olsen, *IMFUFA, University of Roskilde, Denmark*

Iron and vanadium have a very close lattice match with MgO(001) with a misfit within a few procent. Both grow epitaxially on MgO(001) with the (001) planes parallel to the MgO(001) surface and in-plane with the [100] directions parallel to the MgO[110] direction. We have studied the system in the metal-MBE (MBE=Molecular Beam Epitaxy) apparatus in the department. The evaporation of the metals were performed with electron beam evaporators. The pressure in the chamber during deposition was in $10^{-9}$ to $10^{-8}$ torr range, the base pressure in the chamber is in the low $10^{-10}$ torr range. The growth *in-situ* was studied by Reflecting High Energy Electron Diffraction (RHEED).

On top of the metal-films, MgO can be deposited stoichiometrically via electron beam evaporation and sandwich and multilayer structures can be fabricated. To characterize these structures, we have performed X-ray diffraction and X-ray reflectivity studies. An example is shown in the figure. X-ray reflectivity was performed at beamline BW2 in HASYLAB, Hamburg of a [50 Å MgO/100 Å $Fe]_3$ / 300 Å MgO / MgO(001) structure. A model for describing the data is in progress. Reflectivity measurements at the rotating anode source have also been performed. Furthermore, neutron diffraction measurements at TAS 7 have been performed in a feasibility study, showing that sufficient intensity is available to study the properties of these layers.

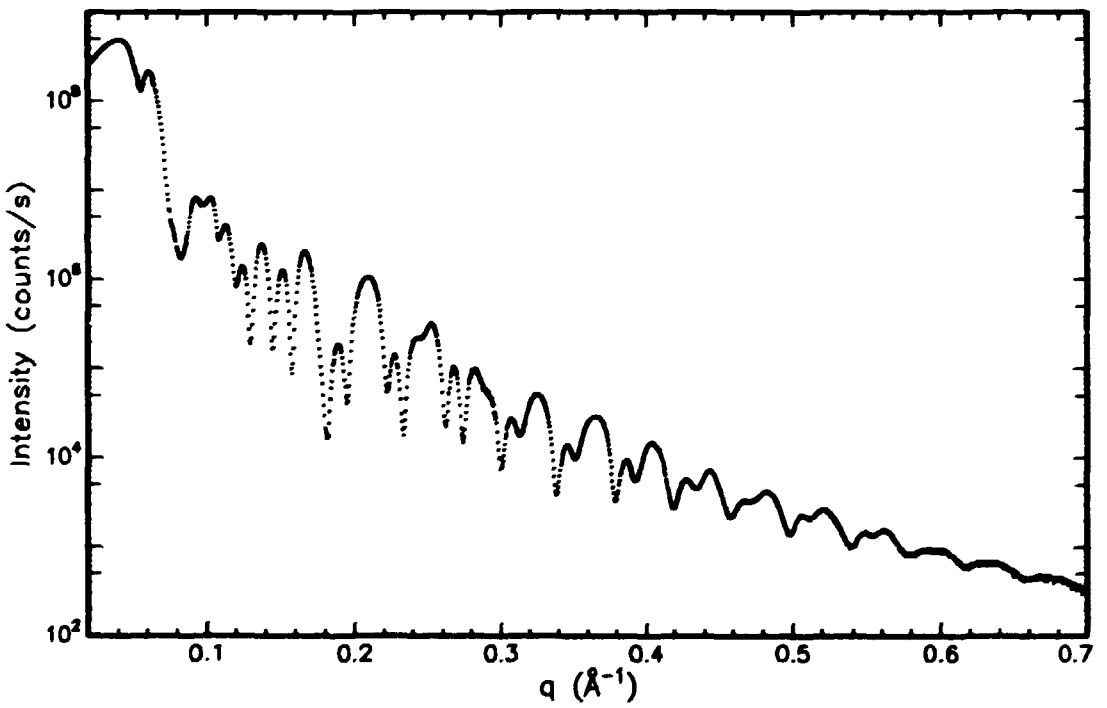


*Fig. 1. X-ray reflectivity measurements of a Fe/MgO multilayer structure. The measurements were performed at beamline BW2 in HASYLAB.*

## 1.47 Determination of the Density and the Amount of Hydrogen in Diamond-Like Carbon Films by X-Ray and Neutron Scattering

E. Findeisen, R. Feidenhans'l, K.N. Clausen, *Department of Solid State Physics, Risø National Laboratory, Denmark*, J.B. Hansen, M. Benzon, *NKT Research Center, Brøndby, Denmark*, and J. Goff, *Harwell Laboratory, Oxfordshire, England*

Specular reflectivity of neutrons or X-rays can be used to determine the scattering density profile of a material perpendicular to its surface. We have applied these techniques to study amorphous, diamond-like, carbon films. By the combination of these two methods one obtains not only the mass density, but also the amount of hydrogen in these films.

Diamond like phases are amorphous. The carbon is predicted to exist in two different kinds of hybridization states, corresponding to tetrahedral ($sp^3$) and trigonal ($sp^2$) bonding. Accordingly, most of the properties of diamond-like carbon (DLC) are between those of graphite and diamond. Due to the unique properties of these film, such as extreme hardness, high thermal conductivity, low friction and chemical inertness, they have potential applications as bearing surfaces and tribological surfaces, and in corrosion protection, electronics and optics.

The films were deposited onto silicon substrates in one of two ways: At the NKT Research Center laser ablation from a graphite target was used, with each sample produced under a different hydrogen partial pressure. At Harwell Laboratory low pressure oil was evaporated onto the silicon wafer with subsequent ion bombardment. The presence of hydrogen is thought to encourage tetrahedral bonding between carbon atoms. The latter deposition method leads, however, to a considerable amount of hydrogen in the film. Measuring this amount of hydrogen is, of course, an important part of characterizing these films.

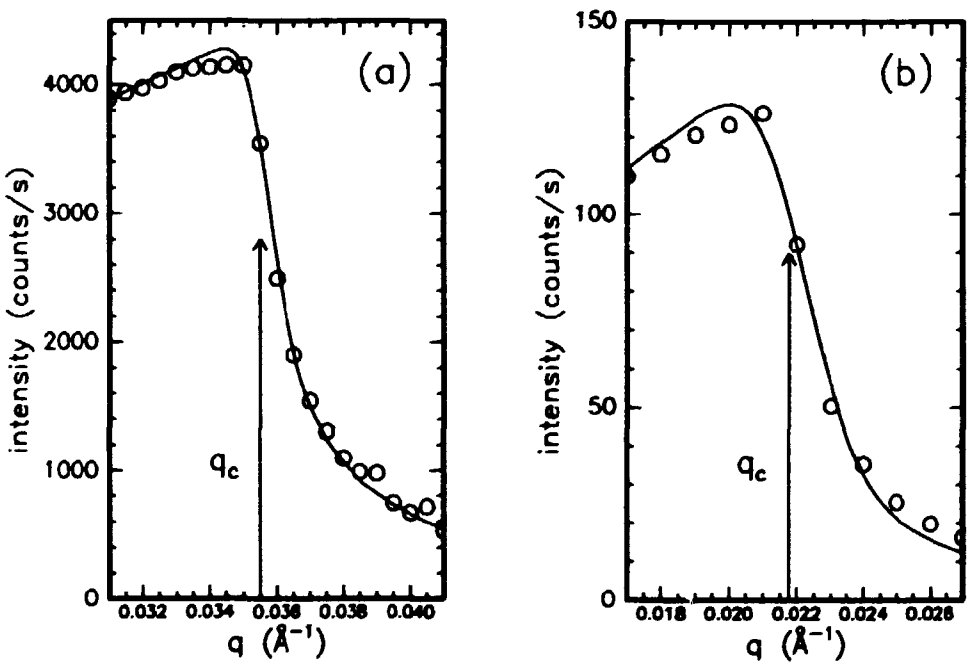


*Fig. 1. Example of the measured reflectivity (o) and fit ( ) for (a) X rays and (b) neutrons.*

In our case, measurements of the density indicate how graphite like ($\rho = 2.25$ g/cm$^3$) or diamond like ($\rho = 3.51$ g/cm$^3$) our films are. For X-rays there is total external reflection for all momentum transfer $q$ less than $q_c = 4\sqrt{\pi n_e r_e}$ (see Fig. 1), where $n_e$ denotes the number of electrons per volume (electron density), and $r_e$ the classical radius of the electron.

Neglecting the hydrogen, we can calculate the mass density as $\rho = n_e m_A/(Z N_A)$, with $m_A$ is the mass of a carbon atom, $N_A$ is Avogadro's number and $Z$ is the number of electrons per carbon atom. By fitting the reflectivity with a dynamical model[1], we obtain the mass densities. For all the laser ablated films, it is 2.8 – 3.0 g/cm$^3$. However, for the ion bombarded sample we find $\rho = 2.33$ g/cm$^3$.

For reflectivity with neutrons (at TAS8), we have $q_c = 4\sqrt{\pi N b}$, where $N$ denotes the average density of nuclei and $b$ the average scattering length. Especially $b$ depends sensitively on the concentration of hydrogen ($c$): in our case, $b = (1 - c)b_C + cb_H$, with $b_C = 0.665 \times 10^{-12}$ cm and $b_H = -0.375 \times 10^{-12}$ cm. Because $b_H < b_C$, the more hydrogen the films contain, the smaller is the critical momentum transfer ($q_c$). In Fig. 2 the momentum transfer is normalized by the calculated value of $q_c$ for no hydrogen, *i.e.* $q_c(c = 0) = 4\sqrt{\pi N b_C}$. By these methods the amount of hydrogen can be determined within an error of about 1 at.%.

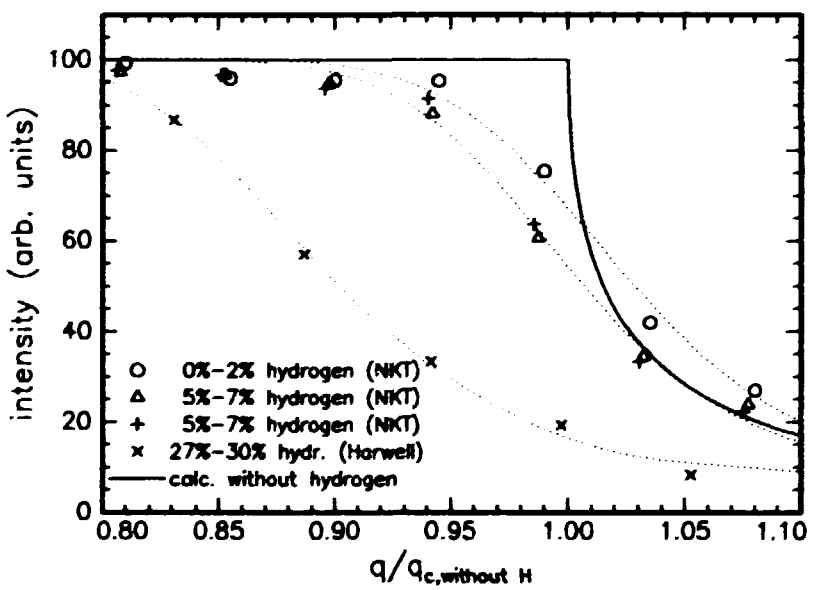


*Fig. 2. Neutron reflectivity of amorphous carbon films containing different amounts of hydrogen. The data of each sample are represented by a certain symbol and the corresponding fit[1] is shown as a dotted line. The solid line indicates the calculated reflectivity for no hydrogen and without taking instrumental resolution into account.*

[1] L. G. Parratt, (1954). Phys. Rev. **95**, 395.

## 1.48 Radial Distribution Function of Amorphous Diamond-like Carbon Obtained by X-ray Scattering

E. Findeisen, R. Feidenhans'l, M. Nielsen, *Department of Solid State Physics, Riso National Laboratory, Denmark*, M. Foss, *University of Århus, Denmark*, J.B. Hansen, and M. Benzon, *NKT Research Center, Brøndby, Denmark*

The structure of diamond-like carbon (DLC)[1] is thought to be a random covalent network, which can be described by the fraction of the two occurring hybridization states of the carbon. For values of the momentum transfer $q$, which correspond to the inverse atomic distances, the scattered intensity contains information about both the $sp^3/sp^2$ ratio and the average distances between carbon atoms.

The DLC films were prepared by laser ablation, using a graphite target as a precursor. In order to obtain a free-standing film, the silicon wafer, used as a substrate during the evaporation process, was etched away afterwards. As carbon is a weak scatterer for X-rays and because the films were less than 1 $\mu$m thick, the experiment was carried out at the intense wiggler beamline BW2 at Hasylab/Hamburg. In order to obtain a reasonable signal to background ratio, we had to use free-standing films, *i.e.* no scattering from a substrate, and a vacuum surrounding the sample, in order to reduce the air scattering.

Figure 1 shows the scattered intensity per atom $I_{eu}/N$ in electron units. Because of instrumental limitations the maximum momentum transfer was $q_{max} = 9$ Å$^{-1}$. However, at $q_{max}$ the intensity still oscillates around the solid curve, which is given by the sum of the incoherent compton scattering $i$ and the square of the atomic form factor $f$.

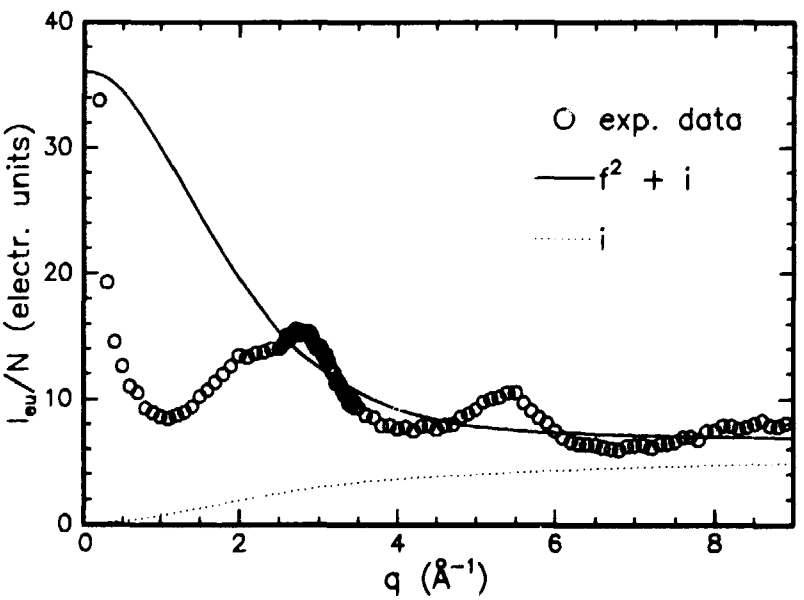


*Fig. 1. Scattered intensity (o), scattering for random distribution of the carbon atoms ( ) and compton scattering (···).*

The structure factor $S(q)$ is defined as

$$S(q) = \frac{I_{eu} - i}{f^2}.$$

If we denote the average mass density $\rho_0$, then the distribution function $\rho(r)/\rho_0$ is obtained mainly by Fourier transformation of the structure factor $S(q)$,

$$\rho(r)/\rho_0 = 1 + \frac{1}{2\pi^2 \rho_0 r} \int_0^\infty q(S(q) - 1) \sin(qr)\, dq.$$

Unfortunately the truncation of the $q$ range causes some oscillations in the distribution function, which makes the analysis more difficult.

The peaks in the distribution function $\rho(r)/\rho_0$ corresponds to shells of neighbours. By fitting the first two peaks with two gaussians, we obtain distances, which are very close to the corresponding values for crystalline diamond (see Table 1). However, there is a considerable difference compared to the graphite values.

| | DLC | diamond | graphite |
|---|---|---|---|
| 1. neighbour distance (Å) | $1.543 \pm 0.003$ | 1.545 | 1.418 |
| 2. neighbour distance (Å) | $2.509 \pm 0.008$ | 2.522 | 2.456 |

*Table 1. Comparison of the distances in DLC, crystalline diamond, and graphite.*

The area under the first peak of the radial distribution function $4\pi r^2 \rho(r)$ is equal to the average coordination number of the carbon (see Fig. 2). Our preliminary result is 3.35, *i.e.* 35% of the carbon atoms are $sp^3$ bonded.

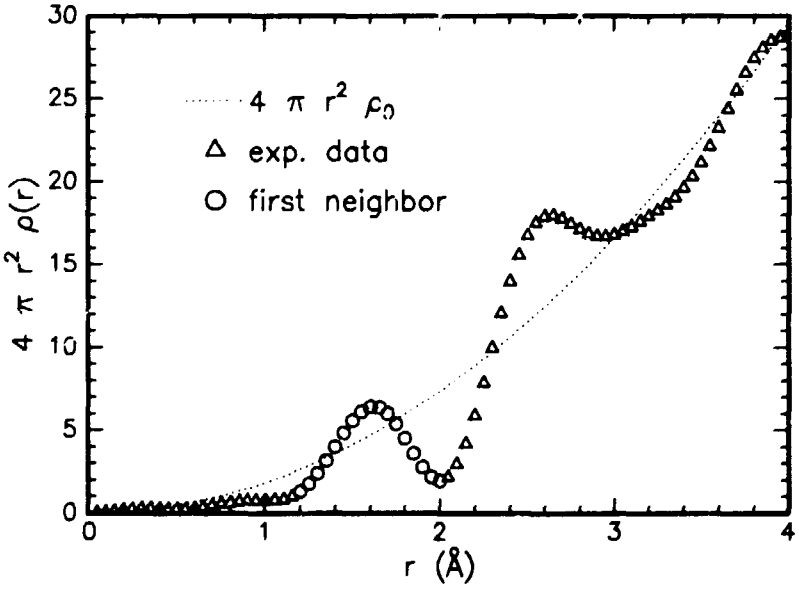


*Fig. 2. Radial distribution function of laser ablated diamond-like carbon.*

[1] see also contribution 1.47

## 1.49 Self-assembled Langmuir Monolayers and Trilayers of Arachidamide at the Air-formamide Interface

S. P. Weinbach, M. Lahav, L. Leiserowitz, *Department of Materials and Interfaces, Weizmann Institute of Science, Rehovot, Israel*, J. Als-Nielsen, and K. Kjær, *Department of Solid State Physics, Risø National Laboratory, Denmark*

We have designed monolayers to mimic the surface of a hydrogen bonded amide crystal, in order to study the role of solvent on the growth of such crystals. A monolayer is spread and serves as a model for the solution from which a three dimensional crystal grows. As part of this study of the structure of hydrogen bonding amphiphiles, we have compared grazing incidence X-ray diffraction (GID) and X-ray specular reflectivity (XR) data from arachidamide ($C_{19}H_{39}CONH_2$) spread at the air-formamide interface with data for the same material spread at the air-water interface.

For monolayers of arachidamide over water, over pure formamide, and over 70 mole% formamide subphases, GID patterns are shown in Fig. 1*a*, Bragg rods are shown in Fig. 1*b* (over pure water), Fig. 1*c* (over pure formamide) and X-ray specular reflectivity (XR) data in Fig. 1*d*. Over water subphases[1], the molecules spontaneously formed highly crystalline monolayers, with correlation lengths $\geq$ 1000 Å (resolution limited). The molecules pack in a unit cell with dimensions $a$ = 4.7 Å, $b$ = 8.7 Å, and are tilted by approximately 18° from the vertical. Over formamide the molecules pack in chain primitive rectangular unit cell with 5.0 Å, b = 7.5 Å (area per molecule $\simeq$ 18.5 Å$^2$) and the molecules oriented vertically. The same plane group was found for longer-chain amphiphiles over formamide (*cf.* next contribution). The FWHM profiles[2] (shown in Fig. 1*b,c*) indicate a film thickness of approximately 75 Å, which corresponds to three times the length of the straight, all-*trans* molecule, indicating that the crystallite is made up, at least in part, of *three molecular layers*. The XR data (Fig. 1*d*) confirm this finding: The position of the first minimum in the reflectivity curve of arachidamide over formamide is at approximately one third the $q_z$-value of that for arachidamide over water, thus indicating that the film is three times as thick. Preliminary fittings of both the GID and XR data suggest the coexistence of monolayers and trilayers in the presence of pure formamide subphase.

All GID experiments in this project were done at HASYLAB, DESY[2].

[1] S. Weinbach, (1993). "The effect of Subphase Carboxylic Acid and Amide Molecules on the Crystallinity of Self-Assembled Crystallites of Amphiphilic Amides at the Air-Solution Interface", *Manuscript in preparation.*

[2] Early experiments at beamline D4; recent measurements at the new undulator beamline BW1, which has much greater intensity, allowing the observation of many high order peaks which could not previously be distinguished from the background. This additional information will allow for more complete understanding of the system. Note that each peak represents the (vertical) $q_z$-integral of a Bragg Rod. The $q_z$-resolved data (not shown) for all these peaks samples the unit-cell structure factor throughout a sizeable volume of reciprocal space.

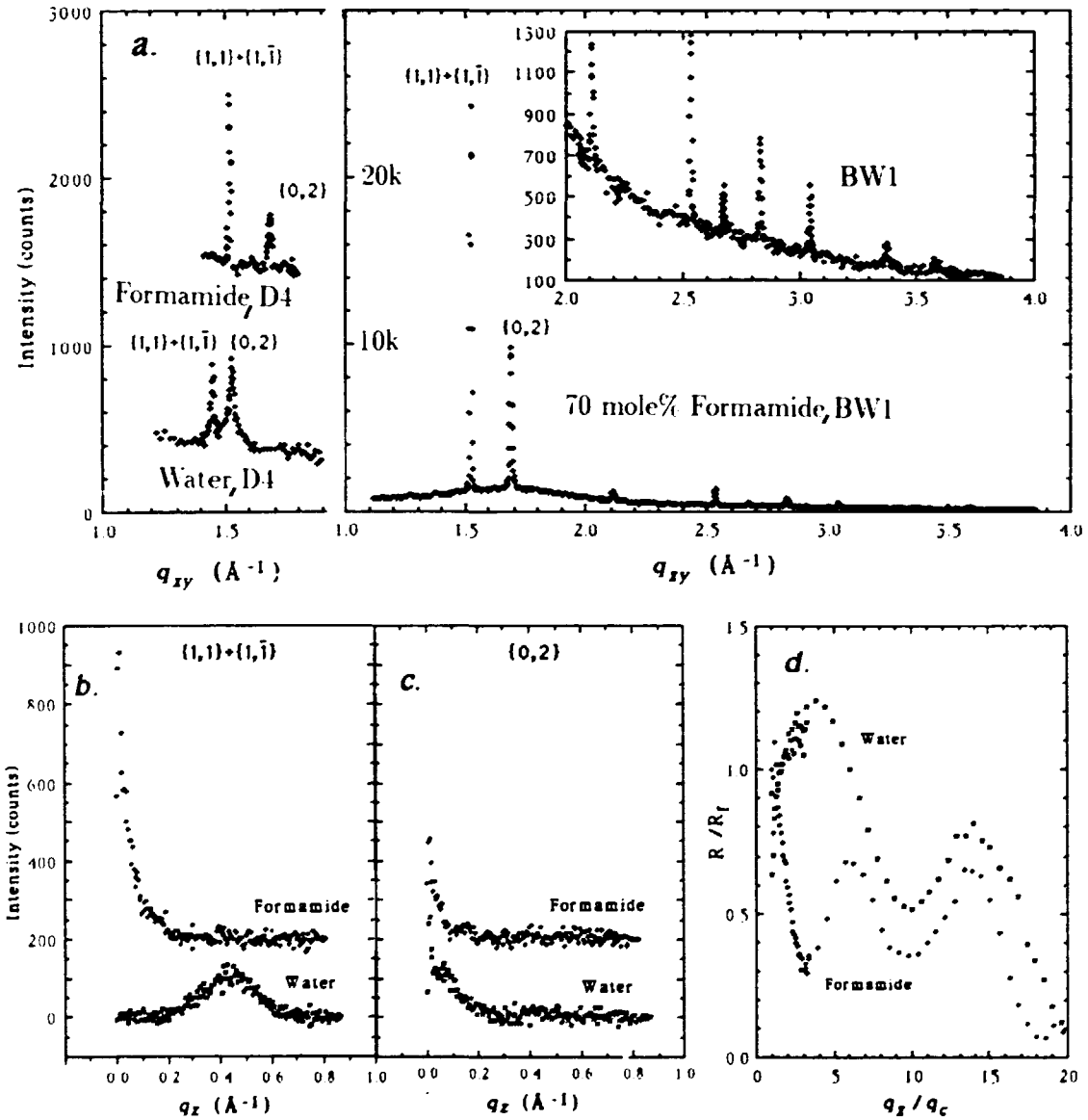


*Fig. 1. a) GID Bragg peaks from uncompressed arachidamide over water and over formamide (offset by 1000 counts) subphases, measured at HASYLAB beamline D4, and over 70 mole% formamide, measured at beamline BW1 (note different intensity scales in plot). The inset shows higher order peaks for arachidamide over 70 mole% formamide. b) Intensity profiles along the Bragg rods of the two reflections, the* $\{1,1\}+\{1,\bar{1}\}$ *at* $q_{xy} = 1.52$ Å$^{-1}$ *for water and at* $q_{xy} = 1.51$ Å$^{-1}$ *for formamide c) the* $\{0,2\}$ *at* $q_{xy} = 1.44$ Å$^{-1}$ *for water and at* $q_{xy} = 1.69$ Å$^{-1}$ *for formamide. d) X-ray specular reflectivity of uncompressed arachidamide over water and over formamide subphases at* $4 \pm 1$°C.

## 1.50 Self-assembly of Long-chain Amide and Carboxylic Acid Amphiphiles at the Air-water and Air-formamide Interfaces

S. P. Weinbach, M. Lahav, L. Leiserowitz, *Department of Materials and Interfaces, Weizmann Institute of Science, Rehovot, Israel*, J. Als-Nielsen, and K. Kjær, *Department of Solid State Physics, Risø National Laboratory, Denmark*

The crystallinity of two dimensional films at the air-aqueous liquid interface has been demonstrated by Grazing-Incidence X-ray Diffraction (GID). In order to expand the usefulness of this technique, and to learn more about crystallization from a variety of solvents, we have now studied such systems at the air-nonaqueous liquid interface. Because of its ability to form hydrogen bonds and excellent solvation properties as well as its high surface tension (58 mN/m at 20°C), we have chosen formamide as the first non-aqueous liquid to be studied. Here we report on structure of hydrogen bonding amphiphiles spread at the air-formamide interface, and amphiphiles spread at the air-water interface. Over both water and formamide subphases, triacontanoic acid ($C_{29}H_{59}CO_2H$) and triacontanoamide ($C_{29}H_{59}CONH_2$) molecules spontaneously formed highly crystalline monolayers, with correlation lengths $\geq$1000 Å (resolution limited). The observed Bragg peaks (Fig. 1) and Bragg rod profiles[1] of $C_{29}H_{59}CONH_2$ over both water and formamide and those of $C_{29}H_{59}CO_2H$ over formamide are strikingly similar, indicating very similar packing arrangements, while those of $C_{29}H_{59}CO_2H$ over water[2] are different. This can be understood in terms of the presence of hydrogen bonding networks within the crystallites of $C_{29}H_{59}CONH_2$. In addition to the hydrogen bonding network which may form within the crystallite, bound formamide molecules from the subphase may form a complementary hydrogen bonding network. While hydrogen bonding between $C_{29}H_{59}CO_2H$ molecules and water molecules undoubtedly takes place[2], no such network exists. Over formamide however, the bound subphase molecules may form hydrogen bonded cyclic mixed dimers with the amphiphiles, analogous to those found for amide amphiphiles. The bound molecules may then form a hydrogen bonded network in precisely the same manner, thereby imposing a packing arrangement which allows this network to occur.

All of these systems gave rise to two low-order reflections, indicating that the molecules pack in a primitive rectangular unit cell. The unit cells of $C_{29}H_{59}CONH_2$ over both water and formamide subphases and those of $C_{29}H_{59}CO_2H$ over formamide have dimensions $a = 5.0$ Å, $b = 7.5$ Å (area per molecule $\simeq 18.5$ Å$^2$) with a packing in which the molecules are nearly vertical. The carboxylic acid over water packs in a different unit cell, of dimensions $a = 5.53$ Å, $b = 7.44$ Å, and with the molecules tilted by $\sim 27°$ in the $a - c$ plane[2].

All GID experiments in this project were done at HASYLAB, DESY (*cf.* previous contribution, note [2]). The GID pattern of triacontanoamide over a water subphase, as measured at each of the beamlines D4 and BW1, is shown in Fig. 2.

[1] S. Weinbach, (1993) "Self-Assembled Langmuir Monolayers and Trilayers at the Air-Formamide Interface", *Manuscript in preparation.*
[2] F. Leveiller, D. Jacquemain, L. Leiserowitz, K. Kjær, and J. Als-Nielsen, (1992). "Towards a Determination at Near-Atomic-Resolution of Two-Dimensional Crystal Structures of Amphiphilic Molecules on the Water Surface", J. Phys. Chem., *In press.*

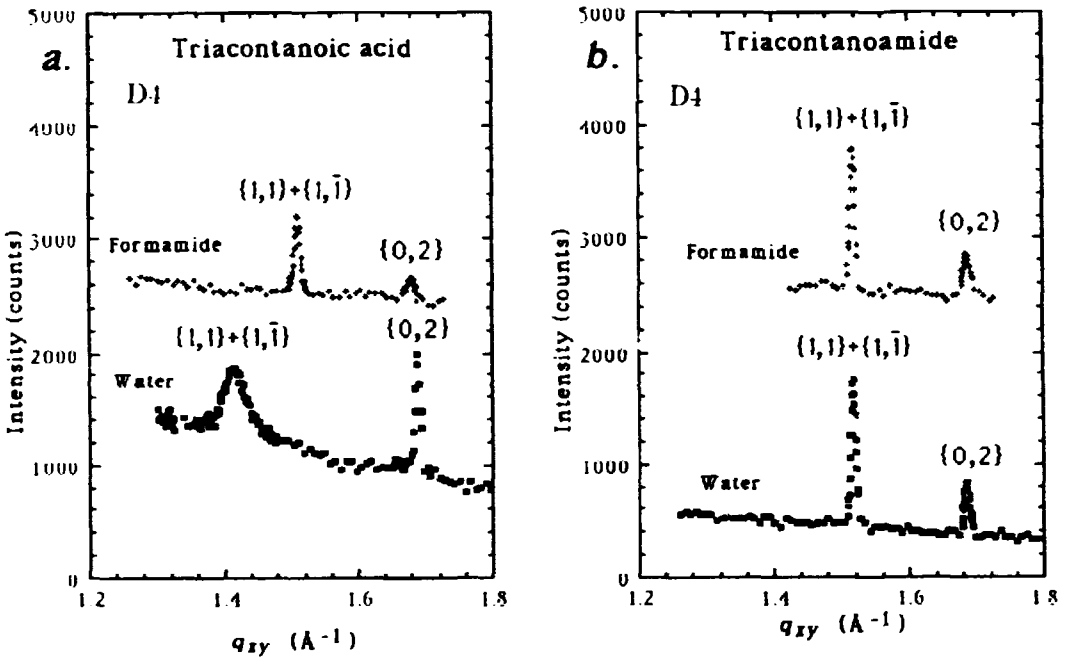


*Fig. 1. GID Bragg peaks of uncompressed a) triacontanoic acid and b) triacontanoamide at 4 ± 1°C over water and formamide (offset by 2000 counts) subphases. The assigned Miller indices are shown for each reflection. All measurements were performed at HASYLAB beamline D4.*

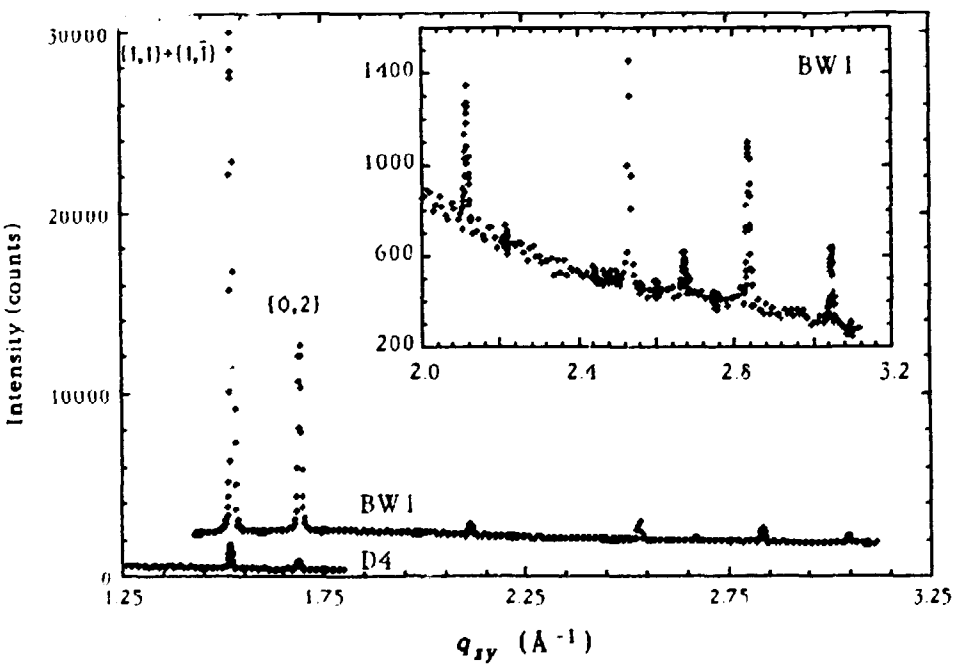


*Fig. 2. GID Bragg peaks of uncompressed triacontatoamide over water measured at beamline D4 (as in Fig. 1) and at beamline BW1 (offset by 1000 counts). Inset: Higher-order peaks measured at BW1.*

## 1.51 Langmuir Films of Surfactant Long-chain Alcohols

J. Majewski, I. Weissbuch, L. Leiserowitz, *Department of Materials and Interfaces, Weizmann Institute of Science, Rehovot, Israel*, J. Als-Nielsen, and K. Kjær, *Department of Solid State Physics, Riso National Laboratory, Denmark*

In connection with a study[1,2] of the ice nucleating properties[3] of Langmuir monolayers of surfactant long-chain alcohols, Grazing-Incidence X-ray Diffraction (GID) measurements were performed at the undulator beam line BW1 on monolayers of alcohols $C_nH_{2n+1}OH$ ($n$ = 31, 20, 16) on pure water at 2°C in order to determine the 2D-crystal structures of the monolayers and, eventually, reach an understanding of the ice-nucleating properties in terms of the crystal structures of the monolayers and the to-be-formed ice crystals. Further, we intend to determine the degrees of crystallinity of the monolayers by comparing the GID data with those from monolayers of $C_{29}H_{59}CONH_2$ on water[4] (the latter is believed to be 100 % crystalline). The GID pattern from $C_{31}H_{63}OH$ exhibited seven diffraction peaks above background. This is to be compared with two peaks obtained at the bending magnet beamline D4 (Fig. 1*a*). Fig. 1*b,c* shows data obtained at BW1 for the shorter-chain alcohols. These molecules are less well organized in the monolayers and so the resulting diffraction signals are weaker. Hence, the the high intensity of the BW1 beam was essential for obtaing good GID data from the $C_{16}H_{33}OH$ monolayer. The data are currently being analyzed.

[1] D. Jacquemain, F. Leveiller, S. P. Weinbach, M. Lahav, L. Leiserowitz, K. Kjær, and J. Als-Nielsen, (1991). J. Am. Chem. Soc. **113**, 7684.
[2] D. Jacquemain, S. Grayer Wolf, F. Leveiller, M. Deutsch, K. Kjær, J. Als-Nielsen, M. Lahav, and L. Leiserowitz, (1992). Angew. Chem. Int. Ed. Engl. **31**, 130.
[3] M. Gavish, R. Popowitz-Biro, M. Lahav, and L. Leiserowitz, (1990). Science **250**, 973.
[4] Contribution 1.50.

*Fig. 1. a)(next page) GID data for monolayers of $C_{31}H_{63}OH$ on water, obtained at beamlines D4 and (offset by 2000 counts) BW1. The inset shows higher-order peaks measured at BW1. Each peak represents the (vertical) $q_z$-integral of a Bragg Rod. The $q_z$-resolved data (not shown) for all these peaks samples the unit-cell structure factor throughout a sizeable volume of reciprocal space. b) Data for a $C_{20}H_{41}OH$ monolayer. BW1 beam line. c) Data for a $C_{16}H_{33}OH$ monolayer. BW1 beam line.*

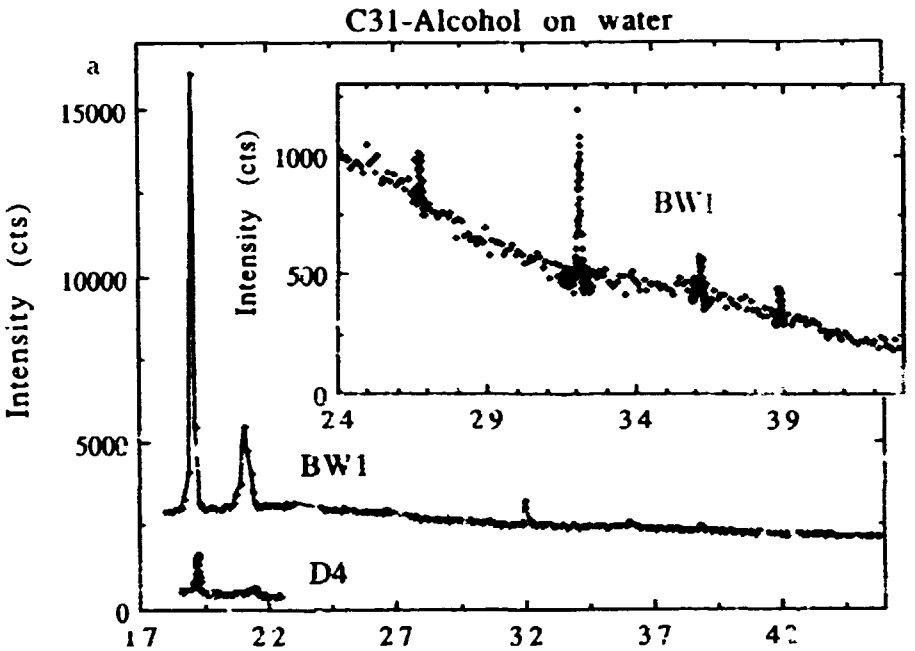


Fig. 1 a)

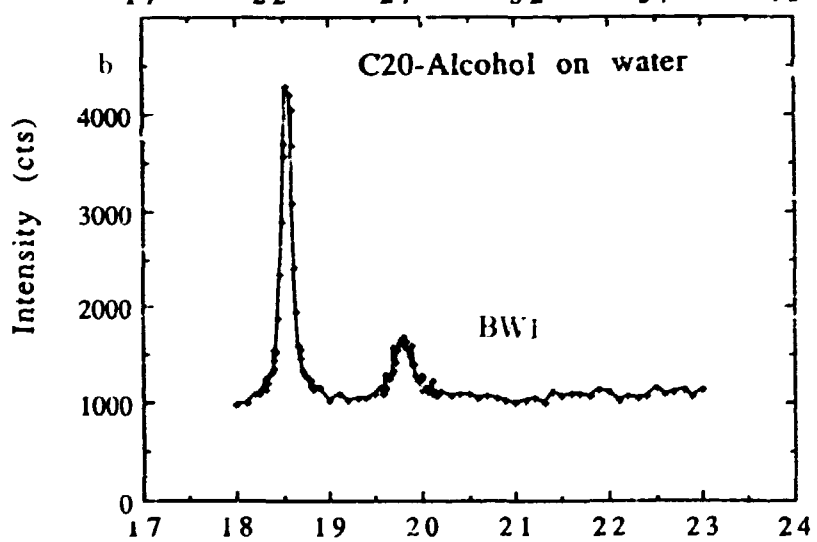


Fig. 1 b)

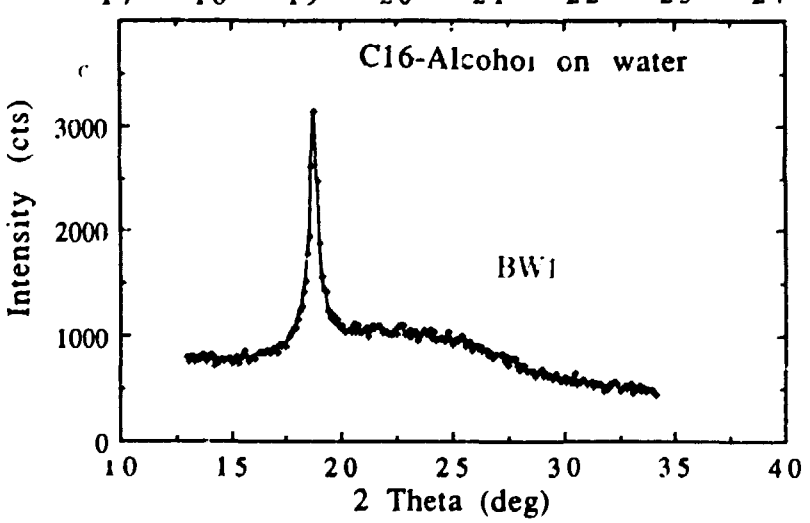


Fig. 1 c)

## 1.52 A Study of $Cd^{2+}$ and $Cl^-$ Ion Binding to a Mixed Monolayer of Octadecylamine and Stearic Acid

D. Gidalevitz, I. Weissbuch, M. Lahav, L. Leiserowitz, *Department of Materials and Interfaces, Weizmann Institute of Science, Rehovot, Israel*, J. Als-Nielsen, and K. Kjær, *Department of Solid State Physics, Risø National Laboratory, Denmark*

These studies are being undertaken as part of a program to determine the concentration profile of ions at the solid-liquid interface. Atomic ions (such as $Cd^{2+}$, $Zn^{2+}$, $Ca^{2+}$, $Cl^-$, $Br^-$, $I^-$) in solution have a pronounced effect on the growth and morphology of crystals containing polar groups (such as sulfates, phosphates, carboxylates or amino), because of preferred binding of the ions to the polar groups at particular faces of the crystal. In order to elucidate whether or not the ions are bound at the crystal surface in an ordered manner we are making use of monolayers to simulate the surface of the crystal and so it is of interest to investigate the binding of ions to the monolayers.

The headgroups of the mixed monolayer Octadecylamine ($CH_3(CH_2)_{17}NH_2$) / Stearic Acid ($CH_3(CH_2)_{16}COOH$) (O/SA) mimic a crystal face of the solid material *β*-alanine ($^+H_3N(CH2)_2COO^-$). The binding of $Cd^{2+}$ and $Cl^-$ ions to the O/SA monolayer has been investigated by means of specular X-ray reflectivity (XR) and Grazing Incidence X-ray Diffraction (GID). XR measurements were done on the liquid surface X-ray reflectometer at the Weizmann Institute on a 1:1 mixture of octadecylamine and stearic acid at normal pH over a number of aqueous subphases with different concentrations of cadmium chloride and was aimed at investigating the ability of the ions to bind to the monolayer. The main result of fitting the reflectivity curves is that increase of the $CdCl_2$ concentration in the subphase leads to a corresponding increase of ions bound to the monolayer, reaching full coverage at 0.1 M $CdCl_2$ concentration in water (Fig. 1).

GID measurements were done at the liquid surface diffractometer at beamline D4 at HASYLAB, Hamburg, on O/SA monolayers over water and over an 0.1 M aqueous solution of $CdCl_2$. The results are shown in Fig. 2. The two reflections were indexed as $\{1,1\}+\{1,1\}$ and $\{0,2\}$ corresponding to a rectangular 2-D structure of the O/SA monolayer. Over a pure water subphase the two reflections are of almost equal intensity (*cf.* Fig. 2*a*). Note that over the $CdCl_2$ solution subphase the intensity of the $\{0,2\}$ reflection disappears almost completely (Fig. 2*b*). This change could be modeled by structure factor calculations showing that the $Cd^{2+}$ and $Cl^-$ ions occupy specific ordered sites under the monolayer. Measurements over a subphase containing $CdCl_2$ and *β*-alanine molecules indicated that the intensity of the $\{0,2\}$ peak was only partially reduced (Fig. 2*c*). This could be interpreted in terms of scavenging of $CdCl_2$ by *β*-alanine. This latter experiment rather shows binding of $Cd^{2+}$ and $Cl_2$ ions to the face of solid *β*-alanine in the presence of *β*-alanine solute molecules in the solvent.

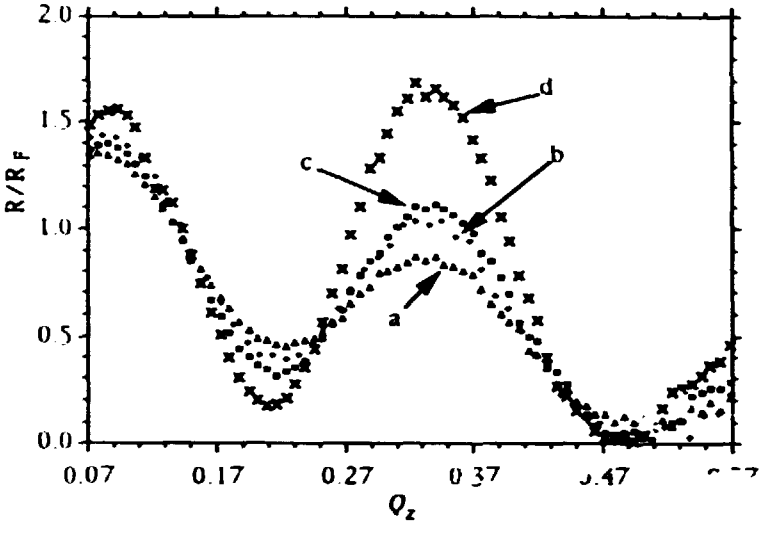


*Fig. 1. Normalized X-ray reflectivity for O/SA monolayers over: a) pure water, b) $10^{-3}$ M, c) $10^{-2}$ M and d) $10^{-1}$ M $CdCl_2$ solutions in water.*

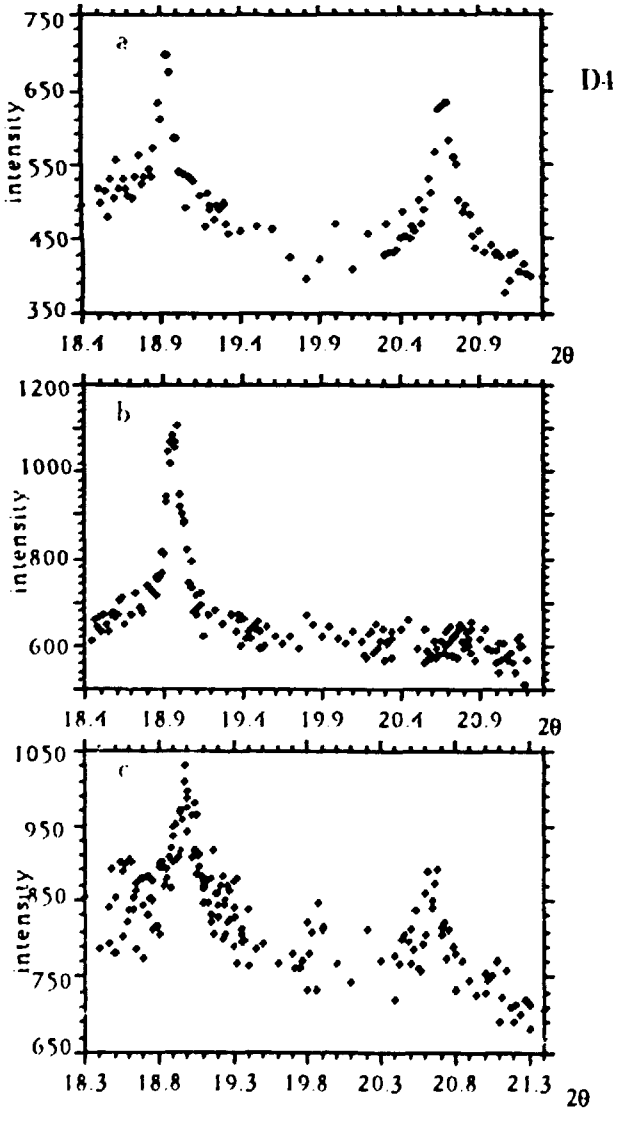


*Fig. 2. GID data for O/SA monolayers over: a) pure water, b) 0.1 M $CdCl_2$ solution in water and c) subphase containing 4 M of β-alanine and 0.1 M of $CdCl_2$.*

## 1.53 2D-Crystalline Monolayers of p-Octadecyl-oxy-benzoic Acid Studied by Grazing-Incidence X-ray Diffraction

I. Weissbuch, M. Lahav, L. Leiserowitz, *Department of Materials and Interfaces, Weizmann Institute of Science, Rehovot, Israel*, J. Als-Nielsen, and K. Kjær, *Department of Solid State Physics, Riso National Laboratory, Denmark*

Monolayers of the surfactant p-octadecyl-oxy-benzoic acid, when present at the surface of solutions of p-hydroxybenzoic acid, were found to induce oriented crystallization of p-hydroxybenzoic acid monohydrate crystals at the surface of the solution[1]. This effect was explained in terms of a model in which the monolayer molecules pack a layer arrangement similar to that of the specific face by which the crystals were attached to the interface.

In order to verify this hypothesis, and to further understand the process, the 2D crystal structure of monolayers of the surfactant was studied by grazing-incidence X-ray diffraction at beam-line BW1 at HASYLAB, Hamburg. Figure 1 shows the results for a monolayer spread on the solution at 14°C, in an uncompressed state. The data are currently being evaluated.

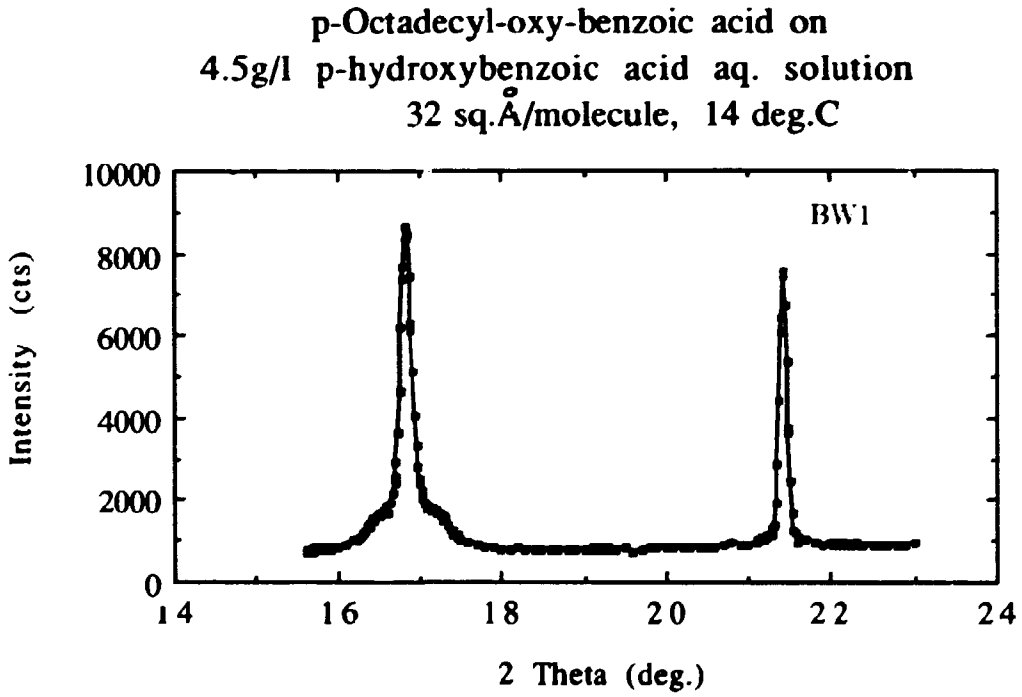


*Fig. 1*

[1] I. Weissbuch, G. Bercovic, L. Leiserowitz, and M. Lahav (1990). J. Am. Chem. Soc. **112**, 5874.

## 1.54 Structural Studies of Langmuir-Monolayers of Electron Donor and Acceptor Molecules

T. Bjornholm, N. B. Larsen, *Centre for Interdisciplinary Studies of Molecular Interactions, University of Copenhagen, Denmark*, J. Als-Nielsen, and K. Kjær, *Department of Solid State Physics, Riso National Laboratory, Denmark*

Two-dimensional interfaces between electron donor and acceptor molecules possess nonlinear optical properties associated with the intermolecular contact between the donor and acceptor layers[1]. By means of the Langmuir-Blodgett technique such layers may be conveniently formed and studied with various donor and acceptor molecules. The physical properties depend crucially on the orientation of the individual molecules in the Langmuir layers and structural information is therefore very important. Such information may be obtained from synchrotron X-ray studies of monolayers of the electron donor and acceptor molecules of interest.

Grazing angle X-ray reflectivity measurements performed at beam line D4 at HASYLAB, Hamburg, for a monolayer of the donor molecule depicted in Fig. 1, show good agreement with the reflectivity calculated for an orientation of the molecules which allows the hydrophilic protonated amine to be in contact with the water surface (Fig. 1). In-plane diffraction measurements revealed no lateral order in the monolayer plane, presumably due to the spatial misfit between the large head groups as compared to the alkyl chains.

The "edge on" molecular orientation deduced is not ideal for achieving an effective electronic contact to other adjacent layers in multilayered films and these structural studies hence give important information for understanding and improving the properties of the materials.

[1] T. Bjornholm, T. Geisler, J. Larsen, and M. Jorgensen, (1992). J. Chem. Soc., Chem. Commun. **1992**, 815;
T. Bjornholm, T. Geisler, J. Larsen, M. Jorgensen, K. Bruntfeldt, K. Schaumburg, and K. Bechgaard, (1992). Synth. Meth., *in press*.
T. Bjornholm, N. B. Larsen, F. E. Christensen, P. Sommer-Larsen, T. Skettrup, and M. Jorgensen, (1992). Synth. Meth., *in press*.

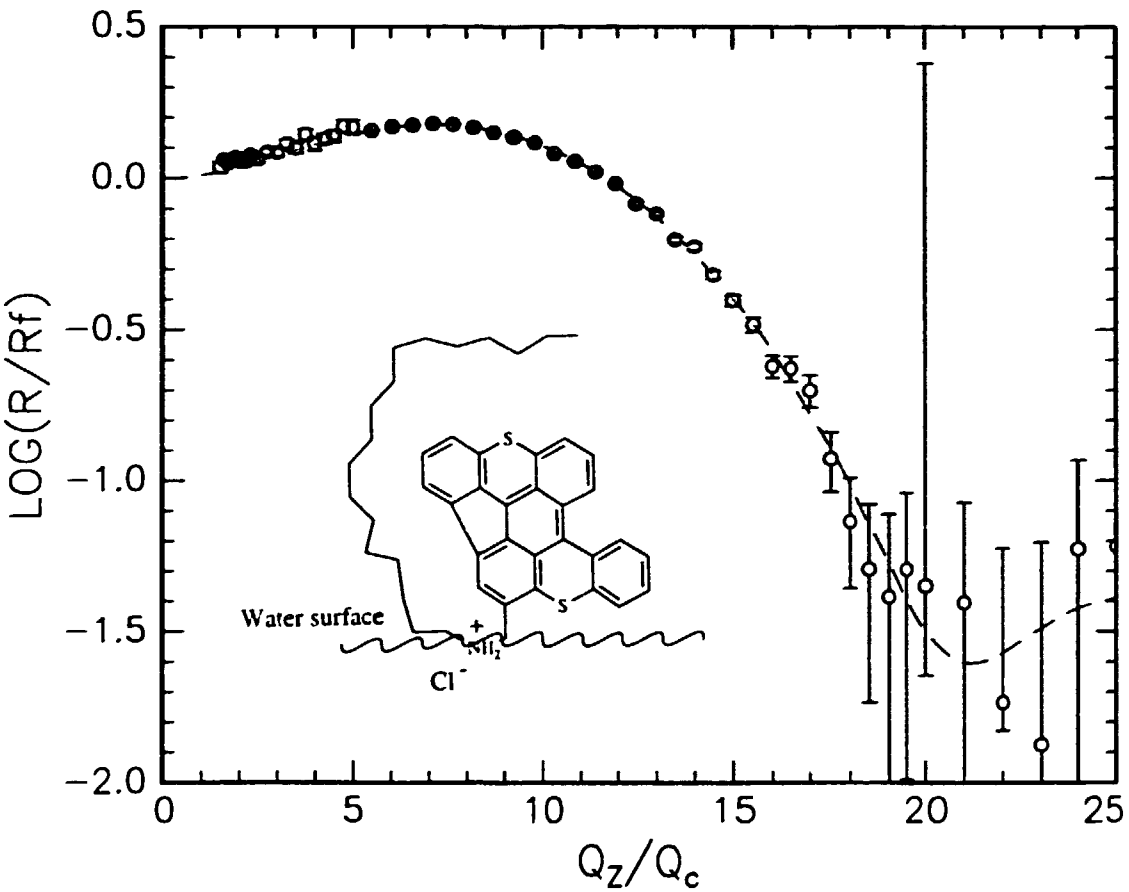


*Fig. 1. Comparison of the measured and calculated reflectivity from a monolayer of poly-aromatic donor molecules derived from corbiene. The orientation of the molecules derived from the fit is also indicated in the figure.*

## 1.55 The Influence of Chirality on the Structure of a Lecithin Monolayer

C. Böhm, H. Möhwald, *Physical Chemistry Department, Mainz University, Germany*, J. Als-Nielsen, and K. Kjær, *Solid State Physics Department, Riso National Laboratory, Denmark*

Grazing incidence X-ray diffraction measurements (GID) of phospholipid monolayers have been performed using the liquid-surface diffractometer at the undulator beamline BW1 in HASYLAB at DESY, Hamburg. Phospholipid monolayers at the air/water interface are model systems for biological membranes. The phospholipids consist of two hydrophobic chains which are linked by a hydrophilic head group (Fig. 1). In recent studies[1] only information about the arrangements of the aliphatic tails of the monolayer molecules could be deduced from the GID powder pattern and no direct information about the head group ordering was obtained. Information thereon could be deduced from a comparative study of the chiral resolved (L: Left-handed molecules only) and racemic (DL: mixtures of Left- and Right-handed molecules) monolayers of DPPE (α-dipalmitoylphosphatidylethanolamine). A centered rectangular unit cell was found in the case of the racemate and a symmetry reduction to a oblique unit cell for the enantiomer, probably due to ordering in the head group region[2]. Now we have investigated monolayers of chiral resolved and of racemic DPPC (α-dipalmitoylphosphatidylcholine). The choline differs from the prevous investigated ethanolamine only in the head group where the H-atoms of the amine N-atom are replaced by methylen groups ($CH_3$). Due to these bulky groups the head group area is larger than the area of the two hydrocarbon chains. Fig. 1 depicts the structural formula of this compound. Fig. 2 shows the GID results for L-DPPC (left) and DL-DPPC (right) at 15°C and a surface pressure of 30 mN/m. The same features were observed for both monolayers with no apparent influence of the chiral carbon atom on the monolayer structure. Two distinct Bragg peaks were detected at $Q_{xy} = 1.32$ and 1.47 Å$^{-1}$ corresponding to $d$ spacings of 4.63 and 4.29 Å. The latter peak has its maximum at $Q_z \simeq 0$ Å$^{-1}$ whereas the intensity of the first peak extends in the region $0.6 \leq Q_z \leq 1.0$ Å$^{-1}$. From the maximum position in $Q_z$ for this peak a molecular tilt of the hydrocarbon chains of 30° towards their nearest neighbours can be deduced which is in agreement with previous results[3]. This extremely large tilt angle, which is due to the large head group, might explain why no chiral influence was observed for this monolayer.

[1] H. Möhwald, R. M. Kenn, D. Degenhardt, K. Kjær and J. Als-Nielsen, (1990). Physica A **168**, 127; and C. A. Helm, P. Lippmann-Krayer, H. Möhwald, J. Als-Nielsen, and K. Kjær, (1991). Biophys. J. **60**, 1457.

[2] C. Böhm, H. Möhwald, L. Leiserowitz, J. Als-Nielsen, and K. Kjær, (1992). Biophys. J., *in press*.

[3] C. A. Helm, H. Möhwald, K. Kjær, and J. Als-Nielsen, (1987). Europhys. Lett. **4**, 697; and D. Vaknin, K. Kjær, J. Als-Nielsen, and M. Lösche, (1991). Biophys. J. **59**, 1325.

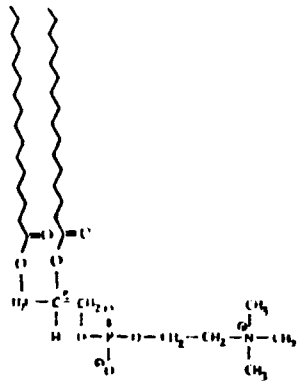

*Fig. 1. Structural formula of DPPC. The chiral C-atom is marked by an asterisk.*

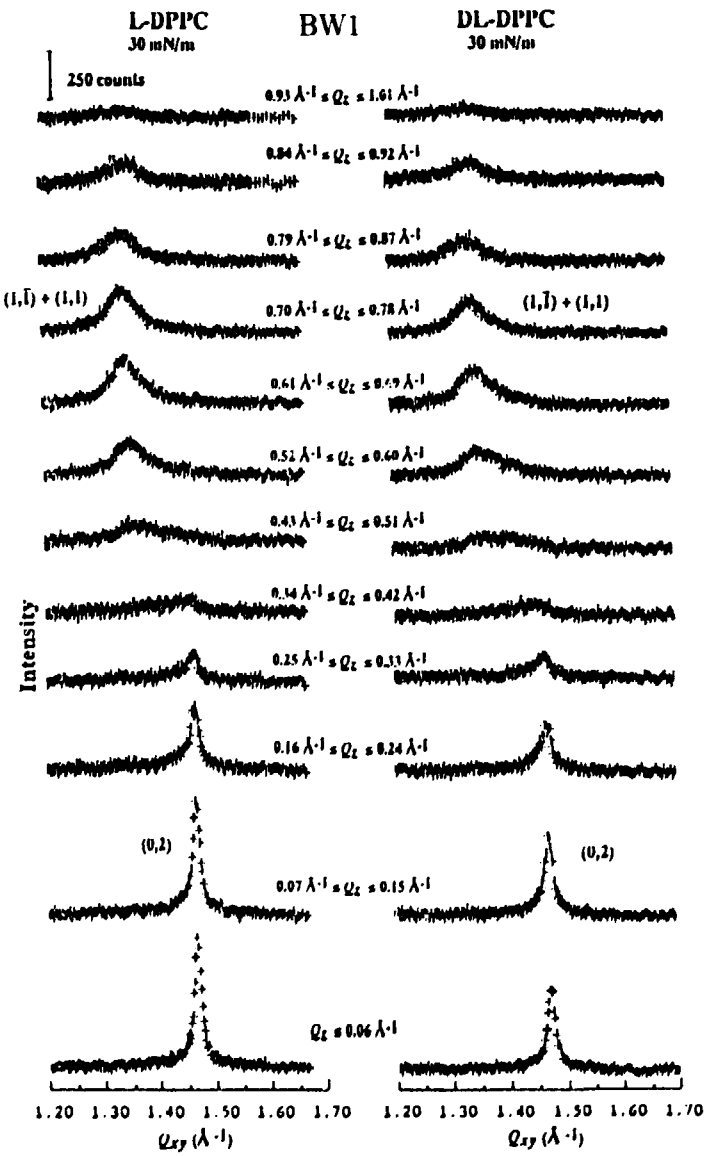


*Fig. 2. GID data (intensity versus horizontal momentum transfer $Q_{xy} = 2\pi/d$) of the chiral resolved L-DPPC (left) and the racemic mixture DL-DPPC (right) monolayer at the air/water interface. Both measurements were carried out at 30 mN/m and 15°C.*

## 1.56 Crystalline Phases in Monolayers of Triple-chain Lecithins on Water

C. Böhm, A. Dietrich, H. Möhwald, *Physical Chemistry Department, Mainz University, Germany*, R. Rietz, G. Brezesinski, *Physical Chemistry Department, University of Halle-Wittenberg, Germany*, J. Als-Nielsen, and K. Kjær, *Solid State Physics Department, Riso National Laboratory, Denmark*

Monolayers of phospholipids are of wide interest due to their importance in biological systems. They enable investigations of the principal features determining the structures of membranes and thin films. In particular, studies of branched chain phospholipids have contributed many important results concerning lipid phases and miscibility properties[1]. The crystalline phases of a triple-chain lecithin (Fig. 1, left) have been investigated by means of Grazing Incidence X-ray Diffraction (GID) measurements using the liquid-surface diffractometer at beamline BW1 in HASYLAB at DESY, Hamburg. Although the phase diagram of the triple-chain lecithin (Fig. 1, right) is qualitatively similar to those of nonbranched lipids, *e.g.* 1,2-dipalmitoylphosphatidylcholine (DPPC), one might expect considerable structural differences: Due to the side chain in the branched compound the area per molecule is larger than the area required by the head group, in contrast the situation for the nonbranched lecithins. Hence, for the branched choline two-dimensional ordering is not hindered by any head group repulsion. The expected structural differences are supported by fluorescence measurements[2] of the monolayer at the air/water interface: where Domain shapes different monolayers were found. Figure 2 shows the GID results for the low temperature phase at 16 mN/m and 10°C and in the so-called liquid crystalline (LC) phase at 32 mN/m and 15°C. At low temperature two diffraction peaks at $Q_{xy} = 1.47$ Å$^{-1}$ and $Q_z \geq 0.25$ Å$^{-1}$ and at $Q_{xy} = 1.44$ Å$^{-1}$ and $Q_z \simeq 0$ Å$^{-1}$ were observed corresponding to $d$-spacings of 4.28 4.34 Å, respectively (Fig. 2, left). The cell dimensions of $a = 5.04$ chains can be deduced by indexing the peak at high $Q_z$ as the coinciding $\{1,1\} + \{1,1\}$ reflections and the one at $Q_z \simeq 0$ Å$^{-1}$ as the $\{0,2\}$ reflection of a rectangular unit cell with the chains tilted towards their nearest neighbours. In the LC phase the two peaks are even closer in $Q_{xy}$, $Q_{xy} = 1.475$ Å$^{-1}$ ($d = 4.26$ Å) for low $Q_z$ and $Q_{xy} = 1.462$ Å$^{-1}$ ($d = 4.29$ Å) for high $Q_z$. This is in strong contrast to the nonbranched choline which was investigated under similar conditions (see previous contribution) and were two well resolved diffraction peaks were observed at $Q_{xy} = 1.32$ analysis is under way.

[1] G. Brezesinski, B. Dobner, H.-D. Dörfler, M. Fischer, S. Haas, and P. Nuhn (1987). Chem. Phys. Lipids **43**, 257.

[2] A. Dietrich , H. Möhwald, W. Rettig, and G. Brezesinski (1991). Langmuir **7**, 539.

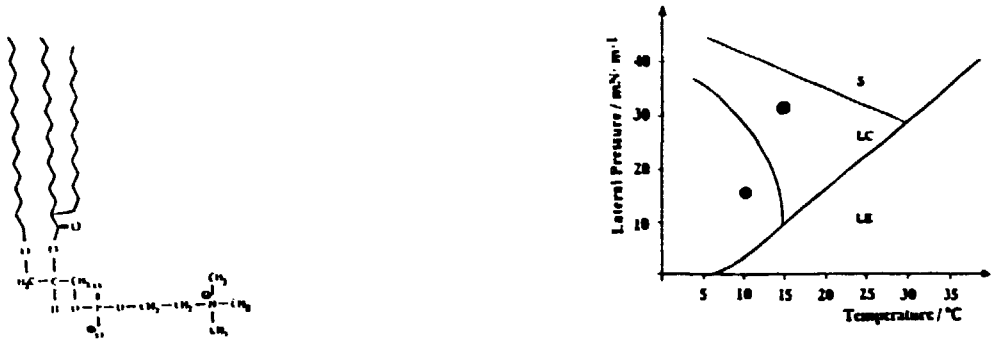


*Fig. 1. Structural formula (left) and phase diagram (right) of the triple-chain lecithin L-2-hexadecyl-1-(2-tetradecylpalmitoyl)glycero-3-phosphocholine. The dots mark points where diffraction data (Fig. 2) were taken.*

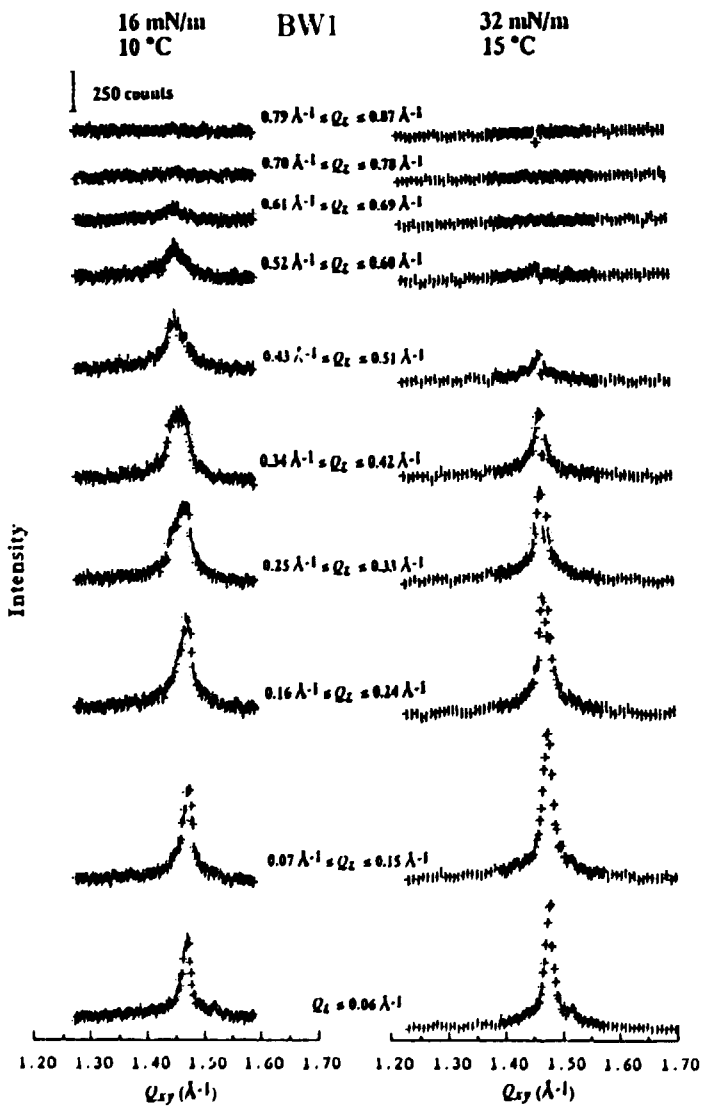


*Fig. 2. GID data (intensity versus horizontal momentum transfer $Q_{xy} = 2\pi/d$) of the triple-chain monolayer at 16 mN/m and 10°C (left) and 32 mN/m and 15°C (right). Data are shown partially resolved in the vertical momentum transfer $Q_z$.*

## 1.57 Control of the Structural Organization of Self-assembled Protein Monolayers at Functionalized Surfaces

M. Lösche, M. Piepenstock, A. Diederich, H. Ringsdorf, C. Erdelen, E. Rump, *Institutes for Physical and Organic Chemistry, Mainz University, Germany*, D. Vaknin, *Physics Department, Ames Laboratory, Iowa, USA*, and K. Kjær, *Solid State Physics Department, Risø National Laboratory, Denmark*

Neutron and x-ray reflectivity measurements have been carried out to characterize the structural organization of self-assembled monolayers of a protein, streptavidin (SA), at aqueous surfaces functionalized with lipids presenting the proteins' natural ligand, biotin, to the fluid subphase. Systematic studies have been conducted to determine the experimental parameters which control the two-dimensional (2D) protein concentration at the interface, the protein hydration within the monolayer, and the distance of the protein monolayer from the functionalized interface.

Foremost, reflectivity measurements have provided unambiguous evidence for the formation of *mono*-molecular protein layers in such systems[1]. Detailed analyses of the reflectivity data were performed in terms of molecular models, by coupling the scattering lengths of the system components to their partial volumes. These volumes were either known from experiments, as in the case of some lipid components[2] and the electrolytic subphase, estimated from computer models, as in the case of the receptor lipids, or, as in the case of the protein, determined[3] from the simultaneous refinement of a general model describing neutron[1] and X-ray reflectivity data (Fig. 1) from identically prepared systems. It was thus possible to determine the water-excluded volume of SA in the aqueous medium with high precision[3]. This enabled both a more correct assessment of the interface structure reported earlier[1] and systematic studies on the control of this structure.

We have varied the length of the spacer moiety between the biotin and its lipid anchor, and have investigated the impact of binary mixtures of functionalized and non-functionalized lipids at the interface. Also, we have *fine-tuned* the organization of protein layers by using lipid molecules with *very* long spacer moieties and controlling the lateral pressures exerted on these lipids. Finally, we have examined the effect of isotopically substituted water subphases or lipid hydrocarbon chains on the structural organization of the protein at the interface. Our conclusions are as follows:

(1) The protein surface density is most effectively controlled by the *effective spacer length* between the biotin and the lipid. When the biotin is immediately bound to the lipid, as in the compound B-BOCEC,[1] the protein density is low, $\sim 1/5000$ Å$^{-2}$. With lipids bearing a caproyl spacer (B-cap-DPPE, added length $l \sim 8$ Å), an increase by $\sim 60\%$ was found and the protein is already densely packed. The reason is probably an increase in flexibility of the bound SA to adjust to its environment within the protein monolayer. Regardless of the spacer length, the protein monolayer was found to be located close to the lipid, and the lipid head groups were dehydrated. As inferred from space filling, the hydration of the protein within the monolayer is inversely related to the protein density.
(2) The introduction of lipids with unfunctionalized head groups (dimyristoylphosphatidylcholine, DMPC) into the lipid monolayer in binary mixtures with B-cap-DPPE (which reduces the *effective* spacer length and introduces electric dipole moments

in-between the relatively hydrophobic spacer moieties) leads back to a reduction of the protein density. Whereas, with the pure functionalized lipids, no water was detected between the protein and the lipid interface layer, the hydrophilic cholines lead to a swelling of the lipid head group region, thus uncoupling the protein layer from the interface. Steric interference between the cholines and the functionalized spacer is *not* the main reason for this uncoupling, since a qualitatively similar observation was made in binary mixtures with cholesteroles, which include a (smaller) dipole moment in their *very* small (-OH) head group.

(3) With lipid molecules bearing a very long spacer moiety (an ethylene-oxide heptamer, $l \sim 30$ Å), we were able to control the distance between the protein and the interface via the lateral pressure $\pi$ exerted on the lipid monolayer prior to protein injection into the subphase: Whereas at $\pi = 8$ mN/m, the slightly hydrophobic spacer is tightly packed and dehydrated, the data are consistent with a distance between protein and the interface of $\sim 10$ Å at $\pi = 25$ mN/m ($\sim 15$ water molecules in the lipid head group).

(4) Isotopic substitutions of both the subphase molecules ($D_2O$ vs. $H_2O$) or the lipid hydrocarbon methylenes ($CD_2$ *vs.* $CH_2$) affect the protein organization to a lesser extent ($\sim 10-15$ % variation in lateral density).

(5) After transfer to suitable solid substrates, protein monolayer systems can be studied by electron diffraction, and are found to show high translational order[4]. With this technique, we have verified the protein surface density as determined from reflectivity measurements, concurrently showing that the protein is organized in a 2D "crystal-like" arrangement.

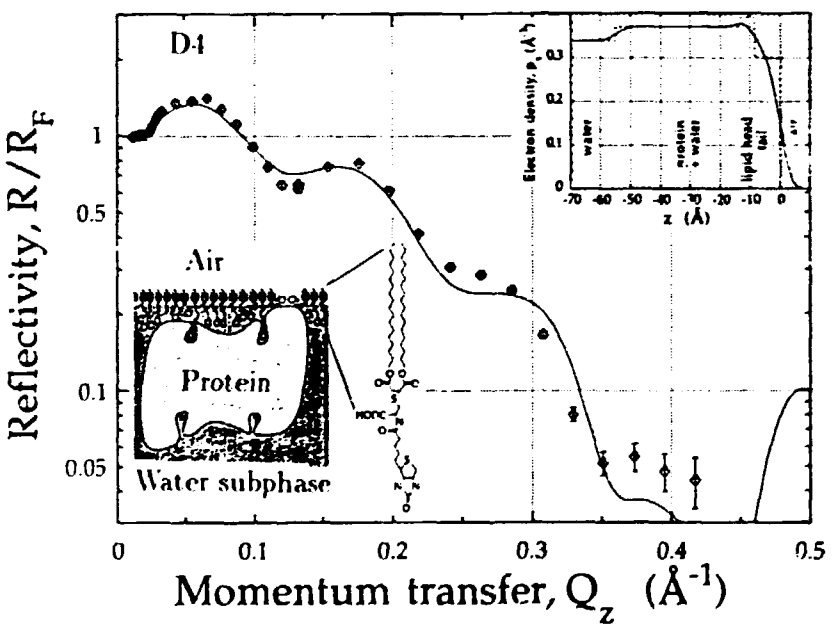


*Fig. 1. X-ray reflectivity data (points), normalized to the reflectivity of the bare subphase, for a functionalized lipid monolayer with bound protein monolayer. The full line corresponds to the scattering density in the top inset, and the bottom inset depicts the geometry as deduced[3] from both neutron[1] and X-ray reflectivities.*


[1] D. Vaknin, J. Als-Nielsen, M. Piepenstock, and M. Lösche, (1991). Biophys. J. **60**, 1545; and Riso report R-610(EN), 67.

[2] D. Vaknin, K. Kjær, J. Als-Nielsen, and M. Lösche, (1991). Biophys. J. **59**, 1325.

[3] D. Vaknin, K. Kjær, H. Ringsdorf, R. Blankenburg, M. Piepenstock, A. Diederich, and M. Lösche, *submitted for publication*.

[4] S. A. Darst, M. Ahlers, P. H. Meller, E. W. Kubalek, R. Blankenburg, H. O. Ribi, H. Ringsdorf, and R. D. Kornberg, (1991). Biophys. J. **59**, 387.

## 1.58 Fullerene-amine Adduct Monolayers at Air-water Interfaces, Studied by Neutron and X-ray Reflection and X-ray Diffraction

D. Vaknin, J. Wang, R. A. Uphaus, *Physics and Chemistry Departments, Ames Laboratory, Iowa, USA*, M. Lösche, *Institute for Physical Chemistry, Mainz University, Germany*, and K. Kjær, *Solid State Physics Department, Risø National Laboratory, Denmark*

Neutron and X-ray reflection measurements and surface-pressure isotherms of spread films of fullerene-amine adducts ($C_{60}$-$(NH_2C_{12}H_{25})_x$, $x \simeq 4$, *cf.* Fig. 1*b*) suggest that single monolayers of these materials can be formed on water surfaces. By contrast, neutron reflection and surface pressure vs. area studies of spread films of pure $C_{60}$ on water surfaces indicate an inhomogeneous multilayered structure. Fig. 2 shows, for a monolayer of the $C_{60}$-dodecyl adduct, the neutron and X-ray reflectivities (normalized to the Fresnel reflectivity of the corresponding substrates). The solid curves represent the calculated reflectivties assuming the scattering density depicted in the insets of Fig. 2. The scattering density profiles were obtained by a nonlinear least square fitting procedure using one global model for all three data sets shown in Fig. 2 (neutron reflectivity on $H_2O$ and on $D_2O$ and X-ray reflectivity on $H_2O$). This global model is defined in terms of the structural dimensions of three layers of scattering density and their chemical contents. All three reflectivities indicate at least one prominent box of higher scattering density which we associate with $C_{60}$. This box is interpenetrated by up to 27 water molecules which presumeably adhere to the fullerene surface. The two boxes on either side of the $C_{60}$ include on average two amine chains. The box at the air interface is dry while the one next the water contains water molecules. This analysis suggests that, on average, at least four amine chains react with each fullerene. Grazing-Incidence X-ray Diffraction data (Fig. 1) of the same monolayer indicate that the $C_{60}$-derivaties are laterally largely uncorrelated. The X-ray data were obtained at the BW1 undulator beam line at HASYLAB, DESY, Hamburg, and the neutron data at the DR3 reactor at Risø. The data analysis is still ongoing.

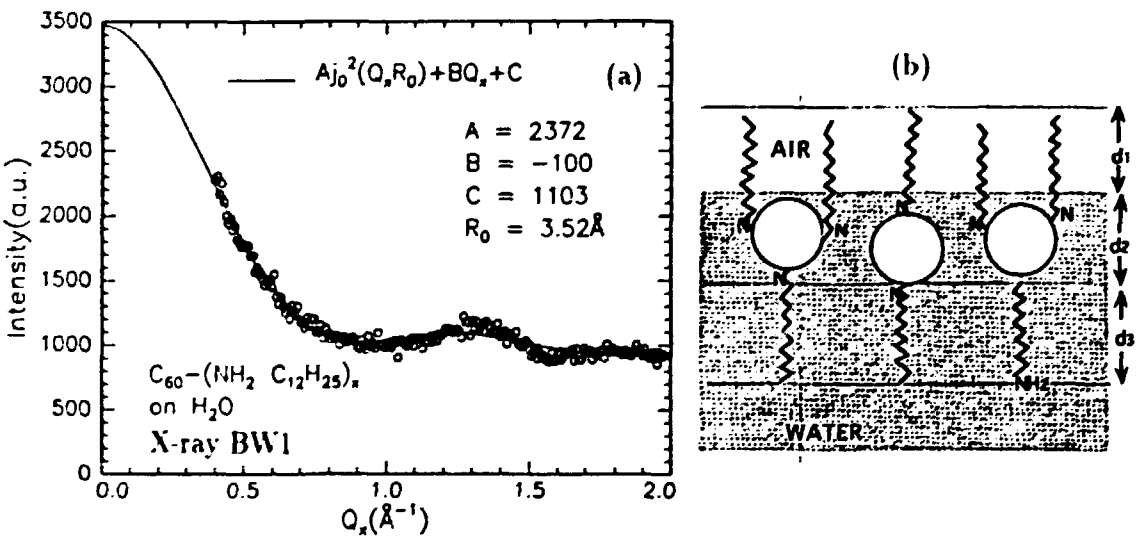


*Fig. 1. a) Grazing-Incidence X-ray Diffraction data (points) from a monolayer of $C_{60}$-dodecyl adduct on $H_2O$. The data are nearly described by the form factor (full line) of a spherical-shell model of the molecules, with no correlations between the fullerenes included. b) Geometrical model deduced from the reflectivity data of Fig. 2.*

(a)

(b)

(c)

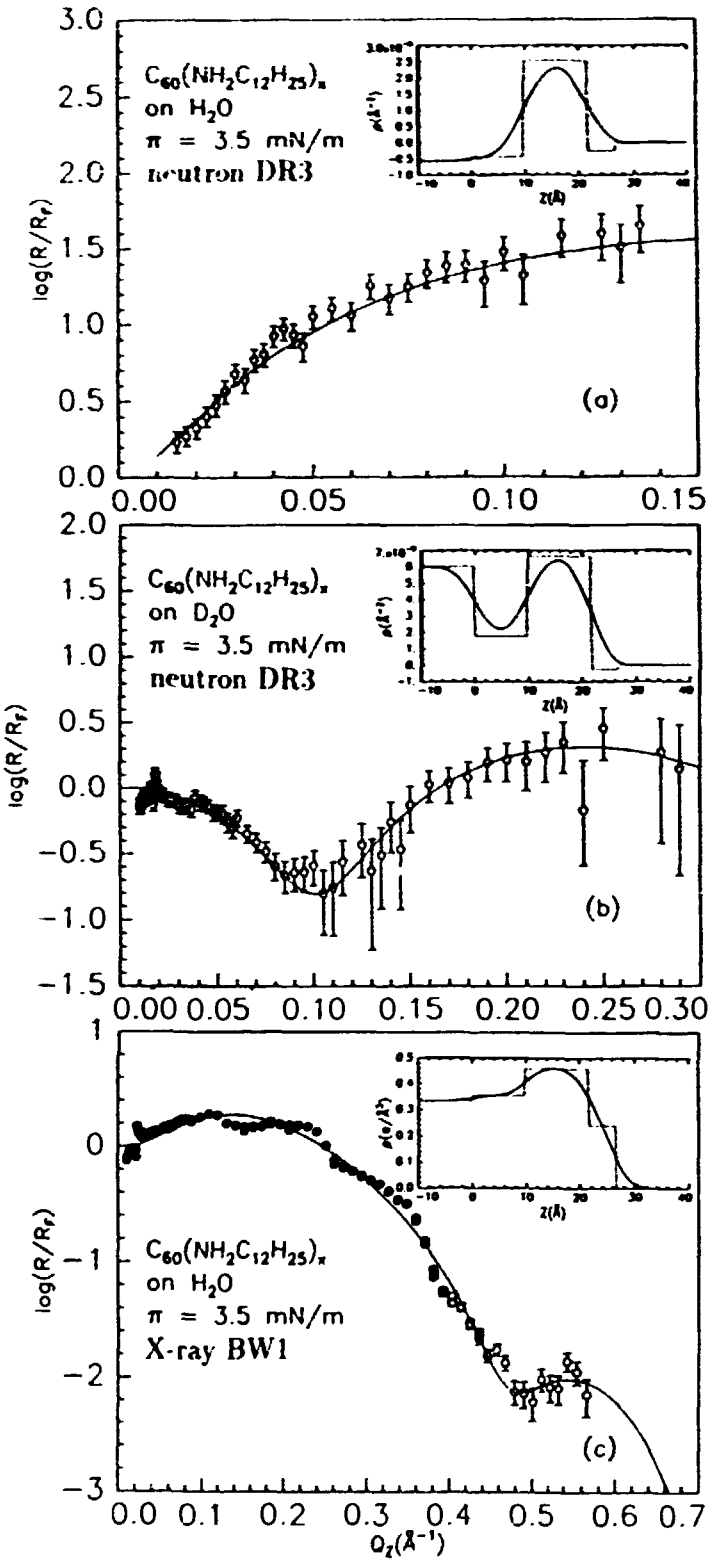


*Fig. 2. a) Neutron reflectivity of a monolayer of $C_{60}$-dodecyl adduct on $H_2O$ and b) $D_2O$, normalized to the Fresnel reflectivity of the corresponding subphase. c) X-ray reflectivity of $C_{60}$-dodecyl adduct normalized to the Fresnel reflectivity of $H_2O$ The solid curves are reflectivities calculated from the scattering densities depicted in the insets.*

## 1.59 On the Origin of Complex Phase Behavior in Block Copolymer Melts

F. S. Bates, K. Koppi, J. H. Rosedale, I. W. Hamley, *Deptartment of Chemical Engineering and Material Science, University of Minnesota, USA*, K. Almdal, *Materials Department, Riso National Laboratory, Denmark*, and K. Mortensen, *Department of Solid State Physics, Riso National Laboratory, Roskilde, Denmark*

In a recent publication[1] we have identified a complex phase behavior in a poly(ethylene-propylene)-poly(ethylethylene) (PEP-PEE) diblock copolymer where the volume fraction of PEP is $f$=0.65. Four distinct phases exist as a function of temperature, with a lamellar ordered phase at the lowest temperature. This finding is inconsistent with the generally accepted concepts of universal block copolymer phase behavior based on the parameters $f$ and $\chi N$ alone, where $\chi$ and $N$ are the Flory-Huggins interaction parameter and the degree of polymerization, respectively. Close to the order-to-disorder transition, extended neutron scattering experiments on shear oriented samples give evidence of fluctuation-induced formation of two distinct ordered hexagonal mesophases[2]. For the highest temperatures, SANS data show a hexagonally packed cylinder structure, whereas a lamellar phase with in-plane hexagonal modulation is observed at slightly lower temperatures.

A prominent feature of the PEP-PEE block copolymer system is the asymmetry in block coil dimensions, *i.e.* difference in the statistical segment length between the blocks. For equal molar mass the radius of gyration of a PEP homopolymer is 44% larger than a corresponding PEE homopolymer. As the volume of the domains in a microstructure is fixed by the overall composition the packing problem presented by the asymmetry in block coil dimension cannot easily be relieved. We have examined the robustness of the complexity in the phase behavior in the PEP-PEE system at $f$=0.65. The value characterizing the molecular weight polydispersity: $M_w/M_n$ is increased by mixing two $f$=0.65 PEP-PEE samples with different molar mass. Differences in the block length distribution are another possible perturbation of the system which is introduced by mixing two PEP-PEE block copolymers of equal molar mass but with $f$=0.53 and $f$=0.75, respectively in such a manner that the overall composition is $f$=0.65. Whereas all samples are characterized by lamellar phases at the lowest temperatures, and disordered phases at the highest temperatures, the complexity in intermediate phases appear to depend critically on perturbing the block length distribution, whereas increasing the overall $M_w/M_n$ have only small effect.

[1] K. Almdal, K.A. Koppi, F.S. Bates, and K. Mortensen, (1992). Macromolecules **25**, 1743

[2] I.W. Hamley, K.A. Koppi, J.H. Rosedale, F.S. Bates, K. Almdal, and K. Mortensen, (1992). Fluctuation induced phasetransitions in an ordered block copolymer melt. *submitted*

## 1.60 Phase Behavior of PEO-PPO-PEO Triblock-copolymer Dissolved in Water

K. Mortensen, *Department of Solid State Physics, Riso National Laboratory, Denmark*

The amphiphilic character of triblock-copolymers made of poly(ethylene oxide) (PEO) and poly(propylene oxide) (PPO) changes substantially as a function of temperature. This leads to interesting phase behavior when the block-copolymers are dissolved in water: micelle formation above a critical temperature and critical concentration, and an apparent "inverse crystallization" characteristic as the micellar liquid "freezes" into a cubic crystal at elevated temperatures, characterized by true long-range correlation in the bond-angle correlation, but absence of long-range order in the bond-length correlation[1]. At higher temperatures a phase of hexagonally packed rods is observed, but between the two crystalline states, a liquid channel appear. It is shown that the micelle concentration depends linearly on both polymer-concentration and temperature, and the cubic crystal is formed whenever the phase-line corresponding to a micellar volume fraction $\phi$=0.53 is crossed, in agreement with crystallization of hard-sphere colloidal suspensions. If the poly-crystalline phases are exposed to shear, they coherently transform into single-crystals. Thus, by performing the scattering experiment under shear, unique insight is obtained in the phase diagram including melting and crystallization into single crystalline states[2].

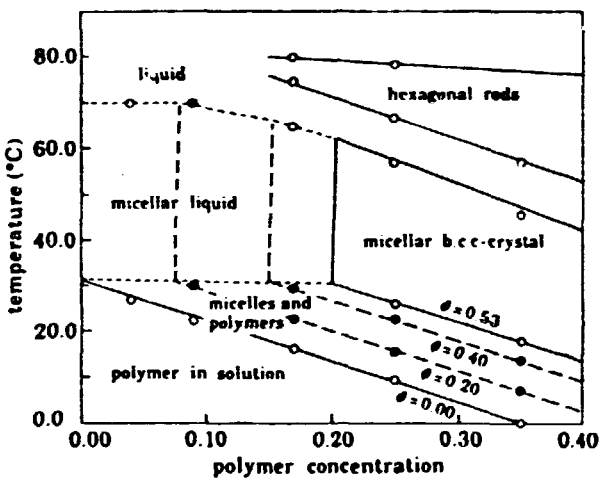


*Fig. 1. Phase diagram of aqueous suspension of PEO-PPO-PEO (P85), showing the fully dissolved polymers at low temperature and low concentration, the critical micellation concentration/temperature $c_{cm}/T_{cm}$-line ($\phi$=0), the $\phi_c$=0.53 transition to bcc micellar crystal, and the high temperature hexagonal phase. At T~60 °C a liquid phase appear between the crystalline bcc and hexagonal phases.*

[1] K. Mortensen, W. Brown, and B. Nordén, (1992). Phys. Rev. Letters **13**, 2340.
[2] K. Mortensen, (1992). Europhys. Letters **19**, 599.

## 1.61 Triblock Copolymers in Aqueous Solution. The Influence of Relative Block Size

K. Mortensen. *Department of Solid State Physics, Riso National Laboratory, Denmark,* and W. Brown. *Department of Physical Chemistry, University of Uppsala, Sweden*

The phase behavior of a series of poly(ethylene oxide) - poly(propylene oxide) - poly(ethylene oxide), $E_mP_nE_m$, tri-block copolymers dissolved in water have been studies using the small-angle neutron scattering technique. The block-copolymers were chosen to have a common polymerization degree of the central $P_n$ block, $n$ = 39, but different degrees of polymerization in the outer $E_m$ blocks, with $m$ ranging from 6 to 97. All polymers show the characteristics of fully dissolved unimers at low temperatures, whereas aggregates are formed at elevated temperatures, due to the hydrophilic-to-hydrophobic transition in PPO. It is observed, that while the aggregates of the polymers with the longest PEO-chains ($m$ = 96) are in the form of spherical micelles up to at least 90°C, the intermediate range copolymer ($m$ = 25) shows abrupt changes from spherical micelle to ellipsoidal form, in the 60-70°C temperature range. The critical micellation temperature $T_{cm1}$ increases with increasing PEO length $m$. In the triblock-copolymer with smallest PEO chains ($m$ = 6), spherical micelle are not the stable aggregate configuration at any temperature. The scattering function of the $m$ = 25-96 aggregates has been analyzed in terms of hard-sphere interacting micelles, characterized by a dense core radius $R_c$, and a hard-sphere interaction radius $R_{hs}$. From the data analysis we find that the core-size, and thereby the aggregation number, increases with increasing temperature. It appears, that the micellar characteristics of all three polymers are the same, when scaled to the reduced temperature $T$-$T_{cm1}(m)$. In the figure are shown a double logarithmic plot of the core-sizes versus reduced temperature for two polymer concentrations. The micellar core radius follows a $R_c \propto (T - T_{cm1})^{0.2}$ relationship, and with the aggregation number given by the core-volume, this gives a $N \propto (T - T_{cm1})^{0.6}$ for the aggregation number. Of special interest is the observation that the aggregation number according to this result approach very small values (N~1) near $T_{cm1}$.

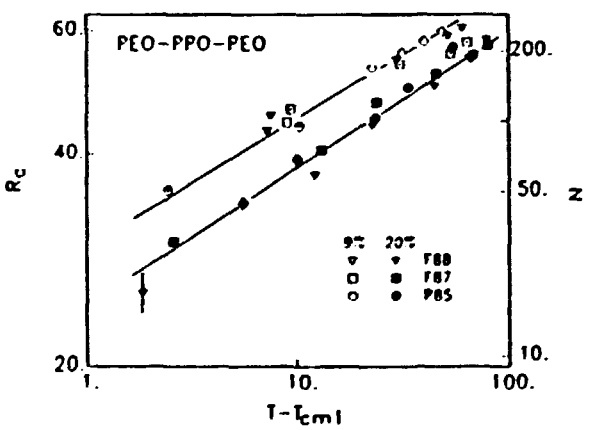


*Fig. 1. Micellar core radius $R_c$ of 9% and 20% aqueous solution of $E_mP_nE_m$, with n=39, and m=27 (P85), m=67 (F87), and m=96 (F88).*

[1] K. Mortensen, and J. Skov Pedersen, (1993). Macromolecules, *in press.*

## 1.62 Pressure Induced Melting of PEO-PPO-PEO Micellar Crystal

K. Mortensen, *Department of Solid State Physics, Riso National Laboratory, Denmark*, D. Schwahn, and S. Janssen, *Institute für Festkörperphysik, Forschungszentrum Jülich, Germany*

Aqueous solutions of triblock-copolymers made of poly(ethylene oxide) ($E_m$) and poly(propylene oxide) ($P_n$). $E_mP_nE_m$, forms within a relative large temperature range a solution of micellar aggregates in thermodynamic equilibrium with dissolved individual polymer chains (unimers)

$$unimers \rightleftharpoons micelles,$$

with the equilibrium constant having a temperature dependence which causes the micellar volume fraction to increase roughly linearly with temperature. This leads to the apparently inverted temperature characteristic, as the volume fraction approach the critical value for hard-sphere crystallization, $\phi$=0.53: an ordered micellar crystalline phase at high temperatures (BCC), and a micellar liquid at low temperatures[1].

In analogy with the inverted temperature dependence, pressure experiments show an "inverted pressure characteristic", *i.e.* when the micellar crystal is exposed to external pressure the cubic crystal melts. This is shown in the figure by the marked change in correlation-length going from the low-pressure crystalline to the high-pressure liquid phase. Upon pressure, the thermodynamic equilibrium balance given in eq. 1 goes toward the left, *i.e.* micelles are dissolved into unimers. This leads to a positive $dP_c/dT_c$ relation between crystallization temperature and pressure, and thereby, according to the Claudius-Clapeyron equation, gain in entropy at $T_c$. This is in spite of the transition to an ordered phase on the 100 Å length scale.

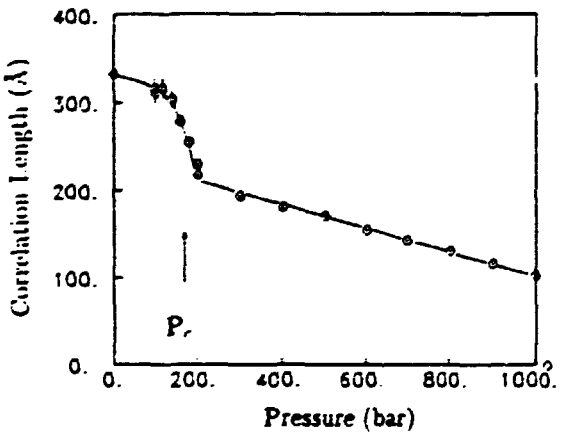


*Fig. 1. Correlation length versus pressure.*

[1] K. Mortensen, W. Brown, and B. Nordén, (1992). Physical Review Letters **13**, 2340-2343.

## 1.63 Pressure Dependence of the Flory-Huggins Interaction Parameter in Polymer Blends

S. Janssen, D. Schwahn, *Institute für Festkörperphysik, Forschungszentrum Jülich, FRG*, and K. Mortensen, *Department of Solid State Physics, Risø National Laboratory, Denmark*

Small angle scattering of neutrons is a very sensitive tool to examine the susceptibility in polymer blends, from which the interaction parameter can be determined. The reciprocal forward scattering reflects critical concentration fluctuations, and can be given as

$$S^{-1}(0) = 2(\Gamma_s - \Gamma)$$

where $\Gamma$ is the Flory-Huggins Interaction parameter of the blend and $\Gamma_s$ indicates its value at the temperature of spinodal decomposition. Many experiments have through the last decade shown that $\Gamma$ can be written in the form[1-3]

$$\Gamma = \frac{\Gamma_h}{T} - \Gamma_\sigma$$

where $\Gamma_h$ and $\Gamma_\sigma$ represent, respectively, the enthalpic and the entropic contribution to the free volume correlated interaction parameter. The aim of our study is to determine the dependence of $\Gamma_h$ and $\Gamma_\sigma$ on the external pressure, $P$, and thereby to examine the concept of the Flory-Huggins parameter with respect to the free volume.

The study was based on the well characterized binary polymer blend of deuterated poly(styrene), dPS, and poly(vinylmethylether), PVME, with molecular weights of $1\times10^6$ g/mol and $6\times10^4$ g/mol, respectively. The PSd/PVME blend decompose at high temperatures[1], *i.e.* it is characterized by a lower critical solution temperature (LCST). The experiments were performed at the critical dPS/PVME composition: $\Phi = 0.13$, where $\Phi$ is the dPS concentration. The study was made as a function of temperature $T$ and pressure between 1 and 1200 bars.

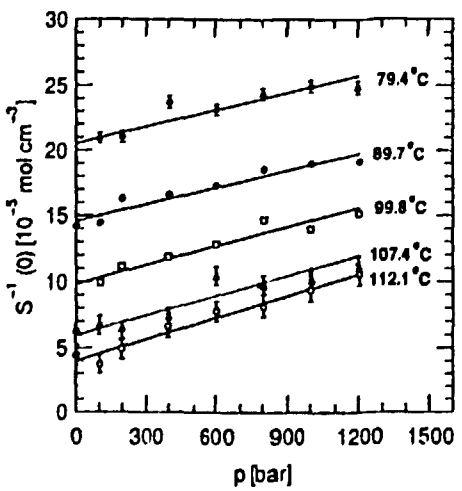


*Fig. 1. Critical scattering, as represented by the reciprocal forward scattering, $S^{-1}(0)$, of the polymer blend dPS/PVME at critical composition.*

Figure 1 shows the pressure dependence of the reciprocal forward scattering for several temperatures in the mixed state. One clearly recognizes a linear dependence of $S^{-1}(0)$ on pressure with a basically constant slope for all five temperatures. In Figure 2*a* and 2*b* $\Gamma_h$ and $\Gamma_\sigma$ are plotted against pressure. It appears that $\Gamma_h$ shows no dependence on $P$, whereas $\Gamma_\sigma$ shows a linearly decreasing function of pressure. This means that only the free volume dependent entropic contribution $\Gamma_\sigma$ is affected by $P$, while the enthalpic interaction $\Gamma_h$ remains constant for pressures up to at least 1200 bars. This result is in qualitative agreement with an equation of state argument of Patterson *et al.*[4].

In the order to get a more complete understanding of the Flory-Huggins parameter in polymer blends, it is the aim to continue the series of small-angle neutron scattering experiments investigating other polymer blends with upper critical solution temperatures, UCST, as well as blends with lower critical solution temperatures, LCST.

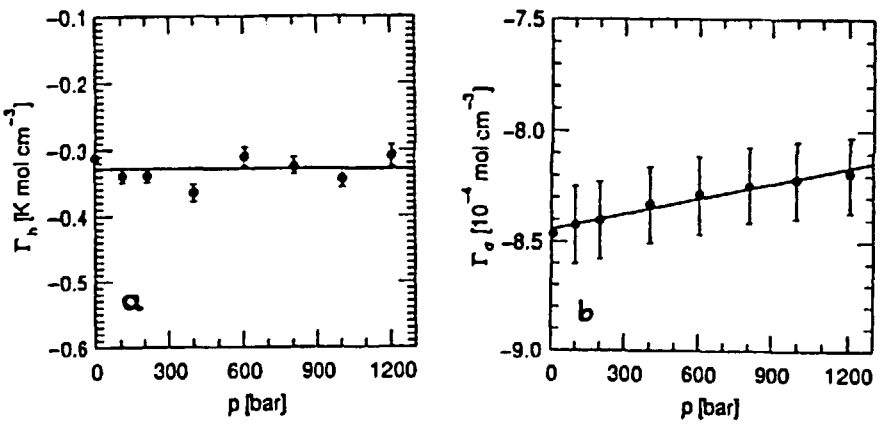


*Fig. 2. Pressure dependence on the Flory-Huggins interaction parameter of dPS-PVME, as represented by the entropic term $\Gamma_\sigma$ (a) and the enthalpic term $\Gamma_h$ (b).*


[1] D. Schwahn, K. Mortensen, T. Springer, H. Y. Madeira, and R. Thomas, (1987). J. Chem. Phys. **87**, 6078.

[2] F. S. Bates, G. D. Wignall, and W. C. Koehler, (1985). Phys. Rev. Lett. **55**, 2425.

[3] S. Sakurai, H. Jinnai, H. Hasagawa, T. Hashimoto, and C. C. Han, (1991). Macromolecules **24**, 4839.

[4] D. Patterson and A. Robard, (1978). Macromolecules **11**, 690.

## 1.64 Critical Scattering in Glassy Syndiotactic Polystyrene

T. Hack, M. Stamm, V. Abetz, *Max Planck Institute for Polymer Research, Mainz, Germany*, and K. Mortensen, *Department of Solid State Physics, Risø National Laboratory, Denmark*

We have used SANS to examine a polymer blend of deuterated polystyrene, PSd, with molecular weight $M_w$=92 kg/mol, and a protonated statistical copolymer poly(cyclohexylacrylate-stat-butylmethacrylate), P(CHA-stat-BMA) with $M_w$=240 kg/mol in different concentrations. The system, which has a lower critical solution temperature (*i.e.*, one-phase system at low temperature and two-phase system at high temperatures), is a good model system because the spinoldal temperature $T_s$ of the blend can be shifted by variation of the copolymer composition. PCHA is compatible with PS and PBMA is incompatible with PS at the used molecular weight. Because the glass transition $T_g$ is not affected by variation of the copolymer composition it is possible to change the difference between $T_g$ and $T_s$ which is responsible for the decomposition kinetics of the system. From measurements in the one phase region of the blend of PSd with copolymer ($CHA_{0.46}$-$BMA_{0.54}$) we have determined the spinodal temperature $T_s$ and the interaction parameter, $\chi$, for four concentrations. The $\chi$-parameters were determined by a fit of the scattering curve $S(q)$ with the de Gennes equation[1] for binary blends. The radius of gyration for polystyrene was fixed to a value from literature[2], $R_{g,PSd}$ = 84 Å. The fit-parameters are the radius of gyration for the copolymer and a temperature dependent interaction parameter $\chi$. The resulting $\chi$ is shown in Fig. 1. For the radius of gyration of the copolymer a value $R_{g,COPO}$=125±10 Å was determined. Performing temperature jumps into the two-phase region of ($CHA_{0.46}$-$BMA_{0.54}$) we find that the kinetics of phase separation is too fast to be resolved by SANS. Incorporating more of the large BMA-blocks into the copolymer, however, cause slower decomposition kinetics. We were therefore able to perform some kinetic studies by SANS, using a 50%-blends with a copolymer composition ($CHA_{0.25}$-$BMA_{0.75}$) and the same polystyrene material.

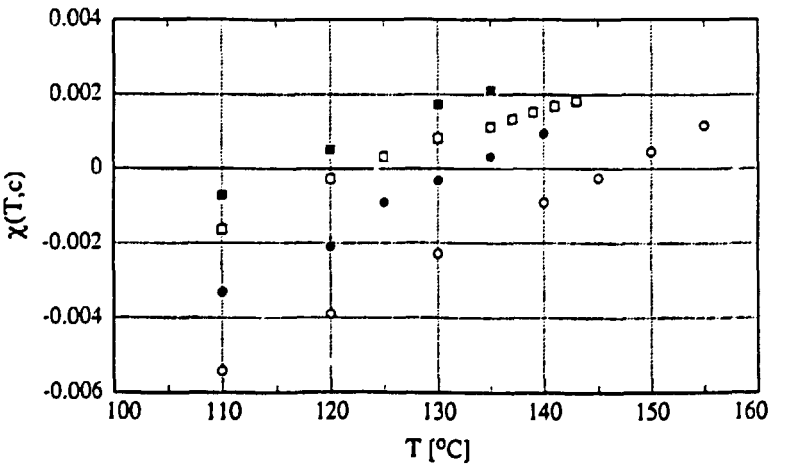


*Fig. 1. Temperature dependence of $\chi$ for four different compositions of the polymer blend: ($CHA_{0.46}$-stat-$BMA_{0.54}$)-PSd).*
*o 20% PSd, • 50%PSd, □ 65%PSd, □ 80%PSd.*

[1] P.G. de Gennes, (1979). *Scaling Concepts in Polymer Physics*, (Cornell University Press, Ithaca).
[2] P.J. Flory, (1969). *Statistical Mechanics of Chain Molecules*, (Interscience Publ., New York).

## 1.65 Structural Properties of Rigid and Plasticed Poly(Vinyl Chloride)

R. Scherrenberg, H. Reynaers, *Laboratory for Macromolecular Structural Chemistry, Catholic University of Leuven, Belgium*, and K. Mortensen, *Department of Solid State Physics, Risø National Laboratory, Denmark*

A comprehensive SANS study on both rigid and plasticized poly(vinyl chloride), PVC, demonstrates the presence of super-structural order in these materials. Comparison of the experimental scattering data with a tentative two-phase model point to specific penetration of the plasticizer in the non-crystalline regions of PVC. Thermal experiments reveal a gradual and thermo-reversible melting of the crystalline regions at temperatures above 80-90°C. On the basis of scattering experiments on uniaxially deformed samples, the existence of a network structure is concluded, where the crystallites act as tie-points in a plasticized medium[1]. Upon uniaxially stretching of the sample, the observed scattering pattern develops into a butterfly pattern, as shown in the figure. Qualitatively similar scattering patterns have been observed in stretched, randomly cross-linked polystyrene gels[2]. In analogy with these chemically cross-linked gels, we conclude that concentration inhomogenities in PVC are formed as a consequence of the random distribution of crystalline tie-points in plasticized PVC. The anisotropy of the scattering pattern gradually disappears on heating, probably resulting from the increasing mobility of the plasticized interstitial medium.

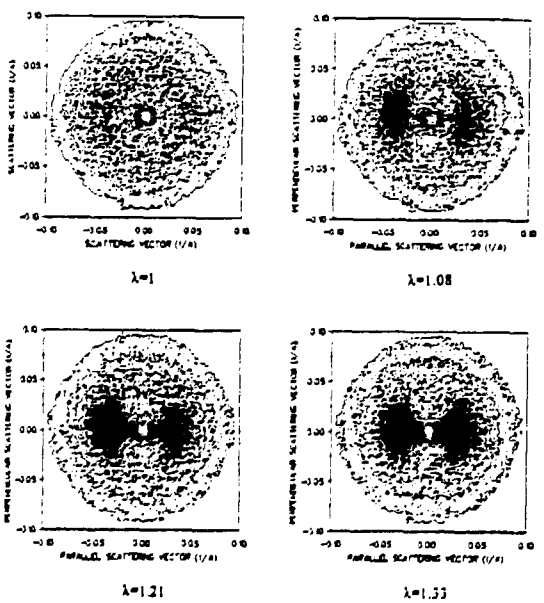


*Fig.1. Two-dimensional iso-intensity scattering patterns of plasticized PVC in relaxed form, λ=1, and uniaxially elongated to λ=1.08, 1.21, and 1.33*

[1] R. Scherrenberg, H. Reynaers, K. Mortensen, W. Vlak, and C. Gondard, (1992), *Submitted to Macromolecules.*

[2] J. Bastide, L. Leibler, and L. Prost, (1990). Macromolecules **23**, 1821

## 1.66 Screening Lengths in Polystyrene Solutions in Toluene Determined by SANS and SAXS

W. Brown, *Department of Physical Chemistry, University of Uppsala, Sweden*, Kell Mortensen, *Department of Solid State Physics, Risø National Laboratory, Roskilde, Denmark*, and George Floudas, *Max Planck Institute for Polymer Research, Mainz, Germany*

Different characteristic lengths have been introduced to describe the effects of chain overlap: $\xi$, $\xi_s$ and $\xi_h$. Here $\xi$ is the correlation length for concentration fluctuations, $\xi_s$ is the screening length of the excluded volume interactions, and $\xi_h$ is the screening length for hydrodynamic interactions. The correlation length for concentration fluctuations, $\xi$, was first introduced by Edwards[1]. In very dilute solutions, intra-molecular interactions are present and these manifest themselves as an excluded volume effect. If the polymer concentration is increased well above the critical overlap concentration, $c^*$, where the chains begin to mutually interpenetrate, the concentration fluctuations are significantly correlated and intermolecular interactions will progressively screen distant segments of the same chain from each other. This diminishes the range of the excluded volume interactions between any two segments on the same chain: the conformation is then that for a random walk process.

Screening lengths have been measured for the polystyrene/toluene system using SANS and SAXS over the concentration interval 0.1 to 0.9 g/ml and in the temperature range from 5 to 70°C. At the lower concentrations covering the semidilute regime ($c < 0.3$ g/ml) the concentration dependence agrees well with literature values: $\xi_s = 2.7 \cdot c^{-0.72}$ Å. At higher concentrations there is a stronger decrease in $\xi_s$ to an approximately constant value: $\xi_s = 1.8$ Å. The observed intensities, $I(q)$, contain contribution from both density and concentration fluctuations and a slow change in slope from a strong ($T > T_g$) to a weak ($T < T_g$) temperature dependence at the glass transition temperature, $T_g$.

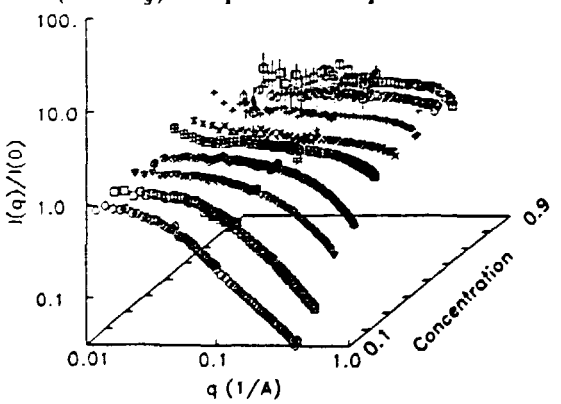


*Fig. 1. Scattering function for polystyrene in deuterated toluene, plotted versus temperature and concentration (g/ml).*

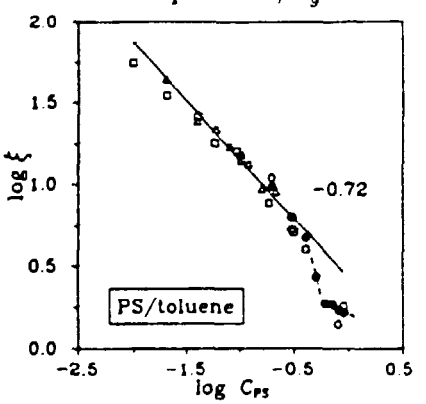


*Fig. 2. Screening length ($\xi_s$) versus polystyrene concentration in semidilute and concentrated solutions. o SANS, • SAXS, △ SANS measurements of King et al.[1], □ SAXS measurements of Hamada et al.[3]*

[1] S.F. Edwards, (1965). Proc. Phys. Soc. **85**, 613.
[2] J.S. King *et al.*, (1985). Macromolecules **18**, 709.
[3] F. Hamada *et al.*, (1985). Macromolecules **18**, 2290.

## 1.67 Structure of Hard Segments in Polyurethanes

G. Planer-Kühne, E. W. Fischer, *Max Planck Institute for Polymer Research, Mainz, Germany*, and K. Mortensen, *Department of Solid State Physics, Risø National Laboratory, Denmark*

Polyurethane elastomers contribute a kind of multiblock copolymers with flexible soft and rigid hard segments. In this case the soft segments is poly(oxytetramethylene), POTM. The socalled hard segments are synthesized monodispersely by a special technique from piparazine and butanediol-bis-chloroformiate[1]. Due to the incompatibility of the two segments the material is phase separated below the melting temperature, $T_m$, of the crystalline hard phase. Above $T_m$ the phases are mixed and small angle neutron scattering, SANS, studies were perform to investigate the structure of the hard segments. The technique used is based on contrast variation[2] of chains with deuterated and protonated hard segments. The structure factor $P(q)$ may be evaluated form the following equation:

$$I(q) = c_d(1 - c_d)K_N n_w P(q)$$

where $c_d$ is the concentration of deuterated segments, $K_N$ is the square of the scattering contrast, $n_W$ is the weight average degree of polymerization, and $I(q)$ the scattering function corrected for background and incoherent scattering. The radius of gyration was evaluated from the Zimm plot: $I(q)^{-1}$ versus $q^2$. This experiment gives a value of 39 Å. Compared to other polyurethanes (on the basis of methylendiphenyldisocyanate, MDI, and polyesters with a stiff backbone and a rigid side chain[3], the value fits very well. The characteristic ratio $C_\infty = 6R_g/L_W$ ($R_g$ being the radius of gyration and $L_W$ the persistence length) gives a value of 13.4 which is much larger than the value for the very flexible polydimethylsiloxane, PDMS, for example. This result implies that in the molten state the socalled hard segments are still in a stretched conformation.

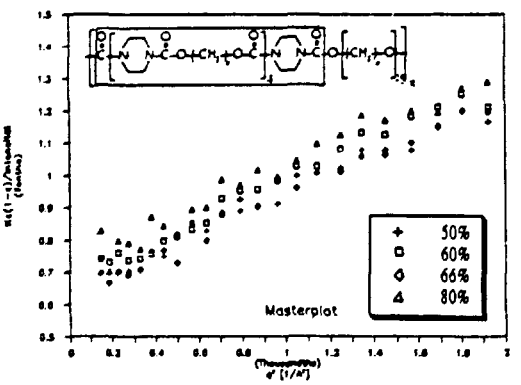


*Fig. 1. Zimm plots for a series of mixtures of hard segment deuterated and protonated polyurethanes. Inset: structure of the investigated polymer; the rectangle includes the hard segments.*

[1] C.D. Eisenbach *et al.*, (1985). Ber. Bunsenges. Phys. Chem. **89**, 1190.
[2] W. Gawrisch *et al.*, (1981). Polymer Bulletin **4**, 90.
[3] E.W. Fisher, (1989). *Pure and Applied Chemistry*, Max Planck Institute Report.

## 1.68 Chain Conformation in Glassy Syndiotactic Polystyrene

S. Stölken, B. Ewen, *Max Planck Institute für Polymer Research, Mainz, Germany,* and K. Mortensen, *Department of Solid State Physics, Risø National Laboratory, Denmark*

The tacticity of vinyl polymers, which describes the ordering of the side groups within the fully extended polymer chain, has an influence on the chain conformation and therefore the scattering function[1], $I(q)$. Small angle neutron scattering (SANS) has been used to study the $I(q)$ on glassy syndiotactic polystyrene (sPS) for different molecular weights at room temperature. (Syndiotactic polymer means that the sidegroup alternates on either sides of the back-bone polymer chain.) As seen from Fig. 1 a plateau was observed at a scattering vector $q < 0.2$ Å$^{-1}$ in the Kratky representation; $I(q)q^2$ versus $q$. In this range the experimental data fit with a Gaussian chain. This is in contrast to previous studies which did not take into account the density fluctuations of the deuterated polymer species. For the $q$ range beyond 0.2 Å$^{-1}$ the scattering behavior depends on concentration. At 3% the data shows an increase in the Kratky plot (Fig. 1). It is not clear, if this effect is due to the density fluctuations or a problem of the sample preparation. There must be more systematic examinations to answer this question. The characteristic ratio $C_\infty = 6\langle R_g^2\rangle / nl^2$, given by the number of monomers of a chain, $n$, and the length of the monomer unit, $l$, was obtained from the radius of gyration $\langle R_g^2\rangle$ determined from the plateau height. On the basis of "the rotational isomeric state model"[1], Flory has calculated the characteristic ratio and the scattering function for polystyrene with different tacticity[2]. The experimental value for sPS is $C_\infty = 8.8$ in contrast to the theoretical value of ~18. In addition the scattering behavior of the used sPS samples also did not show the predicted slope[2] in the Kratky representation.

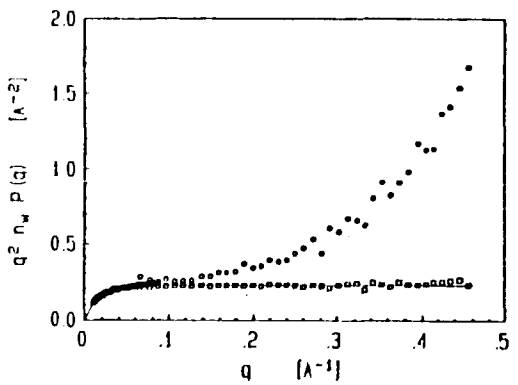


Fig. 1. Kratky representation of sPS with different number of monomers per chain $n$ and volume fraction $c$ of the protonated species in comparison with the Debye function of a Gaussian chain (full line). o $n$=2536 $c$=1%, □ $n$=2296 $c$=3%.

[1] P.J. Flory, (1969). *Statistical Mechanics of Chain Molecules*, (Hanser Publ., New York).
[2] P.J. Flory and D.Y. Yoon, (1976). Macromolecules **9**, 294.

## 1.69 Characteristic Ratio $C_\infty$ of Poly(diethylsiloxane) in the Melt and in a Solution

H. Schlottke, B. Ewen, *Max Planck Institute, Polymer Research, Mainz, Germany*, and K. Mortensen, *Department of Solid State Physics, Risø National Laboratory, Denmark*

In recent years a new class of polymers has been shown to form mesomorphic states, *i.e.* micro-structures with local spatial order. Poly(diethylsiloxane) PDES and poly(dipropylsiloxane) PDPS are examples of this new class, which, in spite that they do not contain any classical "mesogenic" groups in the molecular structure, still form mesophases. The molecular origin of the mesophase formation is not understood, but it has been argued that the chain structure of the macromolecules has great influence on the self-ordering. An important parameter describing the chain structure is the characteristic $C_\infty$-parameter, given by $C_\infty = 6R_g/L_W$. $R_g$ is the polymer radius of gyration and $L_W$ is the persistence length. With the aim to investigate the correlation between polymer chain stiffness, and the ability of mesophase formation, we have measured the $C_\infty$ parameter for a PDES polymer as a function of temperature. $C_\infty$ was determined from the scattering function measured by small angle neutron scattering, see preceeding contribution. From optical polarization microscope measurements[2], PDES was shown to form mesophase below $T \simeq 323$ K.

A slight change is observed in the low-$q$ part of the scattering function going from the mesophase below 323 K to the disordered phase above 323 K (Fig. 1). In the disordered phase, on the other hand, very little temperature dependence is observed. Moreover, we find that in the the high temperature disordered phase, the $C_\infty$ value of PDES is 17.5, which is significant different from the theoretically expected value. This indicates that even in the disordered phase, significant "mesomorphic" fluctuations are present.

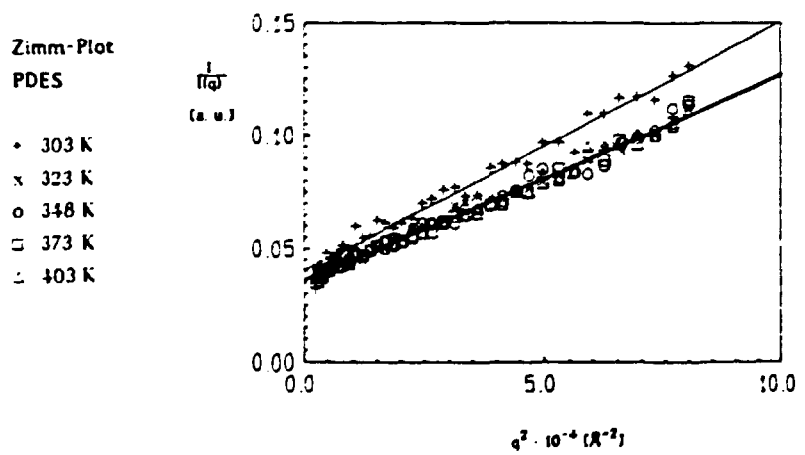


*Fig. 1. Zimm plots for PDES obtained in the 303-403 K temperature regime.*

[1] M. Müller and S. Siffrin, (1990). Macromol. Chem. Macromol. Symp. **34**, 171.
[2] H. Schlottke, (1990). Diploma Thesis, Max Planck Inst., Mainz.

## 1.70 A Model for the Microscopic Structure of Equilibrium Swollen PDMS Networks Randomly Cross-Linked

A.N. Falcão, J. Skov Pedersen and K. Mortensen, *Department of Solid State Physics, Risø National Laboratory, Denmark*

The current thermodynamic treatment explains the equilibrium swelling of polymeric networks by the cancellation of two contributions to the Gibbs function: a mixing term derived from the Flory lattice model, and an elastic term for which several models have been proposed, all assuming that the network strands have a random walk conformation. Although these models explain reasonably well the qualitative features of macroscopic measurements, they fail to explain the microscopic structure as revealed by scattering measurements. Based on an analogy with a percolation problem, a model was proposed[1] to describe the network structure, and the microscopic changes that take place when the network is deformed either by stretching or swelling. This model explains general qualitative features of the scattering patterns obtained from gels, but predicts some scaling relations which have generally not been observed. It also predicts that the intensity scattered in the limit of zero scattering vector should have a maximum when plotted as a function of cross-link density, which has never been observed.

We analyzed scattering data obtained from equilibrium swollen networks with a broad range of linking densities. The analysis was based on a model[2] that describes the structure as resulting, at large scales, from a fractal arrangement of *particles*, formed by polymer segments. The model introduces two characteristic lengths: one, $\xi_L$, associated with the spatial extent of the fractal fluctuations at large scales; the other, $\xi_S$, is the characteristic size of the *particle*. $\xi_S$ was identified with the correlation length that characterizes the polymer solution with the same concentration. With a fixed fractal dimension $D_F = 5/3$, the model fitted very well the scattering data for all of the linking densities.

The results obtained show that the structure of the swollen network is well described as resulting, for distances below $\xi_L$, from the establishment of excluded volume interactions between large connected units with average size $\xi_S$. Both $\xi_L$ and the intensity in the limit of zero scattering vector should scale with polymer concentration as $\sim c^{-3/2}$, and this was well verified by the experimental data. Furthermore, a comparison of $\xi_L$ with values of the average molecular weight in between elastically effective links, $N_C$, previously obtained both from macroscopic measurements and a statistical approach, leads to the scaling relation $\xi_L \sim N_C^{3/5}$. This indicates that, at least for the networks studied, the average size of the network strands obtained from classical theories is compatible with the scattering pattern.

[1] J. Bastide, E.Mendes, F. Boué, M. Buzier, and P. Lindner, (1990). Makromoleculare Chemie **40**, 81.
[2] A.N. Falcão, J. Skov Pedersen, and K. Mortensen, (1992). Macromolecules, *submitted.*

## 1.71 Effect of the Extractable Components in the Microscopic Structure of Swollen PDMS Cross-Linked Networks

A.N. Falcão, J. Skov Pedersen, and K. Mortensen, *Department of Solid State Physics, Riso National Laboratory, Denmark*

Irradiating a melt of linear polymer chains with high energy electrons randomly creates radicals that, after diffusion processes, react forming chemical links. At a certain radiation dose threshold a macroscopic network is formed. With increasing dose above this threshold, the weight fraction of the irradiated polymer that will be part of the network first increases exponentially and then saturates reaching a limit that will be close to unity if the irradiation process has low probability of inducing main-chain scission in the polymer chains. The material not incorporated in the macroscopic network can be removed by standard chemical procedures. In contact with a good solvent for the polymer, both the extracted and non-extracted systems will absorb the solvent, expanding progressively from an initial volume $V_0$ to a maximum equilibrium value $V_{eq}$. The use of deuterated solvent enables the local structure of the polymer chains to be probed by the neutron scattering technique.

We accessed the influence of the extractable components in the microscopic structure of the swollen system, by measuring the small-angle neutron intensity scattered by extracted and non-extracted networks. The study was done as a function of cross-link density. The scattering data were analyzed using a model[1] that describes the fluctuations of polymer concentration in the swollen system as resulting, for distances below a characteristic length $\xi_L$, from excluded volume interactions established between large connected units, each including several monomers. The correlation lengths $\xi_L$ and the intensity scattered in the limit of zero scattering vector obtained from the scattering data, for both the extracted and non-extracted systems, scale with polymer volume fraction as expected from the model. Furthermore, the scaling relations obtained for the extracted and non-extracted systems are indistinguishable within experimental accuracy, suggesting that the extractable components act essentially as network strands. This is expected from the excluded volume picture if the mass distribution in the extractable components is similar to the one present in the average sample, with the same size, collected from the network itself.

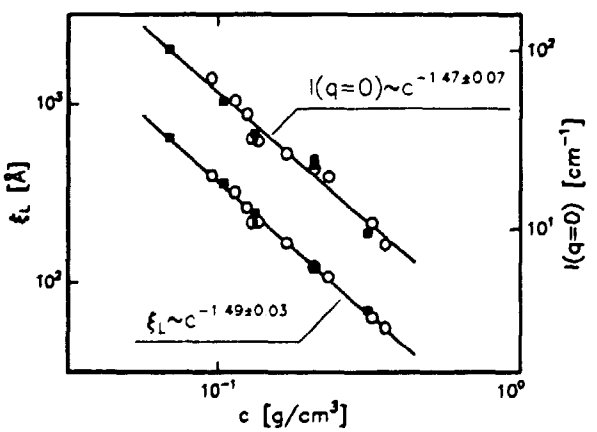


*Fig. 1. Correlation lengths $\xi_L$, and intensities in the limit of zero scattering vector given, in a double logarithmic plot, as a function of polymer concentration in the swollen systems. Open circles: non-extracted networks; filled squares: extracted networks.*

[1] A.N. Falcão, J. Skov Pedersen and K. Mortensen (1992). Macromolecules, *submitted. (se also the previous contribution).*

## 1.72 Bending Rigidity of Sodium Octyl Sulfate/Water/Decanol Lamellae

E. Y. Sheu, *Texaco R&D, Beacon, New York, USA*, J. Samseth, *Institute for Energy Technology, Kjeller, Norway*, S.-H. Chen, *Massachusetts Institute of Technology, Cambridge, Massachusetts*, K. Mortensen, *Department of Solid State Physics, Riso National Laboratory, Denmark*

The bending rigidity of microemulsions in the lamellar phase is an important characterization parameter. Experimentally, it can be determined by measuring the structure factor in a scattering experiment. The conventional data analysis involves detailed analysis of the peak shape. Alternatively, the bending rigidity can be determined from the small angle regime where the scattering contribution is dominated by fluctuations in the lamellar bilayers. In a small-angle neutron scattering study, we have measured the lamellar phase of the sodium octyl sulfate (SOS)/water/decanol micremulsion, along the water dilution line with fixed SOS/decanol weight ratio (W) at 45:55. Figure 1 shows the evolution of the scattering peak as a function of water content. The peak evolves toward higher $q$-values with decreasing water content, indicating the decreasing inter-layer spacing. The small angle scattering is substantial for all samples, signifying important fluctuation within the lamellar plane. At the highest water concentration (the 1.62 % curve in Fig. 1), the system is close to the lamellar boundary, presumably to a bicontinuous "L3" phase. The peak intensity is smaller than that of the 1.44% curve (see also Fig. 2). For water content beyond ~1.44% the peak intensity decreases monotonically until a new phase appear. The 0.56% system is very close to the neigboring phase, consisting of reversed cylindrical micelles. The bending rigidity was obtained using the "average fluctuating mode" as the mean persistence length according to the de Gennes-Taupin model[1]. The values obtained spanned from 0.3 $k_BT$ to about 1.5 $k_BT$, depending on the water content.

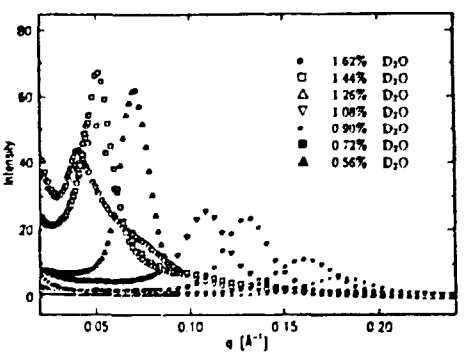


*Fig. 1. Scattering functions of SOS/$D_2O$/Decanol with fixed weight ratio of [SOS]/[$D_2O$]=45:55, and $D_2O$ concentration varying from 0.56 to 1.62 %.*

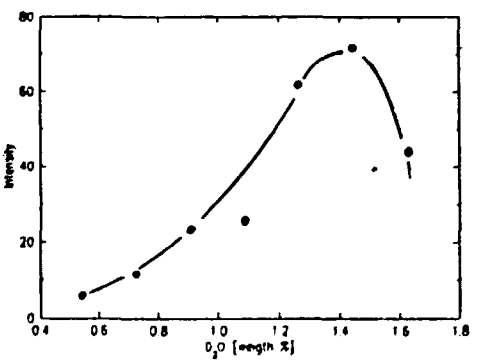


*Fig. 2. Peak Intensity versus $D_2O$ content, as obtained from Fig. 1.*

[1] P.G. de Gennes and C. J. Taupin, (1992). J. Phys. Chem. **86**, 2294.

## 1.73 A SANS study of the Emulsification Failure of a Nonionic Microemulsion

U. Olsson, H. Bagger-Jorgensen, *Division of Physical Chemistry 1, Chemical Center, Lund University, Lund, Sweden*, and K. Mortensen, *Department of Solid State Physics, Risø National Laboratory, Denmark*

The structural properties of a water rich microemulsion composed of nonionic surfactant (pentaethyleneglycol dodecyl ether, $C_{12}E_5$), water ($D_2O$) and decane has been investigated by small-angle neutron scattering. Particular attention was drawn to the so-called emulsification failure[1] (EF) phase boundary, where the microemulsion phase separates with excess oil, and we address the question concerning particle (oil-swollen micelles) size and shape on this boundary. The surfactant-to-oil ratio was kept constant at a volume fraction ratio $\Phi_s/\Phi_o=0.815$ for which the emulsification phase boundary occur at a temperature of about 24°C, independent of $\Phi=\Phi_s+\Phi_o$.

In the absence of long-range (electrostatic) interactions, a description of surfactant-water-oil systems in terms of the elastic properties of the surfactant film has been shown to be very fruitful. In the simplest case (neglecting Gaussian curvature and entropy effects), the EF occur when $H_o^{-1}<R$, where $H_o$ is the spontaneous curvature of the surfactant film and $R=3\Phi_o l_s/\Phi_s$ is the spherical radius associated with the given surfactant-to-oil ratio, where $l_s$ is the surfactant length. Since $H_o$, for nonionic surfactants, is known to decrease monotonically with increasing temperature[2], the model predicts a $\Phi$ independent EF temperature with spherical oil-swollen micelles on the phase boundary. Furthermore, we expect the particles to grow in size (a sphere to rod transition) with increasing the temperature (decreasing $H_o$) away from the EF phase boundary.

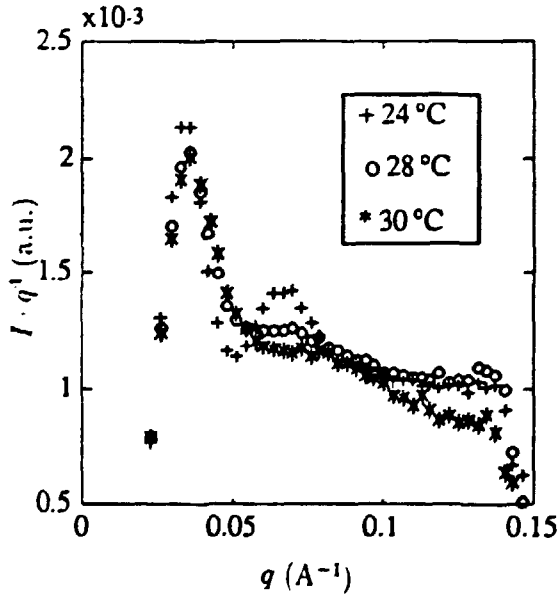


*Fig. 1. SANS data at three different temperatures from a microemulsion with $\Phi$=0.25.*

Fig. 1 shows the SANS data from a sample with $\Phi$=0.25, plotted as $I \cdot q^4$ versus $q$, at three different temperatures. At 24°C, close to the EF phase boundary, the data are consistent with spherical micelles having a radius of roughly 75 Å and a polydispersity (when instrumental resolution is taken into account) of the order of 15% (relative standard deviation). A similar radius is obtained from analyzing the data in the Guinier regime and the value is consistent with the known headgroup area of the surfactant as measured in lamellae phases. The change in the scattering pattern observed when increasing the temperature is consistent with a particle growth. The intensity falls off slightly faster than $q^{-4}$ at high $q$ due to the fact that the scattering length density profile is not perfectly sharp - there is a $D_2O$ concentration profile out from the hydrocarbon core within the hydrated ethylene oxide region.

[1] S. A. Safran, (1992). In: *Structure and Dynamics of Strongly Interacting Colloids and Supramolecular Aggregates in Solution*. S. H. Chen, J. S. Huang and P. Tartaglia (eds.), (Kluwer Academic Publishers, Dordrecht, the Netherlands)
[2] D. Anderson, H. Wennerström, and U. Olsson, (1989). J. Phys. Chem. **93**, 4243.

## 1.74 Phase Behavior of DPPC-Cholesterol Mixtures

T. Brumm, T. Bayerl, E. Sackmann, *Technical university of München, Garching, Germany*, and K. Mortensen, *Department of Solid State Physics, Riso National Laboratory, Denmark*

Cholesterol has great effect on the phase behavior of bilayer membranes, and thereby important influence on biological systems. The phase behavior of binary mixture of lecitin bilayer membranes and cholesterol is very complex and have already been extensively studied by a number of experimental techniques, including electron microscopy[1], NMR[2], and SANS[3], as well as theoretical studies[4]. While the low temperature phase behavior, as measure by various techniques, agrees very well, the high temperature and high cholesterol regimes are the subject of some controversy. Spectroscopic NMR studies indicate a phase boundary between the high and the low temperature part of the socalled liquid-ordered (lo) phase.

For the study, we used a binary mixture of 1,2-dipalmitoyl-sn-3 glycerophosphocholine (DPPC) with 25 mole% cholesterol. The samples were thin-walled vesicles prepared by the size extrusion technique with an average diameter of 200 nm. The measurements were performed in the range of scattering vectors $q$=0.002–0.1 Å$^{-1}$ within the temperature regime 8–50°C. Five contrasts were measured: completely protonated DPPC and completely chain deuterated DPPC (DPPC-d62) as well as three mixtures of DPPC and DPPC-d62 with a scattering length around the theoretical matching point.

The analysis of the data shows that within the experimental error no demixing of the binary system can be observed at any temperatures studied. We therefore conclude, that the existence of a phase boundary in the lo phase is outside the scale of neutron scattering.

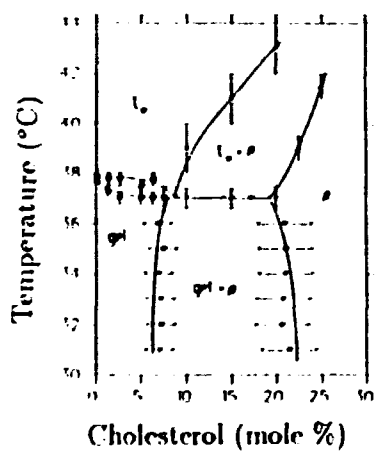


*Fig. 1. Phase diagram of DPPC-Cholesterol* [2]

[1] A. Hicks *et al.*, (1987). Biochim. Biophys. Acta **903**, 177.
[2] M.R. Vist and J.H. Davis, (1990). Biochemistry **29**, 451.
[3] K. Mortensen *et al.*, (1988). *Biochim. Biophys. Acta* **945**, 221.
[4] J.H. Ipsen *et al.*, (1987). Biochim. Biophys. Acta **905**, 162.

## 1.75 Phase Behavior of Gramicidin-Phosphatidylcholine Mixtures

T. Hønger, O. Mouritsen, J. H. Ipsen, *Department of Physical Chemistry, The Technical University, Denmark,* K. Mortensen, J. Skov Pedersen, *Department of Solid State Physics, Risø National Laboratory, Denmark,* and R. Bauer, *Department of Mathematics and Physics, Royal Veterinary and Agricultural University, Frederiksberg, Denmark*

Gramicidin is a hydrophobic peptide, which in biological membranes, as well as in model membranes, is known to form cation specific trans-membrane channels[1]. The channel is formed by hydrogen bonding of the N-terminal parts of two gramicidin molecules, present in a single stranded $\beta$-helical configuration. In addition to the ability of forming the trans-membrane channel, gramicidin also has a dramatic effect in the macroscopic organization of membrane lipids. For example, high concentrations of gramicidin induces a transition from a lamellar organization of the lipids to a hexagonally ordered phase[2]. Mismatch between the length of the lipid acyl chains and the length of gramicidin has been proposed as the driving force for this transition.

In the low concentration regime, NMR studies has given evidence of a small regime of two-phase coexistence[3]. In the attempt to understand the lecitin-gramicidin phase behavior, we have studied in detail the lamellar phases by small-angle neutron scattering technique. For this studied, we used deuterated DMPC (DMPC-d54) incorporated with a 0-5% concentration gramicidin. The mixtures were dissolved in deuterated water, forming a suspension of large multi-bilayer vesicles.

The scattering experiments shows that incorporation of gramicidin in the membrane strongly effects the scattering intensity as a function of $q$. The scattering from the lamellae phase of pure DMPC shows a distinct minimum in the $q$ value of the (100) Bragg reflection at the *main* transition temperature (separating the crystalline $L_\beta$ phase and the disordered $L_\alpha$ phase). This apparent thickening of the bilayer close to $T_m$ is suppressed by incorporating only small amount of gramicidin.

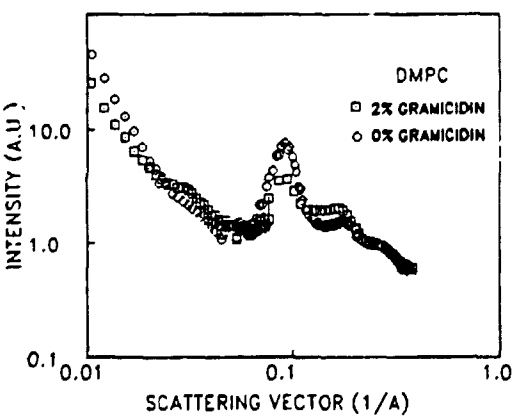


*Fig. 1. Raw scattering data of DMPC and DMPC bilayers incorporated with 2% gramicidin.*

[1] O.S. Andersen, (1984). Annu. Rev. Phisiol. **46**, 531.
[2] J.A. Killian *et al*, (1989). Biochim. Biophys. Acta **978**, 341.
[3] M.R. Morrow and J.H. Davis, (1988). Biochemistry **27**, 2024.

## 1.76 Investigation of Highly Concentrated Solutions of Biological Macromolecules

B. Sjöberg, *Department of Medical Biochemistry, University of Göteborg, Sweden,* and K. Mortensen, *Department of Solid State Physics, Risø National Laboratory, Denmark*

Studies of biological macromolecules are by tradition normally performed on either dilute solutions, or on crystalline phases. Neither of these extreme conditions does, however, represent the true conditions in living systems. For instance the concentration of the dissolved components in blood plasma is about 8% and the corresponding intracellular value is as high as 20-40%. In such systems we can expect the conditions to be quite different from those in a dilute solution, or in the crystalline phase. It is thus desirable to develop both experimental and theoretical methods for the investigation of the structural and thermodynamic properties of highly concentrated macromolecular solutions.

The SANS method is of great potential value for the investigation of such systems because the signal reflects not only the structure of the individual macromolecules but also the interparticle structure of the solution. In traditional SANS investigations the interparticle scattering normally is neglected, or eliminated by extrapolating to zero concentration.

In our investigations we use human serum albumin (HSA), and other proteins which can easily be obtained in highly purified form, as model compounds and we are making a systematic investigation of the structural and thermodynamic properties of the solutions as function of the basic parameters like ionic strength, pH, temperature, viscosity, *etc.* So far SANS data have been collected for HSA concentrations up to 0.4 g/cm$^3$ at varying concentrations of NaCl.

In the analysis of the data we have tried several different approaches. The classical "integral equation" methods (Born-Green, hypernetted chain, Percus-Yevick, *etc.*) are of limited value due to their approximative nature and the assumption of spherically symmetric interactions. We have, however, found computer simulations and the Monte Carlo method to be extremely powerful in the analysis of our experimental data. The advantage of the method is that any type of model, with any type of intermolecular interaction, can be considered. The only problem is to formulate the model into mathematical terms and to implement the algorithm into the computer.

Since the shape of the HSA molecule can be approximated as an ellipsoid of revolution we have started simply by using the hard ellipsoid of revolution type of interaction. Canonical ensemble average of the scattering is calculated by generating Markov chains of configurations for a periodic cubic box containing from a few hundred up to several thousand HSA molecules. It follows that the SANS data at higher ionic strengths can be well approximated by the hard ellipsoid of revolution type of interaction. This information can be used to simulate other properties of the solutions which are not directly attainable by experiments. At lower ionic strengths we are at present analyzing more complicated types of interactions, where the electrical forces between the molecules are considered.

## 1.77 Solution Conformation of a Coiled-coil Protein from Salmonella typhimurium

K. Österlund, R. Hurme, P. Koski, M. Rhen, M. Torkkeli, *Departments of Biochemistry and Physics, University of Helsinki, Finland,* B. Sjöberg, *Department of Medical Biochemistry, University of Göteborg, Sweden,* and K. Mortensen, *Department of Solid State Physics, Risø National Laboratory, Denmark*

Double-alpha helical coiled-coil proteins are important building blocks of, for instance, the functional unit in the musculoskeletal system of vertebrates, the actin-myosin-tropomyosin complex[1]. Important examples are myosins, troponins and tropomyosins which constitute the fundamental chemo-mechanical linkage enabling animal locomotion. Recent extensions of the family are leucine zipper proteins with DNA binding capacity[2].

The first bacterial coiled-coil protein, called M6, was found in Streptococcus pyogenes[3], soon proving to be involved in pathological conditions of streptococcal infections, where the immune system of the human host is unable to recognize the bacterial invader. A tropomyosin-like coiled-coil protein, TLPA, from Salmonella typhimurium has recently been discovered and characterized[4]. The molecular organization of TLPA is somewhat different from that of M6, and the biological function is therefore not expected to be identical. A dominant feature is, however, the existence of a similar repeat in the amino acid sequence, with a heptad pattern of alternating hydrophobic and charged amino acid residues. This results in a tendency for monomers to pair up into tightly associated dimers, in a manner reminiscent of the streptococcal M-proteins.

For understanding the mode of action of TLPA, the overall shape of the dimer in solution should be known. For this purpose, small-angle scattering methods are ideally suited. The additional possibility to accurately control sample temperature at the Risø SANS-facility offers the option of being able to monitor molecular dissociation, following temperature increase. Thus the stability of this bacterial protein can be studied for different mutated chains and at varying temperatures. This is hoped, in combination with other methods, to provide a key to the understanding of the proliferation of the bacterium, when it invades the host, and ultimately suggesting the route for possible remedy.

[1] C. Cohen and B.A.D. Parry, (1990). Proteins: structure, function and genetics **7**. 1.
[2] E. O'Shea, R. Rutkowski, and P. Kim, (1989). Science **243**, 538.
[3] V.A. Fischetti, (1991). Sci. Am. **264**:6, 32.
[4] P. Koski, H. Saarilahti, S. Sukupolvi, S. Taira, P. Riikonen, K. Österlund, R. Hurme, and M. Rhen, (1992). J. Biol. Chem. **267**, 12258.

## 1.78 Humic Acids in Aqueous Solution, a System Characterized by Fractal Geometry and Kinetic Growth

R. Österberg, *The Swedish University of Agricultural Science, Uppsala, Sweden*, and K. Mortensen, *Department of Solid State Physics, Risø National Laboratory, Denmark*

The importance of humus substances in the biosphere cannot be overestimated since they are the key component in soil responsible for the transport of nutrients to the plant kingdom. Using small-angle neutron scattering, we have shown[1] that the structure of humic acids over one to two orders of magnitudes in length scale, obey a power law dependence of the scattering vector, $q$, indicating that the particles in solution are fractals. Analyses of the data yield a fractal dimension $D$ of 2.3 ± 0.1 and an upper cut-off parameter of 385 Å. This latter parameter is related to the radius of gyration, $R_g$, and it is of the same order of magnitude as reported for the $R_g$-values of humic acids obtained from various geographic sources[2]. However, it should be noted that the parameters, $R_g$ and the intensity at $q = 0$, $I(0)$, depends on both time, temperature and concentration. SANS-data as well as high-precision electromotive force titrations indicate that humic acids are random colloid aggregates characterized by kinetic growth. One finding that might have important implications for the function of humic acids in soil is a temperature dependent restructuring occuring in the temperature range 4 - 20°C. Neutron scattering from humic acid particles in solution, which were prepared and stored at 4 - 8°C, show a fractal dimension of $D = 1.8$. When the temperature is increased to 21°C the fractal dimension of the particles in solution increases with time approaching a constant value of $D$=2.35 after 40 hours (Fig. 1). This observation can be explained by the assumption that the low-temperature aggregation proceeeds via diffusion limited cluster-cluster interactions and that these clusters at higher temperatures re-structure into more compact particles[3].

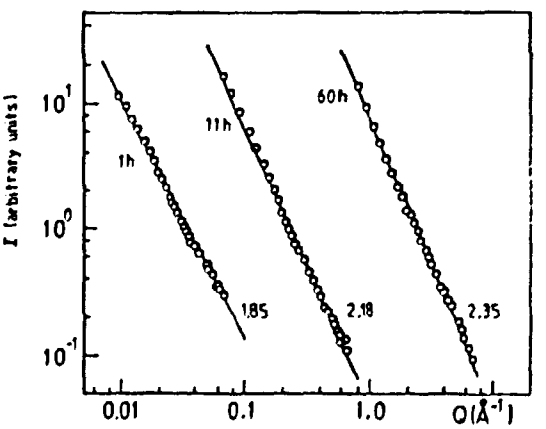


*Fig. 1. SANS data of humic acid solutions. Time of incubation of the samples at 21°C is indicated. For clarity, the data of 11 hours and 60 hours are shifted one and two units along the q-axis. The fractal dimensions are indicated in the lower part of the figure.*

[1] R. Österberg and K. Mortensen, (1992). Eur. Biophys. J., **21**, 163.
[2] R. Österberg, I. Lindqvist, and K. Mortensen, (1992). Soil Sci. Soc. Am. J., *in press.*
[3] R. Österberg and K. Mortensen, (1992). Proceedings of 6th International Meeting Humic Substances Society, *submitted.*

## 1.79 Contrast Variation Study of the 50S Subunit of the E. Coli Ribosome

D.I. Svergun, P. Brouillon, M.H.J. Koch, *EMBL, Hamburg Outstation, Germany*, I.N. Serdyuk, *Institute of Protein Research, Pouschino, Russia*, and J. Skov Pedersen, *Department of Solid State Physics, Risø National Laboratory, Denmark*

Neutron small-angle scattering curves from the solutions of the 50S ribosomal subunit were recorded for different $H_2O/D_2O$ mixtures. Two samples were investigated, containing protonated and deuterated ribosome particles, respectively. For the protonated 50S, samples containing 0, 17, 42, 66, and 98% $D_2O$ were measured, and for the deuterated particles, the $D_2O$ proportions were 0, 66, 80, and 95%. Two instrumental settings were used for each sample, i) 8 Å wavelength, sample-detector distance 3 m, and ii) 6 Å, 1 m, correspondingly. This allowed to cover the range of momentum transfers from 0.01 to 0.23 $Å^{-1}$.

The matching point for the protonated 50S is 59% $D_2O$, and for the deuterated it is around 100% $D_2O$. The radius of gyration extrapolated to the infinite contrast is 78 Å, in good agreement with previous studies. The radii of gyration of the RNA and protein part are 65 Å and 98 Å, respectively.

The samples of the 50S ribosomal subunit were also measured with synchrotron radiation on the X33 camera of the EMBL in HASYLAB (DESY, Hamburg). Contrast variation was performed by adding sucrose (up to 50%). The range of contrasts is much narrower than for the SANS measurements, but the synchrotron data have been measured at point collimation with a good statistical accuracy (approximately the same angular range as for the neutron measurements is covered). Preliminary estimates show that the X-ray and neutron data are well correlated (Fig. 1). The joint processing of the synchrotron and neutron scattering data is now in progress.

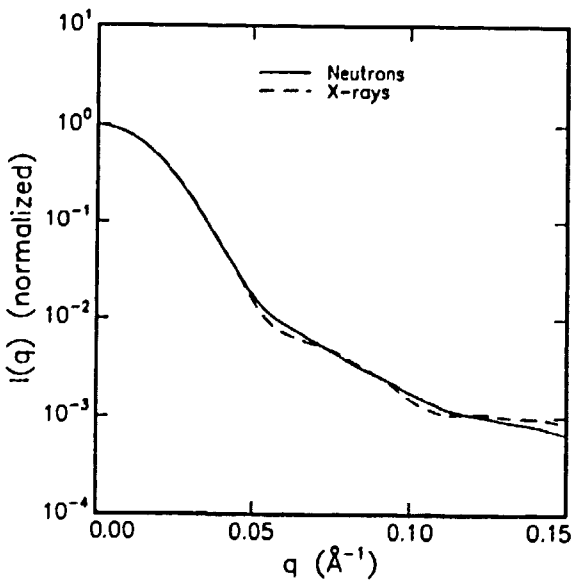


*Fig. 1. Processed solution scattering curves from 50S ribosomal subunits: neutron scattering in $H_2O$ (full line); X-ray scattering in $H_2O$ (broken line).*

## 1.80 The Aggregation of Zinc-free Insulin in Solution Studied by Small-angle Neutron Scattering

R. Bauer, S. Hansen *Department of Mathematics and Physics, The Royal Veterinary and Agricultural University, Frederiksberg, Denmark*, J. Skov Pedersen, *Department of Solid State Physics, Risø National Laboratory, Denmark*

The aggregation properties of the protein hormone insulin in aqueous solutions has been studied as a function of pH, ionic stregth, and protein concentration. In order to reduce the incoherent background from hydrogen in the measured spectra and to enhance the scattering contrast the solutions were based on 100% $D_2O$. The data sets include two concentration series at respectively pH 11, 10 mM NaCl, and pH 8, 100 mM NaCl. The concentrations measured were 1, 2, 5, and 10 mg/ml. Also pH variation series with constant protein concentration (10 mg/ml) were measured for 10 mM and 100 mM NaCl.

The measured data were analysed by indirect Fourier transformation which gives $p(r)$, the correlation function multiplied by $r^2$. For low ionic strength the $p(r)$ function has a negative part, showing significant particle correlations or interactions. At low ionic strength and high pH the results show that the maximum average diameter of the aggregates are less than 50 Å, independent of protein concentration. For higher ionic strength and lower pH the $p(r)$ functions show changes which reflect the aggregation of the insulin. Furthermore, for the concentration variation series at low pH and high ionic strength the results show that the aggregation number is higher at higher concentrations. The largest aggregates have a maximum diameter of about 100 Å. They are found at pH 8, 100 mM NaCl, and 10 mg/ml protein concentration.

The influence of the particle interactions can be eliminated by omitting the part of the scattering curve at small values of the scattering vector, when performing the indirect Fourier transformation. From the $p(r)$ functions determined in this way a forward scattering intensity and a radius of gyration can be determined. As the scattering data are on an absolute scale the forward scattering can be used for calculating average molecular masses. They range from 1.3 to 6.8 times the mass of the insulin molecule (5800 Da).

The data have also been used for determining mass distributions by modelling the structure of the oligomers. The model was based on the crystal structure of cubic zinc-free insulin. The insulin is present as dimers in the crystal structure, and the form of the oligomers were taken as subsets of the unit cell. The model thus contains oligomers with the aggregation numbers 1, 2, 4, 6, 8, 10, .... The distributions show that at high pH and low ionic strength, the aggregates consist of monomers and dimers. At low pH and high ionic strength, the distribution is relatively broad and centered around a mass corresponding to about seven monomers.

The results of the SANS experiments are in very good agreement with recent elastic and dynamical light scattering experiments[1], and agree with the equilibrium model proposed by Kadima *et al.*[1].

[1] W. Kadima, L. Øgendal, R. Bauer, N. Kaarsholm, K. Brodersen, J.F. Hansen, and P. Porting (1993). Biopolymers, *submitted.*

## 1.81 Structure of Clathrin-coated Vesicles from Small-angle Scattering Experiments

J. Skov Pedersen, *Department of Solid State Physics, Risø National Laboratory, Denmark*

Small-angle neutron and X-ray scattering data from coated vesicles, reassembled coats, and stripped vesicles[1,2] have been analyzed in terms of one common structural model. The neutron data sets include contrast variation measurements at three different $D_2O$ solvent concentrations. The model used for interpreting the data has spherical symmetry and explicitly takes into account polydispersity, which is described by a Gaussian distribution. A constant thickness of the clathrin coats is assumed. The fitting of the model shows that the coated vesicles consist of a low-density outer protein shell (clathrin) and a central protein shell (accessory polypeptides and receptors) of approximately six times higher density. For the X-ray scattering and neutron contrast variation data, the polydispersity of the samples is on the order of 90 Å and the average outer radius is approximately 400 Å. The inner high-density shell has an inner and outer radius of 115 and 190 Å, respectively. A simultaneous fit (Fig. 1) to the three neutron contrast variation data sets, identifies the lipid membrane with a thickness of 40 Å and an outer radius of 196 Å. Thus the membrane and the high-density protein shell overlap in space, which shows that the lipid membrane contains protein. The molecular mass of the average particle is $27\times10^6$ Da. The coated vesicles consist, on average, of approximately 85% protein and 15% lipids. About 40% of the protein mass is situated in the central high-density shell, which gives a large amount of protein in the lipid membrane. The densities of the central shell and the lipid membrane show that the hydration is small in the central region. The results from the neutron data for the reassembled coats show that the structure of these particles is very similar to the structure of the native coats. The main difference is a higher density of the central protein shell, which shows that the membrane is replaced by protein in the reassembled coats.

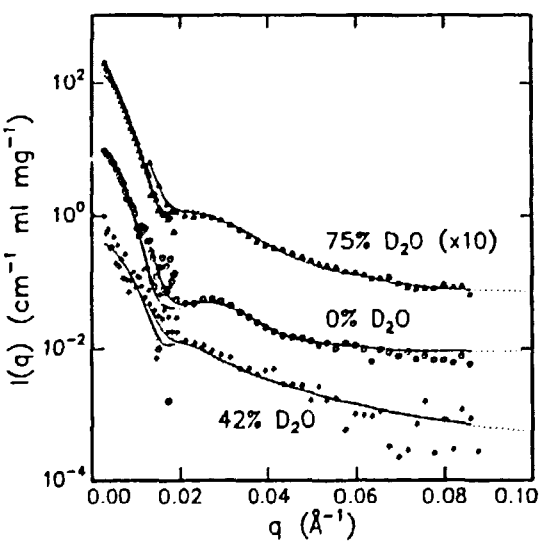


*Fig. 1. Small-angle neutron scattering data for coated vesicles. The lower, middle, and upper data sets are for 42, 0, and 75% $D_2O$, respectively. The data for 75% are multiplied by 10. The solid lines are the simultaneous fit of the two-shell model, smeared by instrumental resolution. The dotted lines are the corresponding ideal fit.*

[1] R. Bauer, M. Behan, S. Hansen, G. Jones, K. Mortensen, T. Særmark, and L. Øgendal, (1991). J. Appl. Cryst. **24**, 815.

[2] R. Bauer, M. Behan, D. Clark, S. Hansen, G. Jones, K. Mortensen, and J. Skov Pedersen, (1992). Eur. Bioph. J. **21**, 129.

## 1.82 Beryllium and Diamond Crystals as Monochromators in Intense Synchrotron Radiation Beams

J. Als-Nielsen and K. Kjær, *Department of Solid State Physics, Riso National Laboratory, Denmark*

The power density in synchrotron radiation (SR) beams from insertion devices (wigglers and undulators) in, *e.g.*, the SR sources DORIS in Hamburg or ESRF in Grenoble is so high that the heat load on the first optical element in the beam presents a very severe problem for obtaining optimal performance of that element. When the first element is a monochromator crystal one simple solution is to use a Be or diamond crystal in transmission (Laue) geometry instead of the conventional perfect crystals of Si or Ge, because Be and carbon are semi-transparent to the X-ray beam so typically only 10% or less of the beam power is absorbed in a crystal. Beryllium crystals are mosaic and the question, then, is whether crystals can be produced with a mosaicity which is acceptable in comparison to the angular divergence of the SR beam. Diamond crystals can be perfect and here the question is whether thin, perfect diamond discs can be produced with a sufficiently large area compared to the SR beam cross section.

A further advantage of Be or diamond monochromators in transmission geometry is that the polychromatic beam may be utilized further downstream on another low-Z monochromator crystal set to Bragg reflect at another wavelength so a number of experimental stations may utilize the same insertion device in simultanous operation. This idea is being implemented at least in one undulator beam at the ESRF.

We have compared the performance of Be(002) and diamond C(111) monochromator crystals in Laue geometry to that of conventional Si and Ge monochromators in (111), resp. (333). Bragg geometry utilizing a relatively low-power SR beam from a bending magnet (D4) at DORIS. Figure 1 shows the monochromatic beam intensity through a 2 mm wide by 0.1 mm high aperture situated about 22 meters from the source (12.12 m bending radius at 4.45 GeV) in photons per second per mA machine current.

In terms of raw flux the Be crystal provides the most intense beam in the entire wavelength range from 0.4 Å to 1.6 Å, but this is at the expense of a comparatively broad wavelength band and some increase of the intrinsic SR beam divergence due to the 0.2 mrad (FWHM) mosaic spread of the Be crystal. This crystal is attractive on a machine like DORIS where the emittance is not particularly low and which is therefore more suited to experiments requiring high flux rather than high brillance. The Be crystal is currently utilized at the undulator beam line BW1 in the DORIS by-pass. Its usefulness in such experiments is demonstrated by-pass in DORIS is report.

The monochromatic beam intensity from the diamond crystal is less than that from Si or Ge, simply because the Darwin width of C(111) is considerably less than that for Si(111) and Ge(111), so for an incident beam of sufficiently low divergence, the reduced intensity is compensated by a correspondingly higher wavelength resolution. Analysis of the data in Fig. 1 indicates that the diamond crystal is perfect. At a low emittance storage ring like the ESRF it should therefore be possible to focus the *monochromatic* beam to a very small size at the sample position.

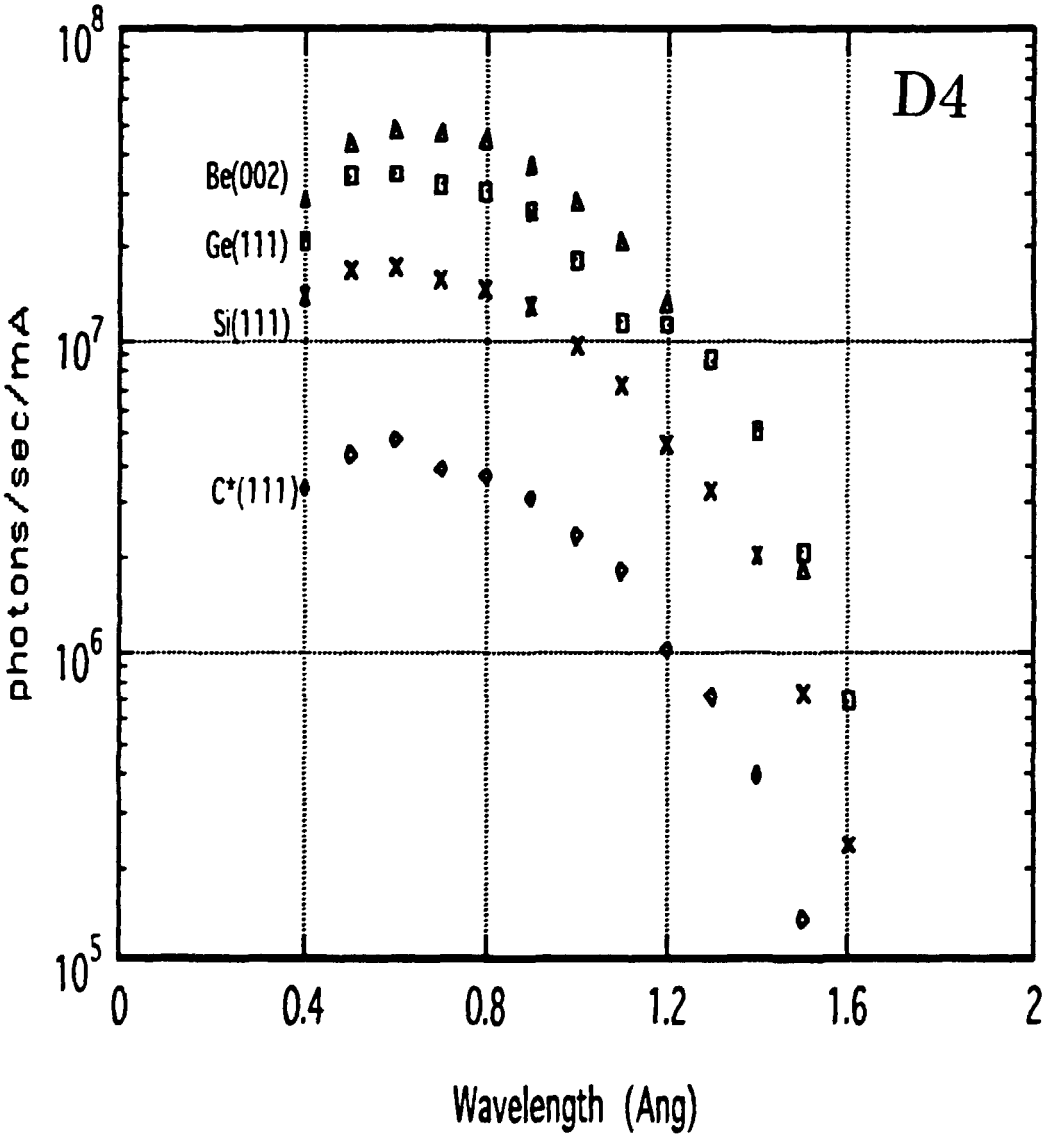


*Fig. 1. Monochromatic beam intensity through a 2 mm wide by 0.1 mm high aperture situated 22 m from the bending magnet D4 in DORIS at 4.45 GeV. Analysis*[1] *of these data in terms of incident brightness (photons per sec. per mA per (mrad)*$^2$ *and per 0.1% band-width) reveals consistency between the results obtained with the four different crystals and good agreement with the theoretically expected brightness.*

[1] J. Als-Nielsen and K. Kjær (1992). Nuclear Inst. Meth. **A323**, 686.

## 1.83 Commissioning and First Results from the Liquid Surface Diffractometer BW1 in HASYLAB

K. Kjær, *Department of Solid State Physics, Risø National Laboratory, Denmark,* J. Majewski, *Department of Materials and Interfaces, Weizmann Institute of Science, Rehovot, Israel,* H. Schulte-Schrepping, and J. Weigelt, *HASYLAB at DESY, Hamburg, Germany*

The BW1 beam line of the HASYLAB Bypass and the Risø BW1 diffractometer were further commissioned and the first scientific results were obtained.

For liquid surface studies, the white synchrotron beam enters the experimental hutch after reflection by a flat and a toroidal mirror to be monochromatized by a beryllium (002) crystal (*cf.* next contribution) 1 meter from the sample. Figure 1 shows the diffractometer. In early October, this mode of operation was tested with the storage ring DORIS-III running at 5.3 GeV and a 1.1 Tesla wiggler as insertion device. For large apertures, the intensity after the second mirror was unstable, decreasing by 90 per cent in a few minutes after the shutter was opened. Most probably, the heat load deforms the first mirror such that the once-reflected beam does not make it past the second mirror. At smaller beam apertures, stable intensities were obtained. However, these tests were cut short by the premature termination (due to vacuum problems) of the 5.3 GeV run.

During the October shut-down, the design insertion device, an undulator with a variable magnetic gap and a maximum field of 0.55 Tesla, was installed by HASYLAB. During November, with DORIS-III running at 4.5 GeV, the undulator beam was tested at a gap of 15.6 mm. With the lower power load, stable intensities were obtained. The beam could be monochromatized and deflected down by the beryllium Laue crystal to hit the water surface. The monochromatic intensity through a 5 mm wide by 0.1 mm high aperture before the sample was *abt;* 100 times that obtained at the unfocussed bending magnet beam line D4, with horizontal $2\theta$-resolution *abt;* 50 percent wider.

With this very intense beam, and with lower background in the BW1 hutch than at D4, Grazing-Incidence-Diffraction data of unprecedented quality could be obtained from Langmuir films at liquid surfaces. A few figures-of-merit:

- For a monolayer of $CH_3(CH_2)_{30}OH$ on water at 2°C, six peaks of the 2D-powder pattern were measureable, with a signal/background ratio of 19 for the lowest-$2\theta$ peak.
- For a monolayer of $CH_3(CH_2)_{18}CONH_2$ on a water/formamide mixture at 4°C, nine peaks could be measured.
- Specular reflectivities could be measured down to $10^{-9}$ of the incident beam.

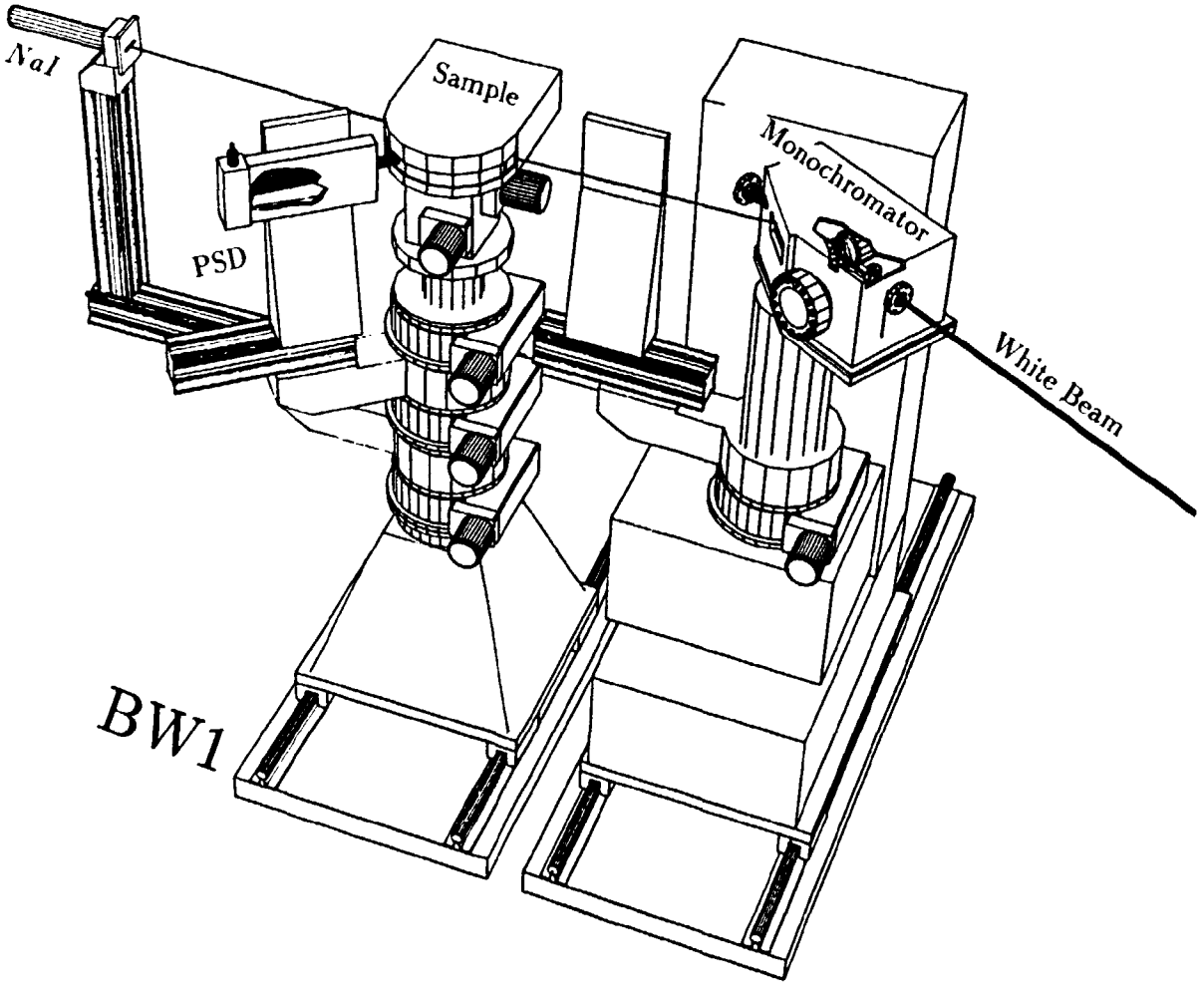


*Fig. 1. The BW1 liquid surface diffractometer with (right to left) white beam entering He-filled box with Be monochromator, monochromatic beam striking the liquid surface sample at a shallow angle from the vertical, position sensitive detector (PSD) for horizontally diffracted beam and NaI detector for the specularly reflected beam.*

## 1.84 Monochromator and Slits for ESRF Undulator Beam

J. Als-Nielsen and J.Linderholm, *Department of Solid State Physics, Riso National Laboratory, Denmark*

We have designed, built and tested a monochromator assembly for use at ESRF undulator beams: the Machine Physics Diagnostics Beamline ID6(1), and the TROIKA beam line ID10(2). The monochromator crystal is Be or Diamond (see 1.xx) mounted in Laue transmission geometry in a water-cooled copper block. Upstream from the monochromator crystal is a vertical and a horizontal aperture. Each of these consists of two parallel cylinders of radius $R$ with a center distance of $2(R + d)$. The midpoint of the centerline coincides with the beam axis and as the two cylinders are rotated around this midpoint the interception of the beam varies. The transmitted beam width $\gamma$ at rotation angle $\phi$ is easily derived:

$$\gamma = 2(R + d)\left[1 - \frac{\cos\phi}{\cos\phi_0}\right].$$

Here $\phi = 0$ corresponds to full open aperture and $\phi = \phi_0$ to the closed position. In this way the aperture can be varied continuously with high precision by a simple rotation of a turn table driven by a stepping motor. The cylinders are water cooled and since the beam hits the cylinder surface under grazing angles the power density is not too high for reliable operation of this simple device in the central cone of an undulator beam.

The two apertures and the monochromator crystal are situated in a vacuum cannister with a Beryllium window to allow $2\theta$ angles of the monochromator between 20° and 100°. Below the cannister is a $2\theta$ arm where one can mount a simple goniometer (ID6) or an entire diffractometer (ID10) on air cushions.

Experiments on the Machine Physics Diagnostics beam line concerning the undulator energy spectrum, stability of the beam, angular emmitance, absolute photon flux an the performance of diamond monochromator under different heat loads were controlled by a PC based mobil station developed in the Electronics Department at Risø. It is similar to the control system used for the X-ray diffractometer at the Solid State Physics Department at Risø.

## 1.85 A Portable Pb Cluster Source for X-ray-scattering Measurements of Freely Suspended Clusters

A.R. Sandy and J. Bohr, *Department of Solid State Physics, Riso National Laboratory, Denmark*

The reliable experimental determination of the geometric structure of freely suspended clusters is one of the fundamental problems in cluster research. Given its long history of success in determining bulk and surface structures, X-ray scattering would seem an obvious choice for determining cluster structures. A principle reason for this success is that X-rays interact weakly with matter so the scattering cross section can be reliably calculated using only the First Born Approximation: but this is also why it has not been possible to study free clusters using X- rays.

However, the high X-ray intensities available from a third-generation X-ray source like the European Synchrotron Radiation Facility (ESRF) in Grenoble, France, makes X-ray-scattering studies of cluster structure feasible. In collaboration with scientists at the Niels Bohr Institute (NBI), Copenhagen, and the ESRF, we are initiating such a research project using a vapour-condensation cluster source and a sputter cluster source.

A picture of the vapour-condensation, Pb cluster source that we have built and are testing at Riso is shown in Fig. 1. It has three main components: the condensation chamber where the clusters are actually produced, the diffraction chamber with a 360° Be window where the resulting beam of freely suspended clusters is studied via X-ray scattering, and an oscillating quartz crystal to monitor the flux of Pb in the cluster beam. The condensation chamber is nearly identical to one of proven design[1].

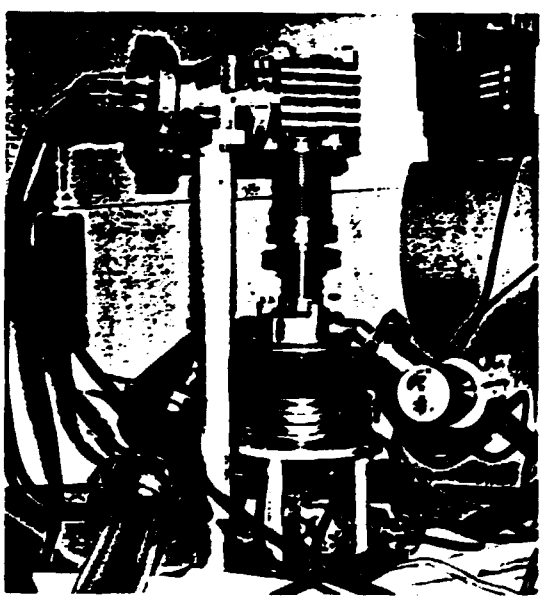

*Fig. 1. The vapour-condensation cluster source. The condensation chamber is at the bottom. Above it is the first differential pumping stage and above this is the diffraction chamber with its 360° Be window. On top is the oscillating-crystal flux monitor.*

[1] O. Echt, K. Sattler, and E. Recknagel, (1981). Phys. Rev. Lett. **47**, 1121.

## 1.86 Performance of the New Neutron Guide

K.N. Clausen, *Department of Solid State Physics, Riso National Laboratory, Denmark*

The three spectrometers in the neutron house are fed by one single neutron guide. The total length of the guide is 22 m. The first 8 m has to be removed every four years during the long shut-down of the reactor. After 15 years in operation the first elements had started to show signs of radiation damage, and had become very difficult to move. Instead of replacing the first few elements, it was decided to replace the whole guide with state of the art components, and at the same time try to optimize the design, for the constraints given by the reactor in one end and the existing instruments in the other.

The new guide has been manufactured by Neutronen Technischen Komponenten in Germany and has been improved in the following ways:

- The guide has been extended by another meter towards the cold source.
- The height of the guide was previously 200 mm. With a 130 mm Ø cold source this led to under illumination. In the new guide the height starts at approximately 150 mm close to the cold source and ends with a height of 200 mm in the neutron house.
- The width of the guide has been increased from 20 to 30 mm.
- The coating on the sides has been replaced by $^{58}$Ni instead of Ni, which increases the angle for total reflection from 6 to 7 arc-minutes/Å.
- The coating on the top and bottom is NiTi super mirror instead of Ni, which increases the angle for total reflection from 6 to 12 arc-minutes/Å. The NiTi mirrors have been manufactured by the ILL.
- The curved part (the first 8 m with a radius of curvature of 1000 m) is now continuously curved. It has a single dividing wall to avoid line of sight in the wider guide, and to improve the cut off of short wavelength neutrons.

The first experiments on the new guide was performed early December. In the 6 Å range the gain in flux on SANS was between 2.5 and 3.5. For TAS7 the results are summarized in Fig. 1. showing a substantial gain of intensity.

The available flux seems to peak at lower energies with the new guide. This is partly due to the wider beam. The present monochromator on TAS7 was designed for the old channel width and is now too narrow for E>5 meV. This could account for another factor factor of 1.5 at 14.5 meV, and hence a spectrum quite similar to previously.

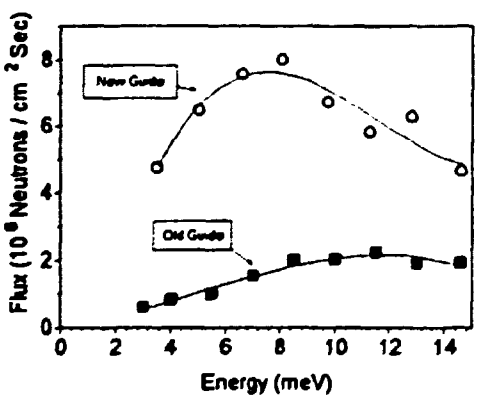


*Fig. 1 Monochromatic flux at the sample position of TAS7 with the Old and New Guide, respectively.*

## 1.87 LIP - CEC Large Installation Programme at Risø

K. N. Clausen, *Department of Solid State Physics, Risø National Laboratory, Denmark,*
A.R. Mackintosh, *Physics Laboratory, H.C. Ørsted Institute, University of Copenhagen, Denmark*

The CEC Large Installation Programme was initiated in order to make Large National Facilities available to users from the whole EC, to promote European collaboration and to make more facilities available to the less favoured regions in the EC.

The cold neutron facilities at DR3 were included in this programme from early 1992. Risø receives funds from the CEC to cover the marginal expenses in connection with neutron scattering experiments. The programme covers 1) Travel and subsistence for the users, 2) Salaries to staff employed to run the user programme, 3) Running expenses (consumable), 4) Purchase of auxiliary equipment requested by the users, and 5) A contribution to the continued modernization and upgrading of the facilities.

The programme is managed by a programme director (A.R. Mackintosh) representing the users and a project leader (K.N. Clausen) responsible for the facilities and the practical arrangements in connection with the experiments.

Proposals for experiments are refereed by a group of 4 international experts, in collaboration with the programme director. Beam time is allocated four times a year, and amounts to 79 instrument weeks per year, approximately 30% of the available resources. Experiments are generally collaborative efforts between the User and Risø via the local contact. The duration of a single experiment is from 1/2 - 3 weeks, and both junior and senior visiting scientists participate in the experiment. In total approximately 100 EEC-scientist have spent up to 3 weeks at Risø during 1992 in connection with LIP experiments.

Below is a list of the titles of the LIP experiments performed in 1992. The column "Proposer" contains the first name on the proposal. The local contact at Risø is shown by initials (**NHA:** N.H. Andersen, **KNC:** K.N. Clausen, **DJJ:** D.J. Jensen, **KK:** K. Kjær, **BL:** B. Lebech, **TL:** T. Lorentzen, **KM:** K. Mortensen, **TM:** T. Mason, **MN:** M. Nielsen, **JSP:** J. Skov Pedersen). Reports on the experiments below will be published in the annual LIP report.

| Proposer | Local contact | Title |
|---|---|---|
| M. Alba | TM | Mode Coupling Theory and Critical Dynamics of Disordered Ferromagnets |
| G. Albertini | TL | Residual Strain in a Tig Welded Component of AlSi304 Steel |
| T.M. Bayerl | KM | Curvature Dependence of Mixing Behavior of Binary Phospholipid/Cholesterol Mixtures |
| N.R. Bernhoeft | BL | Magnetic Structures in MnSi and FeGe |
| A.T. Boothroyd | NHA | The Magnetic Structures in $PrBa2Cu_3O_7$ |
| J. Bradshaw | JSP | SANS Studies of Influenza Virus |
| G. Caglioti | DJJ | Mechanical Damage of Highly Deformed Aluminium Alloys |
| R.A. Cowley | KNC | Magnetic Structure of Er in a Magnetic Field |
| R.A. Cowley | KNC | The Magnetic Structures of Holmium-Yttrium Multilayers |
| R.A. Cowley | KNC | Magnetic Structure and Excitations of Erbium |
| R.A. Cowley | KNC | Magnetic Structure of Rare Earth Multilayers |
| H.W. de Wijn | MN | Ordering of Frustrated Two-Dimensional Magnetic Systems |
| M. Enderle | KNC | Test of Haldane's conjecture in $CsNiCl_3$ and $CsMnI_3$ |
| Olaf Engler | DJJ | Neutron Texture Determination in Two-Phase fcc/bcc Materials |
| E.M. Forgan | BL | Critical Scattering and Magnetic Ordering in $CeAl_2$ |
| E.M. Forgan | KM | Flux Lattice Structures in Superconductors |
| M. Garcia-Hernandez | TM | Low Frequency Dynamics of Liquid Glassy Selenium |
| J.E. Greedan | JSP | Magnetic Microstructure in the Frustrated Nearly Ferromagnetic Oxides $R_2Mn_2O_7$; R=Ho,Y,Lu |
| T. Hack | KM | Critical Scattering and Spinodal Decomposition Kinetics of Polystyrene/Polyacrylate Blends |
| A. Harrison | TM | Dispersion of Spin-waves in the S=1/2 Square Heisenberg Antiferromagnet $Cu(DCO_2)_{2.4}D_2O$ |
| A. Harrison | KNC | Static Spin Correlations in the S=1/2 Triangular Heisenberg Antiferromagnet $NaTiO_2$ |
| S.M. Hayden | TM | Examination of Magnetic Correlations in $La_{2-x}Sr_xNiO_4$ Single Crystals |
| S. Hayden | TM | Magnetic Fluctuations in High Temperature Superconductors |
| W. Hayes | NHA | Diffuse Scattering from $YBa_2Cu_3O_{6.5}$ Single Crystal |
| M. Heidelmann | BL | The Magnetic Phase Diagrams of $RECu_2$ Compounds (RE=Tm;Er) |

| | | |
|---|---|---|
| M.T. Hutchings | KNC | Energy Broadening of Phonon Modes in Hyperstoichiometric $UO_{2+x}$ |
| J.E. King | TL | Residual Macro- and Interphase Stresses in Crack Propagation in Metal Matrix Composites |
| G.H. Lander | BL | Crystallographic Examination of $Nd_2Fe_{14}$ and $Ho_2Co_{17}$ Single Crystals |
| M. Lösche | KK | Interactions between Photoreceptor Extrinsic Proteins and the Visual Membrane |
| K.A. McEwen | KNC | Magnetic Field Dependence of Structures and Excitations in Pr |
| R.L. McGreevy | NHA | Short Range Correlations in the Spin Glass CuMn and the Dilute Semiconductor ZnMnTe |
| R.L. McGreevy | NHA | Structural Disorder in Co Substituted $YBa_2Cu_3O_{6+y}$ |
| D. MacMorrow | KNC | Magnetic Structure of Rare-earth Superlattices (Ho-Lu) |
| G.F. Modlen | DJJ | Preferred Orientation in Cold-Extruded Rods |
| P. Müller | KNC | Elastic Neutron Diffraction on New Deuterides and Chalcogenides |
| B.D. Rainford | TM | Magnetic Excitations in a Sinusoidal Magnetic Structure |
| H. Reynaers | KM | Exploration of Network Structure in Plasticized PVC on Orientation and Relaxation |
| E. Sackmann | KM | Phase Diagram of Lecithin/Cholesterol Mixtures in the Critical Region |
| D. Schwahn | KM | The Pressure and Temperature Dependence of the Flory-Huggins Parameter |
| R.N. Sinclair | KNC | Depth Profile of Implanted Atoms in Metals and $UO_2$ |
| R.N. Sinclair | KM | Evolution of Irradiation Damage Microstructures in Model Alloys |
| D.J. Smith | TL | Measurement of the Redistribution of Residual Stresses after Mechanical Loading |
| U. Steigenberger | KNC | Magnetic Excitations of $UPd_3$ in a Field |
| J.R. Stephenson | JSP | SANS Studies on the Mechanism of Virus Neutralisation |
| W. Stirling | BL | Critical Scattering in $USb_{0.8}Te_{0.2}$ |
| G. Strobl | NHA | Correlated Rotational Motion in the High- Temperature Phase of Polytetra- fluoroethylene |
| G. Strobl | NHA | Confined Segmental Motion in the Amorphous Regions of Polyethylene |
| D. Svergun | JSP | Contrast Variation Study of the 50S Subunit of the E. Coli Ribosome |

| | | |
|---|---|---|
| G. Swallowe | TL | Physics of Strain Measurements Using Neutrons |
| R.I. Todd | TL | Internal Stresses in Platelet-reinforced Ceramic-ceramic Composities |
| P. Van Houtte | DJJ | Texture Analysis during Phase Transformation in Low Carbon Steel |
| D. Visser | TM | Magnetic Excitations in the Modified Triangular Induced Moment Antiferromagnet $RbFeBr_3$ |
| M.R. Wells | TM | Magnetic Order in Barium Holmium Fluoride |
| M.R. Wells | TM | Magnetic Order in $BaHo_2F_8$ and $BaEr_2F_8$ |
| M. Winkelman' | NHA | Magnetic Structure Determination of $MgCu_2O_3$ |
| E. Woldt | DJJ | The Recrystallization Transformation Curve of Copper based on Texture Measurements |

### 1.88 The Liquid He Plant

K. Christensen and M. Nielsen, *Department of Solid State Physics, Risø National Laboratory, Denmark*

For the year 1992 the following quantities of liquid He were delivered: 60150 liters. Of this 53100 liters He are used outside Risø. From March 1993 Risø will stop liquefying helium and buy liquid helium on the commersial market.

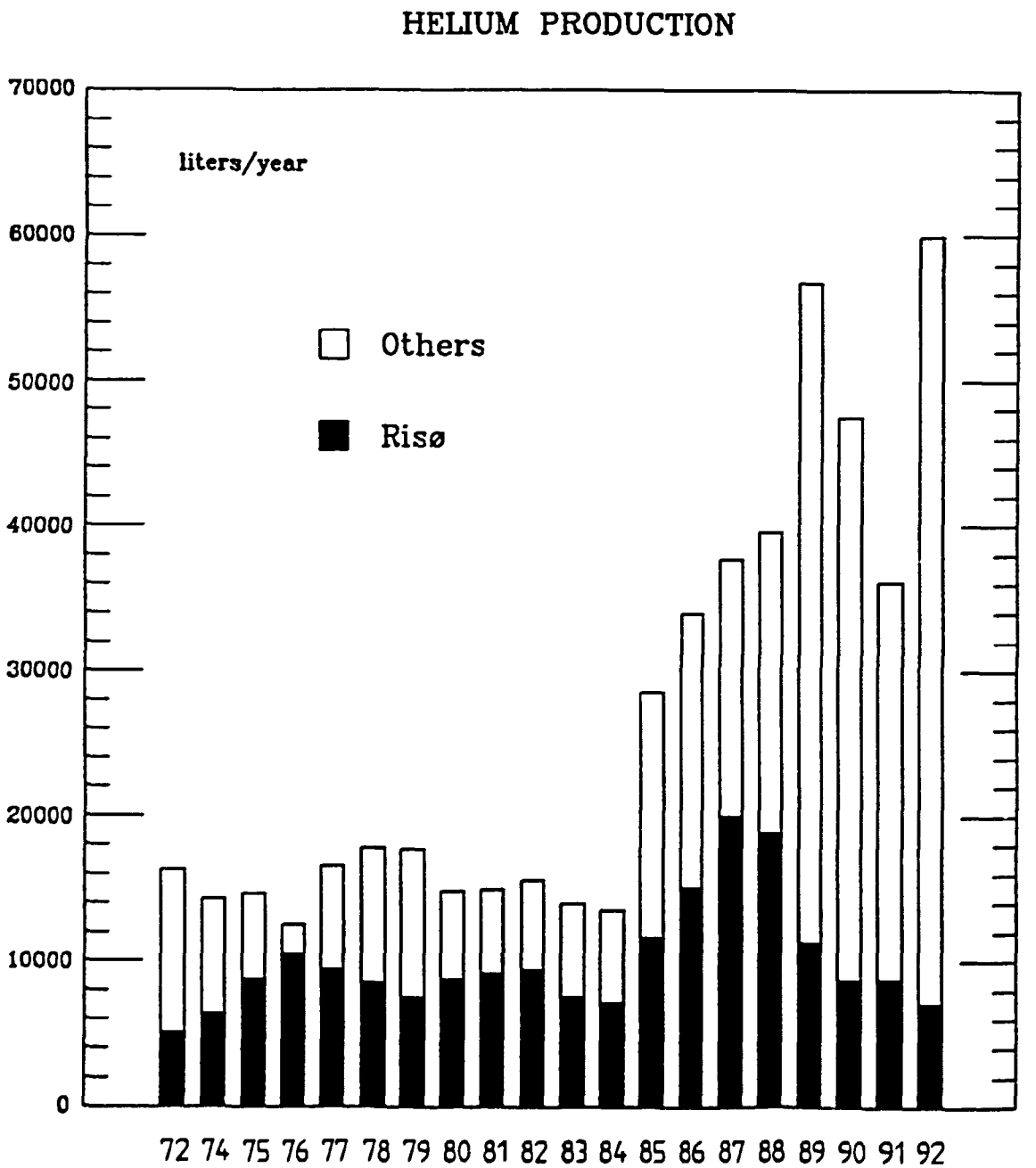

# 2 PARTICIPANTS IN THE WORK IN THE DEPARTMENT

### Scientific Staff

Als-Nielsen, Jens (Head) (Until 1 September)
Andersen, Niels Hessel
Bohr, Jakob
Buras, Bronislaw (Part time consultant)
Clausen, Kurt Nørgaard
Feidenhans'l, Robert
Kjær, Kristian
Lebech, Bente
Lebech, Jens
Lindgård, Per-Anker
Mackintosh, Allan R. (Part time consultant)
Mason, Thomas E.
Mortensen, Kell
Nielsen, Mourits
Pedersen, Jan Skov
Schou, Jørgen

### Ph.D. Students and Students

Falcão, Antonio
Fiig, Thomas
Findeisen, Eberhard (From 1 February)
Foss, Morten (From 1 February, with IFA, Århus University)
Gerstenberg, Michael Christian (From 31 August)
Harris, Pernille
Jensen, Carsten Povl (From 31 August)
Kromann, Rasmus (Until 1 August 1992)
Lefmann, Kim
Petersen, Thomas (From 1 April)
Poulsen, Henning Friis (Until 31 January)
Scherzer, Joseph (From 8 August)
Thoft, Nina Bjørn

### Temporary Students Assistants

Madsen, J.
Oddershede, L.
Paulsen, J.

### Technical Staff

Bang, Steen

Christensen, Kaj
Eiby, Jan (Temporary assistant)
Hansen, René
Kjær, Torben
Linderholm, Jens
Lund, Morits
Nielsen, Steen
Nordskov, Arne
Petersen, Henrik (Temporary assistant)
Rasmussen, Ove
Saxild, Finn B. (From 1 September)
Stahl, Kim
Theodor, Keld
Thuesen, Allan (Until 1 November)
Wichmann, Poul E. (Temporary assistant)

### Secretaries

Frederiksen, Lajla
Kloster, Margit
Korgaard, Charlotte (Apprentice from 1 April until 12 June)
Studinski, Ca Thi (From 15 January)
Thomsen, Susanne (Apprentice from 1 September until 30 November)

### Guest Scientists, Long Time Visitors and Post Docs

| | |
|---|---|
| Pengra, David | |
| de Reus, Roger | (Until 1 April) |
| Sandy, Alec R. | (From 8 June) |
| Vives, Eduard | University of Barcelona, Spain (Until 28 August 1992) |

**Short Time Visitors (more than one week)**

| | |
|---|---|
| Aeppli, G. | AT&T Bell Laboratories, Murray Hill, New Jersey, U.S.A. |
| Bates, F. | University of Minnesota, U.S.A. |
| Besold, G. | Erlangen University, Germany |
| Bishop, D. | AT&T Bell Laboratories, Murray Hill, New Jersey, U.S.A. |
| Boué, F. | Laboratorie Léon-Brillouin, Saclay, France |
| Bänninger, R. | ETH, Zürich, Switzerland |
| Calderon, H. | ETH, Zürich, Switzerland |
| Casalta, H. | Université de Paris-sud, Orsay, France |
| Diderich, A. | University of Mainz, Germany |
| Dutkiewicz, L. | Jagellonian University, Krakow, Poland |
| Falicov, L. | University of California, Berkely, USA |
| Fisk, Z. | Los Alamos National Laboratory, New Mexico, U.S.A. |
| Fjellvåg, H. | University of Oslo, Norway |
| Gammel, P. | AT&T Bell Laboratories, Murray Hill, New Jersey, U.S.A. |
| Grandbois, M. | University of Quebec, Canada |
| Hadfield, R.A. | Clarendon Laboratories, University of Oxford, U.K. |
| Hamley, I. | University of Minnesota, U.S.A. |
| Honger, T. | The Technical University, Denmark |
| Kakurai, K. | University of Tokyo, Japan |
| Kawano, S. | University of Kyoto, Japan |
| Kleimann, R. | AT&T Bell Laboratories, Murray Hill, New Jersey, U.S.A. |
| Koppi, K.A. | University of Minesota, USA |
| Mohama, Y. | AT&T Bell Laboratories, Murray Hill, New Jersey, U.S.A. |
| Mook, H.A. | Oak Ridge National Laboratory, U.S.A. |
| Nordby, P. | University of Odense, Denmark |
| Norlund Christensen, A. | University of Aarhus, Denmark |
| Pedrys, R. | Jagellonian University, Krakow, Poland |
| Rasmussen, J. | ESRF, Grenoble, France |
| Rosedale, J. | University of Minnesota, U.S.A. |
| Scherrenberg, R. | University of Leuven, Belgium |
| Schneiders, D. | KFA, Jülich, Germany |
| Schultz, M. | University of Minnesota, U.S.A. |
| Sequeira, A. | ETH, Zürich, Switzerland |
| Sjöberg, B. | University of Gothenburg, Sweden |
| Smetana, Z. | Charles University, Prague, Czechoslovakia |
| Stassis, C. | Ames Laboratories, U.S.A. |
| Stühn, B. | University of Freiburg, Germany |
| Vaknin, D. | Iowa State University, U.S.A. |
| Vyskocil, P. | ETH, Zürich, Switzerland |
| Wang, J. | Iowa State University, U.S.A. |

## Visitors under the CEC Large Instalation Program (more than one week)

| | |
|---|---|
| Alba, M. | Institut Laue-Langevin, Grenoble, France |
| Albertini, G. | Universita di Ancona, Italy |
| Auffermann, G. | RWTH, University of Aachen, Germany |
| Bayerl, T. | Technical University, München, Germany |
| Bernhoft, N.R. | University of Durham, U.K. |
| Bleaney, B. | Clarendon Laboratories, University of Oxford, U.K. |
| Boothroyd, A.T. | Clarendon Laboratories, University of Oxford, U.K. |
| Bradshaw, J. | University of Edinburgh, U.K. |
| Brouillon, P. | EMBL, Hamburg, Germany |
| Brumm, T. | Technical University, München, Germany |
| Ceretti, M. | Universita di Ancona, Italy |
| Cicognani, G. | ENEA, Bologna, Italy |
| Clarke, S.J. | Inorganic Chemistry Laboratory, University of Oxford, U.K. |
| Cowly, R.A. | Clarendon Laboratories, University of Oxford, U.K. |
| Crooks, A. | Division of Biologies, PHLS, U.K. |
| Duff, K. | University of Edinburgh, U.K. |
| Enderlee, M. | University of Mainz, Germany |
| Fitzpatrick, M.E. | Materials Science and Metallurgy, University of Cambridge, U.K. |
| Forgan, E.M. | University of Birmingham, U.K. |
| Garcia-Hernandez, M. | Instituda de Estructura de la Materia, Spain |
| Goff, J.P. | AEA Industrial Technology, Oxford, U.K. |
| Greedan, J.E. | ISMRA, Caen, France |
| Gregory, C.I. | University of Durham, U.K. |
| Hack, T. | Max-Planck-Institute, Mainz, Germany |
| Hadfield, R.A. | Clarendon Laboratories, University of Oxford, U.K. |
| Harrison, A. | Inorganic Chemistry Laboratory, University of Oxford, U.K. |
| Hayden, S.M. | University of Bristol, U.K. |
| Heidelmann, M. | KFA, Jülich, Germany |
| Holzer, B. | University of Freiburg, Germany |
| Hutchings, M.T. | AEA Industrial Technology, Oxford, U.K. |
| Janssen, S. | KFA, Jülich, Germany |
| Jehan, D. | Clarendon Laboratory, University of Oxford, U.K. |
| Kimming, M. | University of Freiburg, Germany |
| Knowles, D.M. | Materials Science and Metallurgy, University of Cambridge, U.K. |
| Lander, G.H. | The Transuranium Institute, Karlsruhe, Germany |
| Langridge, S. | University of Keele, U.K. |
| Leask, M.J.M. | Clarendon Laboratories, University of Oxford, U.K. |
| Lee, S.L. | University of Birmingham, U.K |
| Longmore, A. | Clarendon Laboratories, University of Oxford, U.K |
| Lösche, M. | University of Mainz, Germany |
| Marshall, W. | Birkbeck College, London, U.K. |
| Martinez, J. | Institut Laue-Langevin, Grenoble, France |
| McEwen, K.A. | Birkbeck College, London, U.K. |
| McGreevy, R.L. | Clarendon Laboratories, University of Oxford, U.K. |
| McKeighan, P. | University of Bristol, U.K. |

| | |
|---|---|
| McMorrow, D.F. | Clarendon Laboratories, University of Oxford, U.K. |
| Modlen, G. | Loughborough University of Technology, U.K. |
| Moze, O. | Instituto ISM del CNR, Frascati, Rome, Italy |
| Müller, P. | RWTH University of Aachen, Germany |
| Nutley, M. | Institut Laue-Langevin, Grenoble, France |
| Osborne, J. | Loughborough University of Technology, U.K. |
| Paul, D. Mck. | University of Warwick, U.K. |
| Pouget, S. | Institut Laue-Langevin, Grenoble, France |
| Rainford, B. | University of Southampton, U.K. |
| Rumpp, E. | University of Mainz, Germany |
| Schmid, B. | Institut Laue-Langevin, Grenoble, France |
| Schouwenaars, R. | University of Leuven, Belgium |
| Schwahn, D. | KFA, Jülich, Germany |
| Shaikh, S.J. | University of Birmingham, U.K. |
| Simpson, A. | Clarendon Laboratories, University of Oxford, U.K. |
| Sinclair, R.N. | AEA Industrial Technology, Oxford, U.K. |
| Smith, D.J. | University of Bristol, U.K. |
| Steigenberger, U. | Rutherford Laboratory, U.K. |
| Stirling, W.G. | University of Keele, U.K. |
| Stölken, S. | Max-Planck-Institute, Mainz, Germany |
| Svergun, D.I. | EMBL, Hamburg, Germany |
| Swaddling, P. | Clarendon Laboratories, University of Oxford, U.K. |
| Swallowe, G. | Loughborough University of Technology, U.K. |
| Tood, R.I. | Clarendon Laboratories, University of Oxford, U.K. |
| Visser, D. | Loughborough University of Technology, U.K. |
| Webster, P.J. | Loughborough University of Technology, U.K. |
| Wells, M.R. | Clarendon Laboratories, University of Oxford, U.K. |
| Wicks, J. | Clarendon Laboratories, University of Oxford, U.K. |
| de Wijn, H.W. | University of Utrecht, The Netherlands |
| Windsor, C.G. | AEA Industrial Technology, Oxford, U.K. |
| Winkelmann, M. | Hahn-Meitner-Institute, Berlin, Germany |
| Withers, P.J. | Materials Science and Metallurgy, University of Cambridge, U.K. |
| Woldt, E. | Technical University, Braunschweig, Germany |

## Awards and Degrees

Poulsen, H. Friis, Ph.D., Copenhagen University, Denmark
Kromann, R., Ph.D., The Technical University, Denmark

# 3 PUBLICATIONS AND EDUCATIONAL ACTIVITIES IN THE DEPARTMENT

## 3.1 Publications


AEPPLI, G., BUCHER, E., and MASON, T.E. (1992). Neutron Scattering and High Field Experiments on Kondo Metals and Insulators. In: Physical Phenomena at High Magnetic Fields, Proceedings. E. Manousakis, P. Slottmann, P. Kumar, K.S. Bedell, and F.M. Mueller (eds.), (Addison-Wesley Publishing Co., Redwood City), 175-183.

AEPPLI, G., FISK, Z., HAYDEN, S.M., HUNDLEY, M.F., HOOK, H., and RYTZ, D. (1992). The Marginal Fermi Liquid Hypothesis and Magnetic Fluctuations in $La_{1.95}Ba_{0.05}CuO_4$. J. Magn. Magn. Mat., **104/107**, 505-507.

ALMDAL, K., BATES, F.S., and MORTENSEN, K. (1992). Order, Disorder, and Fluctuation Effects in an Asymmetric Poly(ethylene-propylene)-Poly(ethylethylene) Diblock Copolymer. J. Chem. Phys. **96**, 9122-9132.

ALMDAL, K., KOPPI, K.A., BATES, F.S., and MORTENSEN, K. (1992). Multiple Ordered Phases in a Block Copolymer Melt. Macromol. **25**, 1743-1751.

ALS-NIELSEN, J. (1991). Synchrotron X-ray and Cold Neutron Studies of Amphiphilic Monolayer Structures. In: Structure and Dynamics of Strongly Interacting Colloids and Supramolecular Aggregates in Solution. NATO Advanced Study Institute on Structure and Dynamics of Strongly Interacting Colloids and Supramolecular Aggregates in Solution, Acquafredda di Maratea, Italy, 11-21 June, Chen, S.-H., Huang, J.S., Tartaglia, P. (eds.), (Kluwer Academic Publishers, Dordrecht, 1992) (NATO Advanced Science Institutes Series C: Mathematical and Physical Sciences, 369), 589-616.

ALS-NIELSEN, J. (1992). Synkrotron Røntgenstråling - (Frem)tidens Værktøj i Fysik, Kemi og Molekylær Biologi (Synchrotron X-rays - The Tool of the Future in Physics, Chemistry and Molecular Biology). Forskning **8**, 20-21.

ALS-NIELSEN, J. and KJÆR, K. (1992). Crystal Spectroscopy of X-ray Synchrotron Source Brigthness. Nucl. Inst. Meth. Phys. Res. A **323**, 686-693.

ANDERSEN, N.H., BANDARANAYAKE, P.W.S.K., CAREEM, M.A., DISSANAYAKE, M.A.K.L., WIJAYASEKERA, C.N., KABER, R., LUNDÉN, A., MELLANDER, B.-E., NILSSON, L., and THOMAS, J.O. (1992). Paddle-wheel versus Percolation Mechanism for Cation Transport in Some Sulphate Phases. Solid State Ionics **57**, 203-209.

ANDERSEN, N. H., FRELTOFT, T., BINDSLEV HANSEN, J., HEDEGÅRD, P., and GUTZON LARSEN, J. (1992). Højtemperatur-superledere (High Temperature Superconductors). (Industriens Forlag, København, 1992) (Det Materialeteknologiske Udviklingsprogram, temahæfte 6) 33 p.

ANNILA, A.J., CLAUSEN, K.N., OJA, A.S., TUORINIEMI, J.T., and WEINFURTER, H. (1992). Neutron-Diffraction Studies of the Nuclear Magnetic Phase Diagram of Copper. Phys. Rev. B **45**, 7772-7788.

BAUER, R., BEHAN, M., CLARKE, D., HANSEN, S., JONES, G., MORTENSEN, K., and PEDERSEN, J. SKOV. (1992). Contrast Variation Studies of Clathrin Coated Vesicles by Small-Angle Neutron Scattering. Eur. Biophys. J. **21**, 129-136.

BOHR, J., GIBBS, D., SINHA, S.K., KRÄTSCHMER, W., TENDELOO, G. VAN, LARSEN, E., EGSGAARD, H., and BERMAN, L.E. (1992). Order, Disorders, and Structure of Crystals of C60/C70. Europhys. Lett. **17**, 327-332.

BOHR, J. and GREY, F. (1992). Epitaxial Rotations and Finite Size Effects. Condens. Matter News **3**, (No. 1), 12-15.

BOHR, J. and GREY, F. (1992). Roterede Krystaller (Rotated Crystals). Kvant **2**, 1-3.

BROWN, W., MORTENSEN, K., and FLOUDAS, G. (1992). Screening Lengths in Concentrated Polystyrene Solutions in Toluene Determined Using Small Angle Neutron and Small Angle X-ray Scattering. Macromol. **25**, 6904-6908.

CLARKE, S.J., HARRISON, A., MASON, T.E., McINTYRE, G.J., and VISSER, D. (1992). Magnetic Ordering and Fluctuations in the S=1/2 Square Heisenberg Antiferromagnet $Cu(DCO_2)_24D_2O$. J. Phys.: Condens. Matt. **4**, L. 71-76.

CLAUSEN, B.S., STEFFENSEN, G., FABIUS, B., VILLADSEN, J., FEIDENHANS'L, R., and TOPSØE, H. (1991). In Situ Cell for Combined XRD and On-line Catalysis Tests: Studies of Cu-based Water Gas Shift and Methanol Catalysts. J. Catal. **132**, 524-535.

CLAUSEN, K.N. (1991). Neutron Scattering at nK Temperatures. Neutron News **2**, 4, 25-28.

DORNISCH, D., MORITZ, W., SCHULZ, H., FEIDENHANS'L, R., NIELSEN, M., GREY, F., JOHNSON, R.L., and LE LAY, G. (1992). Ag on Ge(111): 2D X-ray Structure Analysis of the $\sqrt{3} \times \sqrt{3}$ Superstructure. Surf. Sci. **274**, 215-221.

ELLEGAARD, O., SCHOU, J., STENUM, B., SØRENSEN, H., and PEDRYS, R. (1992). Sputtering Yields and Energy Distributions from Nonoverlapping Subspikes in Ion Bombarded Volatile Solids. Nucl. Instrum. Methods Phys. Res. B **62**, 447-455.

ELLEGAARD, O., SCHOU, J., STENUM, B., SØRENSEN, H., and PEDRYS, R. (1992). Enhanced Sputtering of Solid Neon by Molecular Ions. Nucl. Instrum. Methods Phys. Res. B **67**, 549-553.

FEIDENHANS'L, R. (1991). Surface X-ray Crystallography and STM Images. In: Surface X-ray and Neutron Scattering. 2. International Conference on Surface X-ray and Neutron Scattering, Bad Honnef, Germany, 25-28 June 1992. Zabel, H.; Robinson, I.K. (eds.), (Springer-Verlag, Berlin, 1992) (Springer Proceedings in Physics, 61), 5-9.

FIIG, T. and JAUHO, A.P. (1992). Self-Consistent Modelling of Resonant Tunnelling Structures. Surf. Sci. **267**, 392-395.

FIIG, T., and JAUHO, A.P. (1991). Self-Consisten: Model for Two-Dimensional Accumulation Layer States in Resonant Tunneling Devices. Appl. Phys. Lett. **59**, 2245-2247.

FORREST, J.A., BROOKS, R.L., HUNT, J.L., STENUM, B., SCHOU, J., SORENSEN, H., GÜRTLER, P., MAGNOTTA, F., MAPOLES, E.R., SOUERS, P.C., and COLLINS, G.W. (1992). Continuum Emission from Irradiated Solid Deuterium. Phys. Rev. B **46**, 13820-13825.

GAULIN, B.D., REIMERS, J.N., MASON, T.E., GREEDAN, J.E., and TUN, Z. (1992). Spin Freezing in the Geometrically Frustrated Pyrochlore Antiferromagnet $Tb_2Mo_2O_7$. Phys. Rev. Lett. **69**, 3244-3247.

GOFF, J.P., CLAUSEN, K.N., FÅK, B., GODFRIN, H., HADFIELD, R., HAYES, W., HULL, S., and HUTCHINGS, M.T. (1992). Diffuse Neutron Scattering from Anion-Excess Strontium Chloride. Physica B **180/181**, 819-821.

GREY, F. and BOHR, J. (1992). A Symmetry Principle for Epitaxial Rotation. Europhys. Lett. **18**, 717-722.

GRÅBÆK, L., BOHR, J., ANDERSEN, H.H., JOHANSEN, A., JOHNSON, E., SARHOLT-KRISTENSEN, L., and ROBINSON, I.K. (1992). Melting, Growth, and Faceting of Lead Precipitates in Aluminium. Phys. Rev. B **45**, 2628-2637.

HABEKOST, S., NORLUND CHRISTENSEN, A., LEBECH, B., WROBLEWSKI, T., and O'REILLY, K.P.J. (1992). Superconducting Cuprates and Related Oxides. IV. Temperature - Unit Cell Parameter Relationships of $HoBa_2CU_3O_{7-\delta}$. Acta Chem. Scand. **45**, 966-967.

HARMON, B.N., WANG, X.-W., and LINDGÅRD, P.-A. (1992). Calculation of the Ruderman-Kittel Interaction and the Nuclear Magnetic Ordering in Silver. J. Magn. Magn. Mater. **104/107**, 2113-2115.

HARRIS, P., LARSEN, S., and LEBECH, B. (1992). A Single Crystal Neutron Diffraction Study of $KMnCl_3$. Its Twinning and Magnetic Structure. J. Phys. Chem. Solids **53**, 1021-1025.

HARRISON, A., CLARKE, S.J., MASON, T.E., and VISSER, D. (1992). Dispersion of Spin Waves in the S=1/2 Square Heisenberg Antiferromagnet $Cu(DCO_2)_2{\cdot}4D_2O$. J. Magn. Mat. **104/107**, 557-558.

HEIDELMANN, M., LEBECH, B., SMETANE, Z., and LOEWENHAUPT, M. (1992). Aspects of the Magnetic Structure of $TmCu_2$. J. Phys.: Condens. Mat. **4**, 8773-8782.

HELM, C.A., TIPPMANN-KRAYER, P., KENN, R.M., MÖHWALD, H., ALS-NIELSEN, J., and KJÆR, K. (1991). The Phases of Phosphatidyl Ethanolamine Monolayers. In: Surface X-ray and Neutron Scattering. 2. International Conference on Surface X-ray and Neutron Scattering, Bad Honnef, Germany, 25-28 June 1991. Zabel, H.; Robinson, I.K. (eds.). (Springer-Verlag, Berlin, 1992) (Springer Proceedings in Physics, 61). 147-149.

HELM, C.A., TIPPMANN-KRAYER, P., MÖHWALD, H., ALS-NIELSEN, J., and KJÆR, K. (1991). Phases of Phosphatidyl Ethanolamine Monolayers Studied by Synchrotron X-ray Scattering. Biophys. J. **60**, 1457-1476.

HENDRIKSEN, P.V., LINDEROTH, S., and LINDGÅRD, P.-A. (1992). Finite-size Effects in the Magnetic Properties of Ferromagnetic Clusters. J. Magn. Magn. Mater. **104/107**, 1577-1579.

JACQUEMAIN, D., GRAYER WOLF, S., LEVEILLER, F., DEUTSCH, M., KJÆR, K., ALS-NIELSEN, J., LAHAV, M., and LEISEROWITZ, L. (1992). Zweidimensionale Kristallographie an Amphiphilen Molekülen an der Luft-Wasser-Grenzfläche (Two-dimensional Crystallography of Amphiphilic Molecules at the Air-Water Interface). Angew. Chem. **104**, 134-158.

JACQUEMAIN, D., GRAYER WOLF, S., LEVEILLER, F., DEUTSCH, M., KJÆR, K., ALS-NIELSEN, J., LAHAV, M., and LEISEROWITZ, L. (1992). Two-dimensional Crystallography of Amphiphilic Molecules at the Air-Water Interface. Angew. Chem. Int. Ed. Engl. **31**, 130-152.

JORGENSEN, J.-E., and ANDERSEN, N.H. (1992). Crystal Structure and Charge Localization in $Pb_2Sr_2Ho_{0.625}Ca_{0.375}Cu_3O_8$. Acta Chem. Scand. **46**, 122-125.

KABER, R., NILSSON, L., ANDERSEN, N.H., LUNDÉN, A., and THOMAS, J.O. (1992). A Single-Crystal Neutron Diffraction Study of the Structure of the High-Temperature Rotor Phase of Lithium Sulphate. J. Phys. Condens. Matter **4**, 1925-1933.

KAWANO, S., ONODERA, A., ACHIWA, N., NAKAI, Y., and LEBECH, B. (1992). Neutron Diffraction Studies on Ho, Tb and Er under High Pressure. In: The Proceedings of the European Workshop on Neutron Scattering at High Pressures, Abingdon, U.K., 85-86.

KENN, R.M., BÖHM, C., MÖHWALD, H., KJÆR, K., and ALS-NIELSEN, J. (1992). Behenic Acid as a Structural Model for Fatty Acid Monolayers at the Air/Water Interface: An X-ray Diffraction Study. In: Surface X-ray and Neutron Scattering. 2. International Conference on Surface X-ray and Neutron Scattering, Bad Honnef, Germany, 25-28 June 1991. Zabel, H.; Robinson, I.K. (eds.), (Springer-Verlag, Berlin, 1992) (Springer Proceedings in Physics, 61), 139-142.

KJÆR, K., ALS-NIELSEN, J., KENN, R.M., BÖHM, C., TIPPMANN-KRAYER, P., HELM, C.A., MÖHWALD, H., LEVEILLER, F., JACQUEMAIN, D., LAHAV, M., LEIS-

EROWITZ, L., and DEUTSCH, M. (1992). X-ray Scattering Studies of Organic Monolayers on Electrolytic Solutions: Arachidic Acid on $CdCl_2$. In: Surface X-ray and Neutron Scattering. 2. International Conference on Surface X-ray and Neutron Scattering, Bad Honnef, Germany, 25-28 June 1991. Zabel, H.; Robinson, I.K. (eds.), (Springer-Verlag, Berlin, 1992) (Springer Proceedings in Physics, 61), 143-146.

KLEIMAN, R.N., BROHOLM, C., AEPPLI, G., BUCHER, E., STÜCHELI, N., BISHOP, D.J., CLAUSEN, K.N., MORTENSEN, K., PEDERSEN, J. SKOV, and HOWARD, B. (1992). Neutron Diffraction from the Vortex Lattice in the Heavy-Fermion Superconductor $UPt_3$. Phys. Rev. Lett. **69**, 3120-3123.

KROMANN, R., BILDE-SØRENSEN, J.B., REUS, R. de, ANDERSEN, N.H., VASE, P., and FRELTOFT, T. (1992). Relation Between Critical Current Densities and Epitaxy of $YBa_2Cu_3O_7$ thin Films on MgO(100) and $SrTiO_3$(100). J. Appl. Phys. **71**, 3419-3426.

LARSEN, E., EGSGAARD, H., SKYTTE JENSEN, B., and BOHR, J. (1992). C60/C70, Fysik og Kemi (C60/C70, Physics and Chemistry). Dansk Kemi **6/7**, 10-13.

LEBECH, B., and CLAUSEN, K. N. (1992). Neutron Scattering Facilities at Risø National Laboratory, Denmark. Notiziario Neutroni **2** (No.1), 26-30.

LEBECH, B., and WOLNY, J. (1992). Commensurate-incommensurate Magnetic Phase Transitions in dhcp Nd Metal. J. Magn. Magn. Mater. **104/107**, 1501-1502.

LEVEILLER, F., JACQUEMAIN, D., LEISEROWITZ, L., ALS-NIELSEN, J., and KJÆR, K. (1992). Towards a Determination at Near-Atomic-Resolution of Two-Dimensional Crystal Structures of Amphiphilic Molecules on the Water Surface. J. Phys. Chem. **96**, 10380-10389.

LINDGÅRD, P.-A. (1992). Vibrationally Reduced Magnetic Interactions in Cu and the Magnetic Ordering in a Magnetic field. J. Magn. Magn. Mater. **104/107**, 2109-2110.

LINDGÅRD, P.-A. (ed.), (1992). Proceedings of the Joint Nordic Spring Meeting '92. Extended abstracts. 3. Nordic Conference on Surface Science; 6. Nordic Symposium on Computer Simulation; 3. Nordic Symposium on Superconductivity, Nyborg Strand, Denmark, 7-10 May 1992. Risø-R-628(EN) 346 p.

MA, Y., ROMMING, C., LEBECH, B., GJØNNES, J., and TAFTØ, J. (1992). Structure Refinement of $Al_3Zr$ Using Single-crystal X-ray Diffraction, Powder Neutron Diffraction and CBED. Acta Cryst. B **48**, 11-16.

MANGELSHOTS, I., ANDERSEN, N.H., LEBECH, B., WISNIEWSKI, A., and JACOBSEN, C.S. (1992). Crystal Structure, Magnetic Susceptibility and Thermopower of Superconducting and Non-superconducting $Nd_{1.85}Ce_{0.15}CuO_{4+\gamma}$. Physica C **203**, 369-377.

MASON, T.E., AEPPLI, G., and MOOK, H. (1992). The Magnetic Dynamics of Superconducting $La_{1.86}Sr_{0.14}CuO_4$. Phys. Rev. Lett., **68**, 1414-1417.

MASON, T.E., AEPPLI, G., RAMIREZ, A.P., CLAUSEN, K.N., BROHOLM, C., STÜCHELI, N., BUCHER, E., and PALSTRA, T.T.M. (1992). Spin Gap and Antiferromagnetic Correlations in the Kondo Insulator CeNiSn. Phys. Rev. Lett. **69**, 490-493.

MASON, T.E., YANG, Y.S., COLLINS, M.F., GAULIN, B.D., CLAUSEN, K.N., and HARRISON, A. (1992). Tetracritical Dynamics of $CsMnBr_3$. J. Magn. Magn. Mater. **104/107**, 197-198.

MAYER, H.M., STEINER, M., STÜSSER, N., WEINFURTER, H., DORNER, B., LINDGÅRD, P.-A., CLAUSEN, K.N., HOCK, S., and VERHOEF, R. (1992). Inelastic Neutron Scattering Measurements on $Nd_2Fe_{14}B$ and $Y_2Fe_{14}B$ Single Crystals. J. Magn. Magn. Mater. **104/107**, 1295-1297.

MORTENSEN, K. (1992). Phase Behaviour of Poly(ethylene oxide)-Poly(propylene oxide)-Poly(ethylene oxide) Triblock-copolymer Dissolved in Water. Europhys. Lett. **19**, 599-604.

MORTENSEN, K., BROWN, W., and NORDÉN, B. (1992). Inverse Melting Transition and Evidence of Three-Dimensional Cubatic Structure in a Block-Copolymer Micellar System. Phys. Rev. Lett. **68**, 2340-2343.

NORDÉN, B., ELVINGSON, C., HAGMAR, P., KUBISTA, M., BATY, D., MORTENSEN, K., and TAKAHASHI, M. (1992). RecA Protein-DNA Complexes Studied by Flow Linear Dichroism, Fluorescence and Small Angle Neutron Scattering. Structure & Function. **2**, Proteins. R.H. Sorma and M.H. Sarma (eds.). (Academic Press) 61-68.

NORDÉN, B. ELVINGSON, C., KUBISTA, M., SJÖBERG, B., RYBERG, H., RYBERG, M., MORTENSEN, K., and TAKAHASHI, M. (1992). Structure of RecA-DNA Complexes Studied by Combination of Linear Dichroism and Small-angle Neutron Scattering Measurements on Flow-oriented Samples. J. Mol. Biol. **226**, 1175-1191.

PEDERSEN, J. SKOV. (1992). Model-independent Determination of the Surface Scattering- length-density Profile from Specular Reflectivity Data. J. Appl. Cryst. **25**, 129-145.

PENGRA, D.B., and DASH, J.G. (1992). Edge Melting in Low-coverage Adsorbed Films. J. Phys.: Condens. Matter **4**, 7317-7332.

POSSELT, D., PEDERSEN, J. SKOV, and MORTENSEN, K. (1992). A SANS Investigation on Absolute Scale of a Homologous Series of Base-catalysed Silica Aerogels. J. Non-Cryst. Solids **145**, 128-132.

POULSEN, H.F. (1992). Oxygen Ordering and Superconductivity in the High $T_c$ Superconductor $YBa_2Cu_3O_{6+x}$. Risø-R-608(EN), p. 94.

ROTHARD, H., SCHOU, J., and GROENEVELD, K.-O. (1992). Projectile- and Charge-

State-Dependent Electron Yields from Ion Penetration of Solids as a Probe of Preequilibrium Stopping Power. Phys. Rev. A **45**, 1701-1710.

ROTHARD, H., SCHOU, J., KOSCHAR, P., and GROENEVELD, K.-O. (1992). Electron Yields from Solids: a Probe for the Stopping Power of Swift Charged Particles? Nucl. Instrum. Methods Phys. Res. B **69**, 154-157.

SAMSETH, J., MORTENSEN, K., BURNS, J.L. and SPONTAK, R.J. (1992). Effect of Molecular Architecture on Microstructural Characteristics in Some Polysiloxaneimide Multiblock Copolymers. J. Appl. Pol. Sci. **44**, 1245-1256.

SANCHEZ, J.P., LEBECH, B., WULFF, M., LANDER, G.H., TAMALA, K., MATTENBERGER, K., VOGT, O., BLAISE, A., REBISANT, J., SPIRLET, J.C., and BROW, P.J. (1992). Examination of the Magnetic Properties of $NpCo_2$. J. Phys.: Condens. Matter **4**, 9423-9440.

SANDY, A.R. (1992). Atomernes Vej til Faste Stoffer (The Route of Atoms into the Solid State). Risø Nyt **4-92**, 2-3.

SCHAMPER, C., DORNISCH, D., MORITZ, W., SCHULZ, H., FEIDENHANS'L, R., NIELSEN, M., GREY, F., and JOHNSON, R.L. (1992). Au Adsorption on Si(111) Studied by Grazing Incidence X-ray Diffraction. In: Surface X-ray and Neutron Scattering. 2. International Conference on Surface X-ray and Neutron Scattering, Bad Honnef, Germany, 25-28 June 1991. Zabel, H.; Robinson, I.K. (eds.), (Springer-Verlag, Berlin, 1992) (Springer Proceedings in Physics, 61), 17-20.

SCHINS, A.G., NIELSEN, M., ARTS, A.F.M., and WIJN, H.W. de. (1992). Neutron Scattering Study of $Rb_2Cu_{1-x}Co_xF_4$: A Two-dimensional Randomly Ferromagnet-antiferromagnet. Physica B **180/181**, 161-164.

SCHOU, J. (1992). Iskugler af Brint er Brændstof til Fusionsreaktorer (Ice Balls of Hydrogen are Fuel in Fusion Reactors). Risø Nyt (1992) **2**, 8-9.

SCHOU, J., ELLEGAARD, O., PEDRYS, R., and SØRENSEN, H. (1992). Sputtering of Solid Neon and Argon by Medium Mass Ions. Nucl. Instrum. Methods Phys. Res. B **65**, 173-176.

SCHOU, J. (1992). Electron Emission from Solids, Risø-I-588 (EN), 1-71.

SIEMENSMEYER, K., STEINER, M., WEINFURTHER, H., CLAUSEN, K.N., LINDGÅRD, P.-A., ANNILA, A.J., LOUNASMAA, O.V., OJA, A.S., and TUORINIEMI, J.T. (1992). The Phase Diagram and the Magnetic Structure of Nuclear Spins in Elemental Copper Below 60 nK. Physica B **180/181**, 29-30.

VAKNIN, D., ALS-NIELSEN, J., PIEPENSTOCK, M., and LÖSCHE, M. (1992). Protein Recognition Processes at Functionalized Lipid Surfaces: A Neutron Reflectivity Study. In: Surface X-ray and Neutron Scattering. 2. International Conference on Surface X-ray and Neutron Scattering, Bad Honnef, Germany, 25-28 June 1991. Zabel, H.; Robinson, I.K.

(eds.), (Springer-Verlag, Berlin, 1992) (Springer Proceedings in Physics, 61), 155-157.

WEI, W., TUN, Z., BUYERS, W.J.L. GAULIN, B.D., MASON, T.E., GARRETT, J.D., and ISAACS, E.D. (1992). Long Range Antiferromagnetic Order and Its Coexsistence with Superconductivity in the Heavy Electron System $URu_2Si_2$. J. Magn. Magn. Mat. **108**, 77-78.

WINKELMANN, M., GRAF, H.A., ANDERSEN, N.H., ZEISKE, T., and HOHLWEIN, D. (1992). Magnetic and Electroni Properties of $Mg_{1-x/2}Li_xCu_{2-x/2}O_3$. J. Magn. Magn. Mater. **104/107**, 871-873.

ÖSTERBERG, R. and MORTENSEN, K. (1992). Fractal Dimension of Humanic Acids. A Small Angle Neutron Scattering Study. Eur. Biophys. J. **21**, 163-167.

### 3.2 Conferences

ALMDAL, K., MORTENSEN, K., KOPPI, K.A., and BATES, F.S., On the Origin of Complex Phase Behaviour in Block Copolymer Melts. Joint Nordic Spring Meeting '92: Nyborg Strand, Denmark (May).

ALMDAL, K., MORTENSEN, K., KOPPI, K.A., ROSEDALE, J.H., and BATES, F.S. Asymmetry in Diblock Copolymer Phase Behaviour. Gordon Research Conference on Polymer Physics, Newport, Rhode Island, U.S.A. (August).

ALMDAL, K., MORTENSEN, K., KOPPI, K.A., and BATES, F.S. On the Origin of Complex Phase Behaviour in Block Copolymer Melts. 4th International EPF Symposium on Polymeric Materials, Baden-Baden, Germany (September).

ALS-NIELSEN, J., Structures of Two-Dimensional Soft Condensed Matter. Joint Nordic Spring Meeting '92: Nyborg Strand, Denmark (May).

ALS-NIELSEN, J., X-ray Studies of Langmuir Films. VI International Conference of Solid Films and Surfaces (ICSFS), Paris, France (June).

ALS-NIELSEN, J., X-ray Studies of Langmuir Films. American Crystallographic Association, Pittsburg, U.S.A. (August).

ALS-NIELSEN, J., X-ray Study of Ion Structures in Solution. Gordon Research Conference on Polymer Physics, Newport, Rhode Island, U.S.A. (August).

ANDERSEN, N.H., Structural Properties and Superconductivity of High Tc Superconductors. Kemisk Forenings Årsmøde (Annual Meeting of the Chemical Society), Odense, Denmark (June).

ANDERSEN, N.H., Risø Facilities and Structural Studies on High Temperature Superconductors. Workshop of the EC Working Group on: "The Influence of the local Structure on the Macroscopic Superconducting Properties for Samples in the Y-Ba-Cu-0 and Related Systems". El Escorial, Madrid, Spain (October).

ANDERSEN, N.H., ANDERSEN, J.V., BÖRJESSON, L., HADFIELD, R., KAKIHANA, M., McGREEVY, R., MOURITSEN, O.G., and POULSEN, H.F., The Role of Disorder and Defect Structures in High Temperature Superconductivity. Two Day Contractors Workshop on EC Activities in High Temperature Superconductivity. Strasbourg, France (November).

ANDERSEN, N.H., ANDERSEN, J.V., BÖRJESSON, L., HADFIELD, R., KAKIHANA, M., McGREEVY, R., MOURITSEN, O.G., and POULSEN, H.F., Structure and Superconductivity in Co, Fe, and Al Doped $YBa_2Cu_3O_{6+x}$. European Materials Research Society 1992 Fall Meeting. Strasbourg, France (November).

BOHR, J., Structural Investigations in C60. Joint Nordic Spring Meeting '92: Nyborg Strand, Denmark (May).

BOHR, J., A Critical Review of Magnetic X-ray Scattering. Magnetism and Structure in Systems of Reduced Dimension. NATO Advanced Research Workshop, Cargese, France (June).

BOHR, J., An Alternative Explanation for Epitaxial Rotation. VI International Conference of Solid Films and Surfaces (ICSFS), Paris, France (June).

BOHR, J., Generation of the 3-Dimensional Protein Structure from Distance Inequalities. Biological Sequences: Finding Structure and Function by Neural Networks. Institute for Scientific Interchange Foundation, Torino (July).

BOHR, J., An Alternative Explanation for Epitaxial Rotation. STATFYS 18 (Statistical Physics), Berlin, Germany (August).

BOHR, J., $C_{60}$ a New Form of Carbon. Norwegian Physical Society. Annual Meeting on Solid State Physics. Rondablik, Norway (September).

BOHR, J., Samtidsinformation om Grundvidenskabelig Forskning Illustreret ved Eksempler (Contemporary Information on Basic Science Research Illustrated by Examples). Danmarks Skolebiblioteksforenings Årsmøde (Annual Meeting of Danish Association of Schoollibraries). Copenhagen, Denmark (October).

BOHR, J., Kulstof-60 (Carbon 60). LMFK Årsmøde (Annual Meeting of Danish Highschool Teachers of Mathematics, Physics and Chemistry).(October)

CLARKE, S.J., HARRISON, A., and MASON, T.E., Spin Wave Dispersion in $Cu(DCO_2)_2 \times 4\ D_2O$, A S=1/2 square Heisenberg Antiferromagnet. 37th Annual Conference on Magnetism and Magnetic Materials, Houston, U.S.A. (December).

CLAUSEN, K.N., An Introduction to Risø. 1992 UK Neutron and Muon Beam Users' Meeting, University of Reading, UK (April).

CLAUSEN, K.N., The Magnetic Phase Diagram of Nuclear Spins in Copper as Determined by Neutron Diffraction. Symposium on Collective Effects in Metals Arising from Nuclear Magnetic Interactions, Sjøkulla, Finland (April).

ELLEGAARD, O., SCHOU, J., STENUM, B., SØRENSEN, H., PEDRYS, R., OOSTRA, D.J., HARING, A., and de VRIES, A.E., Sputtering of Thick Nitrogen and Oxygen Films by keV Hydrogen Ions. Joint Nordic Spring Meeting '92: Nyborg Strand, Denmark (May).

ELLEGAARD, O., STENUM, B., SCHOU, J., PEDRYS, R., and SØRENSEN, H., Sputtering of Solid Hydrogenic Targets by keV Hydrogen Ions. Symposium on Sputtering, SPUT92. Fundamental Processes in Sputtering of Atoms and Molecules. Copenhagen, Denmark (August).

FALCAO, A.N., SKOV PEDERSEN, J., MORTENSEN, K., and BOUÉ, F., Over-Scattering from Expanded Gels (PDMS). Swelling from Dry State to Maximum Swelling. Joint Nordic Spring Meeting '92: Nyborg Strand, Denmark (May).

FEIDENHANS'L, R., X-ray Diffraction from Surfaces - Status and Prospects. National Synchrotron Day. Groningen, The Netherlands (November).

FEIDENHANS'L, R., NIELSEN, M., and CLAUSEN, K., Investigations of Diamondlike Carbon Films by X-ray and Neutron Scattering. National Synchrotron Day. Groningen, The Netherlands (November).

FIIG, T., Solving the 3D-ASYNNNI Model on the Connection Machine. STATFYS 18 (Statistical Physics), Berlin, Germany (August).

FIIG, T. and JENSEN, H.J., Diffusive Description of Lattice Gas Models. Joint Nordic Spring Meeting '92: Nyborg Strand, Denmark (May).

FIIG, T., POULSEN, H.F., ANDERSEN, N.H., LINDGÅRD, P.-A., and MOURITSEN, O.G., Solving the 3-D ASYNNNI Model on the Connection Machine. Joint Nordic Spring Meeting '92: Nyborg Strand, Denmark (May).

FINDEISEN, E. and FEIDENHANS'L, R., Investigation of Laserablated Diamond-Like Carbon Films (a-C) by Neutron and X-ray Scattering. 25. Danske Krystallografmøde (25th Danish Crystallography Meeting). H.C. Ørsted Institute, Copenhagen, Denmark (June).

FORLAND, G.M., SAMSETH, J., HØILAND, H., and MORTENSEN, K., The Effect of Medium Chain Length Alcohols on the Micellar Properties of Sodium Dodecyl Sulfate in Brine Solutions. VI European Colloid and Interface Society Conference, Graz, Austria (September).

GAULIN, B.D., REIMERS, J.N., TUN, Z., MASON, T.E., and GREEDAN, J.E., Neutron Scattering from the Geometrically Frustrated Pyrochlore Antiferromagnet $Tb_2Mo_2O_7$. 37th Annual Conference on Magnetism and Magnetic Materials, Houston, U.S.A. (December).

GREEDAN, J.E., MAIGNAN, A., SIMON, C., RAVEAU, B. and PEDERSEN, J. SKOV, Re-entrant Spin-glass Behaviour in the Frustrated Pyrochlore $Y_2Mn_2O_7$. 37th Annual Conference on Magnetism and Magnetic Materials, Houston, U.S.A. (December).

GREGORY, C., BERNHOEFT, N., LEBECH, B., HARRIS, P., PEDERSEN, J. SKOV, MORTENSEN, K., Study of the Magnetic Phase Diagram of MnSi Close to the Critical Temperature. 12. General Conference of the Condensed Matter Divison of the EPS, Prague, Czechoslovakia (April).

HARRIS, P., LEBECH, B., and ACHIWA, N., Diffraction Study of the Nuclear and Magnetic Ordering of the Layered Perovskite PAMC. Joint Nordic Spring Meeting '92: Nyborg Strand, Denmark (May).

HARRIS, P., LEBECH, B., ACHIWA, N., and LARSEN, F.K. Vekselvirkning mellem $(CH_3CH_2CH_2NH_3)_2MnCl_4$ (PAMC)'s Krystal- og Magnetiske Struktur. (Interaction between $(CH_3CH_2CH_2NH_3)_2MnCl_4$ (PAMC)'s Crystal and Magnetic Structure) 25. Danske Krystallografmode (25th Danish Crystallography Meeting), Copenhagen, Denmark (June).

HARRIS, P., LEBECH, B., and ACHIWA, N., Diffraction Study of the Nuclear and Magnetic Ordering of the Layered Perovskite PAMC. Physique en Herbe 92, Marseille, France (July).

HENDRIKSEN, P.V., LINDEROTH, S., and LINDGÅRD, P.-A., Magnetic Properties of Clusters. Joint Nordic Spring Meeting '92: Nyborg Strand, Denmark (May).

JORGENSEN, J.-E. and ANDERSEN, N.H., Crystal Structure and Charge Localization in $Pb_2Sr_2Y_{1-x}Ca_xCu_3O_8$ for x=0.0-0.5. Joint Nordic Spring Meeting '92: Nyborg Strand, Denmark (May).

KINGSTON, J.J., KROMANN, R., MIKLICH, A.H., SAGDAHL, L., SAITO, Y., DANTSKER, E., and CLARKE, J., High-$T_c$ Multilayers for Josephson Junctions and Interconnects. 1992 March Meeting of the American Physical Society, Indianapolis, U.S.A. (March).

KJÆR, K., Monolayers at Liquid Surfaces: 2D Systems on a Smooth Substrate. Joint Nordic Spring Meeting '92: Nyborg Strand, Denmark (May).

KROMANN, R., KINGSTON, J.J., MIKLICH, A.H., SAGDAHL, L.T., SAITO, Y., and CLARKE, J., High $T_c$ SQUID's and Magnetometers. Joint Nordic Spring Meeting '92: Nyborg Strand, Denmark (May).

KROMANN, R., REUS, R. de, ANDERSEN, N.H., BILDE-SØRENSEN, J.B., VASE, P., and FRELTOFT, T., Relation Between Critical Current and In-Plane Ordering of $YBa_2Cu_3O_{6+x}$ on MgO(001) and $SrTiO_3$(001). Joint Nordic Spring Meeting '92: Nyborg Strand, Denmark (May).

LINDGÅRD, P.-A., Theory and Modelling of Martensitic Transformations. Workshop on Martensitic Transformations. Ames Lab. Iowa, U.S.A. (March).

LINDGÅRD, P.-A., Elastically Driven Phase Transitions Studied by a Continous Monte Carlo Method. NATO ASI on Phase Transformation, Rhodos, Greece (July).

LINDGÅRD, P.-A., Ordering by Disorder in Adsorbed Layers on Graphite. Workshop on Statistical Physics, Århus University, Århus (August).

LEBECH, B., HARRIS, P., GREGORY, C., BERNHOEFT, N., PEDERSEN, J. SKOV, and MORTENSEN, K., Neutron Diffraction Study of the Magnetic Phase Diagram of MnSi Close to the Critical Temperature. Joint Nordic Spring Meeting '92: Nyborg Strand, Denmark (May).

LEBECH, B., Magnetic Ordering in Nearly Ferromagnetic Antiferromagnetic Spirals. International Symposium on Recent Progress in Materials Physics, Osaka, Japan (June).

MASON, T.E., Magnetic Dynamics of $La_{2-x}Sr_xCuO_4$. Joint Nordic Spring Meeting '92, Nyborg Strand (May).

MASON, T.E., Magnetic Fluctiations in Superconducting $La_{2-x}Sr_xCuO_4$. 37th Annual Conference on Magnetism and Magnetic Materials, Houston, U.S.A. (December).

McCRACKEN, C.G., TALBOT, D.E.J., and PEDERSEN, J. SKOV, The Effects of Hydrogen on the Aging of an Aluminium- 2wt% Lithium Alloy. 1992 Materials Week Conference, Chicago, U.S.A. (November).

MIKLICH, A.H., KINGSTON, J.J., WELLSTOOD, F.C., KROMANN, R.F., SAGDAHL, L.T., DANTSKER, E., CLARKE, J., CHAR, K., COLCLOUGH, M.S., and ZAHARCHUK, G., High-$T_c$ Thin Film Magnetometers for Low Frequency Applications. SC Global 92, San Diego, California, U.S.A. (January).

MORTENSEN, K., Block Polymer in Aqueous Solution: Micelle Formation and Crystallization. Gordon Research Conference on Macromolecule and Polyelectrolyte Solutions, Oxnard, California, U.S.A. (February).

MORTENSEN, K., Strukturelle Studier af Miceller ved Neutronspredning (Structural Studies of Micelles by Neutron Scattering). Biologiske Systemers Fysiske Kemi (The Physical Chemistry of Biological Systems), Kemisk Forening (Chemical Society), Copenhagen, Denmark (April).

MORTENSEN, K., Small-Angle Neutron Scattering on Polymers. Symposium on Characterization of Polymer Materials, Copenhagen, Denmark (May).

MORTENSEN, K., ALMDAL, K., and BATES, F.S., Crystalline Mesophases in Polymer Materials. 25. Danske Krystallografmøde (25th Danish Crystallography Meeting). H.C. Orsted Institute, Copenhagen, Denmark (June).

MORTENSEN, K., Block Copolymer in Aqueous Solution: Micelle Formation and Hard-sphere Crystallization. VI European Colloid and Interface Society Conference. Graz, Austria (September).

MORTENSEN, K., Aggregation of Amphiphilic Molecules. Physics and Chemistry of Biological Systems. Technical University, Lyngby, Denmark (September).

MORTENSEN, K., PEDERSEN, J. SKOV, and BROWN, W., Block Polymer in Aqueous Solution: Micelle Formation and Crystallization. Joint Nordic Spring Meeting '92: Nyborg Strand, Denmark (May).

PEDERSEN, J. SKOV, Structure of Clathrin-coated Vesicles from Small-Angle Neutron Scattering Experiments. VI European Colloid and Interface Society Conference, Graz, Austria (September).

PEDRYS, R., WARCZAK, B., and SCHOU, J., Energy Spectra from Solid Rare Gases Sputtered by Light Ions. Ninth International Workshop on Inelastic Ion Surface Collisions. Centre Paul Langevin, Aussois, France (September).

PENGRA, D.P., Edge Melting: Surface Melting in 2 D. The 12th General Conference of the Condensed Matter Division of the European Physical Society. Prague, Czechoslovakia (April).

PENGRA, D.B. and BOHR, J., Charge-Density Wave Phases in $TaS_2$. Joint Nordic Spring Meeting '92: Nyborg Strand, Denmark (May).

POULSEN, H.F., ANDERSEN, N.H., LEBECH, B., ANDERSEN, J.V., BOHR, H., MOURITSEN, O.G., ZEISKE, T., SONNTAG, R., HOHLWEIN, D., and WOLF, T., Oxygen Order and Superconductivity in Pure and Doped $YBa_2Cu_3O_{6+x}$. Joint Nordic Spring Meeting '92: Nyborg Strand, Denmark (May).

REUS, R. de, KROMANN, R., NIELSEN, M., ANDERSEN, N.H., KRINGHØJ, P., VASE, P., HANSEN, K.L., FRELTOFT, T., SEEMANN, R., SEWING, A., and JOHNSON, R.L., Structural Characterization of Thin-Film High-$T_c$ Superconductors. Seminar om Avanceret Elektronik, H.C. Ørsted Institute, Copenhagen, Denmark (April).

REUS, R. de, SEEMANN, R., NIELSEN, M., SEWING, A., and JOHNSON, R.L., Epitaxial Growth of High-Tc Superconducting $Bi_2Sr_2CaCu_2O_{8+x}$ Thin Films on MgO(001), $LaAlO_3$(001), and $NdGaO_3$(001). Joint Nordic Spring Meeting '92: Nyborg Strand, Denmark (May).

SANDY, A.R., MOCHRIE, S.G.J., ZEHNER, D.M., GRÜBEL, G., HUANG, K.G., and GIBBS, D., Au and Pt(111) Surface Studies. 12. International Vacuum Congres/8. International Conference on Solid Surfaces. The Hague, The Netherlands.

SCHOU, J. Secondary Electron Emission from Insulators. Ionization of Solids by Heavy Particles. NATO Advanced Research Workshop. Giardini Naxos, Taormina, Italy (June).

SCHOU, J. and ELLEGAARD, O., Evaporation Yields of Solid Nitrogen Induced by UV-Laser Irradiation. 1992 Summer Gordon Research Conference on Particle-Solid Interactions. Holderness School, Plymouth, New Hampshire, U.S.A. (July).

SCHOU, J., Sputtering of Inorganic Insulators: Experimental Resuits. Symposium on Sputtering, SPUT92. Fundamental Processes in Sputtering of Atoms and Molecules. Copenhagen, Denmark (August).

SCHWAHN, D., JANSSEN, S., MORTENSEN, K., MEIER, G., and SPRINGER, T., Ginzburg-Landau-Criterium for Different Polymer Mixtures with Different Chain Length. Deutschen Physikalischen Gesellschaft (German Physical Society),Regensburg, Germany (March).

SEQUEIRA, A.D., CALDERON, H.A., KOSTORZ, G., and PEDERSEN, J. SKOV, The Effect of Coherency Strains on the Coarsening of Bimodal $\gamma'$ Precipitates Ensembles in Ni-Al-Mo. Fall Meeting of the Material Research Society, Pittsburg, U.S.A. (December).

THOFT, N.B., BOHR, J., JOHNSON, E., ANDERSEN, H.H., JOHANSEN, A., and SARHOLT-KRISTENSEN, L., and BURAS, B., Bismuth Inclusions in Aluminium. Joint Nordic Spring Meeting '92: Nyborg Strand, Denmark (May).

VIVES, E. and LINDGÅRD, P.-A., Monte Carlo Simulation of Two-Dimensional Corrugated Systems. Joint Nordic Spring Meeting '92: Nyborg Strand, Denmark (May).

VIVES, E. and LINDGÅRD, P.-A., Structural Phase Transitions of an Adsorbate on a Corrugated Surface Studied by Monte Carlo Simulation. 1992 March Meeting of the American Physical Society, Indianapolis, U.S.A. (March).

WOLNY, J., FRELTOFT, T., and TOPOLNICKA, A., Small Angle Neutron Scattering on Carbon Fibres. European Conference on Physics for Industry, Industry for Physics, Cracow, Poland (September).

### 3.3 Lectures

ALS-NIELSEN, J., Introductory Lectures on X-ray and Neutron Scattering. The European Course HERCULES, Grenoble, France (February).

ALS-NIELSEN, J., Crystal Spectroscopy of X-ray Synchrotron Brightness - First Results from ESRF Undulator ID6. National Synchrotron Light Source (NSLS), Brookhaven, U.S.A. (August).

ANDERSEN, N.H., Højtemperatur Superledning (High Temperature Superconductivity). Dansk Institut for Økologisk Teknik, (Danish Institute of Ecological Technology) Valby, Denmark (March).

ANDERSEN, N.H., Structural Properties of High-Tc Superconductors. University of Kiel, Germany (January).

ANDERSEN, N.H., Structural Ordering and Superconductivity in Pure and M-doped $YBa_2Cu_{3-y}M_yO_{6+x}$.
Hahn-Meitner-Institute, Berlin, Germany (September).
Physics Department, Chalmers University of Technology, Gothenburg, Sweden (October).
University of British Columbia, Vancouver, Canada (November).

BOHR, J., Kulstof-60 (Carbon-60).
Roskilde University Center, Denmark (April).
Ungdommens Naturvidenskabelige Forening (Youth Science Society), Copenhagen, Denmark (September).

FEIDENHANS'L, R ., X-ray Diffraction from Surfaces. Max-Planck-Institute für Festkörper Forschung, Stuttgart, Germany (January).

FEIDENHANS'L, R., Metal-MBE at Risø. H.C. Ørsted Institute, Copenhagen, Denmark (April).

KJÆR, K., Synchrotron Radiation. Methods in Soft Condensed Matter. PhD course in Experimental Methods for studying Soft Condensed Matter. Roskilde University Center, Denmark (October).

LINDGÅRD, P.-A., Theory and Simulations of Structures in Two Dimensions. NORDITA, Copenhagen (April).

LINDGÅRD, P.-A., Structured Liquids on Corrugated Surfaces. Technical University, Lyngby, Denmark (May).

MASON, T.E., Neutron Scattering as a Probe of Band Structure.
University of Toronto, Canada (April).
Chalk River Laboratories, Canada (April).
McGill University, Canada (April).

MASON, T.E., Magnetic Fluctuations in Superconducting $La_{2-x}Sr_xCuO_4$.
AT&T Bell Laboratories, U.S.A. (November).
Los Alamos National Laboratory, U.S.A. (November).

MORTENSEN, K., Micelle Formation and Micelle Hard Sphere Crystallization. Catholic University of Leuven, Belgium (August).

MORTENSEN, K., Small Angle Scattering. Methods in Soft Condensed Matter. PhD course in Experimental Methods for studying Soft Condensed Matter. Roskilde University Center, Denmark (October).

MORTENSEN, K., Small Angle Scattering of Selfassembling Macromolecular Aggregates. CISMI, University of Copenhagen, Denmark (November).

PEDERSEN, J. SKOV, The Structure of Clathrin-coated Vesicles from Solution Scattering Experiments. European Molecular Biology Laboratory, Outstation Hamburg, Germany (February).

PEDERSEN, J. SKOV, Analysis of Small-angle Scattering Data. Institute für Angewandte Physik, ETH, Zürich, Switzerland (November).

PEDERSEN, J. SKOV, Structure of Clathrin-coated Vesicles: A Small-angle Neutron Scattering Study. Institut für Polymere, ETH Zürich, Switzerland (November).

PENGRA, D., Edge Melting in Neon Films. H.C. Orsted Institute, Copenhagen, Denmark (April).

## 3.4 Organization of Conferences, Schools

### JOINT NORDIC SPRING MEETING '92

7-10 May 1992, Nyborg, Denmark.

The Joint Meeting consisted of three symposia on the topics: Surface Science, Computer Simulation and Superconductivity and three works shops on related topics: Physics of small clusters, Soft condensed matter and Electronic properties. In addition there was an exhibition on scientific equipment with participation of twelve companies. There were 35 invited, international speakers a large number of talks in four parallel sessions, and a poster session. There were in total about 350 participants from all the Nordic countries and from other countries; in particular there was participation from the Baltic countries. The meeting was supported by a large number of funds and by a registration fee. This allowed the meeting to offer support to many of the participating students.

Organization

The Joint meeting and the symposia were organized in collaboration with the physical societies in the Nordic countries and with inter-Nordic symposia committees. Proceedings, in the form of extended abstracts, were published as a Risø Report, 346 pp. The chairmen of the organization were

P.-A. LINDGÅRD, Risø National Laboratory, Denmark,
General chairman of the Joint Nordic Spring Meeting '92 and organizer of the work shops.

N.H. ANDERSEN, Risø National Laboratory, Denmark,
Chairman of the 6th Nordic Symposium on Superconductivity.

O.G. MOURITSEN, The Technical University, Lyngby, Denmark,
Chairman of the 3rd Nordic Symposium on Computer Simulation.

J. ONSGÅRD, The University of Odense, Denmark,
Chairman of the 3rd Nordic Symposium on Surface Science.

### COURSE IN SURFACE SCIENCE

R. FEIDENHANS'L together with J.K. Nørskov and I. Chorkendorff from the Laboratory of Applied Physics, the Technical University (DtH) of Denmark, gave a course in Surface Physics at the DtH. The course consisted of two lectures of 2x35 minutes duration every week together with exercises. R. Feidenhans'l was lecturing in total nine lectures about Surface Crystallography, Phase Transitions at Surfaces, Epitaxy, and Growth.

## 3-WEEK EXPERIMENTAL COURSE

R. FEIDENHANS'L, E. FINDEISEN AND K.N. CLAUSEN gave a three week experimental course in X-ray and neutron reflectometry for four students from the Technical University (DtH) of Denmark. Diamond-like Carbon films were investigated.

## COURSE IN SOLID STATE PHYSICS

T.E. MASON together with A.R. Mackintosh from the H.C. Ørsted Institute, Copenhagen, taught a course in solid state physics using the text book by N.W. Ashcroft and N.D. Mermin ("Solid State Physics" Holt-Saunders International Editions, 1976). The course was taught at the H.C. Ørsted Institute and provided an introduction to basic concepts in solid state physics. Topics included the band theory of metals, semiconductors, magnetic ordering, superconductivity, and neutron scattering. The weekly lectures were given by A.R. Mackintosh. They were supplemented by problem sessions led by T.E. Mason.

### 3.5 Seminars at Risø, 1992

CHEN, S.-H., *Massachusetts Institute of Technology, USA.* Inversion of X-ray and Neutron Reflectivity Data (January).

STAMM, M., *Max Planck Institut für Polymerforschung, Mainz, Germany.* Neutron Reflectivity Studies on Polymer Interfaces (January).

SJÖBERG, J., *Chalmers University of Technology, Gothenburg, Sweden.* A Study of the Structure of Certain Sialons Using X-Ray and Neutron Diffraction, Solid State NMR and EXAFS (January).

SELLSHOP, F., *GSI, Darmstadt, Germany.* The Physics of Diamonds (February).

BOUÉ, F., *Laboratoire Léon Brillouin (CEA/CNRS) CEN-Saclay, France.* Free Chains in a Deformed Polymer Network: Heterogeneity in Deformation and Butterfly Effect (February).

GREY, F., *Aono Atomcraft Project, Ibaraki, Japan.* Prospects of Silicon Nanolithography by STM (March).

BLEANEY, B., *University of Oxford, England.* Magnetic Properties of Rare Earth Fluorides (April).

BAYERL, T., *Technical University, München, Germany.* Structure and Dynamics of Lipid Bilayers on a Solid Support (April).

VARMA, C.M., *AT&T Bell Laboratories, U.S.A.* Superconductivity in the Fullerenes (May).

JIANG, X., *University of Houston, U.S.A.* Diffuse X-Ray Scattering Study of Tetragonal Y $Ba_2(CU_{1-x}Al_x)_3O_7$ Crystals (June).

BESOLD, G., *Institut für Angewandte Physik, Universität Erlangen-Nürnberg, Germany.* Monte Carlo Simulation of Ordering on Surfaces (June).

DAHMEN, U., *National Center for Electron Microscopy, Lawrence Berkeley Laboratory, California, U.S.A.* Ledge Growth and Roughening Transitions in Interfaces (July).

SCHIPPERS, S., *University of Osnabrück, Germany.* The Interaction of Highly Charged Ions with Metal Surfaces (June).

FISK, Z., *Los Alamos National Laboratory, U.S.A..* Kondo Insulators (June).

MOTIZUKI, K., *Sinshu University, Faculty of Science, Matsumoto, Japan.* A Role of Electron-Phonon Interaction in Oxide Superconductors (July).

MAY, S.E., *University of Pittsburgh, U.S.A.* Capillary Wave Relaxation for a Meniscus between Miscible Liquids (July).

CHAIKIN, P., *Princeton University, U.S.A.*, The Most Remarkable Material ever Discovered - from Copenhagen - The Bechgaard Salt$(TMTSF)_2PF_6$ (August).

FALICOV, L., *University of Berkeley, U.S.A.*, The Current Hot Topics - A Personal Overwiev (August).

MACKINTOSH, A., *University of Copenhagen, Denmark*, Competing Interactions and Novel Magnetic Structures (August).

MASON, T., *Risø National Laboratory, Denmark*, Magnetism in Heavy-Fermion Superconductors and Semiconductors (August).

ITOH, N., *Nagoya University, Japan*, Electronic Processes in Laser-Induced Particle Emission and Ablation (August)

FALICOV, L., *University of Berkeley, U.S.A.*, Surface, Interface and Thin-Film Magnetism (September).

ANDERSEN, N.H., *Risø National Laboratory, Denmark*, Structural Aspects of High-Temperature Superconductivity (September).

BECHGAARD, K., , Organic Superconductors: Recent Developments (September).

NØRSKOV, J., Crystal Growth and Pattern Formation (September).

MONTFROOIJ, W., *Chalk River Laboratories, Ontario, Canada*, Helium at $T_\lambda$: the Transition from a Classical to a Quantum Fluid (September).

SVENDSEN, W., *Physics Department, University College, Dublin*, Laser-produced Plasma and their Applications (September).

SPANNINGA, W., *Rijksuniversiteit of Groningen, The Netherlands*, Structural Phase Transition in Buried $CoSi_2$ Layers. A Mößbauer and Channeling Study (October).

MIKHEEV, L., *NORDITA, Copenhagen*, Surface Ordering vs. Fluctuations in Wetting, Surface Melting and Roughening (November).

JOHNSON, E., *H.C. Ørsted Institute, Copenhagen*, Nano-size Crystalline Inclusions in a Crystalline Matrix: Electron Microscope Study (December).

SMILGIES, D.M., *Rutgers University, U.S.A.*, Structure and Dynamics of the MO(001) Reconstruction by Helium Atom Scattering and X-Ray Diffraction (December).

FIG, T., *Department of Solid State Physics, Risø National Laboratory*, 1/f Noise (December).

**Bibliographic Data Sheet** **Riso-R-660(EN)**

Title and author(s)

Annual Progress Report of the of Department of Solid State Physics
1 January - 31 December 1992

J. Skov Pedersen, B. Lebech and P.-A. Lindgård (eds.)

| ISBN | ISSN |
|---|---|
| 87-550-1868-8 | 0106-2840<br>0907-0249 |

| Dept. or group | Date |
|---|---|
| Department of Solid State Physics | January 1993 |

| Groups own reg. number(s) | Project/contract no. |
|---|---|
| - | - |

| Pages | Tables | Illustrations | References |
|---|---|---|---|
| 164 | 1 | 101 | 165 |

Abstract (Max. 2000 char.)

Research in the department is in the field of condensed matter physics. The principal activities of the department in the period from 1 January, to 31 December, 1992, are presented in this Progress Report.

The department's research is predominantly experimental - utilising diffraction of neutrons and X-rays - and includes studies of two- and three-dimensional structures, magnetic ordering, heavy fermions, high $T_c$ superconductivity, phase transitions in model systems, precipitation phenomena, and nano-scale structures in various materials. The major interest of the department is in basic research but projects of a more applied nature are often taken up, prompted by the applicability of the developed techniques and expertise.

For clarity, the contributions to this report are organized into 12 categories with the following headings:

- Theory, Monte Carlo simulations, and methods for data analysis
- Magnetic structures, magnetic phase transitions, and spin dynamics
- High $T_C$ superconductivity
- Structures and structural phase transitions
- Inclusions and precipitates in alloys and metals
- Interaction of particles and photons with surfaces
- Surfaces, interfaces, and amorphous structures
- Langmuir films
- Polymers
- Microemulsions and biological systems
- Instrumental developments
- Other activities

Descriptors INIS/EDB

MAGNETISM; PROGRESS REPORT; RISOE NATIONAL LABORATORY; SOLID STATE PHYSICS; SUPERCONDUCTIVITY

Available on exchange or request from:
Risø Library, Risø National Laboratory (Risø Bibliotek, Forskningscenter Risø)
P.O. Box 49, DK-4000 Roskilde, Denmark
Phone (+45) 42 37 12 12, ext. 2268/2269 · Telex 43 116 · Telefax (+45) 46 75 56 27

Available on request from:
Risø Library
Risø National Laboratory,
P.O. Box 49, DK-4000 Roskilde, Denmark
Phone +45 42 37 12 12, ext. 2268/2269
Telex 43116, Telefax +45 46 75 56 27

ISBN 87-550-1868-8
ISSN 0106-2840
ISSN 0907-0249